Sediment Capping Effects on Gas ebullition, Hyporheic Exchange and Benthic Microbial Community Structure

BY

RAJA SHANKAR KALIAPPAN

B.E., College of Engineering, Guindy, Anna University, 2005

M.Eng., Illinois Institute of Technology, Chicago, 2008

THESIS

Submitted as partial fulfillment of the requirements

for the degree of Doctor of Philosophy in Civil Engineering

in the Graduate College of the

University of Illinois at Chicago, 2016

Chicago, Illinois

Defense Committee:

Karl J. Rockne, Chair and Advisor

Amid P. Khodadoust

Benjamin L. O'Connor

Craig D. Foster

Asha Rani, College of Medicine

To

இறச்சகுளம் ஸ்ரீ பத்திரகாளி அம்மன் *and my family*

Kaliappan Sudalyandi, Thilaga Kaliappan, Radhika, Kalisha, Sunil, Kiranmai and Kalisvarupan

ACKNOWLEDGEMENTS

It has been a long journey and I have been fortunate to have the support and encouragement of many along the way. I would like to take this opportunity to thank some of them here.

First and foremost, I am sincerely grateful to my advisor, Dr. Karl J Rockne for his invaluable support. This thesis would not have been possible without his guidance. The challenges he presented to me allowed be to attain invaluable skills and has given me the confidence to analyze any research problem. The four years of tough field-work performed under his tutelage will always be fondly remembered and etched forever in my memory.

I thank my committee members Professors Amid Khodadoust, Benjamin O'Connor, Craig Foster and Dr. Asha Rani for their suggestions and help. I am especially thankful to Prof. Khodadoust for his guidance during the early years of my PhD program, Dr. Asha for all the guidance she provided for the microbiology work and Prof. O'Connor and Prof. Foster for their guidance on heat transport modeling.

I am thankful to Gary Johnson for his valuable help with field work and laboratory analysis. Ammar Elmajdoub and Peter Doskar for their assistance with laboratory work. I would also like to thank my laboratory friends Solidea Bonina, Soheil Hosseini, Azivy Aziz, Kelly Granberg, Gregory Bourgon, Priscilla Viana, Hamed Babaei, Itzel Godinez and Dorin Bogdan. I am grateful to my friends Saikrishnan Ramamurthy, Arunkumar Vijayakumar, Naveen Sudarshan, Agnel Antony, Dhanasekar Murugan and Simon Johnson for their support.

I would also like to thank all the teachers in my life, especially teachers from Anna Gem Science Park School and Professors from College of Engineering Guindy – Anna University, IIT – Chicago and UIC, who have imparted their knowledge in me.

Finally, I am eternally thankful to my parents Dr. Kaliappan Sudalyandi and Thilaga Kaliappan for their unfailing love and belief in me, my wife Radhika and daughter Kalisha for their love and patience during this long journey and my brother Sunil Manikandan for his guidance and support.

TABLE OF CONTENTS

CHAPTER I INTRODUCTION 1

CHAPTER II LITERATURE REVIEW 7

2.1 Sediment Contamination in United States of America 7

2.2 Factors influencing sediment contamination 8

2.3 Sediment Contaminants 10

2.4 Impacts of Sediment Contamination 12

2.5 Strategies for Contaminated Site Remediation 13

2.5.1 Site Assessment 13

2.5.2 No Action Alternative or Monitored Natural Recovery 14

2.5.3 Dredging 15

2.5.4 Capping 16

2.5.5 Bioremediation 19

2.6 Gas Production and Microbial Ecology 22

2.7 Factors affecting ebullition rates and field gas measurement 23

2.7.1 Methanogenesis 25

2.7.2 Methanogenic Archaea 26

2.7.3 Hydrogenotrophic Methanogens 27

2.7.4 Acetotrophic Methanogens 28

2.7.5 Methane production in aquatic environment 29

2.8 Factors Affecting Methanogenesis 32

2.8.1 Temperature: 33

2.8.2 Presence of alternate electron acceptors 35

2.8.3 Sulfate reduction 35

2.8.4 Nitrification and Denitrification: 38

2.8.5 Fe and Mn reduction 40

2.8.6 Methane Oxidation by Methanotrophs 42

2.9 Ground Water Surface Water Exchange 44

2.9.1 Heat as a surrogate measurement to estimate GW-SW exchange 45

2.9.2 General Characteristics of a Streambed temperature profile 46

2.9.3 Theoretical Background: 47
2.9.4 Darcy's Law 48
2.9.5 Heat Transport in porous media: 49
2.10 Analytical Solutions to Heat Transport Equation to estimate GW-SW exchange 55
2.10.1 Analytical solution using Harmonic Temperature Fluctuation 55
2.10.2 Analytical Solution using Exponential Type Curves: 56
2.10.3 Analytical solution for Temperature Profiles in a stream 57
2.10.4 Silliman's Analytical Solution for time series dataset. 58
CHAPTER III Effect of Sediment capping on gas ebullition rates and temperature dynamics in a polluted urban river 61
3.1 Abstract 61
3.2 Introduction 62
3.3 Materials and Methods 64
3.3.1 Site Description 64
3.3.2 Gas Flux Measurement 65
3.3.3 Sediment Sampling and Analysis 67
3.3.4 Sediment Incubation Study: 67
3.3.5 Sediment Temperature and Water Depth Measurement 68
3.4 Results and Discussion 69
3.4.1 Effect of Temperature and Water Depth 69
3.4.2 Pre- and Post-Cap Sediment Characteristics: 71
3.4.3 Comparison of Pre and Post-Capping Gas Fluxes: 72
3.4.4 Underlying contaminated sediment is a significant source of gas production 77
3.4.5 Modeling post-cap gas production rates 81
3.5 Conclusions 82
3.6 Supporting Information 84
CHAPTER IV Effectiveness of the active cap in controlling ebullition-facilitated contaminant release 96
4.1 Abstract 96
4.2 Introduction 97
4.3 Materials and Methods 99

4.3.1 Ebullition Facilitated Contaminant Flux Measurement 100
4.3.2 Sediment Sampling and Analysis: 102
4.3.3 Sediment Temperature and Water Depth 102
4.4 Results and Discussion 103
4.4.1 Pre and Post-Capping Metal Fluxes: 103
4.4.1 Pre and Post-Capping PAH flux: 109
4.4.3 Comparison of Pre-cap and Post-capping PAH transport mechanism 113
4.5 Supporting Information 119
CHAPTER V Archaeal Community Structure in Pre and Post Cap West Branch Grand Calumet River Sediments 139
5.1 Introduction 139
5.2 Objectives 141
5.3 Materials and Methods 143
5.3.1 DNA extraction 144
5.3.2 16S rRNA sequencing 146
5.3.3 MGRAST Pipeline 147
5.4 Results and Discussion 149
5.4.1 Sequence Statistics 149
5.4.2 Species Richness and Diversity in Pre-Capping Sediments 151
5.4.3 Species Richness and Diversity in post-cap sections 156
5.4.4 Indigenous Archaeal Community Structure in Pre-Capping Sediment 159
5.4.5 Trends in distribution of Archaea in pre-capping surficial sediment 163
5.4.6 Relationship between field-measured gas production rates, sediment physical characteristics and distribution of archaeal community structure 167
5.4.7 Functional significance of Methanoarchaea in Pre-cap GCR Sediments 183
5.4.8 Archaeal Community Structure in Post-capping Sediment 187
5.4.9 Trends in post-capping distribution of Archaeal community structure, sediment physical characteristics and field gas ebullition rates 198
5.5 Conclusion 203
CHAPTER VI Groundwater Surface Water Exchange Modeling 223
6.1 Introduction 223

6.2 Materials and Methods 227
6.3 Analytical Methods for Flux Measurement from Temperature Time Series 229
6.3.1 Combining Amplitude Ratio (Ar) and Phase(ΔØ) shift to calculate thermal diffusivity and thermal front velocity 235
6.4 Processing Temperature Data 236
6.5 Results and Discussion 240
6.5.1 Streambed temperature fluctuations 240
6.5.2 Dynamic Harmonic Regression Analysis 247
6.5.3 McCallum Method Darcy Flux Estimation 260
6.5.4 Limitations and Uncertainty in flux estimates 263
6.5.5 Forward Modelling of Streambed Temperature Data for depths below -25cm 268
6.5.6 Implications for capped sites 273
6.6 Conclusion 274
CHAPTER VII Conclusions and Implications 276
REFERENCES 281
APPENDIX 300
VITA 331

LIST OF TABLES

Table 2.1 Classification of methanogenic *Archaea* 28

Table 2.2 Common methanogenic reactions and their representative genera (Chaban, Ng, and Jarrell 2006, Demirel and Scherer 2008) 30

Table 2.3 Genera of SRB commonly found in the environment..... 38

Table 2.4 Genera of denitrifiers found in the environment. 40

Table 2.5 Different genera of DNRA found in the environment (Zehnder 1988) 40

Table 2.6 Different genera of Fe(III) and Mn(IV) reducers in the environment 42

Table 2.7 Thermal Conductivity of different materials (Anderson 2005, Domenico and Schwartz 1998) 54

Table 3.1 Descriptive statistics of streambed temperature data for 0cm depth. Negative temperature differences represent temperature increase in comparison to previous year and positive values represent temperature decrease. 85

Table 3.2 Descriptive statistics of streambed temperature data for -25cm depth. Negative temperature differences represent temperature increase in comparison to previous year and positive values represent temperature decrease. 86

Table 3.3 Sediment physical parameters for pre-cap surface grab samples and post-cap cores from sites GCR2, GCR6, GCR11 and GCR13. Average values are presented for section depths corresponding to New Deposit (ND), Gravel Armoring (GAL), Organoclay (OrgC) and Contaminated Sediment (CSed) layers. 87

Table 3.4 Descriptive Statistics of Pre-capping sediment grab samples..... 90

Table 3.5 Descriptive statistics of post-cap water depth data derived from weekly averages. 91

Table 3.6 Average gas flux at all sites with percentage decrease in post-capping fluxes compared to pre-capping levels. Negative values represent the corresponding percent increase in gas fluxes. Bold values in parentheses represent an increase in ebullition post-capping. 93

Table 3.7 Mean annual gas flux and independent variables used for regression model development. GCR11-1, 11-2, 2-1 and 2-2 represent duplicates at each site..... 94

Table 3.8 Biogenic gas production reaction rate constant k (d^{-1}) at the four incubation temperatures and Arrhenius Activation Energy E_a (KJ/mol) for incubations of ND, GAL, OrgC and CSed at different temperatures. 95

Table 4.1 Ebullition facilitated metal fluxes during the pre-capping sampling campaign in 2010. Non-detects are reported as zero. Gas flux data from GCR 13 was not included in mean calculation as one week of sampling was obtained due to low water levels. ND= No data available. 119

Table 4.2 Ebullition facilitated metal fluxes during the post-capping sampling campaign in 2012. 120

Table 4.3 Ebullition facilitated metal fluxes during the post-capping sampling campaign in 2013. Data from GCR 6 was not included in mean and SE calculation as it was an outlier. 121

Table 4.4 Ebullition facilitated metal fluxes during the post-capping sampling campaign in 2014. 122

Table 4.5 Metal concentrations in pre-capping surficial sediment obtained using a Ponar dredge sampler during the 2010 sampling campaign. 123

Table 4.6 Ebullition facilitated PAH fluxes during the pre-capping sampling campaign in 2010. Non-detects are reported as zero. ND= No data available. 125

Table 4.7 Ebullition facilitated PAH fluxes during the post-capping sampling campaign in 2012. 126

Table 4.8 Ebullition facilitated PAH fluxes during the post-capping sampling campaign in 2013. 127

Table 4.9 Ebullition facilitated PAH fluxes during the post-capping sampling campaign in 2014. 128

Table 4.10 PAH concentrations in pre-capping surficial sediment obtained using a Ponar dredge sampler during the 2010 sampling campaign. 129

Table 4.11 PAH flux reduction for all three post-cap monitoring years. Cases with negative values represent increase in post-capping PAH flux. The negative reductions observed for anthracene and phenanthrene is attributed to negligible fluxes observed in the pre-capping data. 130

Table 4.12 Metal flux reduction for all three post-cap monitoring years. 130

Table 4.13 Chemical properties of PAHs including molecular weight, organic carbon water partitioning coefficient (K_{oc}) and Henry's constant (K_H) of PAHs used in equilibrium partition model (USEPA 1996). 131

Table 4.14 Pore-water concentration of PAHs predicted by the equilibrium partition model (EPT), C_w (mg/L). 132

Table 4.15 Partial pressure of PAHs in the gaseous phase as predicted by the equilibrium partitioning model (EPT), C_a (atm)..... 133

Table 5.1 Properties and DNA content of sediment core sections chosen for analysis. 143

Table 5.2 Statistics for pre- and post-quality control of post-capping DNA sequences submitted to MGRAST..... 148

Table 5.3 Sequence statistics for pre-capping DNA sequencing data from sediment surface grabs..... 149

Table 5.4 Pre-capping domain level distribution of sequences expressed as percentage and number of sequences..... 155

Table 5.5 Post-capping domain level distribution of sequences expressed as percentage and number of sequences..... 155

Table 5.6 Chemical characteristics of pre-capping surface sediment and α-diversity of archaeal sequences. 157

Table 5.7 Comparison of **s**ediment chemical characteristics and Archaeal α-diversity for the ND, GAL, OrgC and CSed layers for sediment cores sampled in 2012 at sites GCR 2, 6, 11 and 13..... 158

Table 5.8 Dominant archaeal genera and sequence count in pre-capping sediment. Sequence count is shown in parenthesis. 169

Table 5.9 Archaeal abundance in new deposit (ND) layer sediments at sites GCR2, 6, 11 and 13. 193

Table 5.10 Archaeal abundance in new deposit (GAL) layer sediments at sites GCR2, 6, 11 and 13..... 194

Table 5.11 Archaeal abundance in new deposit (OrgC) layer sediments at sites GCR2, 6, 11 and 13..... 195

Table 5.12 Archaeal abundance in new deposit (CSed) layer sediments at sites GCR2, 6, 11 and 13..... 196

Table 6.1 Porosity and dry bulk density measurements obtained from sediment cores at sites GCR2, GCR6, GCR11 and GCR13. Shown are mean ± SEM (σ)..... 239

Table 6.2 Average daily temperature recorded for different depths at the start and end of a distinct surface warming period and observed streambed response represented as temperature increase. 246

Table 6.3 Estimated Darcy velocity at all model sites for depth -50, -75 and -100cm depths. . 272

Table A9.1 Genus level classification and abundance of the15 most abundant *Archaea* in pre-capping surface sediment of site GCR 1. 300

Table A9.2 Genus level classification and abundance of the15 most abundant *Archaea* in pre-capping surface sediment of site GCR 2. 301

Table A9.3 Genus level classification and abundance of the15 most abundant *Archaea* in pre-capping surface sediment of site GCR 3. 302

Table A9.4 Genus level classification and abundance of the15 most abundant *Archaea* in pre-capping surface sediment of site GCR 4. 303

Table A9.5 Genus level classification and abundance of the15 most abundant *Archaea* in pre-capping surface sediment of site GCR 5. 304

Table A9.6 Genus level classification and abundance of the15 most abundant *Archaea* in pre-capping surface sediment of site GCR 6. 305

Table A9.7 Genus level classification and abundance of the15 most abundant *Archaea* in pre-capping surface sediment of site GCR 7. 306

Table A9.8 Genus level classification and abundance of the15 most abundant *Archaea* in pre-capping surface sediment of site GCR 8. 307

Table A9.9 Genus level classification and abundance of the15 most abundant *Archaea* in pre-capping surface sediment of site GCR 9. 308

Table A9.10 Genus level classification and abundance of the15 most abundant *Archaea* in pre-capping surface sediment of site GCR 10. 309

Table A9.11 Genus level classification and abundance of the15 most abundant *Archaea* in pre-capping surface sediment of site GCR 11. 310

Table A9.12 Genus level classification and abundance of the15 most abundant *Archaea* in pre-capping surface sediment of site GCR 12. 311

Table A9.13 Genus level classification and abundance of the15 most abundant *Archaea* in pre-capping surface sediment of site GCR 13. 312

Table A9.14 Genus level classification and abundance of the15 most abundant *Archaea* in post-capping sediment layer GCR 2 –ND. 313

Table A9.15 Genus level classification and abundance of the15 most abundant *Archaea* in post-capping sediment layer GCR 2 –GAL. 314

Table A9.16 Genus level classification and abundance of the15 most abundant *Archaea* in post-capping sediment layer GCR 2 –OrgC. 315

Table A9.17 Genus level classification and abundance of the15 most abundant *Archaea* in post-capping sediment layer GCR 2 –CSed..... 316

Table A9.18 Genus level classification and abundance of the15 most abundant *Archaea* in post-capping sediment layer GCR 6 –ND. 317

Table A9.19 Genus level classification and abundance of the15 most abundant *Archaea* in post-capping sediment layer GCR 6 –GAL. 318

Table A9.20 Genus level classification and abundance of the15 most abundant *Archaea* in post-capping sediment layer GCR 6 –OrgC. 319

Table A9.21 Genus level classification and abundance of the15 most abundant *Archaea* in post-capping sediment layer GCR 6 –CSed..... 320

Table A9.22 Genus level classification and abundance of the15 most abundant *Archaea* in post-capping sediment layer GCR 11 –ND. 321

Table A9.23 Genus level classification and abundance of the15 most abundant *Archaea* in post-capping sediment layer GCR 11 –GAL. 322

Table A9.24 Genus level classification and abundance of the15 most abundant *Archaea* in post-capping sediment layer GCR 11 –OrgC. 323

Table A9.25 Genus level classification and abundance of the15 most abundant *Archaea* in post-capping sediment layer GCR 11 –CSed..... 324

Table A9.26 Genus level classification and abundance of the15 most abundant *Archaea* in post-capping sediment layer GCR 13 –ND. 325

Table A9.27 Genus level classification and abundance of the15 most abundant *Archaea* in post-capping sediment layer GCR 13 –GAL. 326

Table A9.28 Genus level classification and abundance of the15 most abundant *Archaea* in post-capping sediment layer GCR 13 –OrgC. 327

Table A9.29 Genus level classification and abundance of the15 most abundant *Archaea* in post-capping sediment layer GCR 13 –CSed..... 328

Table A9.30 Pearson's coefficient between dominant pre-cap methanogenic archaeal genera, sediment chemical parameters and field gas ebullition rates..... 329

Table A9.31 Pearson's coefficient between dominant post-cap methanogenic archaeal genera, sediment chemical parameters and field gas ebullition rates. 330

LIST OF FIGURES

Figure 1.1 The location of 96 watersheds with Areas of Probable (APCs) Concern identified in the USEPA sediment survey (USEPA 2004)..... 4

Figure 2.1 Pictorial representation of sources and sinks for sediment contamination (USEPA 1987) 9

Figure 3.1 Gas collection system comprised of two concrete-block footings supporting the hollow PVC gas collection frame, fitted with a funnel and ball valve for gas measurement. 66

Figure 3.2 Comparison of measured pre-cap gas ebullition rates to three literature model predictions based on measured field condition. 73

Figure 3.3 Average gas ebullition fluxes during pre-cap and post-cap sampling campaigns..... 74

Figure 3.4 Comparison of pre- and post-cap average sampling campaign gas fluxes. 77

Figure 3.5 Total gas production for laboratory incubations of ND, GAL, OrgC and CSed over 369d as a function of sediment site and incubation temperature. 80

Figure 3.6 Comparison of predicted to measured gas fluxes for sites GCR2, 6, 11 and 13. 82

Figure 3.7 A) Pre-capping and B) Post-capping aerial view of the study area. 84

Figure 3.8 Poast-capping sediment temperature (0cm depth) and gas flux measured during 2012 sampling campaign. All sites except GCR6 exhibited a decreasing trend in gas prduction rates with decreasing surface temeprature. 89

Figure 3.9 Increase in water depth over the three years of monitoring. Trend-line represents the overall pattern in water depth fluctuation during each monitoring year. 90

Figure 3.10 Weekly field gas fluxes (mmol/m^2/d) measured (A) pre-capping in 2010 and post capping in years B) 2012, C) 2013, and D) 2014. Note: Site GCR 7 was not monitored in post-capping years 92

Figure 3.11 Cumulative gas production as a function of incubation temperature. Dotted lines represents the CSed layer and dash-dot line represents the ND layer 95

Figure 4.1 Mean metal fluxes observed at all sites pre and post-capping. Pre-capping fluxes are plotted in the secondary y-axis with all post-capping fluxes are plotted at 1:10 scale the primary y-axis to show detail. 104

Figure 4.2 Mean pre-capping PAH flux measured in 2010 and post-capping PAH fluxes measured in 2012, 2013 and 2014. ACE = acenaphthene, ACY = acenaphthylene, ANT = anthracene, BNA = benzo[a]anthracene, BaP = benzo[a]pyrene, BbFL = benzo[b]fluoranthene, BPY = benzo[g,h,i]perylene, BkFL = benzo[k]fluoranthene, CHR = chrysene, DBAN = dibenzo[a,h]anthracene, FLAN = fluoranthene, FLEN = fluorene, PHE = phenanthrene, PYR = pyrene 110

Figure 4.3 Comparison of fractional contribution of individual PAHs to total PAHs in the sediment, pre-cap, 2013 and 2014 glass wool (GW) measured fluxes along with the predicted fractional contribution in the air and water phase using an equilibrium-partitioning model. Data for 2012 GW is not presented, as Chrysene was the only detectable PAH flux measured only at GCR6. 116

Figure 4.4 Comparison plot of fraction of individual PAHs to total PAHs in glass wool and contaminated sediment for A) pre-capping B) 2013 and C) 2014 134

Figure 4.5 Comparison plot of fraction of individual metals to total metals in glass wool and contaminated sediment for A) pre-capping B) 2012 C) 2013 and D)2014 135

Figure 4.6 Predicted ebullition facilitated PAH fluxes for A)Pyrene (PYR), B)Chrysene (CHR) C)Phenathrene (PHE) plotted as a function of gas flux and compared with field measured fluxes. 136

Figure 4.7 Comparison plot of Viana et al predicted metal and PAH flux and field measured ebullition facilitated flux. 137

Figure 5.1 Sediment samples obtained from four cores in the WBGCR The dark grey material (1-5 cm) represents new sediment. Brown material (5-25cm) represents the armoring layer, greyish material (25-35cm) represents the organoclay cap and the black material represents the underlying contaminated sediment. 142

Figure 5.2 Texture of the sediment core sections from the A) new sediment deposit, B) armor layer (gravel-sand mixture with high percentage of gravel), C) organoclay layer (sandy texture), and the D) underlying contaminated sediment (clayey texture). 144

Figure 5.3 Rarefaction curves depicting species richness in pre-capping surficial sediments in A) Reach-1 and B) Reach-2. 152

Figure 5.4 Rarefaction curves for archaeal sequences in new deposit (ND), gravel armor layer (GAL), organo-clay layer (OrgC) and contaminated sediment (CSed) layers in sediment cores from Reach-1 sites A) GCR2 and B) GCR6. 153

Figure 5.5 Rarefaction curves for archaeal sequences in new deposit (ND), gravel armor layer (GAL), organo-clay layer (OrgC) and contaminated sediment (CSed) layers in sediment cores from Reach-2 sites A) GCR11 and B) GCR13. 154

Figure 5.6 Composition of the most abundant archaeal genera for all pre-capping sites as revealed by the M5RNA database. Detailed classification at the Family and Order level can be found in Tables A4.1 – 13. 164

Figure 5.7 Trend in *Methanomethylovorans*, *Methanocella* and *Methanospirillum* abundance relative to proximity to the HSD outfall. 165

Figure 5.8 Heat map analysis of pre-capping surficial sediment. The dendrogram in x-axis depicts similarity in the genomes with similar samples clustered in the dendrogram. Transition in colors from red to green represents increasing abundance of sequences. 166

Figure 5.9 Distribution of archaeal community structure in pre-capping sediment at site GCR1. 170

Figure 5.10 Distribution of archaeal community structure in pre-capping sediment at site GCR2. 171

Figure 5.11 Distribution of archaeal community structure in pre-capping sediment at site GCR3. 172

Figure 5.12 Distribution of archaeal community structure in pre-capping sediment at site GCR4. 173

Figure 5.13 Distribution of archaeal community structure in pre-capping sediment at site GCR5. 174

Figure 5.14 Distribution of archaeal community structure in pre-capping sediment at site GCR6. 175

Figure 5.15 Distribution of archaeal community structure in pre-capping sediment at site GCR7. 176

Figure 5.16 Distribution of archaeal community structure in pre-capping sediment at site GCR8. 177

Figure 5.17 Distribution of archaeal community structure in pre-capping sediment at site GCR9. 178

Figure 5.18 Distribution of archaeal community structure in pre-capping sediment at site GCR10. 179

Figure 5.19 Distribution of archaeal community structure in pre-capping sediment at site GCR11. 180

Figure 5.20 Distribution of archaeal community structure in pre-capping sediment at site GCR12. 181

Figure 5.21 Distribution of archaeal community structure in pre-capping sediment at site GCR13. 182

Figure 5.22 Water column ammonia levels during pre-cap monitoring at sites GCR 13 to GCR1 (Site GCR13 is marked as origin on x-axis). 186

Figure 5.23 Dominant archaeal groups in the ND, GAL, OrgC and CSed layers. *Methanosaeta* dominates at most sites. 197

Figure 5.24 Distribution of Archaeal community structure in post-cap GCR2 –ND layer. 207

Figure 5.25 Distribution of Archaeal community structure in post-cap GCR2 -GAL layer. 208

Figure 5.26 Distribution of Archaeal community structure in post-cap GCR2 -OrgC layer..... 209

Figure 5.27 Distribution of Archaeal community structure in post-cap GCR2 -CSed layer..... 210

Figure 5.28 Distribution of Archaeal community structure in post-cap GCR6 -ND layer..... 211

Figure 5.29 Distribution of Archaeal community structure in post-cap GCR6 -GAL layer. 212

Figure 5.30 Distribution of Archaeal community structure in post-cap GCR6 -OrgC layer..... 213

Figure 5.31 Distribution of Archaeal community structure in post-cap GCR6 -CSed layer..... 214

Figure 5.32 Distribution of Archaeal community structure in post-cap GCR11 -ND layer..... 215

Figure 5.33 Distribution of Archaeal community structure in post-cap GCR11 -GAL layer. .. 216

Figure 5.34 Distribution of Archaeal community structure in post-cap GCR11 -OrgC layer... 217

Figure 5.35 Distribution of Archaeal community structure in post-cap GCR11 -CSed layer... 218

Figure 5.36 Distribution of Archaeal community structure in post-cap GCR13 -ND layer..... 219

Figure 5.37 Distribution of Archaeal community structure in post-cap GCR13 -GAL layer. .. 220

Figure 5.38 Distribution of Archaeal community structure in post-cap GCR13 -OrgC layer... 221

Figure 5.39 Distribution of Archaeal community structure in post-cap GCR13 –Csed layer... 222

Figure 6.1 Shows the location of temperature arrays during three years of post-cap monitoring in a 2 Km stretch of West Branch Grand Calumet River (WBGCR) from Columbia Ave to Indianapolis Blvd. 228

Figure 6.2 Approximate location of temperature sensors in relation to the sand-gravel armor and organoclay layers of the active cap and contaminated sediment zone shown in black. 229

Figure 6.3 Sediment temperature from June 1 to Nov 7 at sites GCR 1-3. 242

Figure 6.4 Sediment temperature from June 1 to Nov 7 at GCR4-6. Note: 0 cm probe malfunctioned at GCR5 resulting in no recorded temperature. 243

Figure 6.5 Sediment from June 1 to Nov 7 at GCR8-10. September to November for sites GCR8 and 10 and June to November for GCR9. Note: 0cm probe at GCR9 malfunctioned, resulting in no recorded temperature. 244

Figure 6.6 Sediment temperature from June 1 to Nov 7 at sites GCR11-13 245

Figure 6.7 ARSPEC output for sites GCR1 and GCR2 at model depths 0 and -25 cm. Strong peaks are observed at the fundamental period for both sites. 251

Figure 6.8 ARSPEC output for sites GCR3 and GCR4 at model depths 0 and -25cm. Strong peaks are observed at the fundamental period for both sites. 252

Figure 6.9 ARSPEC output for sites GCR6 and GCR8 at model depths 0 and -25cm. Strong peaks are observed at the fundamental period for GCR6. A strong peak is not observed at the -25cm depth for GCR8 indicating weak diurnal temperature fluctuation. 253

Figure 6.10 ARSPEC output for sites GCR10 and GCR11 at model depths 0 and -25cm. Strong peaks are observed at the fundamental period at both depths for GCR11 and 0cm depth at GCR10. No identifiable peak is seen for -25cm depth for GCR10. 254

Figure 6.11 ARSPEC output for sites GCR12 and GCR13 at model depths 0 and -25cm. Strong peaks are observed at 0cm depth for both sites with and no identifiable peak at -25cm depth for GCR13..... 255

Figure 6.12 DHR fit to temperature data and trend are shown in A) and B). Extracted signal at the fundamental period, first and second harmonics are shown in C) and D). 256

Figure 6.13 Calculated Darcy fluxes compared to river stage over the monitoring period for sites A) GCR1, B) GCR2 and C) GCR3. 257

Figure 6.14 Calculated Darcy fluxes compared to river stage over the monitoring period for sites A) GCR4, B) GCR6 and C) GCR11. 258

Figure 6.15 Calculated Darcy fluxes compared to river stage over the monitoring period for sites A) GCR12 and B) GCR13. 259

Figure 6.16 Box and whisker plot of fluxes for all modeled sites. (-) beyond the whiskers represent max and min, (-) inside the box represent the mean, box represents 75th percentile and 25th percentile and horizontal line across the box represents the median. 260

Figure 6.17 Fluxes measured by piezometer at three uncapped locations immediately east of GCR1 in 2014/2015. Data from James Wescott, TetraTech, Chicago. 263

Figure 6.18 Monte Carlo Analysis of flux estimate incorporating uncertainty in porosity and specific heat capacity for sites A) GCR1, B) GCR2, C) GCR3 from Aug-Oct 2013..... 265

Figure 6.19 Monte Carlo Analysis of flow estimates incorporating uncertainty in porosity and specific heat capacity for sites A) GCR4, B) GCR6, C) GCR11 from Aug-Oct 2013..... 266

Figure 6.20 Monte Carlo Analysis of flow estimates incorporating uncertainty in porosity and specific heat capacity for sites A) GCR12, B) GCR13 from Aug-Oct 2013. 267

Figure 6.21 Measured and simulated temperature at depths -50cm, -75cm, -100cm for sites GCR2, 6 and 8..... 270

Figure 6.22 Measured and simulated temperature at depths -50cm, -75cm, -100cm for sites GCR9, 11and 13.Less temperature is variability observed at these sites compared to GCR2 and GCR6..... 271

LIST OF ABBREVIATIONS

AOC.....Area of Concern

BC..... Black carbon

CDF .....Combined Disposal Facility

CSO ..... Combined Sewage Outfall

ECSD.....East Chicago Sanitary District

GAC.....Granular Activated Carbon

GCR.....Grand Calumet River

GW-SW..... Groundwater – Surface water

HMW..... High Molecular Weight

HOC .....Hydrophobic Organic Contaminant

HSD ..... Hammond Sanitary District

IHC.....Indiana Harbor Canal

LMW .....Low Molecular Weight

MGD..... Million Gallons per Day

MLSR..... Multiple Least Square Regression

NCBI .....National Center for Biotechnology Information

OC.....Organic Carbon

OM.....Organic Matter

ORP ..... Oxidation reduction potential

PAH ..... Polycyclic Aromatic Hydrocarbon

PBB..... Polybrominated Biphenyl

PBDE..... Poly-Brominated Diphenyl Ether

PCB..... Polychlorinated biphenyl

PCDD .....Polychlorinated Dybenzodioxin

PCDF.....Polychlorinated Dibenzofurans

SWI..... Surface Water Interface

USEPA ..... United States Environmental Protection Agency

USGS ..... United States Geological Survey

V ..... Volume

WBGCR ..... West Branch Grand Calumet River

WWTP ..... Wastewater Treatment Plant

CHAPTER I INTRODUCTION

Rapid industrialization and economic growth in the United States from the beginning of the 19th century resulted in large-scale pollution of the lakes, rivers and coastal areas. Although the United States economy benefited greatly from these historical events, the lack of environmental regulations for waste disposal and understanding of long-term impacts heavily impaired the health of the environment, leaving a large reservoir of contamination in the environment. Pollution enters the aquatic ecosystem through a variety of pathways including surface runoff, spills, point source effluent and atmospheric deposition. Once in the water column, the contaminants undergo transport and transformation processes depending on their chemical properties. Hydrophobic organic contaminants (HOCs) are of primary concern in aquatic ecosystems as they can be immobilized by sequestration in the sediment or undergo bio-geochemical transformation to more toxic compounds.

Implementation of the Clean Water Act of 1972 and the National Pollution Discharge Elimination System (NPDES) resulted in the regulation of release of contaminants into waterways and resulted in rapid improvement in national water quality. However, HOCs such as PCBs, PAHs, PBDEs and PCDD/PCDF, heavy metals and pesticides continue to persistent in the environment due to their resistance to degradation and affinity to sediment organic matter. The legacy pollution in the sediments now can act as a contaminant source, releasing toxic chemicals to the water column and atmosphere. These persistent chemicals can be taken up by aquatic organisms and bio-accumulate in the food chain, posing a significant risk to human and ecological health.

Contaminated sediment is defined by the United States Environmental Protection Agency (USEPA) as, "aquatic sediment which contains chemical substances in excess of appropriate geochemical, toxicological, or sediment quality criteria or measures; or is otherwise considered to pose a threat to human health or the environment" (Section 503 WRDA 1992). The United States has more than 15.94 million hectares of lakes, 2.9 million km of rivers, 82880 square kilometers of estuaries and 45000 km of coastline (USEPA 1987) which require effective sediment management strategy to protect the navigational, drinking water, agricultural and recreational use of the water body. The USEPA has estimated that approximately ten percent of US surface water bodies are contaminated (USEPA 1998) representing around 2 billion cubic meters of contaminated sediments, (assuming an upper 20cm bioactive zone). A National Level Sediment Quality Survey conducted by the USEPA in 2004 (USEPA 2004) identified 96 different watersheds as Areas of Probable Concern (APCs) characterized by severe sediment contamination, posing a significant risk to the environment. Considering the extent of sediment contamination, it is important to effectively manage sediment remediation efforts and restore sites to acceptable conditions to protect human and ecological health. It is estimated that the cost of sediment remediation and cleanup of all contaminated sites in the US alone is five billion dollars ($\$50/m^3$) making sediment contamination a challenging environmental problem (Kuiper et al. 2004).

Sediment remediation is a multi-step process involving extensive site investigation exploring the sources of pollution, site-specific geo-hydrological processes and the extent of the contamination. This is followed by identification of remediation goals and objectives along with plausible remediation alternatives. Sediment remediation alternatives are broadly classified into monitored natural recovery, dredging, capping and bioremediation with each one having its own

advantages and disadvantages. The selection of an appropriate alternative is based on site-specific conditions, remediation goals and economic considerations. Dredging is a conventional technique and provides long-term risk reduction as the contaminated sediment is permanently removed and disposed in landfills or combined disposal facility (CDF). However, the destructive action of dredging can damage benthic communities and lead to temporary increases in contaminant levels in the water column caused by sediment re-suspension. Also, dredging can be cost prohibitive at sites requiring extensive sediment removal and handling. Monitored natural recovery (MNR) and bioremediation strategies provide a permanent and low cost solution. MNR typically requires a long-term monitoring plan to collect substantial evidence of natural processes that reduce risk and are employed at sites where the human health risk is not an immediate concern. Bioremediation involves introduction of microbes or nutrients that promote the growth of specific groups capable of contaminant degradation. Although laboratory studies have provided promising results, the difficulty in implementing biological treatment methods and relatively limited real world performance validation make their application less favorable. In contrast, capping serves as an effective remediation alternative providing physical separation for benthic organisms to thrive, retardation against advective/diffusive contaminant migration and eliminating the need for extensive dredging. More recently, active and thin layer capping is beginning to be widely adopted adding contaminant sequestration and transformation capabilities in the cap material. Active caps are especially beneficial at sites with ground water discharge where enhanced advective transport can lead to shorter contaminant breakthrough times in sand caps.

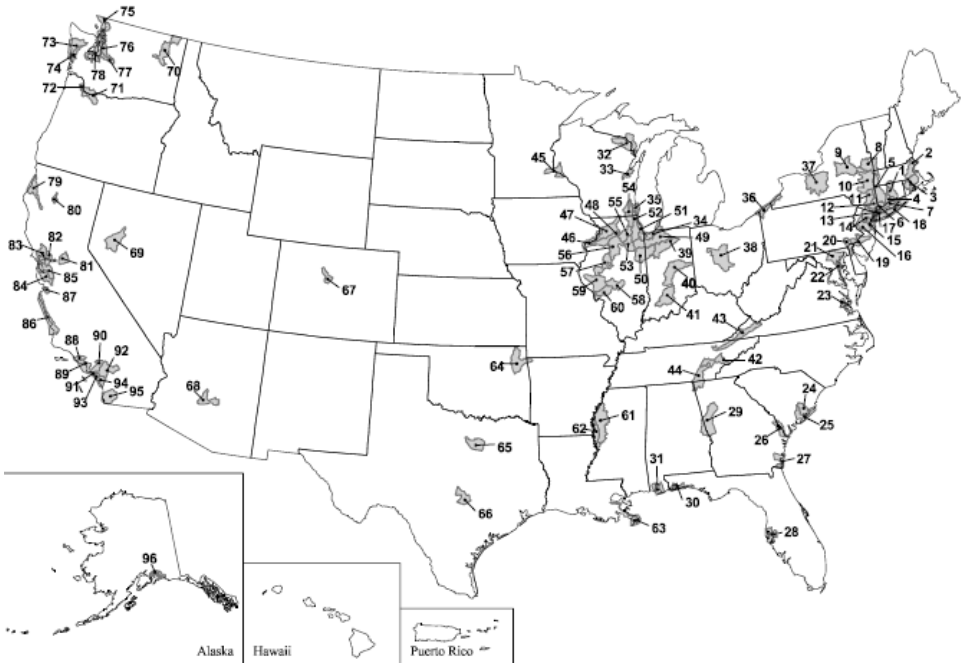

Figure 0.1 The location of 96 watersheds with Areas of Probable (APCs) Concern identified in the USEPA sediment survey (USEPA 2004).

Although capping has been widely implemented at many sites (Reible et al. 2006, Quadrini et al. 2003, Olsta and Hornaday 2007) its impact on gas production, ebullition-facilitated transport, contaminant transformation, biodegradation, sediment temperature regulation, benthic/microbial community structure and ground water-surface water interaction needs to be clearly understood. Several studies have investigated some of the aforementioned aspects such as microbial re-colonization of cap material (Himmelheber, Thomas, et al. 2008), changes in biogeochemical processes (Himmelheber, Taillefert, et al. 2008), chemical transformation and degradation (Johnson, Reible, and Katz 2010, Liu et al. 2001, Himmelheber, Pennell, and Hughes 2007). In comparison there has been a limited number of studies on the impact of capping on sedimentary gas production (Zhu et al. 2015), and no studies on post-capping ebullition facilitated contaminant fluxes. Gas production from methanogenic activity leads to accumulation of biogenic gases in the sediment with production rates primarily dependent on sediment

physiochemical characteristics, temperature and water depth. Ebullition of sediment gases can facilitate contaminant transport and can be a significant transport mechanism in highly ebullition active sediments contaminated with high levels of HOCs such as NAPL, PAHs and PCBs (Viana, Yin, and Rockne 2012, Huls and Costello 2005, McLinn and Stolzenburg 2009, Yuan et al. 2007). Post-capping gas ebullition from underneath the cap can rupture impermeable caps and form preferential pathways for enhanced advective transport (Reible et al. 2006, McDonough and Dzombak 2005) in permeable caps, reducing the time for natural recovery. Although capping reduces contaminated sediment re-suspension, partitioning of HOCs from the pore-water to gas bubbles and the subsequent release to the water column could still be a significant contaminant transport pathway. Capping can also change the native hydraulic properties of the streambed due to consolidation and introduction of new material, which can lead to changes in the nature of post-capping groundwater-surface water (GW-SW) interaction and potentially compromise the effectiveness of the cap. With the perspective outlined above, the research described in this thesis serves to address the impact of capping on gas ebullition rates, GW-SW interactions, changes in the microbial community structure and the effectiveness of the cap in controlling ebullition facilitated contaminant fluxes. With these broad objectives, the specific goals for this study is as follows:

1. Perform a pre-capping study to
    a. Assess sediment physical characteristics and identify the severity of contamination and primary contaminants in West Branch Grand Calumet River (WBGCR)
    b. Measure field gas ebullition rates and magnitude of ebullition-facilitated chemical fluxes

2. Perform a long-term post-capping study to
    a. Measure post-capping ebullition rates and assess the impact of the cap on long-term gas ebullition rates after stoppage of new organic matter input to the previously ebullition active zone
    b. Measure ebullition facilitated contaminant fluxes to assess the effectiveness of the active-cap in controlling contaminant migration
3. Identify the primary post-capping gas production zone
    a. Perform a laboratory incubation study to assess the gas production potential and biodegradability of the cap/sediment material. Measure physical characteristics of the cap/sediment material to assess influence of sediment physical parameters on the observed laboratory and field gas production rates
    b. Assess the microbial community structure of methanogenic Archaea at different depths of the sediment/cap material to support the identification of the primary gas production zone.
4. Perform DNA sequencing and microbial community structure analysis in the pre and post-capping surficial sediment zone to study changes in Archaeal populations
5. Apply heat tracer techniques to measure the magnitude and direction of post-capping GW-SW interactions and assess the feasibility of using heat tracer techniques in long-term monitoring of near surface ground water fluxes in sediment remediation projects.

CHAPTER II LITERATURE REVIEW

This literature review is also organized into three sections focusing on the three aspects of my research. The first section talks about sediment contamination and capping followed by microbiology of biogenic gas production and application of heat tracer techniques in measuring groundwater surface water interaction.

2.1 Sediment Contamination in United States of America

Sediment contamination is a major concern in lakes, reservoirs, rivers, harbors and coastal areas affected by long-term environmental contamination originating from point and non-point sources such as industrial and municipal discharges, surface runoff, mining activity etc. The United States economy greatly benefited from the rapid industrialization at the beginning of the 19th century but the lack of waste disposal regulations and knowledge of long term impacts greatly impaired the health of the environment. The sediment zone being the final resting place for pollutants discharged into the nation's waterways, the continued pollution led to accumulation of toxic chemicals in the sediment. The implementation of Clean Water Act of 1972 and NPDES (National Pollution Discharge Elimination System) led to rapid improvement in national water quality, however the repository of historical pollution in the sediment now acts as a source of continuous contaminant release into the environment affecting human and ecological health. The enactment of Comprehensive Environmental Response Compensation and Liability Act (CERCLA) in 1980 mandated the cleanup of hazardous waste sites including contaminated sediments that can endanger human or environmental health. In a National Level Sediment Quality Survey conducted by the EPA in 2004 (USEPA 2004), 96 different USGS watersheds were identified to be considered as Areas of Probable Concern (APC) with an estimated 2 billion cubic meters of contaminated sediment that require treatment. The cost of sediment remediation

and cleanup in the US alone is five billion dollars ($50/m^3) (Kuiper et al. 2004) making development of economical and effective sediment remediation technologies a high priority. Hydrophobic organic contaminants such as PAHs, PCBs, PBDEs and PCDD/PCDF are of primary concern in aquatic ecosystems as they can be immobilized by sequestration into the sediment or could be further transformed by bio-geochemical processes. The sediment-phase organic contaminants can be a continuous source of pollution to the water column and are known to bio accumulate in the food chain affecting ecological and human health.

2.2 Factors influencing sediment contamination

Sediment contamination is influenced by factors such as contaminant source, sedimentation rates, chemical properties of the contaminant and physical/chemical characteristics of the sediment such as organic content and area to volume ratio, groundwater exchange and human activity. Pollution enters the aquatic ecosystem through a variety of pathways including point discharges from wastewater treatment plants, industries, combined sewer outflows, spills, mines, nonpoint sources like urban and agricultural surface runoff, and atmospheric deposition. Sediment contamination can also be influenced by hydraulic factors that control sediment movement including water currents and periodic storm events. In some water bodies pollutants discharged in the upper reaches of the watershed can travel hundreds of kilometers before they can settle and accumulate in quiescent waters of harbors, lakes and reservoirs. Physical properties of the sediment such as surface-area to volume (A/V) ratio and organic matter content influence the spatial variability observed in sediment contamination. Finer sediment has a higher surface-area to volume ratio and tends to adsorb more contaminants than coarse-grained sediment. A highly contaminated site within a water body is referred to as a “hot spot” (USEPA). Organic contaminants have high affinity to sediments with high organic content and act as sinks

to organic and inorganic pollutants (Perelo 2010). Human activities such as ship traffic, dredging and recreational use of water bodies are also major factors that impact sediment contamination and remediation efforts. Sediment contamination is commonly observed in rivers, estuaries and harbors serving heavily industrialized areas near major cities, as they receive run off from industrial and urban point sources, contaminated sediment load from rivers and are also subject to commercial uses.

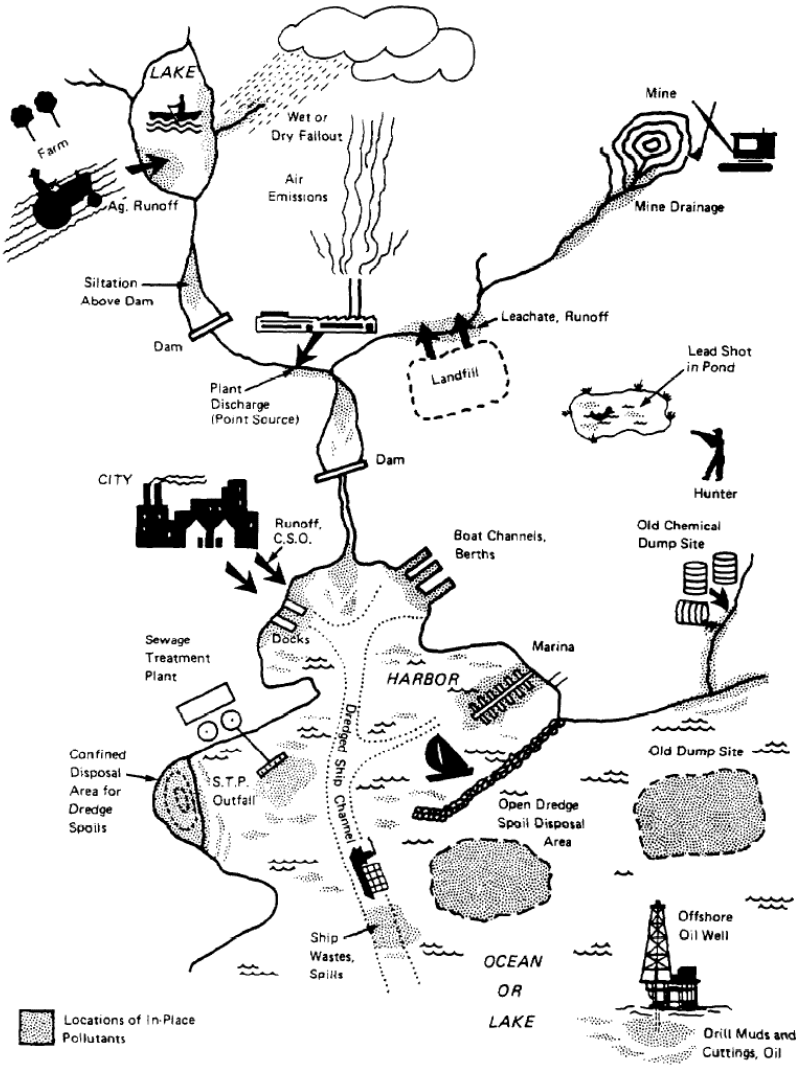

Figure 2.1 Pictorial representation of sources and sinks for sediment contamination (USEPA 1987)

2.3 Sediment Contaminants

Some of the most persistent sediment contaminants in the environment include semi-volatile organic pollutants such as Polycyclic Aromatic Hydrocarbons (PAHs), Polychlorinated biphenyls (PCBs), Polychlorinated dibenzo-p-dioxins and dibenzofurans (PCDD/Fs), DDT and metals like lead, mercury, manganese, cadmium, zinc, arsenic and selenium (Perelo 2010). Organic contaminants, due to their hydrophobic nature, get adsorbed onto organic carbon fraction in sediment particles. Metals on the other hand are not biodegradable but can be subject to biological uptake by microorganisms and transport processes (Martínez-Jerónimo, Cruz-Cisneros, and García-Hernández 2008). Anthropogenic organic contaminants originate from industrial chemicals, petroleum processing and incomplete combustion of hydrocarbons. Natural sources include forest and grass fires, biosynthesis by aquatic fauna, biotransformation of naturally synthesized precursors and diffusion from deep petroleum reserves in the earth's mantle.

PAHs are found in creosote and heavy fraction of crude oil, as well as being formed by incomplete combustion of organic substances such as coal, oil, gas and garbage. Few PAHs are also used in medicine, dye plastic and pesticides (Office 1998). PAHs can also occur naturally in the environment (USEPA 2008) and are highly persistent due to their low water solubility, high affinity to organic matter and low degradation potential in the sediment, especially the higher molecular weight PAHs. PAHs due to their high carcinogenic and mutagenic potential are highly toxic to biota and bio-accumulate in the environment. Sixteen PAHs have been identified by USEPA as high priority pollutants due to their high toxicity and/or mutagenic effects (Monograph 1983). These include Naphthalene, Acenaphthylene, Acenaphthene, Fluorene, Phenanthrene, Anthracene, Fluoranthene, Pyrene, Benz[a]anthracene, Chrysene,

Benzo[b]fluoranthene, Benzo[k]fluoranthene, Benzo[a]pyrene, Dibenz[a,h]anthracene, Benzo[g,h,i]perylene, Indeno[1,2,3-cd]pyrene.

PCBs are among the most toxic pollutants in the environment due to their adverse health effects. Studies on animal subjects have shown PCBs to cause cancer and non-cancer effects on the immune system, nervous system, endocrine system and reproductive system (USEPA). PCB's high chemical stability, non-flammability and electrical insulating properties have led to them being used in chemical and industrial applications since 1929 until their production was banned in 1979. PCBs are persistent in the environment and can be transported over long distances through air currents and deposited in lakes and reservoirs; especially the light molecular weight PCBs. PCDD/Fs (dioxins) are another group of recalcitrant organic compounds found in contaminated sediment and are primarily produced by incineration. Dioxins are resistant to degradation in the environment with high toxicity and carcinogenic potential (Kaiser 2000).

Metals are the most commonly occurring contaminant in sediments followed by pesticide, PCBs and PAHs. From a survey of 184 contaminated sites located in 10 EPA regions across United States heavy metals were detected in 69 percent, PCBs in 34 percent, PAHs in 19 percent and pesticides in 26 percent of the sites (USEPA 1987). Although metals, PAHs, PCBs, pesticides like DDT are the most common sediment contaminants, it is important to point out that the contaminated sites are monitored for these chemicals and other contaminants of specific interest to the site. The levels and extent of contamination of other chlorinated organic compounds, polymers and products of biodegradation of anthropogenic chemicals that are not currently monitored is not clearly understood.

2.4 Impacts of Sediment Contamination

The impact of sediment contamination is diverse affecting the navigational and recreational use of the water body, human, aquatic and ecological health. Channels with high levels of sediment contamination have become uneconomical to maintain with sufficient depth for navigation due to the high cost of navigational dredging associated with contaminated sediment (USEPA 1987). Sediment contamination is also typically associated with high levels of nutrients, pathogens, high oxygen demand, salinity and habitat alteration.

Bioavailability of the contaminant is an important factor that influences the impact of sediment contamination. Bioavailability depends on several factors including the chemical properties of the contaminant such as chemical speciation and partitioning, background concentration of the chemical, physical properties of the sediment such as bulk density, porosity and surface area-volume ratio. Contaminants in the sediment undergo adsorption, desorption and transformation processes between the water column, sediment and gas phase. Contaminants in the sediment can be adsorbed onto sediment particles, non-filterable dissolved organic matter or dissolved in the water phase. The partitioning process is also influenced by biogeochemical conditions of the site such as pH, alkalinity and redox potential that affect the sorption and transformation processes. The exposure of aquatic organisms to contaminants in the aquatic ecosystem depends on the above mentioned factors that influence bioavailability and physiological behavior of the organism in the environment (Perelo 2010, USEPA 2004). In the case of metals, bioavailability and toxicity depends on their speciation in the water phase which is greatly influenced by redox conditions at the site (Liu et al. 2001). The primary routes of exposure for aquatic organisms are 1) transport of dissolved contaminants in pore water across cell membrane 2) ingestion of contaminated food or sediment particles. Direct exposure of sediments to benthic organisms and

fish is the most significant exposure pathway for these organisms (Perelo 2010). Sediment contamination has many adverse effects on the ecosystem and human health where benthic communities could be lost or shifted to pollution-tolerant species, which in turn could impact the energy flow; productivity and chemical cycle and affect other components of the ecosystem. It can also indirectly contaminate the food chain affecting aquatic macro fauna like fish. Contamination of the food chain can further affect human health through fish consumption as contaminants tend to bioaccumulation in the food chain. The USEPA issues fish consumption advisory for contaminated sites to prevent human exposure and health risks. Sediment contamination also impacts the effective utilization of the water body by restricting navigational, commercial and recreational use.

2.5 Strategies for Contaminated Site Remediation

Sediment remediation in the US follows a structured approach as outlined in USEPA Sediment Remediation Guidance Document (USEPA 2005). The remediation effort involves a detailed site assessment to understand the extent, source and type of contamination followed by selection one or more remediation alternative appropriate for the site specific contamination and environmental conditions.

2.5.1 Site Assessment

Each site has its own set of site-specific factors that influence the sediment management strategy. There are several factors that need to be considered when choosing a remediation strategy. Site and sediment assessment is the first step in remediation and involves collection of information on the spatial variability (both horizontal and vertical) of contamination, identifying sources of contamination and understanding other hydrologic and geological factors at the site such as groundwater seepage, tidal influence, sedimentation rates, erosion etc. Sediment assessment

methods can be either qualitative or quantitative (USEPA 1992). Quantitative methods are chemical specific and provide information on sediment quality for direct comparison to sediment quality criteria such as National Oceanic and Atmospheric Administration (NOAA) Screening Quick Reference Tables (SQuiRTs). Qualitative methods such as sediment toxicity tests provide assessment of the overall effects of all the chemicals in the sediment. As quantitative methods do not reveal the combined effects of all the chemicals and descriptive methods are not useful to develop sediment quality criteria, both tests complement each other. The second step involves implementation of elimination and control measures to prevent further release of the contaminant into the environment. The effectiveness of any remedial action will be ineffective unless the contaminant source is controlled. A remedial measure should be focused on minimizing human risk, cost of remediation and any habitat destruction/disturbance.

Sediment surveys are essential for identification of zones of sediment contamination and involve using a grab sampler for surficial sediments and sediment corers for subsurface sediment sampling. Grab samples are useful for physical/chemical and benthic community characterization. Core samples are useful for subsurface assessment of environmental contamination for understanding in-situ conditions. The potential for remobilization of contaminants should be considered during site assessment. Remobilization could occur through changes in the environmental conditions such pH, redox, alkalinity, concentration gradients, sediment re-suspension and biotransformation to more mobile forms.

2.5.2 No Action Alternative or Monitored Natural Recovery

The no action alternative is implemented in cases where there is evidence of natural burial, biodegradation, sedimentation, biotransformation or chemical transformation that are ongoing at acceptable rates to eliminate surface-contamination within a reasonable time frame.

Sedimentation results in deposition of a new layer of less contaminated material on top of the contaminated sediments thereby reducing contaminant flux and migration over a period of time. Although sorption of contaminants to new organic material may immobilize the chemical, there is a risk of bulk transport of particles by erosion and other physical forces like wind and wave action. Further benthic animals ingest organic matter and thus will be exposed to much higher levels of contamination (Rockne and Strand 2001). Contaminants can be bio-transformed into less toxic chemical or degraded to their constituent compounds by metabolic activities of microorganisms indigenous to the sediment. Natural bioremediation offers a permanent solution for sediment contamination problem where there is no contaminated sediment that is left in place unlike conventional techniques such as capping or relocation of contaminants in dredging. However, bioremediation has limited real world application and is rarely used as a remedial alternative as will be discussed later. Selection and implementation of MNR as a remediation strategy requires multiple lines of evidence of natural recovery and continued long term monitoring. MNR is most suitable for sites with low contaminant migration and low human/ecological risk. The disadvantages of MNR stems from the inherent slow process of natural recovery and the associated need for long term monitoring.

2.5.3 Dredging

Dredging and disposal in landfills or incineration is a conventional technique for remediation of contaminated sediments and has its advantages and disadvantages. Dredging involves removing the contaminated sediments up to a sufficient depth to maintain the streambed hydrology and is typically performed along with capping to form a barrier between the contaminated sediment and the water column. In dredging the contamination is not left in place and reduces the long-term risk of contaminant migration to the water column. However, dredging necessitates further

treatment and disposal of the contaminated sediment. This typically involves on site dewatering followed by transportation to a landfill, confined disposal facility (CDF) or incinerated (Zhao et al. 2009). The dewatering process requires further treatment of the leachate, to meet the effluent discharge standards, to be discharged into the nation's waterways. The cost associated with transporting large quantities of dewatered sediment and the associated leachate treatment makes dredging a more expensive remediation alternative. Other factors to be considered include re-suspension of contaminated sediment, increased bioavailability and residual contamination during the dredging operation. Also dredging is a more destructive operation whereby entire benthic community and microbial ecology could be lost.

2.5.4 Capping

Capping involves construction of a barrier between the contaminated sediment and the water column, thereby segregating the contamination. This reduces bioavailability and downstream transport of the contaminants. Capping can stop contaminant migration to the water column by providing increased path length for contaminant transport, physical separation, retardation, reduced sediment re-suspension and a clean sediment layer for benthic organisms to flourish (Himmelheber, Pennell, and Hughes 2007, Johnson, Reible, and Katz 2010, Josefsson et al. 2012, Liu et al. 2001). Capping is relatively less expensive than dredging with costs primarily dependent on the type of cap design employed for the project. Traditionally sand has been used as capping material but has low adsorptive properties to sequester and stop contaminant migration. On the other hand a variety of other materials are used in reactive caps (called as active capping) that can sequester contaminants or transform them to less toxic forms (Jacobs and Förstner 1999, Zimmerman et al. 2004). Phosphate and apatite/clay for metal control, organoclay and granular activated carbon/coke have been proposed for organic contaminants

control (Reible et al. 2006, Viana, Yin, Zhao, et al. 2007). In a modeling study to test the effectiveness of sand, granular activated carbon, organoclay, shredded tires and apatite as cap material, organoclay and apatite were found to be suitable for metal (Cd, Cr, Pb, Ag, As, Ba, Hg, CH_3Hg, and CN) contaminated sediments (Viana, Yin, and Rockne 2008). Organoclay consist of bentonite modified with quaternary amines (Knox et al. 2008). The quaternary amines get attached to the clay platelets through cation exchange and are effective against oil, PCBs and PAHs. Organoclay cap layer is prepared as a mixture of sand and organoclay in different proportions (Knox, Paller, and Roberts 2012). Zeolites and natural organic matter have also been used in reactive cap materials. Zeolite is an easily available natural material that can be surface treated to adsorb non-polar contaminants (Jacobs and Förstner 1999). Similarly, natural organic matter from plant material can be activated by treatment with superheated water to improve its sorption and hydrophobic characteristics to be used as capping material. Application of sorbent material such as organic rich soil, coke and activated carbon, organoclay and zeolites as capping material increases the time for breakthrough and decreases contaminant flux from the sediment (Murphy et al. 2006).

Geotextiles are used in sediment capping for a variety of applications. Geotextiles provide isolation from new organic matter and contaminated sediment; improve cap stability and infiltration of groundwater and for sequestration of contaminants when encapsulated with active sorbents. Active sorbents such as coke and activated carbon can be mixed with top sediment to reduce bioavailability and contaminant flux. Effectiveness of contaminant sequestration in mixing sediments with active sorbents such as coke and activated carbon was studied by Zimmerman et al (Zimmerman et al. 2004) and was shown to reduce PCB and PAH levels in the water column by 92% and 84% respectively.

Capping can enhance biodegradation in contaminated sediments by providing anaerobic conditions and enrichment of microbial community at the underlying sediment layer. Also capping provides a separation for contaminated sediment from the water column with environmental and hydraulic conditions similar to that of deep sediment characterized by low porosity, diffusion and pore-water mobility. These conditions hinder contaminant transport and increase breakthrough times. Capping also prevents sediment re-suspension by bioturbation and provides sufficient depth for benthic communities to flourish.

One of the major disadvantages of capping is that the contamination is left in place. This creates the possibility of contaminants breaking-through to the water column from damage to the cap layer, uneven application of cap material during construction, groundwater transport through channels around cap material or gas bubble migration from biogenic gas production (Reible et al. 2006, Yin et al. 2010, Rockne, Viana, and Yin 2010). Biogenic gas production and ebullition affects the transport parameters of the sediment bed and facilitates formation of bubble tubes that can increase diffusivity by as much as 1.2 to 3.1 times the theoretical values (Martens and Val Klump 1980, Viana, Yin, and Rockne 2012). Riverbed groundwater exchange can increase up to 30% due to altered hydraulic conductivity, specific storage and porosity. Ebullition can also affect the thermal diffusivity of the streambed with 4 to 20% increase in temperature fluctuation compared to saturated sediment (Cuthbert et al. 2010). The aforementioned factors necessitate long term monitoring of cap performance to ensure contaminant isolation. Capping can change the benthic community structure in response to the type of cap material installed. Capping can also inhibits biotransformation as the cap isolates the biologically active sediment zone from new carbon and electron source that are required by microorganisms involved in biotransformation (Himmelheber, Pennell, and Hughes 2007).

2.5.5 Bioremediation

Bioremediation is described as "the use of microorganisms to destroy or reduce the concentration of hazardous waste at a contaminated site" (Boopathy 2000). The most important advantage of bioremediation is its low cost in comparison to $5 billion required for treating all contaminated sediment sites using conventional treatment techniques (Dixon 1996). However, monitored natural recovery is the only bioremediation strategy currently in use. Other bioremediation alternatives include bio stimulation and bio augmentation.

Bio stimulation involves addition of nutrients, electron acceptors, electron donors, biopolymers and other stimulating agents to enhance the kinetics of anaerobic degradation of the contaminant by a specific metabolic pathway. Contaminant bioavailability, diffusional losses to the water column and utilization of electron acceptors in the oxidation of non-target organic matter are important factor that influence the effectiveness of bioremediation. Contaminant bioavailability for degradation depends on the physical and chemical properties of the contaminant such as solubility and chemical structure. Higher molecular weight hydrocarbons are less bioavailable than lower molecular weight hydrocarbons (Nakajima et al. 2005). Bio stimulation is also influenced by pH, temperature, and nutrients such as sodium, potassium, calcium, ammonium, iron, chloride sulfur and other trace nutrients (Rockne and Reddy 2003). Several researchers have reported enhanced hydrophobic organic compound biodegradation by addition of electron acceptors such as nitrate and sulfate (Rockne and Strand 1998, Rockne et al. 2000, McNally, Mihelcic, and Lueking 1998, Bedessem, Swoboda-Colberg, and Colberg 1997). Rockne et al (Rockne and Strand 2001) reported enhanced biodegradation of naphthalene, biphenyl and phenanthrene under anaerobic nitrate and sulfate reducing conditions. Lovely et al reported the anaerobic degradation of benzene in sediments with Fe(III) and sulfate as terminal

electron acceptors, with addition of humic substances and nitrilo-triacetic acid (NTA) as a chelating agents (Lovley 2000). The addition of chelators in metal rich sediments enhances the bioavailability of Fe (III). Synthetic and natural bio-surfactants have been shown to increase bioavailability and enhance biodegradation of hydrophobic organic compounds (HOC). Surfactants contain both hydrophobic and hydrophilic part and are termed as amphiphilic. Due to their amphiphilic nature, surfactants accumulate at the interface soil particles and pore water. Above a certain concentration called critical micelle concentration (CMC), surfactants form stable aggregates at the interface and increase bioavailability of HOCs (Makkar and Rockne 2003). Addition of natural surfactants like bile salt (sodium taurocholic acid) and rhamnolipids, or artificial surfactants like triton X-100 and sodium dodecyl sulfate can improve bioavailability and enhance biodegradation (West and Harwell 1992). The disadvantages associated with synthetic surfactant are its toxicity, inhibition of microbial degradation processes, recalcitrant nature and associated manufacturing cost. On the other hand, biosurfactants are biodegradable and are naturally produced by different microorganisms. Biosurfactants fall into three structural classes including glycolipids, phospholipids/fatty acids and lipopeptides/lipoproteins. Biosurfactants operate by changing the affinity of microbial cells to hydrocarbons by increasing the hydrophobicity of cell wall thereby enhancing biodegradation. However several studies have reported conflicting results on the ability of surfactants to enhance in biodegradation (Rouse et al. 1996, West and Harwell 1992, Foght, Gutnick, and Westlake 1989, Oberbremer, Müller-Hurtig, and Wagner 1990).

Bioaugmentation involves addition of new microorganisms with metabolic traits required for degradation of the contaminants of interest. There are several important factors that influence the effectiveness of this approach. It is critical to ensure that the newly introduced

microorganisms survive under the new environmental conditions. Other influencing environmental factors include pH, redox potential, co-contaminants, availability of co-substrates and bioavailability. Factors to be considered in strain selection include *i*) the relative abundance of the strain at the contaminated site, *ii*) tolerance to co-contaminants and *iii*) primary contaminant degradation potential. Reductive dechlorination is a known pathway for microbial degradation of PCBs and PCDD/Fs. Under anoxic conditions certain microorganisms use chlorinated compounds as their terminal electron acceptor to gain energy, replacing the chlorine atoms with hydrogen. *Dehalococcoides* strain are dehalo-respiring organisms that are known to degrade halogenated organics such as PCBs and PCDD/Fs (Perelo 2010). The complexity involved in mixing sediments with bio-stimulating agents and bioaugmenting existing microbial community structure make these methods difficult to implement.

2.6 Gas Production and Microbial Ecology

Soft fine-grained sediments accumulate in water bodies under slow flow conditions such as in estuaries, lakes and rivers. These sediments are typically high in labile organic matter that can be degraded by microbial communities in the sediment. Microorganisms produce CH_4, CO_2, and N_2 gas as end products of organic material degradation through specific pathways that depend on the availability of electron acceptors.

Microbially induced gas production is termed **biogenic gas production** with bubble formation occurring when the total partial pressure of all dissolved gases exceeds the hydrostatic pressure and cohesive forces within the sediment. The bubble phase concentrations of gases in the sediment are in equilibrium with dissolved gases in pore-water with mass distribution in the bubble and dissolved phase exhibiting highly variability. Gas phase methane in sediments can be as much as three times that of dissolved phase methane (Fechner-Levy and Hemond 1996). **Gas ebullition** refers to the release of accumulated gases in the form of gas bubbles from the sediment to water column and the atmosphere. During ebullition events gas produced from labile organic matter in deeper sediment migrate upwards and form preferential pathways. These preferential pathways can enhance transport of contaminants to the water column and nutrients to micro flora in deep sediments (Fendinger, Adams, and Glotfelty 1992). However, the impact of bubble ebullition to chemical transport is not the same in all sediment. Depending on the cohesiveness of the sediment the bubble tube may not last long enough to make a significant impact on transport parameters. Gas ebullition along with biogeochemical processes and human activities contribute to sediments being a constant source of pollution to the water column.

Gas ebullition greatly impacts the performance of an active cap through formation of preferential pathways and it is essential to manage gas production in order to ensure cap performance (Viana, Yin, Xhao, et al. 2007, Viana, Yin, and Rockne 2012). Gas production in sediments is influenced by a variety of geochemical and ecological factors and the impact of capping on gas ebullition rates and depth of biogenic gas production is not clearly understood. The gas ebullition rates exhibit high seasonal variability with temperature and site location. Greater variability in ebullition rates were observed in tidal estuaries (Martens and Val Klump 1980) where ebullition rates are influenced by tidal fluctuation in hydrostatic pressure. Ebullition rates of 411 16.8 mmol/m^2 were observed at a marine basin in North Carolina (Martens and Val Klump 1980). The following sections will delve in detail into factors influencing gas production rates and the highly complex and interlinked microbial processes in gas production.

2.7 Factors affecting ebullition rates and field gas measurement

Chemical and environmental conditions such as temperature, nutrient availability, substrate competition and toxicity from heavy metals/organics can play a major role in microbial ecology and gas production in capped sediment. Organic loading primarily controls the ebullition rate. Other contributing factors also include wind, physical disturbance, atmospheric pressure changes and hydrostatic pressure. Ebullition from shallow lakes have been shown to increase with wind speed and underwater currents causing physical disturbance at sediment water interface and change in overlying hydrostatic pressure. Low tides decrease hydrostatic pressure causing sediment gasses to expand and escape to the atmosphere. In temperate regions air temperature greatly affects ebullition rates with higher rates observed in the summer months. Many of the microbial

reaction kinetics in OM degradation are also temperature dependent, influencing seasonal ebullition rates (Viana, Yin, Xhao, et al. 2007, Yin et al. 2010). In tropical regions water level is the controlling factor in gas production, as temperature remains sufficiently warm throughout the year (Matson and Harriss 2009).

Biogenic gases produced in sediments include CH_4, CO_2, N_2, H_2S, CH_3SH (methane-thiol), DMS (dimethyl sulfide) and CS_2 (carbon disulfide) (Matson and Harriss 2009). Methane emissions from submerged soils contribute 21% (115 Mt/yr.) of the total natural and anthropogenic emissions to the environment (Mosier et al. 2004). When bubbles migrate upwards bubble stripping occurs that impact the concentration of dissolved gases in the pore water in upper layers of the sediment. Gases such as N_2, Ar and Rn are stripped as bubbles rise in the sediment. With increased ebullition rates the bubble CH_4 concentration increases in response to N_2 stripping. Thus seasonal changes in ebullition rates enforce a seasonal trend in N_2 levels as N_2 levels drop in the summer and increase in the fall due to lower gas production and diffusion of N_2 from the water column.

The concentration of dissolved gases in the bubble phase also change as they rise through the water column. CO_2 and H_2S bubble phase concentrations are primarily affected by bubble rise through the water column attributed to high solubility of CO_2 and dissociation of H_2S in water respectively (Chanton, Martens, and Kelley 1989). Methane and other gases in the bubble phase are not affected by bubble rise and measured concentrations are representative of that in the sediment. Gas bubbles released from the sediment are only slightly different than those captured using a trap. The change in gas concentration during bubble rise in the water column primarily affects CO_2 concentrations due to its high solubility (Chanton, Martens, and Kelley 1989). Consequently, field measurement of

trapped sediment gases is influenced by the frequency of measurement. Keller and Stallard (Keller and Stallard 1994) conducted field experiments that showed less than 3% methane was lost after 2 hours in the funnel. The gas phase methane concentration in sediments is highly variable ranging from 11 to 79% (Martens et al. 1992). At a small hypertrophic lake in UK a total gas (diffusion and ebullition of CO_2 and CH_4) flux of 52 mmol/m^2/day was observed with a methane and CO_2 ebullition flux of 12.0 mmol/m^2/day and 0.23 mmol/m^2/day respectively (Casper et al. 2000).

2.7.1 Methanogenesis

Methanogenesis is the conversion of organic carbon and inorganic forms of carbon to methane. As none of the individual microorganisms are capable of complete mineralization of organic carbon, a consortium of microorganisms that use different substrates form a complex food web to completely transform carbon to CH_4 and CO_2. Methanogenesis of organic matter is a complex multi-stage process. The **First stage** involves **hydrolysis** of organic polymers such as carbohydrates, proteins and lipids to monomers, sugars, alcohols, amino acids and fatty acids by hydrolytic bacteria. The **second stage** is termed as **Acidogenesis** involving fermentative bacteria that consume amino acids and sugars releasing H_2, volatile fatty acids, alcohol and CO_2. The volatile fatty acids (VFA) and alcohols can be further fermented to acetate (CH_3COO^-). The **third stage** is termed as **Acetogenesis** where CO_2 and H_2 produced in prior stages are converted to acetate by acetogenic bacteria. Acetogens are called "Reversibacter" as they can also oxidize acetate to CO_2 and H_2. Acetoclastic methanogens compete with acetogens in methane formation with acetate formation favored at high H_2 concentrations (>500Pa) and acetate oxidation to H_2 and CO_2 is favored at low H_2 concentrations

(<40Pa) (Demirel and Scherer 2008). The latter process involves inter-species hydrogen transfer between hydrogenotrophic methanogens and H_2 producing species to maintain an overall thermodynamically favorable reaction energetics. Methanogens can have a syntrophic relationship with obligate H_2 producing acetogens (OHPA) resulting in enhancement of H_2 producing acetogens. In acidic environments H_2 is consumed by homoacetogens to form acetate outcompeting hydrogenotrophs (Whalen 2005). The **fourth stage** is **methanogenesis** involving three groups of archaea; hydrogenotrophs, acetoclasts and methylotrophs. Hydrogenotrophs directly consume H_2 and CO_2 to form methane. Most hydrogenotrophs can also use formate produced by fermentative bacteria in the reduction of CO_2 to CH_4. Acetoclasts cleave acetate to form methane from the methyl-group by methylotrophic methanogens and CO_2 from the carboxyl group by acetoclastic methanogens (Demirel and Scherer 2008). *Methanosarcina* is the only group than can produce methane through all the three-methanogenic pathways.

2.7.2 Methanogenic Archaea

Methanogens are an important group of strict anaerobic archaea controlling CH_4 production in the environment, a key greenhouse gas. Methanogens are known to be difficult to isolate in the laboratory and molecular tools such as 16S rRNA gene analysis have been widely used to study their abundance and diversity.

Methanotrophs are grouped into three nutritional groups a) Hydrogenotrophs b) Methylotrophs and c) Acetoclasts. As the name implies, the three groups metabolize hydrogen, methyl compounds and acetate respectively to form methane. Methyl compounds utilized by methanotrophs include methanol, methylamines and dimethyl sulfide. Some methanogens can use H_2 and methanol or CO_2 and alcohol to form

methane and share nutritional characteristics among the three groups. Genus level classification of the common methanogenic *Archaea* is presented in Table 2.1. In natural environments with molecular sulfur, methanogens can form H_2S through sulfur reduction and could play an important role in the sulfur cycle (Stetter and Gaag 1983). Hydrogenotrophic methanogenesis is the most thermodynamically favorable reaction followed by methylotrophs and acetotrophs. The standard change in free energy ($\Delta G^{\circ\prime}$) of biochemical reactions dictates the order of substrate consumption in aquatic sediments and is proportional to redox potential ($\Delta E_o'$) in a reduction-oxidation reaction. The redox pair with the highest negative reduction potential E_o' (the electron donor) reacts with the redox pair with the highest positive potential to release maximum energy that can be utilized for cell growth.

2.7.3 Hydrogenotrophic Methanogens

Hydrogenotrophic methanogens include Methanomicrobiaceae, Methanobacteriaceae, Euryarchaeota group III and *Methanocellales*. Methanocellales are hydrogenotrophic methanogens utilizing H_2 and CO_2 for methane production. Most hydrogenotrophs can also use formate for methanogenesis (Garcia, Patel, and Ollivier 2000). Considering that hydrogenotrophic methanogenesis is the most thermodynamically favorable reaction, the group is also the most commonly found with more than 61 species identified. This group has been isolated from rice fields, marine sediments, freshwater sediments in different parts of the world indicating their versatile nature in different environments (Conrad, Erkel, and Liesack 2006). Hydrogenotrophic methanogens via H_2/CO_2 pathway are more dominant at higher temperatures (Glissman et al. 2004).

Table 0.1 Classification of methanogenic *Archaea*

Order	Family	Genus
Methanobacteriales	*Methanobacteriacea*	*Methanobacterium* *Methanothermobacter* *Methanobrevibacter* *Methanosphaera*
	Methanothermacea	*Methanothermus*
Methanococcales	*Methanococcaceae*	*Methanococus* *Methanothermococcus*
	Methanocaldoccoccaceae	*Methanocaldococcus jannaschii* *Methanoignis igneus*
Methanomicrobiales	*Methanomicrobiaceae*	*Methanomicrobium* *Methanolacinia* *Methanogenium* *Methanoculles* *Methanosplanus* *Methanofollis* *Methanocalculus*
	Methanocorpusculaceae *Methanospirillacae*	*Methanocorpusculum* *Methanospirillum*
Methanosarcinales	*Methanosarcinaceae*	*Methanosarcina* *Methanolobus* *Methanococcoides* *Methanohalophilus* *Methanosalsus* *Methanohalobium*
	Methanosaetacea	*Methanosaeta*

2.7.4 Acetotrophic Methanogens

The *methanosarcinales* group, comprising of *Methanosarcinaceae* and *Methanosaetacea* form the acetotrophic methanogens. While *Methanosarcinaceae* are the most metabolically diverse utilizing a variety of organic compounds, *Methanosaetacea* can metabolize only acetate (Dubey et al. 2014). *Methanosarcina* are more dominant in acetate rich sediments compared to Methanosaeta. Their presence can be used as an indicator for high levels of acetate in the environment (Chin et al. 2004, Zheng and Raskin 2000). The filamentous Methanosaeta species are found to be dominant at low

acetate levels (Demirel and Scherer 2008). Methane production from acetoclastic methanogens can range between 50-83% of the total methane in bulk sediment (Joulian et al. 1998). Temperature dependent phylogenetic studies indicate that the contribution of acetoclasts to methane production is more pronounced at lower temperatures (Glissman et al. 2004). In the absence of acetoclastic methanogens in acetate rich sediments, it is possible to have a syntrophic relationship with other microbial groups that can oxidize acetate. As evidenced in Lake Kinneret, Israel acetate production was detected in the pore water, however acetoclastic methanogens were not detected in phylogenetic analysis (Nüsslein et al. 2001). The most common methanogenic reactions and its representative methanogenic genera are shown in Table 2.2.

2.7.5 Methane production in aquatic environment

Methane is produced in a wide range of anaerobic environments such as ponds, marshes, swamps, paddy fields, lakes and oceans. Natural methane emissions from submerged soils is estimated at 115 Mt yr-1 accounting for nearly 21% of total CH_4 emissions (Natural and Anthropogenic) and 60% of the total natural emission from the environment (Mosier et al. 2004). Considering the wide range of environments from which methane is produced many studies have been published on the methanogenic community structure of different environments.

Sediment cores from lakes show decreasing microbial diversity with depth with intense microbial activity in the first few centimeters of core evidenced by rapid changes in concentration of substrates such as ammonia, Fe (III) and SO_4^{2-}. In a phylogenetic analysis of sediment cores form the Swiss Lake Rotsee, *Methanosaeta* accounted for 90% of archaeal population. Sediment cores show a shift from hydrogenotrophic methanogens

to acetoclastic methanogens with increasing depth (Falz et al. 1999). DNA extracted from Lake Dagow, Germany also showed the presence of *Methanosaetacea* and *Methanomicrobiaceae* the metabolically diverse groups (Glissman et al. 2004).

Table 0.2 Common methanogenic reactions and their representative genera (Chaban, Ng, and Jarrell 2006, Demirel and Scherer 2008)

Reaction	Genera
Hydrogen: $4H_2 + CO_2 \rightarrow CH_4 + 2H_2O$	Most methanogens (*Methanobacterium*, *Methanococcus*, *Methanobrevibacter*, *Methanopyrus*, *Methanosarcina*
Formate: $4HCOOH \rightarrow CH_4 + 3CO_2 + 2H_2O$	*Methanococcus*, *Methanogenium*, *Methanobacterium*, *Methanocorpusculum*
Acetate: $CH_3COOH \rightarrow CH_4 + CO2$	*Methanosarcina*, *Methanosaeta*
Methanol: $CH_3OH + H_2 \rightarrow CH_4 + H_2O$	*Methanosphaera*, *Methanomicrococcus*
Ethanol: $CH_3CH_2OH + CO_2 \rightarrow CH_4 + 2acetate$	*Methanospirillum*
2-Propanol: $4C_3H_7OH + CO_2 \rightarrow CH_4 + 2acetone + 2H_2O$	*Methanospirillm*, *Methanobacterium*, *Methanocorpusculum*
Carbon monoxide: $4CO + 2H_2O \rightarrow CH_4 + 3H_2CO_3$	*Methanobacterium*, *Methanosarcina*
Monomethylamine: $4(CH_3)NH_2 + 2H_2O \rightarrow 3CH_4 + CO_2 + 4NH_3$	*Methanosarcina*, *Methanococcoides*, *Methanolobus*
Dimethylamine: $2(CH_3)_2NH + 2H_2O \rightarrow 3CH_4 + CO_2 + 2NH_3$	*Methanosarcina*, *Methanococcoides*, *Methanolobus*
Trimethylamine: $4(CH_3)_3N + 6H_2O \rightarrow 9CH_4 + 3CO_2 + 4NH_3$	*Methanosarcina*, *Methanococcoides*, *Methanolobus*
Methyl mercaptans: $2(CH_3)_2S + 3H_2O \rightarrow 3CH_4 + CO_2 + H_2S$	*Methanomethylovorans*, *Methanohalophilus*, *Methanosalsum*

Phylogenetic analysis of sediment cores from the meromictic Lake Pavin revealed a shift in methanogenic community abundance from *Methanosaetacea* and *Methanobacteriaceae* to uncultured archael lineages [Marine Benthic Group – D (MBG-D) and Miscellaneous Crenarchaeal Group (MCG)] with increasing depth (Borrel et al. 2012). Abundance of *Methanosaetacea* was found to be strongly correlated with depth whereas *Methanobacteriaceae* did not exhibit a significant correlation. Archaea accounted for 18% of the prokaryotic cells in the first 40cm on the core. Methanogenic community analysis of five different paddy soils from different regions of India revealed the presence of a diverse group of methanogenic archaea including *Methanomicrobiaceae, Methanobacteriaceae, Methanocellales, Methanosarcinaceae, Methanosaetacea* and *Crenarchaeota*. The abundance of each microbial group was found to be dependent on the soil type and physiochemical properties of the soil with *Methanocellales* present in all the four soils types indicating the versatile nature of these species.

2.8 Factors Affecting Methanogenesis

Methanogens are strict anaerobes that require a very restricted group of substrates for gas production. Methane production in sediments is influenced by (Albert, Martens, and Alperin 1998):

- OM flux to sediment water interface (SWI)
- Biodegradability of OM
- Environmental factors like pH, ORP, temperature
- Presence of alternate high energy alternate electron acceptors in pore water like SO_4^{2-} and NO_3^-
- CH_4 ebullition to water column

After anaerobic conditions are established substrate availability becomes the limiting factor for methanogenesis (Bridgham and Richardson 1992, Roy and Knowles 1994, Morris et al. 1994). In incubation studies of sediment cores with no substrate amendment, methane production decreased with depth indicating lack of substrate availability. Addition of Na^+ and trace metals such as Fe, Ni, Co enhance methanogenesis, as these metals are known to be essential catalysts in electron transport (Schlegel et al. 2012, Basiliko and Yavitt 2001). Presence of Cr and Se inhibit CH_4 and CO_2 production (Dalal et al. 2008).

Methanogens are neutrophilic *archaea* with low CH_4 production at lower pH. Methane production has been reported at a wide pH ranging from 4 to 9 (Chaban, Ng, and Jarrell 2006) with an optimum between 5-7.5 (Inubushi et al. 2005, Segers 1998). In an incubation study, peat soils exhibited inhibition of methanogenesis at low pH (Coles and Yavitt 2002, Yavitt, Lang, and Wieder 1987). Addition of N and P were not found to

impact CH_4 production, suggesting that CH_4 production is independent of nutrient availability (Bridgham and Richardson 1992, Williams and Crawford 1984) as there is sufficient N available in the environment for cell synthesis. Methane production is also influence by redox potential. In paddy soils significant methane production was reported at redox potentials below -100mV (Hou et al. 2000). Strong correlation exists between methane production potential and aerobic CO_2 production, as CO_2 production can be associated with biodegradability of organic matter (Crozier, Devai, and DeLaune 1995). Yavitt et al reported that the amount of acid soluble material in wetland soils explained 50% of the variation in CH_4 production. Resistance to microbial decay such as C:N ratio and lignin:N ratio have also been used as indicators of microbial CH_4 production (Valentine, Holland, and Schimel 1994). Organic acid concentration (OAC) in pore water has been used as a measure of microbial substrate availability including acetate, a precursor for methanogenesis. In a study of wetland methane emissions recorded from a wide range of climatic conditions, soil temperature and OAC was able to explain almost 100% of the variability in CH_4 emissions (Christensen et al. 2003). OAC in pore water can be analyzed by centrifuging the pore water and analyzed using an anion exchange HPLC (Ström, Olsson, and Tyler 1994).

2.8.1 Temperature:

Methanogens are mesophilic with a temperature range of 30° to 40°C for optimum growth (Zinder 1993). A temperature optimum of 35 to 40°C was observed in incubations of lake sediments and wetlands (Zeikus and Winfrey 1976, Boon and Mitchell 1995) with gas production observed at a lowest temperatures of around 5°C (Boon and Mitchell 1995). In a 12 year study on methane emission from wetlands in

Greenland, Iceland and Scandinavia a strong correlation between methane emission and seasonal soil temperature was observed with R^2=0.84 (Christensen et al. 2003). Q_{10} values are used as a measure of the temperature dependence of microbial reactions and represent reaction rate increase for every 10°C rise in temperature. Q_{10} values for methanogenesis in wetland sediments range from 1 to 35. However, Q_{10} values for pure cultures of acetoclastic methanogens (2.9 – 9) and hydrogenotrophs (1.3 – 12.3) show a much narrower range. As methanogenesis is the end process in a complex food web, the wide range of Q_{10} values observed is a composite of temperature dependence of methanogens as well as temperature dependence of microbial activity associated with the production of methanogenic precursors such as acetate, H_2, CO_2 etc. Q_{10} values are also found to vary with depth and season. At high temperatures, hydrogenotrophic *Methanosarcinaceae* dominate methanogenic activity and at lower temperatures *Methanosaetacea* which use acetate as substrate are typically found to dominate (Chin et al. 1999).

Incubation studies and community structure analysis of different soils and sediments suggest that the total *Archaea* do not change at different temperatures. This indicates that temperature dependent changes in CH_4 production are associated with changes in activity of the each Archaeal group rather than enrichment of the specific microbial groups (Glissman et al. 2004).

2.8.2 Presence of alternate electron acceptors

Methanogenesis is affected by the presence of external electron acceptors such as O_2, sulfate (SO_4^{2-}), NO_3^{2-}, and Fe (III) with substrate competition for C and H negatively impacting CH_4 production (Segers 1998, Lovley et al. 1996). In an incubation study of sediment slurries with supplemental Fe (III), it was found that 90% of OM was consumed by ferric iron reduction (Lovley and Phillips 1986), significantly affecting CH_4 production. Methanogenesis is dependent on the presence of internal electron acceptors such as CO_2, acetic acid, formic acid, methylamines, methane thiol and dimethyl sulfide that are produced in the sediment. Sulfate and nitrate reduction requires external electron acceptors such as SO_4^{2-} and NO_3^{2-}. The order of substrate affinity of methanogens is as follows: H_2>propionate>other organic donors (Laanbroek et al. 1984). However the order of biogeochemical reactions in the sediments follows a sequence dependent on the oxidant available in sediment/pore-water that yields the highest energy (Albert, Martens, and Alperin 1998). O_2>NO_3>MnO_2>FeO(OH)>SO_4^{2-}>CO_2 is the order of progressively favorable electron acceptors in environment which follows the order of increasing energy yield.

2.8.3 Sulfate reduction

Sulfate is an external electron acceptor that diffuses from the water column to the sediment and the extent of sulfate reduction is dependent on availability of SO_4^{2-} in pore water. Sulfate reduction by sulfate reducing bacteria (SRB) can induce two types of inhibition to methanogens; primary inhibition by direct competition for substrates such as acetate, propionate and secondary inhibition by sulfide toxicity to other anaerobes including methanogens, acetogens and to SRBs themselves (Winfrey and Zeikus 1977,

McCartney and Oleszkiewicz 1991). As SRBs are capable of utilizing a wide range of substrates and due to thermodynamic advantages, they compete with methanogens, acetogens and fermentative bacteria (McCartney and Oleszkiewicz 1993).

At sulfate concentrations above 30 μM a sulfate reduction zone starts to develop as these microorganisms consume acetate and maintain acetate levels too low for methanogenesis (Lovley and Klug 1986). Sulfate reduction is more energetically favorable with a higher biomass yield per mole of sulphate compared to methanogenesis (shown in the reactions below). The rate of organic matter degradation (i.e. acetate formation) controls the extent of sulfate reduction zone. At high rates of acetate formation, sulfate gets consumed within the first few centimeters from SWI (1-2cm) and a methanogenic zone starts to develop below the sulfate reduction zone. Methanogenesis begins to dominate when acetate concentration is above 21.5μM and SO_4^{2-} <30μM. However methanogenesis can still proceed at high sulfate concentrations through pathways related to noncompetitive methanogenic substrates such as methanol and trimethylamines (Chaban, Ng, and Jarrell 2006).

$$CH_3COO^- + SO_4^- \leftrightharpoons HS^- + 2HCO_3^- \qquad \Delta G^\circ = -47.3\ kJ \qquad (0.1)$$

$$4H_2 + SO_4^- + H^+ \leftrightharpoons HS^- + 4H_2O \qquad \Delta G^\circ = -151.9\ kJ \qquad (0.2)$$

$$CH_3COO^- + H_2O \leftrightharpoons CH_4 + HCO_3^- \qquad \Delta G^\circ = -31.0\ kJ \qquad (0.3)$$

$$4H_2 + HCO_3^- + H^+ \leftrightharpoons CH_4 + H_2O \qquad \Delta G^\circ = -135.6\ kJ \qquad (0.4)$$

SRBs are strict anaerobes that can oxidize volatile acids, alcohols, long chain fatty acids, acetate, H_2, organic acids and aromatic compounds (Hao et al. 1996). In sediments sulfate is reduced to sulfide by two groups of incomplete and complete sulfate reducing bacteria

(SRB). Incomplete SRBs reduce fatty acids such as lactate and propionate to acetate and CO_2 whereas complete SRB's convert acetate to CO_2 and HCO_3^- resulting in complete carbon mineralization.

Lactate:

$$2CH_3CHOHCOO^- + SO_4^{2-} \rightarrow 2CH_3COO^- + 2HCO_3^- + HS^- + H^+ \quad \Delta G° = -160.1 \text{ kJ} \qquad (0.5)$$

Hydrogen:

$$4H_2 + SO_4^{2-} + H^+ \rightarrow 4H_2O + HS^- \qquad \Delta G° = -152.2 \text{ kJ} \qquad (0.6)$$

Acetate:

$$CH_3COO^- + SO_4^{2-} \rightarrow 2HCO_3^- + HS^- \qquad \Delta G° = -152.2 \text{ kJ} \qquad (0.7)$$

SRBs are gram-negative bacteria except for *Desulfonema* species and two SRB genera, *Desulfotomaculum* and *Desulfovibrio*, have been clearly identified in sulfate reduction. *Desulfotomaculum* consume acetate and compete with methanogenesis whereas *Desulfovibrio* degrade lactate to acetate. Most common SRB genera are shown in Table 2.3.

Other forms of sulfur such as sulfite and thiosulfate can also be used as sulfur source by SRBs. SRBs disproportionate sulfite (SO_3^{2-}) and thiosulfate ($S_2O_3^{2-}$) to sulfate, which is again consumed for OM oxidation. *Desulfovibrio sulfodismutans* species has been associated with splitting thiosulfate to sulfate and sulfite (Hao et al. 1996).

$$S_2O_3^{2-} + H_2O \rightarrow SO_4^{2-} + HS^- + H^+ \qquad \Delta G° = -21.9\text{kJ} \qquad (0.8)$$

$$4SO_3^{2-} + H^+ \rightarrow {}^- + HS^- \qquad \Delta G° = -235.6\text{kJ} \qquad (0.9)$$

Table 0.3 Genera of SRB commonly found in the environment

Genus	
Desulfotomaculum	*Desulfosarcina*
Desulfovibrio	*Desulfobacterium*
Desulfomonas	*Desulfonema*
Thermodesulfobacterium	*Desulfotomaculum*
Desulfobulbus	*Desulfovibrio*
Desulfobacter	*Desulfomonas, Desulfococcus*

2.8.4 Nitrification and Denitrification:

Similar to sulfate reduction, nitrification and denitrification are important in controlling gas ebullition from sediments, especially in nitrate rich environments such as near wastewater treatment discharge. Nitrate availability in pore water is dependent on these processes. Sulfate reduction and methanogenesis can commence only after the exhaustion of available nitrate in pore water by denitrification.

Nitrification and denitrification occur in sequence in aquatic habitat resulting in the loss of N to the atmosphere (Roy and Knowles 1994). Nitrification is the rate limiting step and is defined as biological oxidation of reduced forms of nitrogen (NH_4^+) to NO_2^- and NO_3^- by aerobic bacteria (Matson and Harriss 2009). Nitrification occurs in the aerobic zone within a few centimeters of the SWI and N_2O is produced as byproduct (Bremner and BLACKMER 1978, Goreau et al. 1980). Roy et al observed increased nitrification in sediment slurries supplemented with CH_4 with enhanced nitrification observed up to a CH_4 concentration of 24μM. However at CH_4 concentrations above 84μM, nitrification was suppressed resulting in NH_4^+ accumulation in pore water (Roy and Knowles 1994). Bosse et al also observed inhibition of CH_4 oxidation at high concentrations of ammonia (Bosse, Frenzel, and Conrad 1993). Multiple lines of evidence suggest that nitrification

by methanotrophs via enzyme methane monooxygenase is attributed to the enhanced nitrification observed at high CH_4 concentrations. In GCR with WWTP discharge containing ammonia and nitrate, denitrification and nitrification can significantly impact N_2 levels in the sediment.

The nitrate and nitrite formed in the nitrification step can undergo two types of microbially mediated transformation in anaerobic sediment.

Denitrification:	$NO_3^- \rightarrow NO_2^- \rightarrow N_2O \rightarrow N_2$
Dissimilatory Nitrate Reduction to Ammonia (DNRA):	$NO_3^- \rightarrow NO_2^- \rightarrow NH_4^+$

Denitrification is a process of microbial respiration in which nitrate and nitrite are reduced to N_2O and N_2. Incubation studies have shown the presence of nitrate to inhibit methanogenesis and sulfate reduction (Achtnich, Bak, and Conrad 1995). Denitrifiers are aerobic bacteria that can utilize nitrate and nitrite in place of oxygen for respiration in anaerobic conditions. Microorganisms involved in denitrification possess enzyme nitrate reductase and nitrite reductase. Denitrifiers isolated from the environment belong to a variety of taxonomic groups and primarily use organic matter as carbon source. Denitrifiers are also know to utilize H_2, CO_2 and reduced sulfur for growth (Knowles 1982). *Micrococcus denitrificans* can denitrify using hydrogen as electron donor (Davies 1973). Table 2.4 below shows a list of denitrifiers commonly found in the environment (Zehnder 1988, Knowles 1982). *Pseudomonas* is the most common denitrifier in soils and aquatic habitats. At high concentrations of methane certain genera of denitrifiers including *Alcaligenes*, *Achromobacter*, *Pseudomonas* and *Bacillus* utilize CH_4 as carbon source (Davies 1973) and can regulate of CH_4 concentration in pore water.

Table 0.4 Genera of denitrifiers found in the environment.

Genus		
Achromobacter	*Flavobacterium*	*Rhizobium*
Agrobacterium	*Halobacterium*	*Rhodopseudomonas*
Alcaligenes	*Hyphomicrobium*	*Thiobacillus*
Aquaspirillum	*Nitrosomonas*	*Thiomicrospira*
Azospirillum	*Paracoccus*	*Thiospaera*
Bacillus	*Pseudomonas*	*Wolinella, Cytophaga*

Dissimilatory nitrate reduction to ammonia (DNRA) could play an important role in cycling of anthropogenic sources of nitrogen in aquatic and marine habitats (Koike and Hattori 1978, Dong et al. 2009). Unlike denitrifiers that require nitrate reductase enzyme, DNRA is carried out by a variety of organisms and enzymes. List of genera identified with DNRA are presented in Table 2.5. The abundance of nitrifiers and denitrifiers in different layers of the sediment core can be used to identify the microbial process dominating organic matter degradation.

Table 0.5 Different genera of DNRA found in the environment (Zehnder 1988)

Genus		
Achromobacter	*Salmonella typhimurium*	*Escherichia coli*
Agrobacterium	*Klebsiella*	*Citrobacter*
Alcaligenes	*Enterobacter aerogenes*	*Vibrio*
Aquaspirillum	*Serratia marcescens*	*Campylobacter sputorum*
Azospirillum	*Erwina carotovora*	
Bacillus	*Photobacterium*	

2.8.5 Fe and Mn reduction

Dissimilatory Fe(III) and Mn(IV) reduction refers to the utilization of Fe(III) and Mn(IV) as electron acceptors in microbial OM oxidation with Fe (II) and Mn(II) produced as end

products along with CO_2 or carbonic acids. Several incubation studies have shown that sulfate reduction and methanogenesis are inhibited in sediment slurries amended with Fe(III) oxides (Lovley and Phillips 1987, Achtnich, Bak, and Conrad 1995). Iron reducers compete for electron donors such as H_2 and acetate and outcompete sulfate reducers and methanogens by oxidizing H_2 and acetate at a lower threshold concentration (Lovley and Phillips 1987). The degree of competition depends on the type of Fe (III) oxide available. Amorphous Fe(III) oxide is considered as the primary Fe(III) oxide responsible for OM oxidation in anaerobic sediments (Roden 2003, Lovley and Phillips 1986). Fe and Mn reduction is known to play an important role in the development of anaerobic zone in aquatic sediments leading to magnetization of sediments and release of high levels of Fe into groundwater.

A variety of aerobic and anaerobic, fermentative, sulfur, H_2, organic matter and aromatic compound oxidizing species have been associated with Fe and Mn reduction in natural environments (Lovley 1991). *Escherichia coli, Clostridium pasteurianum, Lactobacillus lactis, Bacillus polymyxa* are some of the fermentative iron reducers. Sulfur oxidizing iron reducers include *Thiobacillus thiooxidans, Thiobacillus ferrooxidans and Sulfolobus acidocaldarius*. Hydrogen oxidizers include *Pseudomonas spp. and Shewanella putrefaciens*. Two important groups of microorganisms capable of complete oxidation of organic carbon to CO_2 have been isolated; *Geobacter metallireducens* (GS-15) and strain 172. Although strain 172 has been shown to completely oxidize acetate with Fe (III) as the sole electron acceptor, the strain has not been well characterized. Strain GS-15 is well characterized and is known to utilize Fe (III) as the sole electron acceptor to oxidize short chain fatty acids, alcohols and mono-aromatic compounds (Lovley et al. 1993, Lovley

and Phillips 1988). GS-15 can also oxidize acetate with Mn (IV), nitrate and U(VI) as electron acceptors (Lovley et al. 1993). Some of the common Fe (III) and Mn(IV) reducers are shown in Table 2.6.

Table 0.6 Different genera of Fe(III) and Mn(IV) reducers in the environment

Genus		
Aerobic	**Aerobic**	**Anaerobic**
Alcaligenes	*Proteus*	*Clostridium*
Arthrobacter	*Pseudomonas*	*Bacteroides*
Bacillus	*Serratia*	*Desulfovibrio*
Citrobacter	*Streptomyces*	*Geobacter*
Corynebacterium	*Vibrio*	
Enterobacter	*Escherichia*	
Micrococcus	*Leptothrix*	

2.8.6 Methane Oxidation by Methanotrophs

Methanotrophs are a large group of aerobic eubacteria that use C-1 compounds such as methane, methanol, methylated amines and halomethanes as substrate. These organisms oxidize CH_4 to methanol, formaldehyde, formate and CO_2 and assimilate formaldehyde (Hanson and Hanson 1996). In this oxidative metabolism, formaldehyde is used in catabolism and anabolism of methanotrophs.

$$CH_4 \rightarrow CH_3OH \rightarrow HCHO \rightarrow HCOOH \rightarrow CO_2$$

The presence of O_2 is essential for methane oxidation as it is the terminal electron acceptor and acts as a catalyst for oxidation of CH_4 to CH_3OH by enzyme methane monooxygenase (MMO). Methane oxidation is known to occur in both aerobic and anaerobic environments but the microbiology and biochemistry of anaerobic methane

oxidation is not well studied. There are two types of MMOs. The pMMO (particulate) form is present in cell membrane is found in all methanotrophs whereas sMMO (soluble) form is encountered less frequently. pMMO has lower O_2 and substrate specificity compared to sMMO and consequently is more active even at low O_2 levels (Whalen 2005). MMO can utilize a variety of substrate including a xenobiotic compounds and has potential for use in bioremediation. An anaerobic bacteria/archaea consortium has been recently identified that can oxidize methane to CO_2 coupled to denitrification (Raghoebarsing et al. 2006).

Methanotrophs include the genera *Methylomonas*, *Methylobacter*, *Methylococcus*, *Methylocystis*, *Methylosinus* and *Methylomicrobium.* Methanotrophs are primarily classified into three groups Type I, Type II and Type X. Type I include *Methylococcus*, *Methylomicrobium*, *Methylobacter*, and *Methylomonas* that use ribulose monophosphate (RuMP) pathway for formaldehyde assimilation. Type II methanotrophs use serine pathway and include the genera *Methylocystis*, *Methylosinus* (Hanson and Hanson 1996). Type X methanotrophs include microorganisms that primarily use RuMP pathway but also possess low levels of the enzyme ribulose- bisphosphate carboxylase and include the species *Methylococcus capsulatus*

2.9 Ground Water Surface Water Exchange

Groundwater and surface water are integral components of a hydrological system and interact in a variety of ways such that the contamination or human impact of one affects the other. The zone of interaction between surface water and ground water is called the hyporheic zone and is characterized by low flow velocities and complete saturation. The zone is marked by either groundwater raising through the streambed and mixing with stream water (gaining stream) or stream water percolating through the sediment into groundwater zone (losing stream). The direction of ground water surface water movement will depend on the hydraulic gradient between groundwater table and stream stage. Typically streams reaches have both gaining and losing zones and many processes like contaminant transport, degradation, precipitation and adsorption characterize the mixing zone. These processes impact the water quality of both ground and surface water. The downwelling of stream water transports nutrients, oxygen and organic carbon into the hyporheic zone. This can have a significant impact on the nutrient and carbon cycle of the subsurface ecosystem and influence the microbial community structure of the streambed sediment. The ground water-surface water (GW-SW) exchange can transport contaminants from the streambed into ground water or vice-versa. The extent and scale of GW-SW exchange is influenced by the streambed morphology, geology and spatial variations in geological heterogeneities.

In capping of a contaminated site, the natural hydraulic properties of the streambed are altered by the installation of the cap. This makes post-capping assessment of ground water and surface water exchange essential to evaluate post-cap GW-SW exchange and ensure safety against contaminant breakthrough. Also, capping can impact the

biogeochemical processes occurring at the site due to changes in redox potential. Post-capping transport of nutrients and electron acceptors by advection can impact the microbial community of deeper streambed sediment and enhance gas generation. Biogenic gas production can induce cap rupture and enhance contaminant transport through ebullition events.

In an effort to understand the impact of capping on groundwater-surface water exchange and the associated transport processes, I have attempted to estimate the magnitude of groundwater fluxes at the sediment water interface (SWI). Conventional techniques for measurement of groundwater surface water exchange such as using seepage meters, mini-piezometers, slug testing or mass balance approach such as incremental steam flow, hydrograph separation and environmental tracer methods are time consuming or laborious (Kalbus, Reinstorf, and Schirmer 2006).

Alternately, heat tracer technique serves as a quick and low cost method to estimate the magnitude of groundwater fluxes at SWI (Becker et al. 2004, Conant 2004). Surface water that percolates into the sediment or groundwater migrating upwards carries with it a heat signature, which can be used as a tracer to estimate GW-SW exchange. The development of low cost heat sensors and data loggers has enabled this technique to be used more widely (Constantz et al. 2002, J.Constantz 2004, Becker et al. 2004).

2.9.1 Heat as a surrogate measurement to estimate GW-SW exchange

The temperature difference between groundwater and surface water can be used as a tracer to estimate the GW-SW exchange at the SWI (Kalbus, Reinstorf, and Schirmer 2006, Constantz 1998, Constantz et al. 2002). Variations in ground water temperatures are relatively stable compared to the diurnal variation in stream temperatures. This

relative difference in temperature variation leaves a distinct signature on the temperature profile at a site depending on whether the reach is gaining or losing water to the streambed. A time series of the temperature profile at a streambed can be used to identify the magnitude and direction of the exchange using the heat transport equation in porous media. In gaining reaches, the temperature profile is marked by a concave upward curve and in losing reaches the profiles are convex upward. The direction of GW-SW exchange is not always stable and can change temporally induced by changes in stream stage or ground water table. Streambed temperature records can be used to observe temporal changes in in GW-SW exchange whereas field measurement only provides a single point estimate.

The temperature profile at a streambed records the exchange of heat between surface water and the sediment. At sites where the reach is losing, the temperature time series are marked by a sinusoidal temperature pattern in response to diurnal heating and cooling of the surface water. The extent of penetration of the sinusoidal pattern is dependent on the magnitude of ground water flux into the sediment, the clarity of the water column to solar irradiation and the heat transfer properties of the sediment water matrix. In a losing stream the amplitude of temperature variation decreases with depth and is marked by an offset in phase. Geomorphological formations like pool-riffle sequences, changes in streambed slope, fractures and obstacles can also induce cause local variability in GW-SW exchange interactions (Kalbus, Reinstorf, and Schirmer 2006).

2.9.2 General Characteristics of a Streambed temperature profile

There are two distinct zones in the sediment subsurface, the surficial zone and geothermal zone. The surficial zone refers to the shallow subsurface zone immediately below the

SWI and is characterized by temperature changes influenced by diurnal heating and cooling cycles. Silliman et al observed that at depths below 1.5 m the streambed temperature is more stable and away from the effects of diurnal temperature fluctuations at the surface (Silliman and Booth 1993). The geothermal zone is typically below a depth of 10 m and is influenced by geothermal heat. In general the temperature in the geothermal zone increases 1°C for every 20 – 40m (Parsons 1970). The geothermal zone shows no seasonal variability and any temperature fluctuations are induced by groundwater movement. In the case of groundwater moving upward or gaining reaches, the surface water temperature is close to that of groundwater the profile is marked by a convex upward curve with pore water temperature increasing with depth in the surficial zone. In losing reaches the temperature profile has a concave upward curve, with pore water temperature decreasing with depth in the surficial zone and increasing with depth in the geothermal zone. The streambed temperature profile fluctuates with changes in pore water temperature caused by surficial temperature changes and hydraulic head. Consequently, temperature profiles monitored over a longer period of time form an envelope of temperature profile curves representing recharge and discharge during the year. In the case of a losing reach, the temperature profiles form an elongated and wide temperature envelope. The temperature envelope is more narrow and compressed in the case of gaining reaches.

2.9.3 Theoretical Background:

The underlying theory in using streambed temperature measurement to determine ground water flux is based on modeling the combined process of heat conduction and advection resulting from movement of water in the interstitial spaces of the sediment matrix. The

combined heat-fluid transport equation is used to estimate stream-groundwater interaction. Pioneering work done in the early 1960s by Suzuki, Stallman, Bredehoeft and Papadopulos et al (Suzuki 1960, Stallman 1965, Bredehoeft and Papaopulos 1965) laid the foundation for using streambed temperature measurement to estimate GW-SW flux. The heat transport equation that defines the movement of heat in porous media is linked to fluid flow in porous media by the velocity term in Darcy's law.

2.9.4 Darcy's Law

Darcy's law states that the volume of water, Q, passing through a homogenous column of sand is proportional to:

- The cross-sectional area of the column, A
- The difference in water level elevation at inflow and outflow of the column, (h_1-$h_{2)}$, the hydraulic head of the column
- The inverse of the length of the column, L

$$Q = KA\frac{h_1 - h_2}{L} \tag{0.10}$$

$$q = \frac{Q}{A} = K\nabla H \tag{0.11}$$

Where K is a coefficient of proportionality called the hydraulic conductivity of the porous media, q is the seepage flux with units L/T and ∇H is the hydraulic gradient, $\frac{h_1-h_2}{L}$. K defines the ability of fluids to flow through a soil matrix and is dependent on both soil properties and fluid properties. The soil properties include, grain size distribution, grain shape, tortuosity, specific surface and porosity. The effect of soil matrix properties on hydraulic conductivity is lumped together in a coefficient called the hydraulic

permeability of the medium, k. Hydraulic conductivity and permeability are related by the following expression:

$$K = k\frac{\rho g}{\mu} = \frac{kg}{\nu} \tag{0.12}$$

Where g is the acceleration due to gravity, μ and ν are dynamic and kinematic viscosities of the fluid respectively. The dimension of K is L/T with commonly used units of m/d, cm/s, and cm/d. The hydraulic permeability has dimension of L^2 with commonly used units of cm^2, m^2. Both ρ and μ are temperature dependent and temperature has a profound effect on the hydraulic conductivity of the medium and the temporal variability of groundwater fluxes. Jaynes et al (Jaynes 1990) observed increased infiltration rates from a pond in the afternoon and minimum infiltration rates at night. Warming of the water column and streambed in the afternoon and the resultant increase in hydraulic conductivity of the medium can increase the GW-SW exchange.

2.9.5 Heat Transport in porous media:

Heat transport in porous media occurs by three processes: conduction, convection and radiation. Conduction is the process of heat transport caused by a temperature gradient. Fourier's law describes the conduction of heat as follows,

$$H = -\kappa \nabla T$$

The heat flux between two points, H is directly proportional to the thermal gradient ∇T where κ is the constant of proportionality called thermal conductivity, which is a property of the medium. Convective heat transport refers to the movement of heat associated with the bulk movement of ground water. There are two type of convective transport, free and

forced convection. Forced convection occurs when external forces are at play such as movement of groundwater in the absence of density differences. Darcy's law is applicable in such cases. Free convection is the movement of groundwater caused by density gradients. Free convection is encountered in the subsurface geothermal systems caused by geothermal heating of groundwater. Forced convection is normally encountered at shallow depths typically near the sediment water interface and in shallow aquifer. A mixed convection zone develops in the transition zone between the shallow subsurface and the geothermal zone. This transition zone has both free and forced convection. Radiation refers to the heat emitted by a substance in response to the temperature of the body. Such radiative heat transfer is negligible in the surficial zone.

The three dimensional differential equation for simultaneously non-steady heat and fluid transport (HFT) through a homogeneous porous medium is given by Eq 2.13 (Bredehoeft and Papaopulos 1965) assuming that the temperature of the fluid and solid are at thermal equilibrium

$$\frac{\partial^2 T}{\partial x^2} + \frac{\partial^2 T}{\partial y^2} + \frac{\partial^2 T}{\partial z^2} - \frac{c_w \rho_w}{\kappa_e}\left[\frac{\partial (v_x T)}{\partial x} + \frac{\partial \left(v_y T\right)}{\partial y} + \frac{\partial (v_z T)}{\partial z}\right] = \frac{c\rho}{\kappa_e}\frac{\partial T}{\partial t} \qquad (0.13)$$

Where,

T = Temperature at any point at time t (K)

c_w = Specific heat of water (J/[g * K])

ρ_w = Density of water (kg/m^3)

c = Specific heat of saturated sediment matrix (J/[g * K])

ρ = Density of saturated sediment matrix (kg/m^3)

κ_e = Thermal conductivity of saturated sediment-fluid matrix (W/m. K)

v_x, v_y, v_z = Components of fluid velocity or seepage velocity in the *x, y* and *z* direction

x, y, z = Cartesian coordinates

t = Time since start of flow (s)

For the one-dimensional (1D-HFT) case with flow in the z (vertical) direction the Eq 2.13 simplifies to the following form:

$$\frac{\partial^2 T}{\partial z^2} - \left[\frac{c_w \rho_w v_z}{\kappa_e}\right]\left(\frac{\partial T}{\partial z}\right) = \frac{c\rho}{\kappa_e}\frac{\partial T}{\partial t} \tag{0.14}$$

or

$$\frac{\partial T}{\partial t} = \frac{\kappa_e}{c\rho}\frac{\partial^2 T}{\partial z^2} - \left[\frac{c_w \rho_w v_z}{c\rho}\right]\left(\frac{\partial T}{\partial z}\right) \tag{0.15}$$

$$\frac{\partial T}{\partial t} + \left[\frac{c_w \rho_w v_z}{c\rho}\right]\left(\frac{\partial T}{\partial z}\right) = \frac{\kappa_e}{c\rho}\frac{\partial^2 T}{\partial z^2} \tag{0.16}$$

The 1D-HFT equation (2.15) is analogous to the 1D advection-diffusion equation (1D-ADE) written as follows.

$$\left(\frac{\partial C}{\partial t}\right) = D\frac{\partial^2 C}{\partial z^2} - U_x\left(\frac{\partial C}{\partial x}\right) \tag{0.17}$$

The second term in Eq 2.15 represents heat transport by conduction and thermal dispersion and is analogous to the diffusion/dispersion (second) term in 1D-ADE (2.17). The term κ_e thus represents the conduction of heat through the solid matrix and thermal

dispersion caused by velocity changes in the interstitial spaces of the sediment. The following equation relates κ_e to the effective thermal conductivity of the medium, κ_o.

$$\eta = \frac{\kappa_e}{\rho c} = \frac{\kappa_o}{\rho c} + \alpha^* |q| \qquad (0.18)$$

Where $\kappa_o = n\kappa_w + (1-n)\kappa_g$, is the effective thermal conductivity of the solid-fluid matrix, n is the porosity, κ_w is the thermal conductivity of fluid, κ_g is the thermal conductivity of solid phase. Thermal conductivity has units of (W/m°C) watts (J/s) per degree Celsius per meter. From the above relationship it is clear that the thermal conductivity is dependent on the porosity and level of saturation in the sediment-fluid matrix. The values of thermal conductivity range from 0.2 W/m°C in the case of dry sediments up to 4.5 W/m°C for sandstone whereas that of water, κ_w, is 0.6 W/m°C. Similar to effective thermal conductivity, the heat capacity of the sediment-fluid matrix is given by, $\rho c = n(\rho_w c_w) + (1-n)\rho_g c_g$, where ρ_w, c_w, ρ_g, c_g are the heat capacity and density of the fluid and solid phase respectively. The term $\kappa_o/\rho c$, is similar to the diffusion coefficient term in the 1d-ADE and represents thermal diffusivity. In equation (2.18) α^* represents the thermal dispersion and is analogous to the solute dispersivity term, where $|q|$ is the magnitude of the specific discharge. When there is no groundwater flow $\alpha^* = 0$ and $\kappa_e = \kappa_o$, the effective thermal conductivity. The thermal diffusivity ranges from 10^{-2} to 10^{-3} cm^2/s, whereas the molecular diffusion coefficient values are around 10^{-6} cm^2/s. The contribution of thermal dispersivity, α^*, to heat transport is thus negligible and is typically assigned a value zero (Hopmans, Šimunek, and Bristow 2002, Bear 2013) . The thermal conductivity of different porous media is shown in Table 2.7 and fall within a short range for saturated sediments.

The third term in equation (2.15) represents transport of heat by moving water (convection) and is analogous to the advection term in equation (2.17). There are three types of convection, free, forced and mixed convection. Forced convection is the predominant mechanism in sediment pore water and refers to heat transfer induced by groundwater flow in the interstitial spaces. Mixed convection refers to heat flow induced by both free and forced convection. The Peclet number gives the relative magnitude of convective heat transport in comparison to conductive transport given by equation (2.19). Peclet number (Pe) is the ratio of heat transfer by convection to heat transfer by conduction in a sub-surface environment. The Peclet number is also used in solute transport model and is defined as the ratio of advective to dispersive transport. The heat transport equation and ground water flow equations are linked by the velocity term in both equations.

$$Pe = \frac{c_w \rho_w q L}{\kappa_e} \tag{0.19}$$

Table 0.7 Thermal Conductivity of different materials (Anderson 2005, Domenico and Schwartz 1998)

Material/Phase	Thermal Conductivity (W/m°C)
Dry Sediments	0.18 – 0.26
Saturated sediments	1.4 – 2.2
Shale	1 – 2
Water	0.46
Air	0.025
Clay	0.84 – 1.26
Quartz	8.37
Dolomite	1.67 – 4.19
Sandstone	2 – 4.5
Limestone	2 – 4
Granite	3 – 4
Basalt	1.5 – 2.5

The thermal conductivity of saturated sediments falls within a short range of 1.4 – 2.2 and an appropriate value can be assumed for modeling purposes. This enables heat tracer technique to be a powerful tool for inexpensive and convenient long term monitoring of ground-water surface water interaction at the SWI.

Investigators have taken two approaches to solve the heat transport equation to estimate groundwater fluxes. Initial contribution by researchers in this area (Suzuki 1960, Stallman 1965, Becker et al. 2004, Silliman and Booth 1993) focused on an analytical approach to solve the problem assuming appropriate boundary conditions. More recent research has utilized computer programs with numerical solutions and more complex boundary conditions. There are several numerical models with codes and graphical user interface that are available to model heat transport in a shallow aquifer including VS2DH, SUTRA, HST3D and FEFLOW.

2.10 Analytical Solutions to Heat Transport Equation to estimate GW-SW exchange

2.10.1 Analytical solution using Harmonic Temperature Fluctuation

Suzuki (1960) was the first to use sediment temperature measurements to estimate percolation of water in a rice field. Temperature measurements were taken using sensors and the following solution applies of 1D steady state HFT. If the temperature variation at the surface exhibits a pattern similar to a simple harmonic fluctuation, the solution for sediment temperature measured as a function of depth is given as

$$T = T_0 + Ae^{az}\sin\left(\frac{2\pi t}{T} - bz\right) \tag{0.20}$$

Where

$$a = \left[\frac{\pi c\rho}{T\kappa}\right]^{1/2} - \frac{v_z}{2\kappa} + the\ second\ order\ of\ v_z/2\kappa \tag{0.21}$$

$$b = \left[\frac{\pi c\rho}{T\kappa}\right]^{1/2} + the\ second\ order\ of\ v_z/2\kappa \tag{0.22}$$

T_0 = Mean temperature

A = Amplitude of temperature wave at soil surface

"a" can be calculated, if the maximum and minimum temperatures T_1^+, T_1^-, T_2^+ and T_2^- at two different depths z_1, z_2, are known.

$$a = [\ln(T_1^+ - T_1^-) - \ln(T_2^+ - T_2^-)]/(z_2\text{-}z_1)$$

b can be calculated from the phase shift between two temperature waves at two different depths, where t_2 and t_1 are the time of occurrence of the maximum or minimum at depths z_2 and z_1 respectively.

$$b = 2\pi(t_2 - t_1)/T(z_2 - z_1)$$

Solving equations 2.21 and 2.22 the velocity of groundwater flow can be calculated as

$$v_z = 2\kappa_e(b - a) \tag{0.23}$$

2.10.2 Analytical Solution using Exponential Type Curves:

Bredehoeft and Papadopulos (1965) (Bredehoeft and Papaopulos 1965) constructed type curves to solve for seepage velocity. The method involves temperature measurements at three different depths; surface (z=0), at a depth z=h and at a depth z=L and assumes the following boundary conditions

$$T_z = T_0 \; at \; z = 0$$

$$T_z = T_L \; at \; z = L$$

Where

T_z= Temperature measurement at any depth z

T_0 = Temperature measured at the surface

T_L = Lowermost temperature measurement

L = Length over which temperature is measured.

The solution for Eq (2.15) applying the above boundary conditions is given as:

$$\frac{T_z - T_0}{T_L - T_0} = f(\beta, \frac{z}{L}) \tag{0.24}$$

Where

$$f\left(\beta, \frac{z}{L}\right) = \frac{\left[\exp\left(\frac{\beta z}{L}\right) - 1\right]}{[\exp(\beta) - 1]} \quad (0.25)$$

$$\beta = c_0 \rho_0 v_z L/\kappa \quad (0.26)$$

β is positive or negative depending on the direction of movement of groundwater and is similar to the Peclet number. Bredehoeft et al constructed type curves for $f\left(\beta, \frac{z}{L}\right)$ for a practical range of values. The groundwater velocity is calculated from Eq 2.25 ($v_z = \beta\kappa/c_0\rho_0 L$). The ratio $\frac{T_z - T_0}{T_L - T_0}$ of the measured values of temperature is plotted in the x-axis and z/L is plotted in the y-axis and compared with type curves to get appropriate values of β, from which the velocity can be calculated.

2.10.3 Analytical solution for Temperature Profiles in a stream

Schmidt et al (Schmidt, Bayer-Raich, and Schirmer 2006) used Bredehoeft and Papadopulos one-dimensional solution to study GW-SW interaction in a 220 m long stretch of a man made stream in Germany. Temperature profiles were measured along two transects 3 m apart with a total of 140 measurements. Streambed temperatures were recorded at 0, 0.1, 0.15, 0.2, 0.3 and 0.5 m for each profile. The solution for ID-HFT is given as:

$$\frac{T_z - T_0}{T_L - T_0} = \frac{\left[\exp\left(\frac{c_0 \rho_0 v_z}{\kappa} z\right) - 1\right]}{\left[\exp\left(\frac{c_0 \rho_0 v_z}{\kappa}\right) - 1\right]} \quad (0.27)$$

Where, T_L is the observed temperature at a large depth (L) beyond the influence of diurnal temperature variations at the surface, T_0 is the surface temperature and T_z is the temperature at model depth. The above equation can be solved for v_z, assuming that the

change in measured temperature is only a function of v_z. An objective function of the form below can be formulated using Eq 2.27.

$$Error_k(L) = \sum_{j=1}^{5}\left[T_{jk} - \left(\frac{\exp\left(\frac{c_0\rho_0 v_{zk}}{\kappa} z\right) - 1}{\exp\left(\frac{c_0\rho_0 v_{zk}}{\kappa}\right) - 1}(T_L - T_0) + T_0\right)\right]^2 \qquad (0.28)$$

Where v_{zk} is the value of v_z, that minimizes the $Error_k(L)$ for a given L. For each measured temperature profile (k), a value for v_{zk} can be computed that minimizes the error function (Eq 2.28). Schmidt et al (2006) also tested the influence of L on the computed v_{zk} using profile data with different values of L ranging from 0.6 to 10m and concluded that for L greater than 1 m the value of v_{zk} is independent of L.

To test the quality of fit, the difference between observed and simulated temperature ΔT was calculated as,

$$\Delta T = T(z) - \frac{\left[\exp\left(\frac{c_0\rho_0 v_z}{\kappa} z\right) - 1\right]}{\left[\exp\left(\frac{c_0\rho_0 v_z}{\kappa}\right) - 1\right]}(T_L - T_0) + T_0$$

Using this method, the groundwater flux can be calculated using a single temperature profile measurement.

2.10.4 Silliman's Analytical Solution for time series dataset.

Silliman et al (Silliman and Booth 1993) presented an analytical solution to estimate flux through the SWI for a time series of temperature profile. The solution is based on the assumption of one-dimensional recharge conditions with temperature changes in the sediment induced by temperature perturbations at the SWI. Although Silliman et al reported that this method can be utilized only for recharge conditions, Becker et al

(Becker et al. 2004) demonstrated the applicability of the mathematical solution for both recharge and discharge conditions.

Using the one-dimensional heat transport equation with the following boundary conditions,

$$T(x,0) = 0$$

$$T(0,t) = \Delta T_w$$

$$T(x \longrightarrow \infty, t) = 0$$

The solution for equation 17 is given by:

$$T(x,t) = \frac{\Delta T_w}{2}\left[erfc\left(\frac{x - Zt}{2\sqrt{Dt}}\right) + exp\left(\frac{Zx}{D}\right) erfc\left(\frac{x + Zt}{2\sqrt{Dt}}\right)\right] \quad (0.29)$$

Where

$$Z = n\beta v_z \quad (0.30)$$

$$\beta = \frac{\rho_o c_0}{\rho c} \quad (0.31)$$

$$D = \frac{\kappa}{\rho c} \quad (0.32)$$

The erfc is complimentary error function and D is the thermal diffusivity (cm^2/s). In the analysis of time-series temperature profile, as temperature is not known at all times at any point x, the above equation is written in time steps. If ΔT_{wi} is the change in surface water temperature for a time interval of $t_i - t_{i-1}$, the solution for the above equation is given as:

$$\Delta T_{wi} = \Delta T_w(t_i) - \Delta T_w(t_{i-1}) \tag{0.33}$$

The above equation represents the incremental temperature change rather than the actual temperature. To obtain the actual temperature, a reference temperature of T_0 is assumed and solution is given by,

$$T_i(\tau) = T_0 + \sum T_i(x, \tau) \tag{0.34}$$

Becker et al successfully applied Silliman's solution to predict groundwater water surface water interaction using in both losing and gaining reaches.

CHAPTER III EFFECT OF SEDIMENT CAPPING ON GAS EBULLITION RATES AND TEMPERATURE DYNAMICS IN A POLLUTED URBAN RIVER

3.1 Abstract

The West Branch Grand Calumet River (WBGCR) reach 1 and 2 is part of one of the areas of concern (AOC) in the Great Lakes watershed identified by the USEPA. Dredging followed by sediment capping was used at the WBGCR to isolate the contaminated sediment and minimize exposure. Biogenic gas production is a major problem associated with capping as it can negatively impact its effectiveness by enhancing contaminant transport through partitioning into gas phase, formation of preferential fracture pathways and possible cap failure. We measured gas ebullition rates along with environmental variables such as water depth and sediment temperature at twelve monitoring stations prior to and for three years after capping to assess the effectiveness of active capping in controlling gas production. Long-term laboratory incubation studies were also preformed to evaluate the gas production potential of the cap and sediment material. These data were used to identify factors influencing post-cap gas production rates. The study indicates the active-cap and armoring layer can rapidly transport heat to the contaminated sediment zone in contrast to previous suggestions in the literature. Warming of the underlying sediment has the potential to enhance gas production rates post-capping. Mean post-capping gas fluxes in the two reaches were lower than pre-capping gas fluxes, with rates varying from 7.5 – 20 mmol/m^2/d, compared to a mean pre-capping flux of 46 mmol/m^2/d. Post-capping gas ebullition rates were influenced by changes in sediment temperature, water depth, biodegradability and organic matter (OM) content of the

contaminated sediment layer and the presence of newly deposited organic rich sediment on top of the cap. The mean gas fluxes generally increased over the three post-capping years with the magnitude of increase varying by site and environmental factors. Sites GCR 11-13 located closer to a CSO outfall had higher gas fluxes between 1 – 87 mmol/m^2/d. Mean gas flux at sites GCR 1-10 ranged between 1-28 mmol/m^2/d, except for site GCR6 which had very high values (22-360 mmol/m^2/d). Multivariate regression analysis and comparison of sediment characteristics revealed that gas fluxes were higher at sites with higher OM content and lower Arrhenius activation energy (E_a) in the contaminated sediment (CSed) zone. Incubations indicate that biogenic gases originated from both the newly deposited layer and CSed, with most gas production in the latter due to the greater volume of material available for degradation. Although the new deposition was more biodegradable with lower E_a values, the CSed layer had nine times more organic matter and produced more gas per unit weight of sediment. As expected little or no gas was produced in the cap armoring layer and organoclay. The results demonstrate that gas ebullition from the CSed will continue post-capping. These findings emphasize the need for engineered systems to vent sediment gases produced under the cap and ensure that the cap removes contaminants from gas bubbles prior to release.

3.2 Introduction

Sediment contamination is a major problem in the United States with estimates > 10^9 m^3 of contaminated sediments spread across 70% of US watersheds (USEPA 1987). Several strategies for remediation of contaminated sediments have been implemented, including monitored natural recovery, *in-situ* capping, dredging with sediment treatment or disposal in a landfill. More recently, *in-situ* capping has emerged as an effective remediation

strategy and has been implemented at many sites (Reible et al. 2006, Rockne and Kaliappan 2013, Zhu et al. 2015, Huls and Costello 2005). Biogenic gas (CH_4, CO_2, N_2) production from the degradation of organic matter underneath the cap may cause cap rupture and enhance transport by formation of preferential pathways and pore water mixing (Yuan, Valsaraj, and Reible 2009). Gas ebullition rates in sediments are influenced by several factors including temperature, ground-water flux and water depth (Zhu et al. 2015, Martens and Val Klump 1980, Christensen et al. 2003). Gas fluxes from natural environments exhibit large variability with reported fluxes ranging from 2-450mmol/m^2/d in urban waterways (Zhu et al. 2015), 16.8 mmol/ m^2/d, in estuarine sediments (Martens and Val Klump 1980), 2.5-26 mmol CH_4/m^2/d in wetland sediments (Chanton, Martens, and Kelley 1989) and 63 mmol CH_4/m^2/d in a Swiss reservoir (DelSontro et al. 2010). The additional weight of the cap material along with its typically increased hydraulic conductivity compared to native sediment, may enhance nutrient transport to biota in deeper sediments (Fendinger, Adams, and Glotfelty 1992), and thus potentially enable gas production even after controlling new organic matter input. The impact of capping on continued gas ebullition from underlying contaminated sediment and the associated ebullition-facilitated transport of hydrophobic contaminants is yet to be studied in detail at the field scale space (Yuan, Valsaraj, and Reible 2009, Viana, Yin, and Rockne 2012). Further there are few studies on the long term monitoring of post-capping gas ebullition rates (Zhu et al. 2015). This study was thus performed to validate the effectiveness of an active-cap in controlling biogenic gas production and identify the primary zone of post-cap gas production. We also utilized multivariate regression analysis of sediment physical characteristics along with field and laboratory measured

environmental variables, to identify factors influencing the post-cap gas production rates.

3.3 Materials and Methods

3.3.1 Site Description

The Grand Calumet River (GCR) has been heavily contaminated in the past century by both point and non-point sources including fifteen CSOs, thirty-nine industrial outflows, urban runoff and leachate/overflow from landfills and ponds in the surrounding watershed (Brannon et al. 1989). The study area consists of a 1.3-mile long stretch of the West Branch of the GCR (WBGCR) located just south of Lake Michigan close to the Illinois-Indiana border. The 20-MGD Hammond Sanitary District (HSD) and 48-MGD East Chicago Sanitary District (ECSD) wastewater treatment plants (WWTPs) discharge treated effluent into the WBGCR with industrial inflow contributing to 10% and 24% of the total inflow, respectively (Brannon et al. 1989). Both WWTPs are known to have released metals, polycyclic aromatic hydrocarbons (PAHs) and other toxic contaminants into the WBGCR (Sultrac 2010), with discharges contributing up to 90% of the water flow in the river (USEPA 2015, Battelle 2012). The study area is separated into two reaches with the western Reach-2 extending east from Columbia Av. to I-90 interstate bridge, and Reach-1 extending further east from the I-90 bridge to Indianapolis Blvd. The width of the WBGCR in the two reaches ranges between 50-70 m with a typical depth of 0.6-1 m. Twelve sample stations were monitored in the study. Sites GCR1-6 are located in Reach-1 and sites GCR8-13 are located in Reach-2 (Figure 3.7). Site GCR8 was left uncapped due to the presence of an underwater petroleum pipeline in the vicinity. HSD discharges treated effluent into WBGCR between sites GCR 10 and 11 where it flows westward, resulting in markedly improved water quality east of site GCR11. A stagnant

water column created by a sheet pile at the east end of Reach 2 resulted in minimal mixing and flow between sites GCR11 to 13 and anaerobic conditions with poor water quality. A CSO located near GCR 13 discharges untreated sewage and runoff during rain events, further impairing water quality upstream of the outfall. CSOs, algal photosynthesis and vegetation lining the banks of the river are the primary source of new organic matter and sediment input into the river system. The remediation project involved dredging the top 60cm of contaminated sediment followed by capping with 15 cm organoclay barrier and 25 cm sand/gravel armoring layer (USEPA 2015, Battelle 2012). Dredging started in 2011 and the cap was in place by spring 2012. Field data collection was performed each year from September to November. Pre-capping monitoring was completed in 2010, and three years of post-cap monitoring was completed from 2012 – 2014. These time periods were chosen to include a wide range of sediment and water column temperatures during the study.

3.3.2 Gas Flux Measurement

Gas traps were fabricated using PVC tubing and other fittings. The design was based on a modification to those described in Huttunen et al (Huttunen et al. 2001) and Viana et al (Viana, Yin, and Rockne 2012) for use in the shallower water depths in the WBGCR. The gas trap consisted of a 25 cm or 18 cm diameter funnel, attached to a hollow PVC frame constructed using 2.5 cm inside diameter pipes, forming a U-shaped structure with two legs that could either be pushed into the riverbed or placed on concrete footings. A ball valve with a narrow opening was attached to the top of the PVC frame to measure the volume of accumulated gas (**Figure 3.1)**. Footings were fabricated by placing a 60 cm long, 5cm diameter hollow PVC tube in a hollow concrete block and the void was filled

with concrete to bind the two components together. The gas trap was placed into the hollow PVC pipe in the two footings, allowing the gas trap to move vertically, making it height adjustable. The funnel was positioned at approximately mid-depth in the water column by securing the gas traps to the footing at the appropriate height using duct-tape. Glass wool placed inside the funnel allowed for the measurement of ebullition-facilitated contaminant flux by letting gas bubbles to pass through and entrain contaminants on the gas bubble surface and any sediment particles transported with it (Viana, Yin, and Rockne 2012). The entire trap was carefully lowered into the riverbed, the system purged of air, and the ball valve closed to collect gas released from the sediment. Field gas measurements were performed at regular intervals by placing an inverted water filled 1000 ml-graduated cylinder over the ball valve opening and allowing the accumulated gas to move into the cylinder and displace the water inside. Volumetric gas measurements were converted to mmol of gas to account for the compressibility of gas and fluxes are reported in mmol/m^2/d.

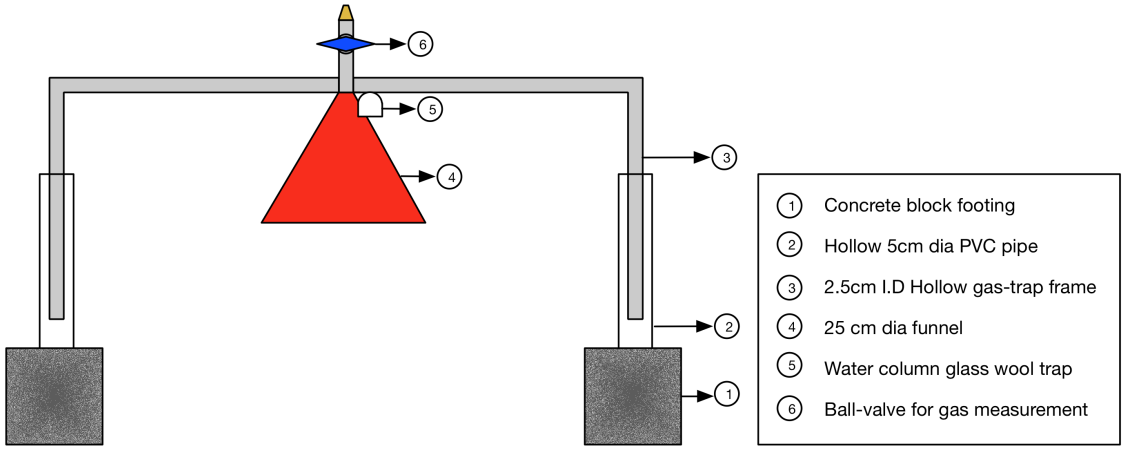

Figure 0.1 Gas collection system comprised of two concrete-block footings supporting the hollow PVC gas collection frame, fitted with a funnel and ball valve for gas measurement.

3.3.3 Sediment Sampling and Analysis

Prior to capping, sediment grab samples were taken at all sampling stations using a 9-inch Ponar dredge sampler and homogenized in a HDPE bucket. A 50 ml subsample was placed in a clean glass jar for sediment physical characterization to measure bulk density, percent moisture, organic matter (OM) and organic carbon (OC) using methods described in Borrel et al (Borrel et al. 2012). Eight months after capping, two intact sediment cores were sampled in each Reach at sites GCR 2, 6, 11 and 13 by pushing a 5 cm inside diameter HDPE tube into the riverbed, as described by Rockne et al (Rockne and Brezonik 2006). Four distinct layers were sectioned: a new-deposit (ND) layer, gravel armor layer (GAL), the organoclay (OrgC) cap and the underlying contaminated sediment (CSed) layer. These layers were homogenized for physical characterization as discussed above. The thickness of the cap layers and new deposit varied widely between reaches, with cap thickness ranging from 32-38 cm in Reach1 and 23-25 cm in Reach 2. New deposition was predominant in Reach 2 with accumulation of up to 6 cm of new organic rich sediment.

3.3.4 Sediment Incubation Study:

Sediment incubations were prepared in duplicate using homogenized sediment sectioned from the aforementioned layers with the exception of the armoring layers, where large gravel particles were excluded from the incubation. Sediment incubations were performed in 120 ml serum bottles filled with butyl rubber stopper and autoclaved and deoxygenated site water, prepared by simultaneous boiling and purging with O_2 free N_2

gas (Butler, Schoonen, and Rickard 1994). Anaerobic resazurin solution (0.1 ml of a 1 g/L solution) was added to site water as anaerobic indicator (Mittal and Rockne 2008). With minimal air exposure, 10 g of wet sediment was mixed with 10 ml of deoxygenated site water in the serum bottle and the head spaced was purged with N_2 gas for three minutes (Dubey et al. 2014) . The serum bottles were closed immediately with butyl rubber stoppers, crimped and incubated upside down in a dark environment at 5, 15, 25 and 35°C. Kill controls were prepared in the in the same but with the addition of 10 ml of 37% formaldehyde solution to the sediment slurry and incubated at 25°C. Gas production was measured at 12, 35, 68, 110, 154, 194, 250, 316 and 369 days using a glass syringe. The rate constant at each temperature was calculated assuming first-order degradation of methanogenic substrate using the Fujimoto method and multivariate fit analysis using OriginPro (v9, OriginLab, Northhampton, MA) (Viana, Yin, Xhao, et al. 2007). The Arrhenius activation energy (E_a) representing the biodegradability of organic matter was calculated as described in Viana et al (Viana, Yin, Xhao, et al. 2007)

3.3.5 Sediment Temperature and Water Depth Measurement

Hobo pendent temperature loggers (UA-002-08) were used to measure sediment temperature data at 45-minute intervals for all post-cap monitoring years. The loggers were attached externally to 0.64 cm hollow PVC tubes at 0, 25 and 50cm depths and pushed through the cap. The data were used to calculate the average sediment temperatures between sampling events. Temperature at the sediment-water interface (SWI) was also measured during weekly sampling events by a glass thermometer on the riverbed. Water depth at each site was also recorded at the weekly sampling events. For sampling years 2013 and 2014, we utilized an In-Situ Rugged Troll 100 water depth

logger at site GCR9 to record water depth at 15-min intervals. The absolute water depth data were corrected for changes in atmospheric pressure using weather data from Lansing Airport located six miles from the site. The water depth measurements were used to calculate the water depth for all other sites in reference to that measured at site GCR9. The GCR9 logger data was adjusted with the average differential water depth at each site for 2013 and 2014 monitoring years, to reverse calculate the depth at all the corresponding sites. For monitoring years with no temperature or depth logger data, weekly field measurements were used for all statistical analyses.

3.4 Results and Discussion

3.4.1 Effect of Temperature and Water Depth

The post-capping streambed temperature decreased from 21-23°C in September to 14-16°C in late October (Figure 3.8). The progressive decrease in streambed temperature resulted in progressively lower gas fluxes over the monitoring period at all sites except GCR6. The HSD WWTP outfall had a strong influence on temperature at sites GCR 8, 9 and 10 immediately downstream, with higher mean temperatures during the sampling period (18.7-20.2, 18.7-20.3 and 18.9-20.2 °C in 2012, 2013 and 2014 respectively) and lower observed temperature fluctuations compared to the other sample sites (Table 3.1, SI). In comparison, sediment temperatures at sites upstream (GCR 11, 12 and 13) were relatively colder and had higher diurnal temperature fluctuations in response to heating of the water column. The mean temperature at GCR 11, 12 and 13 ranged between 17.5-17.9, 16-17.4 and 17.6-17.8 °C, respectively, for the three post-capping sampling campaigns. Although sites GCR 1-6 were not directly influenced by the plant outfall, they had lower diurnal fluctuations compared to sites GCR 11-13 in response to flowing

water from the HSD outfall. The mean temperature at sites GCR 1-6 ranged between 18.4-19.2, 18.3-19.4 and 17.1-18.4 °C for 2012, 2013 and 2014, respectively. Temperature is an important factor in biogenic gas production as microbial biokinetic rates have a strong dependence on temperature (Yin et al. 2010, Viana, Yin, Xhao, et al. 2007, Yuan, Valsaraj, and Reible 2009). Previous research (Reible et al. 2006, Huls and Costello 2005) suggested that a sediment cap can act as an insulating layer preventing heat transport to deeper sediment, thus limiting long-term gas production. The temperature differential between the surface (0 cm) and the 25 cm (in-cap) and 50 cm (below-cap) depths were compared pre-and post-capping for sites GCR6 and GCR11 using temperature logger data collected from Nov 2010 to March 2011 and Nov 2013 to March 2014. A paired t-test showed a statistically significant difference in pre-and post-capping temperature differential at the 95% confidence interval (CI) ($p< 0.001$) for both sites. A pre-capping temperature differential of 1.1 and 1.7°C was observed at the -25 cm and -50 cm depths respectively, compared to the post-capping differential of 0.4 and 1.1 °C, at site GCR6. The temperature differential at GCR 11 was largely similar to GCR6, while the temperature differentials at the two depths were significantly greater (1.4 and 2.6°C post-capping) at the uncapped site GCR8. The consistently lower temperature differential observed in the capped sites suggests that temperature changes in the water column are transported more rapidly to deeper sediment compared to the uncapped site GCR8. The slightly higher post-capping temperature differential for uncapped site GCR8 may be attributed to construction activity performed post-capping to protect an underlying petroleum pipeline located approximately 3 m from GCR8.

Observations of sediment texture during gas sampler deployment indicated that the

surficial sediment was relatively compacted with a clayey texture; in contrast to soft sediment observed prior to capping. Heat transport caused by convection and conduction depends on the physical and thermal properties of the medium such as thermal conductivity, heat capacity, and porosity (Anderson 2005). The sand/gravel cap material has a higher thermal conductivity value (≈3 W/m °C) (Farouki 1986) compared to that of the saturated sediment (≈1.4-2.2 W/m °C) (Anderson 2005). We therefore must conclude that no evidence supports the hypothesis of the cap acting as an insulator to restrict heat transport to the deeper underlying sediment. In fact, the cap appears to be more conductive to heat transport compared to underlying sediment. This has important implications for biogenic gas production rates, discussed below. Average water depth in the three years post-capping progressively increased from ~80 in 2012 to ~120 cm in 2014 (Table 3.5, Figure 3.9).

3.4.2 Pre- and Post-Cap Sediment Characteristics:

The OM content of the surficial sediment prior to capping ranged from 5-25%, with a mean of 14.2% (Table 3.2). Sites GCR 1, 2 and 5 had lower OM (5.2-7.4%) and the maximum OM was 25% at GCR6. The OC content ranged from 3.3-15.2% with a mean of 8.6%. Neither OM nor OC varied as function of distance from CSO. The various capping layers had greatly varying physical and chemical characteristics, necessitating sediment coring to accurately characterize this variability. OM of New-Deposit (ND), gravel armor layer (GAL), organoclay layer (OrgC), and underlying contaminated Sediment layer (CSed) ranged between 1.29-2.9%, 0.46-0.98%, 1.03-1.6% and 10.9-27%, respectively, in sediment cores from sites GCR2, 6, 11 and 13. Average OM of the CSed was 11, 22, 27 and 17% at sites GCR2, 6, 11 and 13, respectively. These values

were comparable to pre-capping surface grab values. The OC/OM ratio of ND sediment decreased from 0.7-0.9 at sites GCR13 and 11 to 0.3-0.45 at sites GCR2 and 6. While this is a limited dataset it would be consistent with a decrease in biodegradability with increasing distance from the CSO located near GCR13. The OC/OM ratio of CSed sediment ranged from 0.5 – 0.8, with a maximum value of 0.83 at site GCR6. Interestingly, GCR6 had the highest post-capping gas fluxes. High OM and OC/OM ratios at sites GCR6, 11 and 13 suggest that the underlying sediment is comprised of more highly biodegradable OM compared to GCR2. Descriptive statistics of all sediment parameters is presented in Table 3.1-2.

3.4.3 Comparison of Pre and Post-Capping Gas Fluxes:

Pre-capping gas fluxes were measured weekly at the twelve sites from 10/15/2010 to 11/4/2010. Only one complete week of sampling was possible at site GCR13 due to low water levels and thus these data were excluded from analysis. Mean pre-cap gas fluxes at the twelve sites varied between 11 to 81 mmol/m^2/d; with an upper and lower 95% CI of 59 and 33 mmol/m^2/d and a mean value of 46 mmol/m^2/d (Figure 3.3, Table 3.6). With one exception higher fluxes were observed typically in the first two weeks of sampling, with progressively lower fluxes as the sediment and water column temperature decreased. In contrast gas fluxes at GCR6 increased over the monitoring period accompanied by a decrease in the water level (**Figure 3.10**). This suggests gradual release of trapped biogenic gases from deeper sediment as the water level dropped, suggestive of a deeper depth of gas production at this site. The pre-capping gas fluxes varied though out the two reaches and did not exhibit any trend in relation to distance from the CSO. These gas ebullition rates were similar to those we have measured in the urban waterways,

Collateral Channel (CC) and Bubbly Creek (BC) in the fall (Viana, Yin, and Rockne 2012).

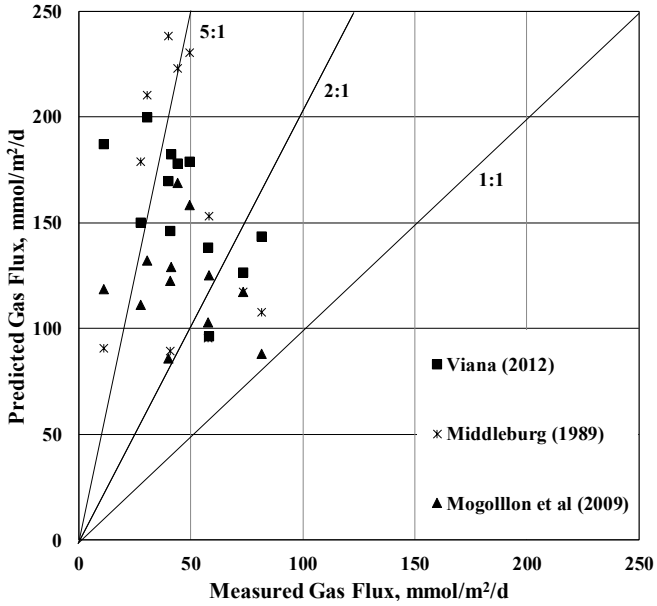

Figure 0.2 Comparison of measured pre-cap gas ebullition rates to three literature model predictions based on measured field condition.

The pre-capping gas fluxes were compared with predictions from three literature models to test their predictive capabilities (Viana, Yin, and Rockne 2012, Winterwerp and Van Kesteren 2004, Mogollón et al. 2009, Middelburg 1989). The literature models generally over-predicted gas fluxes by a factor of 2-5 (Figure 3.2). In general, the Middleburg (1989) model over predicted fluxes by the greatest amount, while the Viana et al (2012) and Mogollon et al (2009) performed best. Interestingly, the Mogollan model (developed for marine sediments) performed as well as or better than the Viana regression model which was developed from data in urban waterways. A likely reason for the latter model over-prediction was its basis on data taken from spring and summer in addition to fall and winter. The Viana study found a consistent increase in spring gas ebullition which was attributed to new OM deposition from leaf fall and other OM. Inclusion of these data in

the regression may result in over prediction for fall results.

Post-capping gas fluxes were measured weekly starting with Julian week 40, 39 and 36 in 2012, 2013 and 2014, respectively. All campaigns ended with Julian week 45. For the 2014 sampling season, only Julian weeks 39-45 were considered for comparison. In 2012, gas ebullition rates decreased on average by 84% compared to pre-capping levels, with a mean flux of 7.5 mmol/m^2/d (2.9-12 mmol/m^2/d U_{95}-L_{95} CI) (Table 3.6). The maximum weekly gas fluxes were 80.5, 66 and 54 mmol/m^2/d at sites GCR6, 11 and 13, respectively (Figure 3.10). Many large bubbling events were observed during field sampling, indicating release of accumulated biogenic gas through fractures in the cap. The higher weekly gas fluxes observed at some sites is thus likely attributable to gas ebullition from such stochastic events.

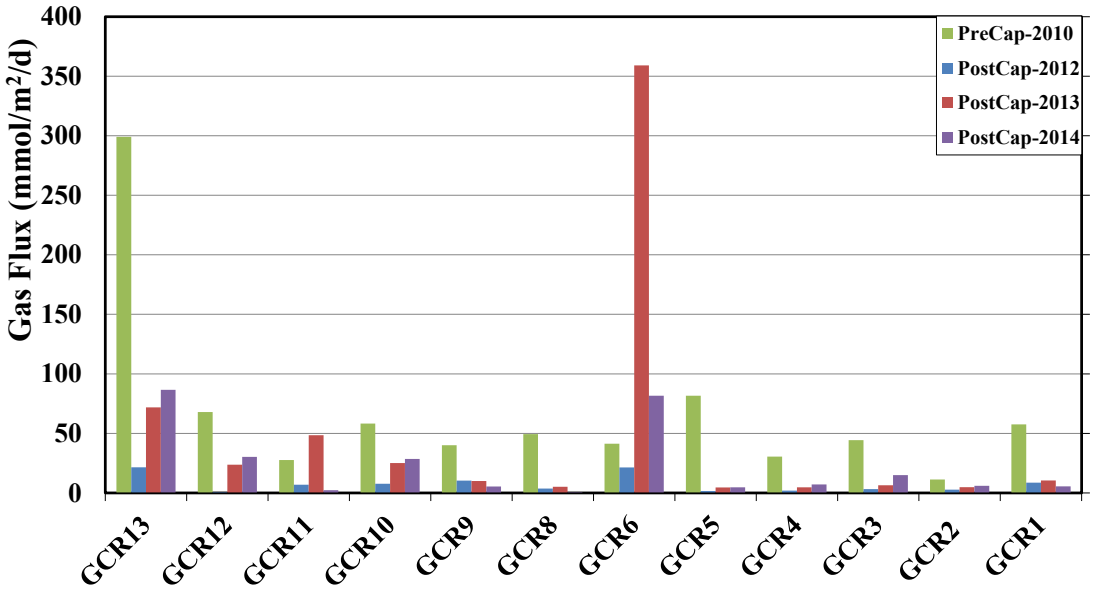

Figure 0.3 Average gas ebullition fluxes during pre-cap and post-cap sampling campaigns.

In the second year of monitoring, significantly higher gas ebullition fluxes occurred at GCR6, with an average flux of 360 mmol/m^2/d. This raises the question of where such

large ebullition events could originate from at site GCR6. The fact that OM content of ND sediment was similar across the study sites, coupled with its relatively thin depth, indicates that ebullition must originate in the CSed layer at GCR6. The mean seasonal gas flux of all sites (excluding GCR6) increased from 7.5 mmol/m^2/d in 2012 to 20 mmol/m^2/d in 2013, a 63% decrease compared to pre-capping levels. Interestingly, 2013 gas fluxes were higher than 2012, even though water depths increased by an average of 20 cm. The greater depth would result in a higher hydrostatic pressure, which would be expected to decrease ebullition. However, sediment temperatures typically increased, likely explaining the higher fluxes (Table 3.7). These observations suggest that a combination of factors including water depth and sediment temperature contribute to the change in gas fluxes.

In addition to physical processes, biological changes may play a role as well. It is possible that the microbial community structure was significantly changed by the 2013 monitoring season, almost twenty months post-dredging/capping. Sites GCR10, 11, 12 and 13 had marked increases in gas fluxes compared to the other study sites. Sediment coring in 2013 clearly showed a layer of newly deposited organ rich sediment above the cap at sites 10-13. This was likely due to high levels of photosynthesis in the quiescent pool to the west of site 10. In addition, we speculate the CSO located close to GCR13 was a significant source of new OM deposition in reach 2. These new deposits likely resulted in the higher gas production from degradation of the labile organic matter in the surficial sediment.

Ebullition fluxes in 2014 were typically similar or slightly higher compared to 2013 except for site GCR11. The mean seasonal gas flux was measured at 20 mmol/m^2/d with

95% CI of 11.9 and 28.6 mmol/m^2/d, respectively, a 60% decrease compared to pre-capping. Ebullition rates at sites GCR12 and 13 continued the increasing trend observed in the previous year, adding credence to our previous argument of greater OM deposition at these sites. Surprisingly, GCR11 showed a marked decrease in ebullition rate with mean flux lower than 2012 fluxes. We believe this is due to the stochastic nature of ebullition events, as gas bubbling was observed around this site throughout the sampling campaign. Site GCR6 continued to exhibit high ebullition rates with a mean flux of 82 mmol/m^2/d, around two times higher than pre-capping levels. Sites GCR1-10 exhibited average flux reductions in the range of 50-90% compared to pre-capping (Table 3.6). Interestingly, ebullition fluxes were similar or higher than 2013 although sediment temperature decreased by around 1.5 ºC and water depth increased by 25cm. This is suggestive of higher gas production in the ND layer and this trend is expected to continue as the thickness of the new deposit increases overtime. Gas flux at GCR8 was the lowest measured in all four monitoring years with flux of 0.71 mmol/m^2/d.

The seasonal gas fluxes reported in our study (7-22 mmol/m^2/d) are comparable to fluxes of 5-35 mmol/m^2/d reported by Zhu et al (Zhu et al. 2015). Although it has been argued (Reible et al. 2006) that gas ebullition rates will decrease over time following capping as the ebullition-active sediment is cut off (Yuan, Valsaraj, and Reible 2009), we did not observe that in the first three years post-capping. Ebullition either remained unchanged or increased from 2012 to 2014; particularly those in reach 2. This does not mean the cap was ineffective as post-cap fluxes were greatly reduced (with the exception of GCR6 in 2013), as shown in Figure 3.4. This study demonstrates that a focus on only one factor (e.g. temperature or sediment depth) and not all of the post remedial changes in the

system as a whole provide an inaccurate picture of future success.

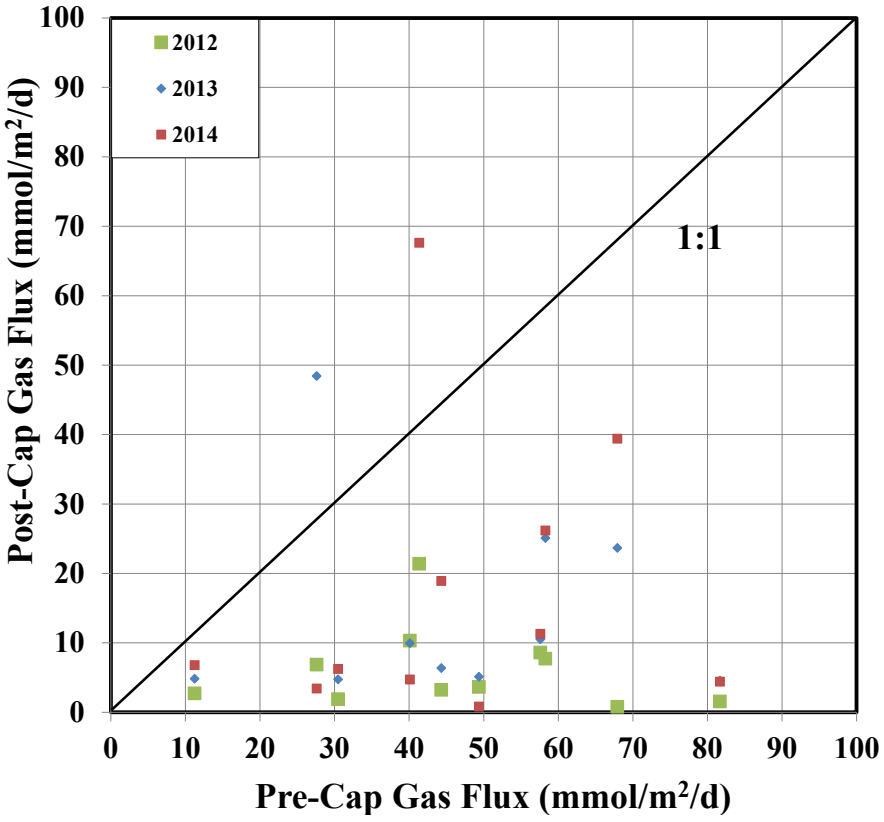

Figure 0.4 Comparison of pre- and post-cap average sampling campaign gas fluxes.

3.4.4 Underlying contaminated sediment is a significant source of gas production

The extensive field study revealed that ebullition rates generally increased over the three years. However, the source of gas generation was not evident from the field observations. To ascertain the primary zone of gas production, incubation experiments were performed on the ND, GAL, OrgC and CSed layers. Cumulative gas production (G_p) was recorded at 62 and 60 mmol/kg and 96 and 94 mmol/kg for ND and CSed layers respectively. GCR2 incubations produced the least gas among the four sites and is in line with low field measurements recorded at this site. GCR13 produced more gas in both ND and CSed layers explaining the higher field gas fluxes. GCR11 exhibited higher G_p in ND

layer measuring 126 mmol/kg compared to 82 mmol/kg in CSed (Figure 3.5). This may explain the low gas production observed in 2014 accompanied by drop in sediment temperature and increase in water levels. GCR6 performed differently to other sites with significantly higher gas production in the CSed (105 mmol/kg) layer, explaining the high field ebullition fluxes and corroborating our argument that sediment gases primarily originate in the CSed. Gas production in GAL and OrgC layers were much lower than other layers with G_p in the range of 30 – 35 mmol/kg, primarily produced from the OM fraction (<1%).

It is interesting to note that gas production in CSed incubations typically increased more rapidly with increasing incubation temperatures compared to ND (Figure 3.11). This suggests the CSed layer is expected to produce more gas at higher sediment temperatures This has significant implications on post-capping gas ebullition rates as higher gas production in CSed increases contaminant migration due to gas ebullition (McLinn and Stolzenburg 2009, Yuan et al. 2007). Also, post-capping ebullition facilitated fluxes are expected to be higher in the summer when sediment temperatures peak.

The rate constant k, d^{-1}, was calculated from the periodic gas production measurements for each incubation temperature. Temperature dependence of methanogenesis was modeled using Arrhenius equation to calculate the activation energy (E_a). Rate constant (k) and E_a values for all sections and incubation temperature is presented in Table 3.8. E_a is a measure of biodegradability of organic matter with lower values representing higher degradability. Values ranged between 10 – 24 KJ/mol for ND layer, 22 – 39 KJ/mol for CSed, 32 – 43 KJ/mol for GAL and 14 – 47 KJ/mol for OrgC layer. GCR6 registered the highest and lowest E_a values among the four sites for ND and CSed layers respectively,

further adding confidence to our previous argument of primary gas production occurring in CSed. Also, the low gas producing site GCR2 had the highest E_a (39KJ/mol) in CSed layer among the four sites, in the range of values observed for GAL and OrgC layers. G_p in GAL and OrgC layers were in the range of 31 – 39 mmol/kg ww with average E_a values of 37 and 31 KJ/mol respectively. The high E_a values and low gas production potential indicate there is limited gas production in the cap layers. The methanogenic E_a values from this study is in the range of 27 – 138 KJ/mol reported in literature (Thebrath et al. 1993, Prieme 1994, Viana, Yin, Zhao, et al. 2007).

The E_a and G_p data clearly parallels the filed data trend with higher gas production rates observed at sites with higher G_p and low E_a in the CSed layer. Cumulative gas production in CSed were in the range of values observed in the ND layer, although E_a values were slightly higher. This suggest that the gas production potential in CSed is comparable to that of ND layer due to the high OM content (17-27%) and OC/OM ratio. Although the CSed is more recalcitrant, the volumetric extent of the material is significantly larger compared to the ND layer (assuming a 1m ebullition active zone). Consequently, significant gas production is expected to originate from the CSed layer and it seems to be the factor controlling the variations observed in measured gas fluxes

From the field study it is not clear if the contaminated sediment zone would continue to produce gas over time. Long-term field monitoring is essential to understand the impact of deeper burial of the CSed layer as the depth of ND layer increases. Hyporheic flows can transport nutrients and dissolved organic carbon to the deeper contaminated sediment zone and can potentially contribute to gas production rates (Zhu et al. 2015, Huls and Costello 2005) even after several years of capping.

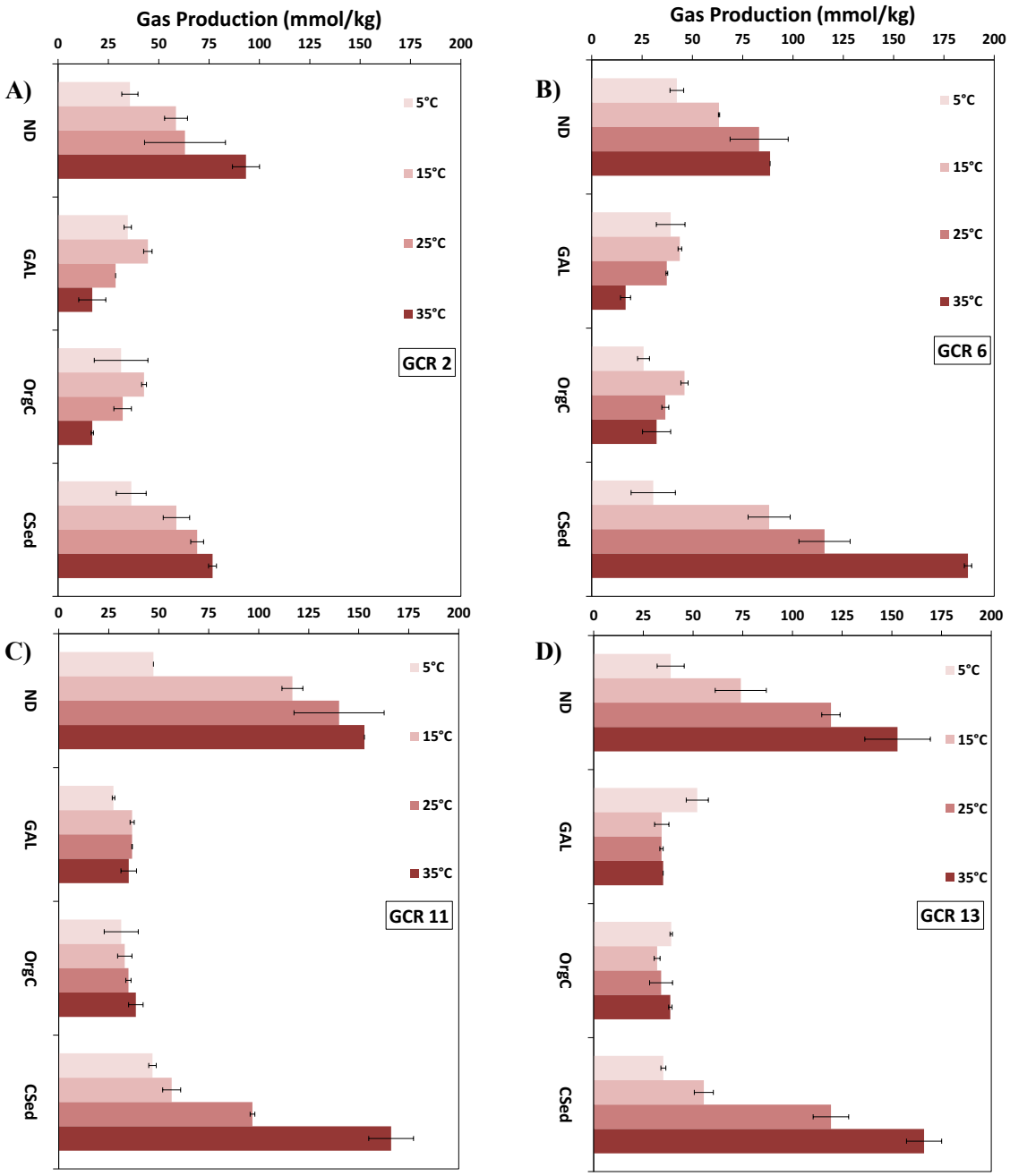

Figure 0.5 Total gas production for laboratory incubations of ND, GAL, OrgC and CSed over 369d as a function of sediment site and incubation temperature.

3.4.5 Modeling post-cap gas production rates

Mean seasonal post-cap gas fluxes (GF_{fall}) for sites with sediment cores; GCR 2, 6, 11, and 13; were regressed with environmental variables such as sediment temperature at 0 and -25cm depth (T_0 and T_{25}), water depth, sediment physical characteristics such as OM content, porosity, wet/dry bulk density and kinetic parameters including first order gas production rate constant (of ND, GAL, OrgC and CSed layers at 5, 15, 25 and 35°C) and Arrhenius activation energy (E_a) (Table 3.7). The dataset (n=17) was subject to a backward stepwise elimination procedure to determine the most significant explanatory variables. Factors including water depth, activation energy and organic matter content were eliminated and a simple linear relationship was found to exist between post-cap gas flux (mmol/m^2/d), first order gas production rate constant of CSed layer at 15°C (k_{15_CSed}) and sediment temperature at -25cm depth (T_{25}), accounting for 53% of the variability. All slopes and the constant were statistically significant with $p<0.05$.

$$GF_{fall} = -1543.89 + 114487.4 \times k_{15\_CSed} + 59.43 \times T_{25} \quad (p=0.006, R^2 = 0.53, n=17)$$

Comparison plot of predicted and measured gas flux is shown in Figure 3.6. Both explanatory variables were positively correlated with $k_{15\_ContSed}$ explaining 35% of the variability. Also the temperature recorded at the 25cm depth proved to be a better predictor, as deeper sediment has limited diurnal temperature fluctuations and is a more representative measure of average sediment temperature.

It is theorized that the ND and CSed contribute to the total filed measured gas flux at each site. The contribution of the ND layer was not captured in the regression analysis, as there was limited variability in the ND rate constants between sites and the volume of material being small compared to the CSed layer. Reiterating our previous observations,

the regression analysis further confirms our findings of the CSed layer controlling variations in post-cap gas fluxes. It is worth noting that the thickness of the ND layer monitored over time could be a potential explanatory factor in evaluating post-cap gas fluxes.

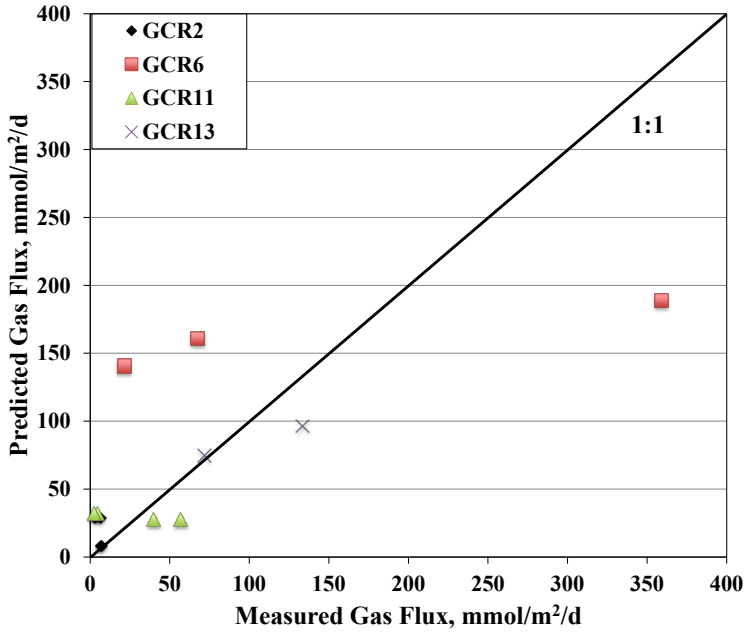

Figure 0.6 Comparison of predicted to measured gas fluxes for sites GCR2, 6, 11 and 13.

3.5 Conclusions

The HSD outfall regulated sediment temperature and OM deposition in the streambed, indirectly affecting gas production rates. Field measured ebullition rates decreased over the monitoring period for most sites in response to lowering of streambed temperatures towards late fall, except for GCR6. Comparison with literature models revealed that Viana et al and Mongollan et al model performed best although both models over predicted ebullition rates. Pre and post-cap temperature profiles showed that the cap does not act as an insulator as suggested by previous studies and is more conductive to heat transport than the native sediment. Capping reduced gas ebullition fluxes in the range of

60 – 80 % with higher fluxes observed at upstream sites GCR12 and 13. The E_a and G_p values of different layers of the cap were able to explain the variation in field measured gas ebullition rates. GCR6 exhibited an increase in gas ebullition rates with primary gas production occurring in the CSed layer. It is postulated that supply of nutrients and substrate to a previously buried ebullition active zone contributed to higher fluxes observed at this site. The low gas ebullition rates at GCR2 was attributed to low E_a and G_p of the ND and CSed layers. Similarly, higher fluxes at GCR13 were attributed to higher biodegradability and gas production potential of ND and CSed layers. Incubation study had several significant findings. Importantly, the experiment showed that the CSed layer could be a significant source of gas production at higher sediment temperatures. This was also observed in the 2013 dataset where gas ebullition rates increased in response to higher sediment temperature. Consequently, the gas fluxes and ebullition facilitated contaminant fluxes are expected to be higher in the summer when sediment temperatures peak. MLR revealed that post-capping fluxes were influenced by gas production rate constant for 15 °C and sediment temperature. The study showed that fluxes were influenced by post-remedial changes in field conditions including temperature, water depth, thickness of new deposition, biodegradability of OM and gas production potential of the CSed layer and focusing on just one of these factors would result in an inaccurate understanding of site specific gas ebullition rates. The increasing trend in gas ebullition rates over the three post-cap years' warrants continued field monitoring to better understand long-term impacts and ascertain whether CSed will continue to be ebullition active.

3.6 Supporting Information

Figure 0.7 A) Pre-capping and B) Post-capping aerial view of the study area.

Table 0.1 Descriptive statistics of streambed temperature data for 0cm depth. Negative temperature differences represent temperature increase in comparison to previous year and positive values represent temperature decrease.

2012	**GCR1**	**GCR2**	**GCR3**	**GCR4**	**GCR5**	**GCR6**	**GCR8**	**GCR9**	**GCR10**	**GCR11**	**GCR12**	**GCR13**
N of Cases	2036	2036	2036	2036	2036	2036	2036	2036	2036	2036	2036	-
Minimum	10.36	10.55	10.75	12.40	13.37	11.92	16.14	16.05	12.69	8.58	7.68	-
Maximum	23.29	23.48	23.58	23.68	23.58	23.39	23.68	23.58	23.39	22.91	21.95	-
Mean	18.36	18.65	18.78	19.05	19.23	18.89	20.17	20.28	20.19	17.48	15.98	-
SD	2.37	2.30	2.18	2.06	1.99	2.19	1.56	1.54	1.57	2.82	3.11	-
2013												
N of Cases	1511	1511	1511	1511	1511	1511	1511	1511	1511	1511	1511	1511
Minimum	14.23	14.71	11.14	15.86	16.81	14.23	17.00	17.38	17.48	12.30	10.94	12.88
Maximum	22.91	22.62	23.68	22.72	22.05	22.53	22.72	22.05	22.14	22.53	22.14	21.28
Mean	18.61	18.81	18.33	19.40	19.55	19.31	19.99	19.95	19.97	17.98	17.18	17.63
SD	2.55	2.48	2.97	2.12	1.87	2.21	1.75	1.62	1.56	3.09	3.15	2.80
$\Delta T_{2012\text{-}2013}$	**-0.25**	**-0.16**	**0.45**	**-0.35**	**-0.32**	**-0.42**	**0.18**	**0.33**	**0.22**	**-0.5**	**-1.2**	-
2014												
N of Cases	1516	1516	1516	1516	1516	1516	1516	1516	1516	1516	1516	1516
Minimum	10.94	11.43	9.57	13.27	12.01	13.65	11.82	11.53	12.01	13.65	13.75	14.71
Maximum	21.95	21.57	22.43	21.57	22.24	21.47	22.05	22.05	21.95	21.00	20.71	20.23
Mean	17.58	17.49	17.06	18.27	18.19	18.40	18.75	18.74	18.88	17.57	17.39	17.81
SD	2.37	2.34	2.68	1.85	1.94	1.78	1.69	1.67	1.58	1.93	1.89	1.63
$\Delta T_{2013\text{-}2014}$	**1.03**	**1.32**	**1.27**	**1.13**	**1.36**	**0.91**	**1.24**	**1.21**	**1.09**	**0.41**	**-0.21**	**-0.18**

Table 0.2 Descriptive statistics of streambed temperature data for -25cm depth. Negative temperature differences represent temperature increase in comparison to previous year and positive values represent temperature decrease.

2012	**GCR1**	**GCR2**	**GCR3**	**GCR4**	**GCR5**	**GCR6**	**GCR8**	**GCR9**	**GCR10**	**GCR11**	**GCR12**	**GCR13**
N of Cases	2,036	2,036	2,036	2,036	2,036	2,036	2,036	2,036	2,036	2,036	2,036	-
Minimum	10.55	11.14	10.46	14.90	13.85	14.33	15.76	15.57	14.80	10.55	14.80	-
Maximum	23.20	22.33	22.14	22.72	23.00	22.53	23.10	23.20	23.20	22.05	23.20	-
Mean	18.52	18.88	19.03	19.31	19.24	18.94	20.36	20.27	20.32	17.67	20.32	-
SD	2.32	2.11	2.09	1.70	1.90	1.92	1.10	1.46	1.48	2.43	1.48	-
2013												
N of Cases	1,511	1,511	1,511	1,511	1,511	1,511	1,511	1,511	1,511	1,511	1,511	1,511
Minimum	15.57	15.86	13.85	16.90	16.81	15.86	17.86	17.38	17.95	13.94	12.69	13.94
Maximum	22.05	21.86	22.33	22.43	22.05	21.95	21.76	22.05	22.14	21.86	21.47	21.09
Mean	18.90	19.00	18.61	19.81	19.55	19.49	20.12	19.95	20.23	18.32	17.53	18.01
SD	2.20	2.21	2.59	1.94	1.87	2.02	1.33	1.62	1.42	2.75	2.86	2.51
$\Delta T_{2012\text{-}2013}$	**-0.38**	**-0.12**	**0.42**	**-0.5**	**-0.31**	**-0.55**	**0.24**	**0.32**	**0.09**	**-0.65**	**2.79**	
2014												
N of Cases	1,516	1,516	1,516	1,516	1,516	1,516	1,516	1,516	1,516	1,516	1,516	1,516
Minimum	12.98	14.04	12.30	15.19	14.42	14.80	16.71	13.56	12.01	14.52	14.42	15.86
Maximum	21.00	21.00	21.28	20.81	21.00	20.81	20.42	21.57	21.95	20.42	20.23	19.66
Mean	17.82	18.04	17.55	18.48	18.39	18.45	18.97	18.85	18.90	17.72	17.64	18.09
SD	1.97	1.87	2.25	1.53	1.62	1.55	1.04	1.51	1.61	1.68	1.66	1.17
$\Delta T_{2013\text{-}2014}$	**1.08**	**0.96**	**1.06**	**1.33**	**1.16**	**1.04**	**1.15**	**1.1**	**1.33**	**0.6**	**-0.11**	**-0.08**

Table 0.3 Sediment physical parameters for pre-cap surface grab samples and post-cap cores from sites GCR2, GCR6, GCR11 and GCR13. Average values are presented for section depths corresponding to New Deposit (ND), Gravel Armoring (GAL), Organoclay (OrgC) and Contaminated Sediment (CSed) layers.

Sample	Parameter	Units	GCR13	GCR12	GCR11	GCR10	GCR9	GCR8	GCR6	GCR5	GCR4	GCR3	GCR2	GCR1
Pre-capping Surface Grabs	% Water	%	62.86	70.72	72.18	57.30	76.27	57.13	74.39	48.24	59.52	53.10	30.23	37.76
	ρ_b	g/cm^3	1.11	1.00	1.06	1.16	0.96	1.09	1.00	1.11	1.02	0.99	1.32	1.25
	Porosity	%	53.62	56.71	54.67	52.32	58.78	54.33	55.48	55.92	57.12	58.14	48.22	51.04
	OM	%	15.74	20.22	19.24	12.20	19.78	16.26	25.05	7.41	15.76	17.30	5.24	5.85
	OC	%	9.07	11.77	10.36	6.53	10.46	9.25	15.24	4.50	11.09	12.01	5.35	5.17
	BC	%	5.67	3.43	2.49	1.04	1.77	1.93	5.68	4.03	5.24	5.04	3.48	3.33
ND	% Water	%	40.80	_	46.04	_	_	_	30.36	_	_	_	27.71	_
	ρ_b	g/cm^3	1.56	_	1.51	_	_	_	1.74	_	_	_	1.83	_
	Porosity	%	61.95	_	66.47	_	_	_	55.33	_	_	_	47.66	_
	OM	%	2.26	_	2.96	_	_	_	2.46	_	_	_	1.29	_
	OC	%	2.10	_	2.20	_	_	_	1.13	_	_	_	0.44	_
	BC	%	0.07	_	0.19	_	_	_	0.07	_	_	_	0.07	_
GAL	% Water	%	13.07	_	19.63	_	_	_	12.46	_	_	_	11.88	_
	ρ_b	g/cm^3	1.97	_	2.03	_	_	_	1.91	_	_	_	1.92	_
	Porosity	%	36.18	_	38.23	_	_	_	36.82	_	_	_	35.34	_
	OM	%	0.54	_	0.98	_	_	_	0.47	_	_	_	0.46	_
	OC	%	0.20	_	0.37	_	_	_	0.79	_	_	_	0.17	_
	BC	%	0.02	_	0.07	_	_	_	0.03	_	_	_	0.05	_

Sample	Parameter	Units	GCR13	GCR12	GCR11	GCR10	GCR9	GCR8	GCR6	GCR5	GCR4	GCR3	GCR2	GCR1
OrgC	% Water	%	14.83	_	15.69	_	_	_	17.05	_	_	_	16.50	_
	ρ_b	g/ml	1.88	_	1.95	_	_	_	1.85	_	_	_	1.87	_
	Porosity	%	37.66	_	37.25	_	_	_	41.44	_	_	_	40.59	_
	OM	%	1.54	_	1.55	_	_	_	1.60	_	_	_	1.03	_
	OC	%	1.11	_	1.45	_	_	_	1.12	_	_	_	0.69	_
	BC	%	0.10	_	0.12	_	_	_	0.13	_	_	_	0.10	_
CSed	% Water	%	53.09	_	73.10	_	_	_	64.70	_	_	_	45.60	_
	ρ_b	g/ml	1.31	_	1.15	_	_	_	1.19	_	_	_	1.46	_
	Porosity	%	73.99	_	86.09	_	_	_	81.80	_	_	_	67.48	_
	OM	%	17.81	_	27.61	_	_	_	22.12	_	_	_	10.94	_
	OC	%	9.09	_	21.13	_	_	_	18.46	_	_	_	7.02	_
	BC	%	0.86	_	1.73	_	_	_	1.39	_	_	_	1.38	_

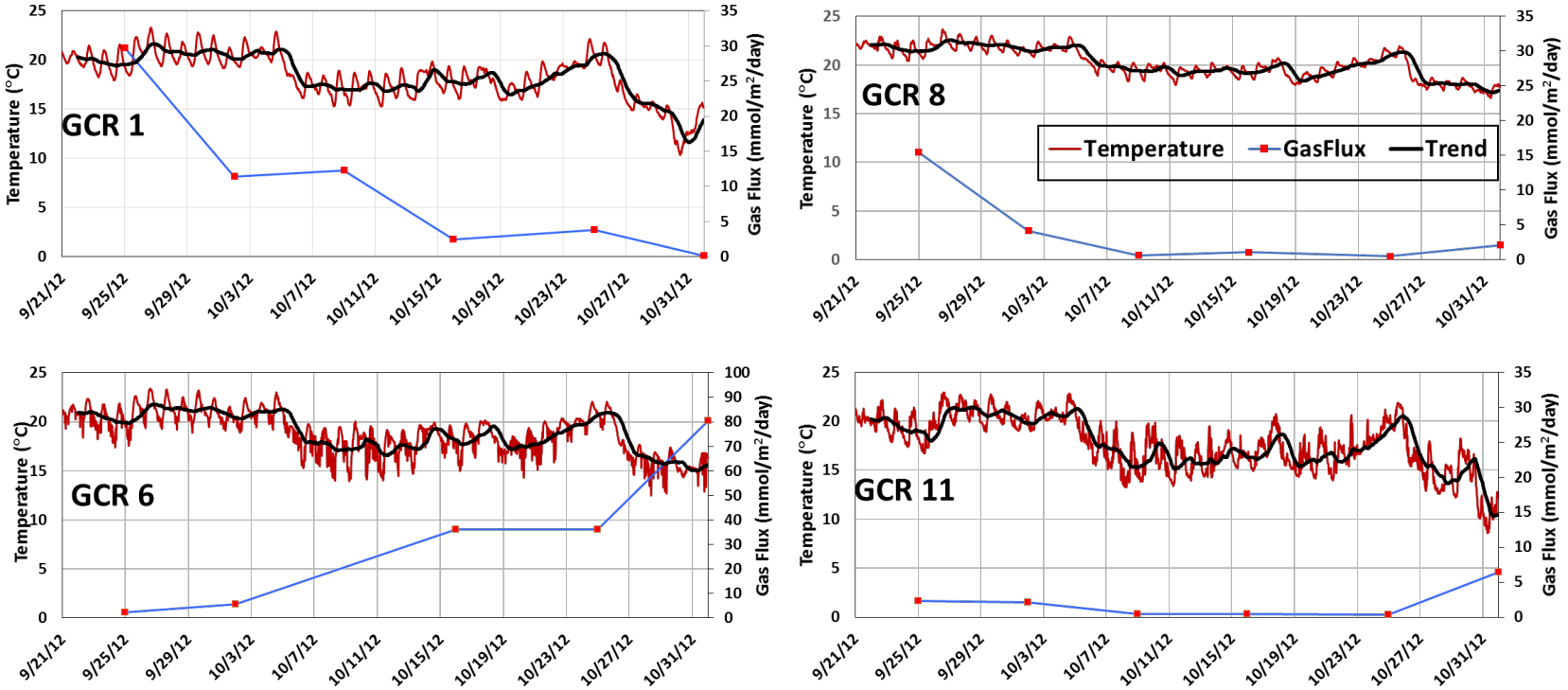

Figure 0.8 Poast-capping sediment temperature (0cm depth) and gas flux measured during 2012 sampling campaign. All sites except GCR6 exhibited a decreasing trend in gas prduction rates with decreasing surface temeprature.

Table 0.4 Descriptive Statistics of Pre-capping sediment grab samples

Statistic	% Water	ρ_b, g/cm^3	Porosity, %	OM, %	OC, %	BC, %
N of Cases	13	13	13	13	13	13
Minimum	30.23	0.96	46.17	4.95	3.31	0.98
Maximum	76.27	1.38	58.78	25.05	15.24	5.68
Median	57.30	1.09	54.67	15.76	9.25	3.43
Arithmetic Mean	56.28	1.11	54.04	14.23	8.78	3.39
Standard Error of Arithmetic Mean	4.34	0.04	1.04	1.82	0.98	0.47
95.0% LCL of Arithmetic Mean	46.84	1.03	51.77	10.27	6.64	2.38
95.0% UCL of Arithmetic Mean	65.73	1.19	56.31	18.19	10.92	4.41
Standard Deviation	15.63	0.13	3.76	6.55	3.54	1.68

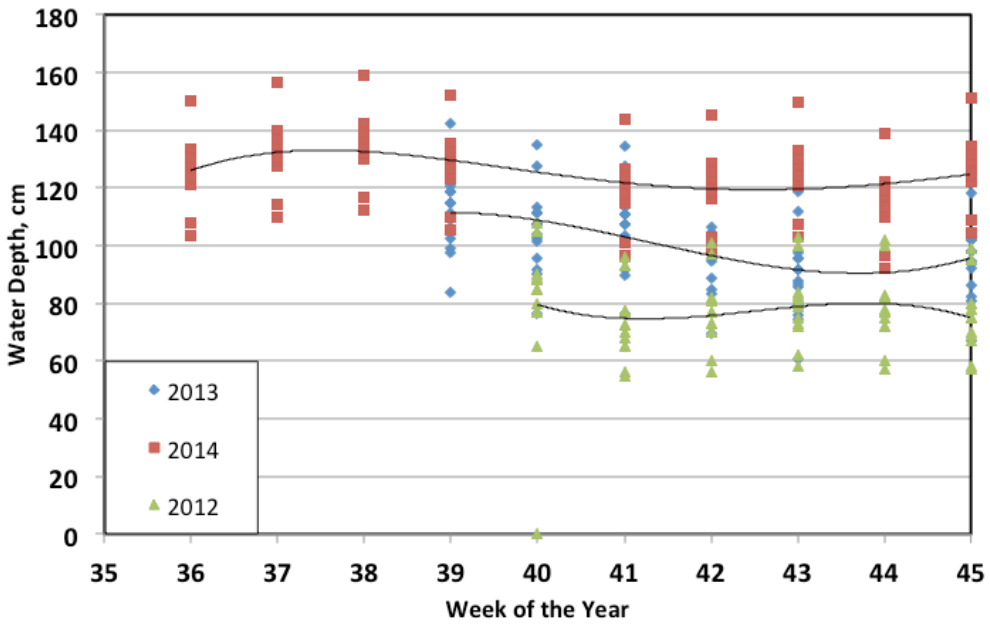

Figure 0.9 Increase in water depth over the three years of monitoring. Trend-line represents the overall pattern in water depth fluctuation during each monitoring year.

Table 0.5 Descriptive statistics of post-cap water depth data derived from weekly averages.

Year	Statistic	GCR1	GCR2	GCR3	GCR4	GCR5	GCR6	GCR8	GCR9	GCR10	GCR11	GCR12	GCR13
2012	N of Cases	6	6	6	6	6	6	5	6	6	6	6	6
	Minimum	65.00	77.50	56.00	77.00	77.00	70.00	55.00	93.00	96.00	72.50	68.00	65.00
	Maximum	77.00	88.00	65.00	90.00	89.00	85.00	58.00	105.00	108.00	85.00	80.00	77.00
	Arithmetic Mean	70.50	81.42	60.17	82.67	82.25	76.67	56.60	98.33	101.50	77.75	73.50	71.00
2013	N of Cases	6.00	6.00	6.00	6.00	6.00	6.00	6.00	6.00	6.00	6.00	6.00	6.00
	Minimum	86.74	91.64	74.24	97.54	85.74	87.94	60.64	91.64	111.64	95.34	75.74	79.44
	Maximum	109.97	114.87	97.47	120.77	108.97	111.17	83.87	114.87	134.87	118.57	98.97	102.67
	Arithmetic Mean	98.50	103.40	86.00	109.30	97.50	99.70	72.40	103.40	123.40	107.10	87.50	91.20
2014	N of Cases	9.00	9.00	9.00	9.00	9.00	9.00	9.00	9.00	9.00	9.00	9.00	9.00
	Minimum	110.05	122.11	96.61	122.17	117.27	113.30	92.11	119.36	139.05	113.17	111.80	113.11
	Maximum	130.15	142.21	116.71	142.28	137.37	133.40	112.21	139.46	159.15	133.28	131.90	133.21
	Arithmetic Mean	120.69	132.75	107.25	132.81	127.90	123.94	102.75	130.00	149.69	123.81	122.44	123.75
Differential Depth, 2014-2012		50.19	50.19	51.33	47.08	50.14	45.65	47.27	46.15	31.67	48.19	46.06	48.94
Differential Depth, 2014-2013		22.19	22.19	29.35	21.25	23.51	30.40	24.24	30.35	26.60	26.29	16.71	34.94
Differential Depth, 2013-2012		28.00	28.00	21.98	25.83	26.63	15.25	23.03	15.80	5.07	21.90	29.35	14.00

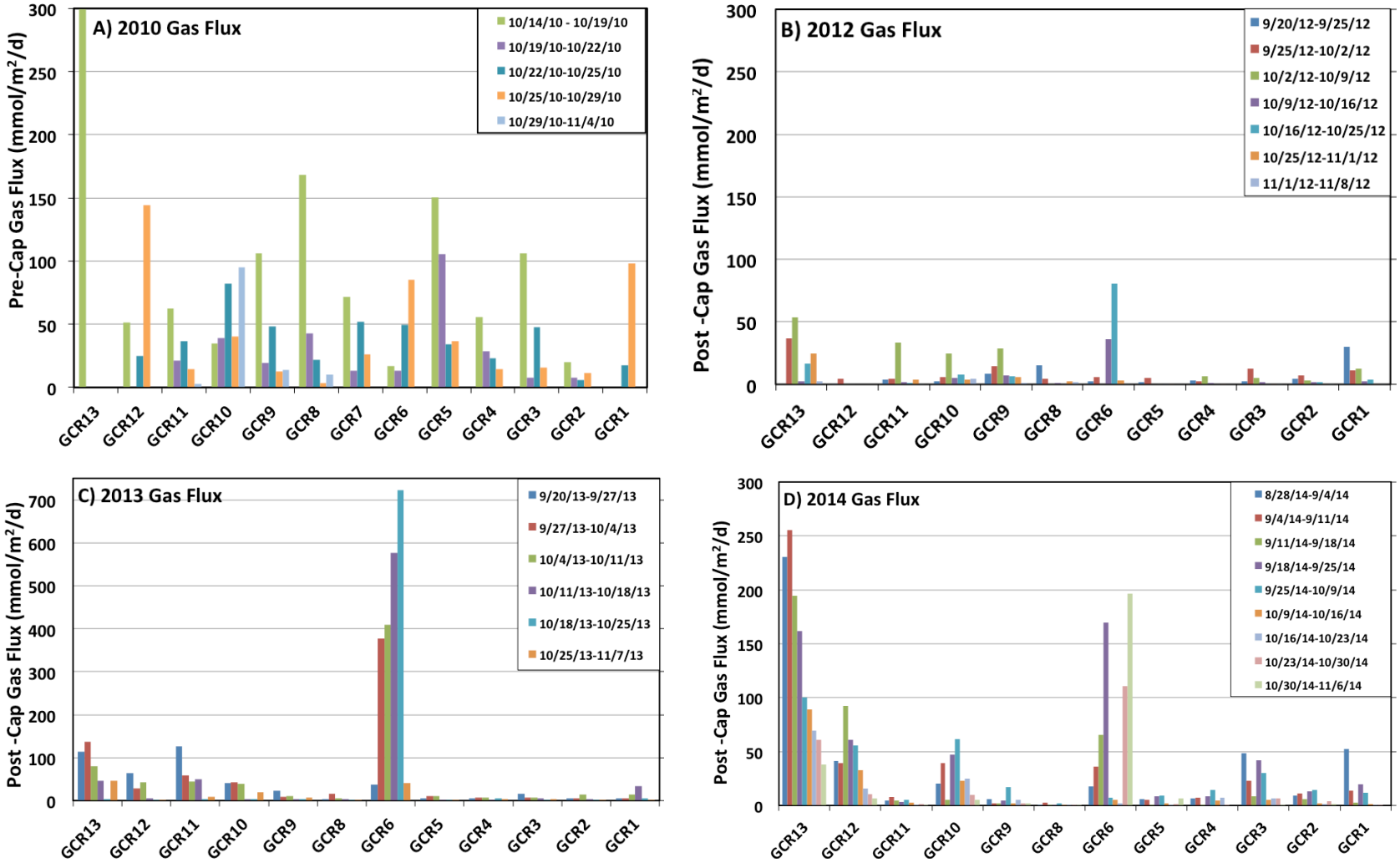

Figure 0.10 Weekly field gas fluxes (mmol/m^2/d) measured (A) pre-capping in 2010 and post capping in years B) 2012, C) 2013, and D) 2014. Note: Site GCR 7 was not monitored in post-capping years

Table 0.6 Average gas flux at all sites with percentage decrease in post-capping fluxes compared to pre-capping levels. Negative values represent the corresponding percent increase in gas fluxes. Bold values in parentheses represent an increase in ebullition post-capping.

	Average Gas Flux, mmol/m^2/d				% Decrease in Gas Flux compared to pre-capping, %			Ratio of pre-cap to post-cap Flux		
Year	**2010**	**2012**	**2013**	**2014**	**2012**	**2013**	**2014**	**2012**	**2013**	**2014**
GCR13	299.04	21.56	71.80	86.59	93%	76%	71%	0.07	0.24	0.29
GCR12	67.91	0.79	23.68	30.27	99%	65%	55%	0.01	0.35	0.45
GCR11	27.59	6.87	48.44	2.32	75%	**(-76%)**	92%	0.25	**(1.76)**	0.08
GCR10	58.27	7.72	25.11	28.49	87%	57%	51%	0.13	0.43	0.49
GCR9	40.09	10.33	9.97	5.43	74%	75%	86%	0.26	0.25	0.14
GCR8	49.35	3.65	5.13	0.71	93%	90%	99%	0.07	0.10	0.01
GCR6	41.34	21.39	359.07	81.63	48%	**(-769%)**	**(-97%)**	0.52	**(8.69)**	**(1.97)**
GCR5	81.66	1.56	4.57	4.72	98%	94%	94%	0.02	0.06	0.06
GCR4	30.47	1.89	4.75	7.14	94%	84%	77%	0.06	0.16	0.23
GCR3	44.30	3.23	6.38	15.00	93%	86%	66%	0.07	0.14	0.34
GCR2	11.23	2.73	4.84	5.91	76%	57%	47%	0.24	0.43	0.53
GCR1	57.59	8.61	10.50	5.48	85%	82%	90%	0.15	0.18	0.10
Mean	46.35	7.53	19.56	22.81	84.58%	62.73%	75.27%	0.15	0.23	0.25
95% UCL of Mean	33.09	2.96	4.80	3.61	84.85%	67.15%	76.23%	0.16	0.28	0.26
95% LCL of Mean	59.60	12.09	34.32	42.01	84.32%	58.30%	74.32%	0.15	0.19	0.24

Table 0.7 Mean annual gas flux and independent variables used for regression model development. GCR11-1, 11-2, 2-1 and 2-2 represent duplicates at each site

		Mean Gas Flux	Temperature at 0 cm	Temperature at -25 cm	Water Depth	Activation Energy (E_a)		First order degradation rate at 15 °C and 25 °C constant (k) for ND and CSed layers			
Site	Year	(mmol/m^2/d)	T_0	T_{25}	(cm)	ND (kJ/mol)	CSed (kJ/mol)	k_{15_ND} d^{-1}	k_{25_ND} d^{-1}	$k1_{5\_CSed}$ d^{-1}	k_{25_CSed} d^{-1}
GCR 2-1	2012	2.54	18.74	18.98	81.42	14.15	37.19	3.70E-03	4.96E-03	3.61E-03	9.63E-03
GCR 2-2	2012	2.91	18.74	18.98	81.42	14.15	37.19	3.70E-03	4.96E-03	3.61E-03	9.63E-03
GCR 6	2012	21.39	18.98	18.99	78.00	24.61	45.83	3.55E-03	9.92E-03	4.86E-03	8.44E-03
GCR11-1	2012	11.97	17.60	17.79	77.75	10.30	22.02	4.94E-03	7.56E-03	4.00E-03	6.86E-03
GCR 11-2	2012	1.77	17.77	17.89	77.75	10.30	22.02	4.94E-03	7.56E-03	4.00E-03	6.86E-03
GCR 13	2012	21.56	ND	ND	71.00	16.32	26.46	4.45E-03	8.06E-03	4.58E-03	6.99E-03
GCR 2-1	2013	3.20	19.29	19.51	103.40	14.15	37.19	3.70E-03	4.96E-03	3.61E-03	9.63E-03
GCR 2-2	2013	6.49	19.29	19.51	103.40	14.15	37.19	3.70E-03	4.96E-03	3.61E-03	9.63E-03
GCR 6	2013	359.07	19.62	19.80	99.70	24.61	45.83	3.55E-03	9.92E-03	4.86E-03	8.44E-03
GCR11-1	2013	39.94	18.39	18.74	107.10	10.30	22.02	4.94E-03	7.56E-03	4.00E-03	6.86E-03
GCR 11-2	2013	56.94	18.39	18.74	107.10	10.30	22.02	4.94E-03	7.56E-03	4.00E-03	6.86E-03
GCR 13	2013	71.80	18.04	18.41	91.20	16.32	26.46	4.45E-03	8.06E-03	4.58E-03	6.99E-03
GCR2-1	2014	6.54	18.75	19.16	132.75	14.15	37.19	3.70E-03	4.96E-03	3.61E-03	9.63E-03
GCR2-2	2014	7.06	18.75	19.16	132.75	14.15	37.19	3.70E-03	4.96E-03	3.61E-03	9.63E-03
GCR6	2014	67.63	19.40	19.32	123.94	24.61	45.83	3.55E-03	9.92E-03	4.86E-03	8.44E-03
GCR11-1	2014	4.47	18.76	18.81	123.81	10.30	22.02	4.94E-03	7.56E-03	4.00E-03	6.86E-03
GCR11-2	2014	2.38	18.76	18.81	123.81	10.30	22.02	4.94E-03	7.56E-03	4.00E-03	6.86E-03
GCR13	2014	133.53	18.86	18.78	123.75	16.32	26.46	4.45E-03	8.06E-03	4.58E-03	6.99E-03

Table 0.8 Biogenic gas production reaction rate constant k (d^{-1}) at the four incubation temperatures and Arrhenius Activation Energy E_a (KJ/mol) for incubations of ND, GAL, OrgC and CSed at different temperatures.

		k, d^{-1}				
Site	**Layer**	**5 ºC**	**15 ºC**	**25 ºC**	**35 ºC**	**E_a, KJ/mol**
GCR2	**ND**	0.005	0.004	0.005	0.005	14.15
	GAL	0.005	0.002	0.002	0.007	40.35
	OrgC	0.002	0.002	0.002	0.005	31.90
	CSed	0.003	0.004	0.010	0.010	39.50
GCR6	**ND**	0.002	0.004	0.010	0.007	24.61
	GAL	0.001	0.001	0.003	0.005	43.81
	OrgC	0.001	0.002	0.004	0.008	47.50
	CSed	0.002	0.005	0.008	0.005	22.38
GCR11	**ND**	0.006	0.005	0.008	0.006	10.30
	GAL	0.005	0.002	0.002	0.005	31.68
	OrgC	0.004	0.002	0.002	0.004	14.10
	CSed	0.004	0.004	0.007	0.007	22.02
GCR13	**ND**	0.006	0.004	0.008	0.007	16.32
	GAL	0.008	0.002	0.002	0.006	32.99
	OrgC	0.008	0.003	0.002	0.002	-11.23
	CSed	0.010	0.005	0.007	0.009	26.46

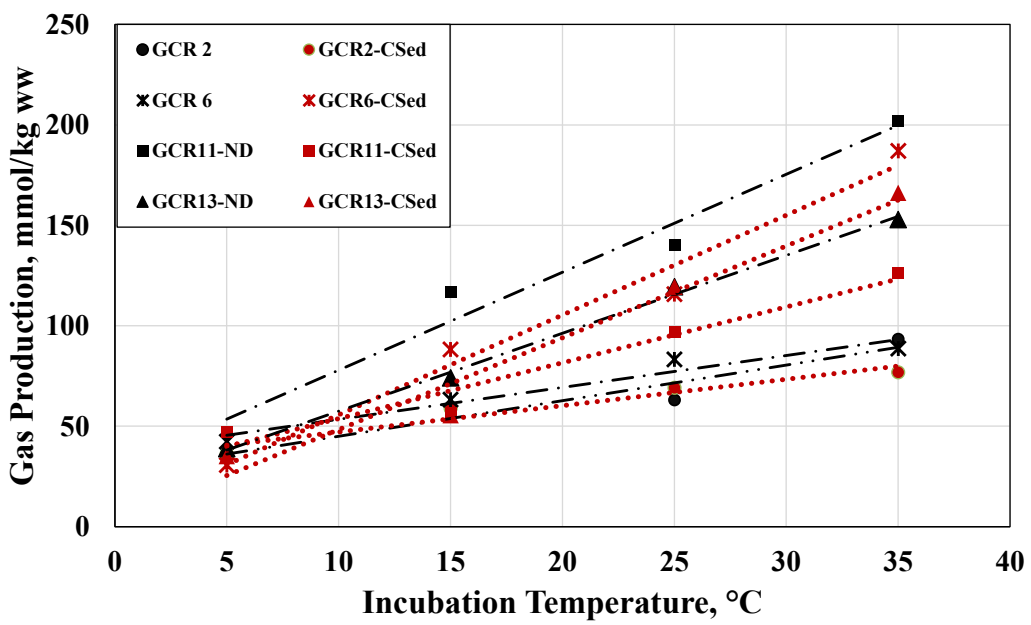

Figure 0.11 Cumulative gas production as a function of incubation temperature. Dotted lines represents the CSed layer and dash-dot line represents the ND layer

CHAPTER IV EFFECTIVENESS OF THE ACTIVE CAP IN CONTROLLING EBULLITION-FACILITATED CONTAMINANT RELEASE

4.1 Abstract

Pre and post-capping field measurements of ebullition-facilitated PAH and metal fluxes were performed at Grand Calumet River, Indiana to assess the effectiveness of the cap in reducing ebullition-facilitated contaminant fluxes to the water column. The fluxes were also compared with literature models to assess the real world applicability of these models to predict ebullition-facilitated fluxes. Capping greatly reduced contaminant fluxes to the water column, with metals and PAHs exhibiting 94-97% and 98%, reduction respectively. PAH fluxes increased in 2013, with only a 38% reduction compared to pre-capping levels primarily attributed to higher gas production below the cap. Analysis revealed that a combination of factors including sediment temperature, water depth and gas flux rates controlled the magnitude of post-cap contaminant fluxes. Post-capping metal fluxes originate primarily from the surficial sediment zone with re-suspension being the primary sediment to water transport mechanism. Post-cap PAH flux to the water column was primarily through gas phase transport of bubbles originating from the contaminated sediment zone. Capping resulted in lower fluxes and the elimination of the re-suspension mode of transport originating from the contaminated sediment. Model results show that the Viana et al model over predicts fluxes, whereas Fendinger et al model under-predicts ebullition-facilitated fluxes for both metals and PAHs. The Yuan et al model based on measured mass transfer coefficients was in close agreement with the measured fluxes. It is postulated that post-cap PAH transport will continue to occur at

lower magnitude (0.001 – 0.004 mg/m^2/d) as long as the contaminated sediment zone remains ebullition active, with the potential for higher fluxes in the summer.

4.2 Introduction

Sedimentary deposition of contaminant bound particles in rivers, lakes, reservoirs and estuaries can act as long-term repository for pollutants including PCBs, PAHs, PCDDs, mercury, methylmercury (MeHg), pesticides and others (Ghosh et al. 2011). Sediment contamination can severely damage the aquatic ecosystem, contaminate the food chain and impair the recreational, navigational or drinking water use of water bodies. With more than 1.2 billion cubic meters of contaminated sediment affecting 10% of the United States surface water (USEPA 1998), sediment remediation is a complex engineering challenge requiring varied remediation approaches tailored to meet site specific conditions such as groundwater flow, water depth, spatial extent of contamination, tidal pumping and erosion (Gidley et al. 2012). Sediment capping and more accurately active capping, has been widely adopted as a remediation measure at many sites (Reible et al. 2006). Dredging followed by capping can stop contaminant migration to the water column by providing increased path length for contaminant transport, physical separation, retardation, reduced sediment re-suspension and a less polluted sediment layer for benthic organisms to re-colonize (Himmelheber, Pennell, and Hughes 2007, Johnson, Reible, and Katz 2010, Josefsson et al. 2012, Liu et al. 2001). Active caps are especially important at sites with groundwater welling as additives in the cap can adsorb and transform the contaminants from the aqueous phase (Gidley et al. 2012, Simpson et al. 2002) providing sufficiently long breakthrough times for natural recovery. Various additives have been used as active sorbents in the cap material including activated carbon, zeolite, apatite,

organoclay and bio char with varying degree of effectiveness depending on the target contaminant of interest (Reible et al. 2007, Ghosh et al. 2011, Zimmerman et al. 2004, Jacobs and Förstner 1999). Although capping can be effective against contaminant migration, cap placement can alter biogeochemical processes in the cap and contaminated sediment, possibly resulting from migration of terminal electron accepting processes (TEAP) thereby increasing the potential for degradation of less mobile higher molecular weight (HMW) hydrophobic organic compounds (HOC) to more mobile and bio accumulative lower molecular weight (LMW) HOCs (Chen, Hale, and Letcher 2015, Brown et al. 1987, Sokol et al. 1994). Capping can also lead to increased mercury methylation rates by sulfate reducing bacteria, particularly in thin caps with limited physical isolation (Johnson, Reible, and Katz 2010). Similarly biogenic gas production below the cap and its subsequent release may result in the transport of contaminants to the water column through sediment particles attached to the gas bubbles and in the vapor phase (Viana, Yin, and Rockne 2012). Though capping has the potential to eliminate or decrease pollutant transport through re-suspension and bubble bound transport of the underlying contaminated sediment through the straining action of the cap during bubble rise through the cap (Yuan 2007), vapor phase transport and re-suspension of newly deposited sediment could still be a significant source of pollution to the water column. Ebullition can transport significant quantities of contaminants to the water column and atmosphere [16], as bubble formation times far exceed chemical equilibration times of less than an hour for pore-water contaminants (Mackay, Shiu, and Sutherland 1979, Bamford, Poster, and Baker 1999, Chanton, Martens, and Kelley 1989). Gas bubble migration is also known to form preferential pathways in the sediment resulting in pore-

water mixing and enhanced advective and diffusive contaminant transport, impacting breakthrough times (Yuan 2007). Ebullition-facilitated contaminant release is a difficult engineering problem considering the stochastic nature of bubble release and the range of influencing factors including lability of organic matter, water level, sediment shear strength and climatic factors like temperature (Zhu et al. 2015). The aforementioned factors make post-capping monitoring an integral part of any sediment remediation effort to ensure cap performance.

Measurement of contaminant migration through the cap using traditional methods such as sediment coring or installation of passive partitioning equilibrium samplers such as polyethylene (PE), polymethylene (POM) and polydimethylsiloxane (PDMS) coated glass fibers (Oen et al. 2011, Thomas, Lampert, and Reible 2014), do not capture the ebullition facilitated fluxes into the water column. Considering the relatively well understood likelihood of decreased contaminant migration from both bioturbation and advection/diffusion following installation of a cap, ebullition facilitated transport represents a large source of uncertainty as source pollution to the water column. This study aims to evaluate the effectiveness of a cap in controlling post-capping ebullition facilitated contaminant fluxes at the Grand Calumet River (GCR) over a course of a three-year field monitoring study using a gas collection system fitted with glass wool samplers.

4.3 Materials and Methods

The grand calumet river (GCR) is located close to the Illinois-Indiana border near the southern end of Lake Michigan. The study area comprises a 2 km stretch of the West Branch of the GCR (WBGCR) located between Columbia Ave and Indianapolis Blvd.

The GCR watershed has a flat terrain draining a 57 sq. km of heavily industrialized area with steel mills, chemical processing and oil refining operations (Battelle 2012). Approximately 90% of flow in WBGCR originates from permitted municipal discharge from the Hammond Sanitary District (HSD) (Battelle 2012). A total of 12 sites were selected for the study with sites GCR 1-6 located in Reach 1 (R1) between Indianapolis Blvd and I-90 Bridge and GCR 8 -13 located in Reach 2 (R2) extending west up to Columbia Ave. A CSO outfall near Columbia Ave discharges untreated sewage and runoff during heavy rain events severely impairing water quality at sites GCR 11 to GCR 13. Treated effluent from the HSD outfall near GCR10 results in significantly improved water quality at downstream sites GCR 10-1 characterized by low ammonia and turbidity levels. Reaches 1& 2 were dredged and capped with a 15 cm organoclay layer and a 25 cm sand/gravel-armoring layer in spring 2012. Site GCR8 was left uncapped because of the presence of an underwater petroleum pipeline. A pre-and post-capping aerial view of study area and site location is show in Figure 3.7, Chapter 3. Ebullition-facilitated contaminant flux monitoring was performed pre-capping in 2010 and for three years post-capping from 2012-2014 in the months of August to November.

4.3.1 Ebullition Facilitated Contaminant Flux Measurement

Gas collectors were fabricated using 2.5 cm diameter hollow PVC pipes and fitted with a funnel to capture the rising gas bubbles across a known surface area (Viana, Yin, and Rockne 2012, Huttunen et al. 2001). The gas collectors had a wide frame and the legs were pushed into the sediment/cap or supported on footings at deeper sites at approximately mid-depth in the water column. Placement of the system did not result in any preferential flow paths that would affect measurement. The PVC frame was equipped

with a ball valve to measure the volume of gas collected between sampling events. Glass wool (Sigma Aldrich, St. Louis, MO) was prepared by combusting it at 375 °C for 4 hrs. to remove organics and approximately 20 g was placed inside the funnel at its apex to capture bubble bound sediment and contaminants as the bubbles rise into the funnel. Another glass wool sample was placed in a perforated PVC cup attached to the exterior of the funnel away from the rising bubbles as control to measure background concentrations in water column. The gas accumulated in the collector was measured weekly using a 1000 ml water-filled volumetric cylinder by the volume of water displaced and weekly gas fluxes were calculated in units of mmol/m^2/day from the known cross-sectional area of the funnel and the number of days deployed with gas volumes converted to mass (moles) using the ideal gas law and measured temperature. The glass wool samples were removed at the end of the 8-10 week sampling period and stored in Teflon lined glass jars at 4 °C until further analysis at a National Environmental Laboratory Accreditation Program (NELAP) certified laboratory. The samples were analyzed for 16 priority PAHs by USEPA Aroclor method SW8270C, heavy metals (As, Ba, Cd, Cr, Cu, Pb) by method SW6020 and mercury by method SW846. Ebullition-facilitated contaminant fluxes were calculated as described in Viana et al (Viana, Yin, and Rockne 2012) in units of mg/m^2/day. For the pre-capping year, glass wool samples, were only available from sites GCR1, GCR2, GCR4, GCR8, GCR11 AND GCR12 due to highly variable water levels leaving some stations exposed due to the occurrence of a seiche in Lake Michigan that reversed the flow of water

4.3.2 Sediment Sampling and Analysis:

Pre-capping sediment grab samples were collected using a 9-inch Ponar dredge (provided by USACE) at all the twelve sites. Samples were homogenized in a high density polyethylene (HDPE) bucket and sub-samples were placed in a Teflon-lined jar of 500ml for PAHs and heavy metal analysis as described earlier for glass wool samples. Another subsample of 50 ml was collected in Falcon tubes to measure sediment physical characteristics including wet bulk density, dry bulk density, percent solids, percent, moisture, organic matter and organic carbon using methods described in Borrel et al (Borrel et al. 2012).

4.3.3 Sediment Temperature and Water Depth

Streambed temperature and water depth were monitored during the study period to assess the influence of temperature on gas and contaminant fluxes. Hobo Pendent® data loggers (Onset Computer Corp, Bourne, MA), model# UA-002-08), were mounted externally on a 0.64cm diameter hollow PVC pipe filled with sand. The loggers were configured to record streambed temperature at the sediment water interface (SWI) and 25 cm depths at 45 min intervals. Sediment temperature was also measured weekly using a thermometer dropped to the streambed. For post-capping years 2013 and 2014, water depth at site GCR9 was recorded at 15-minute intervals using Rugged TROLL 100 automatic depth logger (In-Situ Inc, Fort Collins, CO). Water depth at each site was also recorded using a metered stage during weekly sampling events. The stage measurements were later used to calculate the depth differential between GCR9 and all other sites for each sampling campaign. Automated depth data from site GCR9 was adjusted by the average depth differential to obtain high-resolution stage data at each site. For pre-capping year 2010,

streambed temperature was not recorded using Hobo temperature loggers, and only weekly streambed temperature measurements were used for analysis.

4.4 Results and Discussion

4.4.1 Pre and Post-Capping Metal Fluxes:

The initial pre-capping measurements were performed in the period of August to November in 2010. As and Cd fluxes were measurable above the detection limit at only sites with mean±SEM of 0.23±0.12 and 0.08±0.04 mg/m^2/d, respectively. A maximum Pb flux of 26 mg/m^2/d was observed at site GCR8 and the average for all sites was 11.15± 3.04 mg/m^2/d. For comparison, Pb fluxes were 1.5±0.28 mg/m^2/d in the heavily contaminated urban waterway, Collateral Channel (CC) using similar methodology (Viana, Yin, and Rockne 2012). Ebullition-facilitated fluxes of Ba, Cr, Cu and Hg were 4.97±0.87, 4.35±1.03, 6.57±1.37, and 0.89±3.04 mg/m^2/d, respectively (Figure 4.1). The pre-cap metal fluxes did not have a significant correlation with mean gas ebullition rates, whereas the study in CC exhibited a strong positive correlation. However, site GCR8 that had the highest weekly gas ebullition rate of 168 mmol/m^2/d also had the highest pre-cap metal flux of 49 mg/m^2/d. This suggests that the magnitude of metal fluxes can be influenced by gas ebullition rates as previously argued by Viana et al. Backward stepwise multivariate regression analysis between metal and gas fluxes, sediment metal concentration, water depth and sediment temperature did not reveal any statistically significant relationship ($p<0.05$) between these variables.

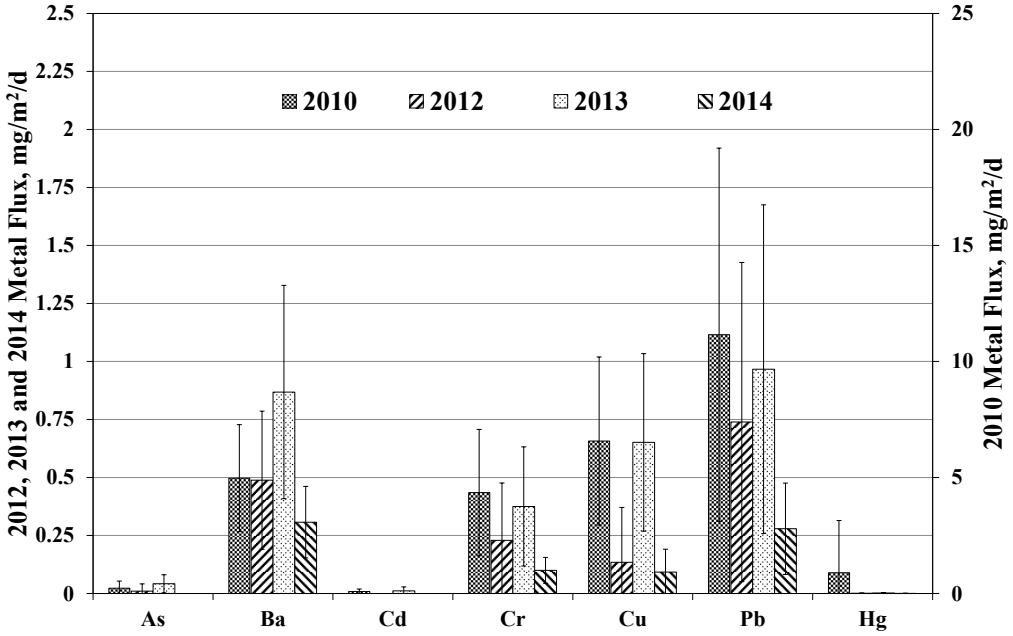

Figure 0.1 Mean metal fluxes observed at all sites pre and post-capping. Pre-capping fluxes are plotted in the secondary y-axis with all post-capping fluxes are plotted at 1:10 scale the primary y-axis to show detail.

The regression model (Eq 4.3, SI) for total metals (TMetals) developed by Viana et al was tested using WBGCR field dataset to assess its performance. A comparison plot of actual and predicted TMetal flux is given in Figure 4.8 in SI. The model provided a good fit to the field data with majority of data points falling close to the 1:1 line. The agreement of field data and observations made at site GCR8, further corroborates previous findings in CC of metal fluxes primarily influenced by sediment re-suspension and gas ebullition rates (Viana, Yin, and Rockne 2012).

In the first post-capping year (2012), As, Cu and Hg fluxes were very low; ranging from 0.001 – 0.01 mg/m^2/d and consequent flux reductions of 94-100% compared to pre-capping. Ba, Cr and Pb fluxes were significantly higher, ranging from 0.25 - 0.79 mg/m^2/d. These represent decreases of 90 – 94% compared to pre-cap conditions (Table

4.12). Cd fluxes were below detection at all sites.

Post-capping ebullition facilitated fluxes of heavy metals were significantly higher in 2013 compared to 2012, but remained well below pre-capping levels. Mean±SEM of As, Ba, Cd, Cr, Cu, Pb and Hg were 0.05±0.01, 0.93±0.13, 0.01±0.01, 0.42±0.07, 0.68±0.11, 1.08±0.2 and 0.002±0.001 mg/m^2/d respectively. These were 79-100% lower than ebullition-facilitated fluxes measured in 2010, prior to capping (Table 4.3, SI). Maximum fluxes of 2.43, 1.63, 1.41 and 0.89 mg/m^2/d were observed for Pb, Ba, Cu and Cr respectively for the uncapped site GCR8.

The magnitude of metal fluxes decreased in 2014 and was lower than fluxes measured in the first post-capping year (2012). A mean±SEM of 0.34±0.05, 0.1±0.02, 0.1±0.3, 0.3±0.06 and 0.001±0 mg/m^2/d were observed for Ba, Cr, Cu, Pb and Hg respectively with arsenic fluxes below detection limit at all sites. The total metal flux was also lower (0.84 mg/m^2/d) compared to 2012 and 2013. Mean ebullition facilitated metal fluxes for the pre and post-cap monitoring years are shown in Figure 4.1.

The monitoring data showed that the cap is effective in controlling metal fluxes to the water column. Hg fluxes were completely eliminated post-capping, suggesting that the cap is effective against Hg migration and the absence of Hg recontamination in the surficial sediment zone. Interestingly, metal fluxes were generally lower in 2014 compared to 2013 even though the gas fluxes were comparable. This was also accompanied by an increase in stream depth of around 25 cm. This trend could be explained by the following reasons. In the post-capping scenario, metal fluxes are lower due to elimination of migration from the underlying sediment is eliminated in response to physical isolation and straining action of the cap removing bubble bound particles. So it

is postulated that the observed metals originate from re-suspension and bubble bound transport of sediments from the surficial zone. The lowering of metal fluxes in 2014 is a direct consequence of higher water depths which lowers the contribution of resuspension mode of metal transport, as the traps were generally place at mid-depth. Also, the larger travel path may result in loss of bubble bound particles in the water column. Another factor that could potentially explain the variation in fluxes is the higher mean temperatures in the range 0.4 to 1.3°C observed in 2013. Water temperature in interstitial spaces can affect metal solubility in sediments as cooler water has more dissolved oxygen than warmer water and increases redox potential in pore water (Fritioff, Kautsky, and Greger 2005). Consequently, metal concentration in pore water may decrease with lower temperature as metals are adsorbed strongly to sediment colloids at higher redox potential (Förstner 1981).

It is important to note that, 2014 fluxes were monitored over a longer period of nine weeks from the first week of August compared to six weeks in 2012 and 2013. Considering the longer monitoring period, metal fluxes and temperature should have been higher, adding credence to our findings that metal fluxes were strongly influenced by sediment temperature and water depth. Considering that ebullition facilitated transport of metals is primarily by bubble-bound transport and sediment re-suspension (Viana, Yin, and Rockne 2012) in pre-capping scenario, we postulated a similar transport mechanism from the newly deposited material on top of the cap and advective-diffusive transport from the underlying sediment.

To further asses the origin of contaminants in the trap, we computed the ratio of the individual metal (As, Ba, Cd, Cr, Cu, Pb, Hg) to the total metals in the cap and pre-

capping contaminated sediment. It is expected the ratios will be similar if the metals originated in the contaminated sediment zone and a comparison plot would result in data points falling close to 1:1 line. The comparison plot shown in Figure 4.6, SI, did not exhibit any similarity in ratio to pre-capping sediments further adding credence to the argument that post-cap metal fluxes originate from surficial zone.

In summary, post-capping metal fluxes were dominated by Ba, Cr, Cu and Pb. Metal fluxes measured over three consecutive years showed that the cap is effective in controlling metal transport to the water column with reduction in fluxes ranging between 89-97% (Table 4.13). The straining action of the cap during bubble rise captures bubble-bound particles from the underlying contaminated sediment resulting in lower post-capping metal fluxes.

Table 4.1. Mean water depth ($D_{w,}$ cm), surface sediment temperature ($T_{0,}$ °C) and gas fluxes ($GF,$ mmol/m^2/d) during each post-cap sampling period from 2012-2014.

	Year	GCR13	GCR12	GCR11	GCR10	GCR9	GCR8	GCR6	GCR5	GCR4	GCR3	GCR2	GCR1
	2012	71	73.5	77.8	101.5	98.3	56.6	76.7	82.3	82.7	60.2	81.4	70.5
D_w, cm	**2013**	91.2	87.5	107.1	123.4	103.4	72.4	99.7	97.5	109.3	86	103.4	98.5
	2014	123.7	122.4	123.8	149.7	130	102.7	123.9	127.9	132.8	107.2	132.7	120.7
	2012	-	16	17.5	20.2	20.3	20.2	18.9	19.2	19	18.8	18.7	18.4
$ST_{0,}$ °C	**2013**	17.6	17.2	18	20	20	20	19.3	19.6	19.4	18.3	18.8	18.6
	2014	17.8	17.4	17.6	18.9	18.7	18.8	18.4	18.2	18.3	17.1	17.5	17.6
	2012	21.6	0.8	6.9	7.7	10.3	3.7	21.4	1.6	1.9	3.2	2.7	8.6
GF	**2013**	71.8	23.7	48.4	25.1	10	5.1	359.1	4.6	4.8	6.4	4.8	10.5
	2014	133.5	39.4	3.4	26.2	4.7	0.8	67.6	4.4	6.3	18.9	6.8	11.3

4.4.1 Pre and Post-Capping PAH flux:

Fluxes for LMW PAHs acenaphthene, fluorene and naphthalene were below detection limit (BDL) for both pre-cap and post-capping monitoring periods and are not discussed further. Similar to metal analysis, the ratios of the sixteen PAHs to total PAH were computed and were compared to ratios in the pre-capping sediment, as an indicator of the source of PAH fluxes. For the pre-capping year, mean±1SE of total LMW (ΣLMW) PAH flux was 0.01±0.004 mg/m^2/d compared to mean total HMW (ΣHMW) PAH flux of 0.212±0.04 mg/m^2/d. The fraction of LMW PAHs ranged between 9 – 11% compared to HMW fraction of 89 – 100 %. Phenanthrene and anthracene were the only detectable LMW compounds with mean±1SE of 0.01±0.003 and 0.001±0.001 mg/m^2/d respectively. Mean±1SE of HMW PAH fluxes in mg/m^2/d were 0.01±0.003 for benz(a)anthracene, 0.03±0.01 for benzo(a)pyrene, 0.03±0.01 for benzo(b)fluoranthene, 0.01±0.003 for benzo(k)fluoranthene, 0.04±0.01 for chrysene, 0.02±0.01 for dibenz(a,h)anthracene, 0.03±0.01 for fluoranthene, 0.007±0.003 for indenopyrene and 0.04±0.01 for pyrene. The measured fluxes were significantly lower than fluxes of 0.61, 0.65, 0.72, 3.51 and 0.85 mg/m^2/d observed in CC for anthracene, benzo[a]-pyrene, chrysene, fluoranthene and fluorene respectively (Viana, Yin, and Rockne 2012). Exploratory regression analysis between PAH fluxes and sediment physio-chemical characteristic did not exhibit any statistically significant relationship. Plots of pre and post-capping fluxes are shown in Figure 4.2.

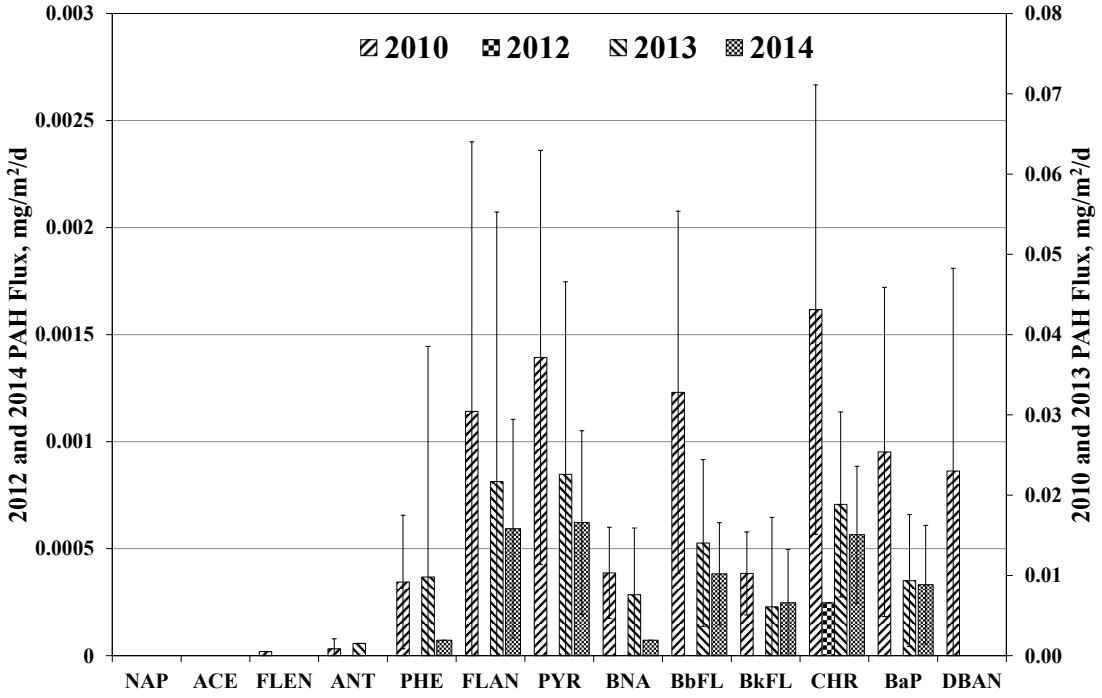

Figure 0.2 Mean pre-capping PAH flux measured in 2010 and post-capping PAH fluxes measured in 2012, 2013 and 2014. ACE = acenaphthene, ACY = acenaphthylene, ANT = anthracene, BNA = benzo[a]anthracene, BaP = benzo[a]pyrene, BbFL = benzo[b]fluoranthene, BPY = benzo[g,h,i]perylene, BkFL = benzo[k]fluoranthene, CHR = chrysene, DBAN = dibenzo[a,h]anthracene, FLAN = fluoranthene, FLEN = fluorene, PHE = phenanthrene, PYR = pyrene

Pre-cap fluxes for HMW PAHs Chrysene (CHE) and Pyrene (PYR) and LMW PAH Phenanthrene (PHE) were compared with Fendinger et al predicted equilibrium partitioning model (Fendinger, Adams, and Glotfelty 1992), shown in Eq. 4.4 in SI. Literature values (Table 4.13, SI) of Henry's constant (K_H), organic carbon water partitioning coefficient (K_{oc}) (USEPA 1996) and mean values of sediment f_{oc} were used in the model. Phenanthrene fluxes were also compared using Yuan et al predicted effective mass transfer coefficient for a gas flux of 1 L/m^2/day, close to the range of fluxes observed in the field. Fendinger et al model grossly under predicted the ebullition-

facilitated fluxes compared to observed values (Figure 4.7). This difference can be primarily attributed to the model not accounting for sediment re-suspension and bubble bound transport. The Yuan et al predicted PHE fluxes (Figure 4.7) was in close agreement with field-measured fluxes. The mass transfer co-efficient accounts for both resuspension and gas phase transport mechanisms, resulting in a better performance. The Yuan model predicted slightly higher fluxes by an order of magnitude. This can be explained by the closed nature of the experimental setup used in the study. PHE concentration in the hexane layer increased over time due to gas-phase transport from methane bubbles and continued mass transfer between the aqueous phase and hexane phase with no loses in the water column thereby resulting in higher mass transfer coefficients. Under field conditions, the continuously moving water column and losses from the gas phase to the atmosphere are higher and are not completely captured by the glass wool trap. Field measured total PAH (TPAH) fluxes were also compared with regression model developed by Viana et al that incorporates sediment concentration (C_{sed}), molar gas flux (GF_m) and sediment physical characteristics such as organic matter, organic carbon and COD/OC ratio as independent variables. The regression model greatly over predicted the observed values for TPAH. This can be explained by the nature of the dataset used in the model development. Mean TPAH of all sites were approximately twenty-seven times higher at 2184 mg/kg-dry compared to 80 mg/kg-dry measured in GCR. Also the mean gas flux was three times higher at 3.3 $L/m^2/d$ compared to 1.1 $L/m^2/d$ at GCR. The regression model represents the higher spectrum of field observed ebullition facilitated PAH fluxes and should be treated with caution.

In 2012, post-capping PAH fluxes were below detection at all sites except for the uncapped site GCR8 and the high flux site GCR6 (Figure 4.2). All LMW PAHs were BDL whereas the mean ΣHMW was 0.0003 mg/m^2/d, which is almost negligible compared to a pre-capping flux of 0.212 mg/m^2/d. At GCR6 chrysene was the only detectable PAH with a flux of 0.003 mg/m^2/d, which also recorded the highest mean gas ebullition rate of 21.4 mmol/m^2/d. At site GCR 8 fluxes for HMW compounds benzo(a)pyrene, benzo(b)fluoranthene, chrysene and pyrene (0.002, 0.002, 0.004 and 0.002 mg/m^2/d) were lower compared to pre-capping fluxes (0.07, 0.07, 0.1 and 0.05 mg/m^2/d)

In 2013, a noticeable increase in ΣPAH flux was observed with mean±1SE of 0.11±0.04 mg/m^2/d. Anthracene and phenanthrene were the only detectable LMW PAHs measured at sites GCR 8, 11, 12 and 13 with fluxes ranging between 0.01 - 0.07 mg/m^2/d. HMW PAHs were detectable at all sites except GCR 3, 9 and 10 with total HMW (ΣHMW) fluxes ranging between 0.04 - 0.4 mg/m^2/d. Mean±1SE of individual PAHs in mg/m^2/d were 0.01±0.004 for benz(a)anthracene, 0.01±0.004 for benzo(a)pyrene, 0.02±0.005 for benzo(b)fluoranthene, 0.01±0.003 for benzo(k)fluoranthene, 0.03±0.01 for chrysene, 0.002±0.002 for dibez(a,h)anthracene, 0.024±0.01 for fluoranthene, 0.005±0.002 for indenopyrene and 0.03±0.01 for pyrene. The mean total PAH (ΣPAH) flux of 0.11±0.04 was comparable to pre-capping flux of 0.22±0.04 mg/m^2/d with LMW fluxes representing 7-18% of ΣPAH.

In 2014 the mean ΣPAH flux decreased considerably to 0.003 mg/m^2/d although gas fluxes were higher at most sites. A similar pattern was also observed in the mean metal flux in response to changes in water depth and lower sediment temperatures as discussed

earlier. Phenanthrene was the only detectable LMW PAH and measured 0.001 mg/m^2/d at GCR11 representing 7% of ΣPAH. HMW PAHs were detectable only at sites in Reach 2 and the high gas flux site GCR6 in Reach 1. The ΣHMW fluxes were in the range of 0.004 – 0.01 mg/m^2/d comparable to the lower fluxes observed in 2012 (Table 4.10). The rise and fall in PAH fluxes in 2013 and 2014 along with rise and fall of sediment temperature in the range of 0.4 to 1.4 ºC has several implications. This trend suggests that the higher temperatures stimulated gas production in the contaminated sediment thereby increasing PAH partition and transport, resulting in higher measured fluxes. In 2014, the sediment temperature decreased and water levels increased by around 25cm in comparison to 2013. However, the gas ebullition rates were slightly higher than 2013. The higher gas fluxes should have increased PAH fluxes to the water column. The reverse trend suggests that gas production in the cleaner new deposit layer probably increased in 2014 resulting in lower PAH fluxes and higher gas ebullition rates. It is postulated that continued deposition will increase the thickness of the new deposition layer further burying the contaminated sediment layer. It is most likely that higher temperatures in the summer can stimulate gas production in the contaminated sediment zone and increase PAH transport to the atmosphere, as show in the incubation study results from Chapter 3.

4.4.3 Comparison of Pre-cap and Post-capping PAH transport mechanism

Ebullition facilitated fluxes of LMW PAHs dibenz(a,h)anthracene and acenapthene were completely eliminated post-capping. Naphthalene fluxes were below detection limit for both pre and post-capping years although sediment concentrations ranged between 0.07-0.6 mg/kg. Also, the overall fluxes were dominated by HMW PAHs in both pre and post-

capping primarily scenario and were dominated by pyrene, chrysene, benzo(a)pyrene, benzo(b)fluoranthene and fluoranthene. The ratios of individual PAHs to TPAHs, LMW and HMW PAHs were compared in the pre and post-capping glass wool to make conclusions on the source of contaminants and its transport mechanism. Ignoring the 2012 post-capping data, where chrysene was the only measurable PAH at GCR6, average chrysene fractions were 20%, 25% and 22% of HMW fluxes for pre-capping, 2013 and 2014 respectively. Similarly, pyrene fraction were 16%, 25%, and 24%; benzo(a)pyrene fraction were 13%, 9% and 10%; benzo(b)fluoranthene fraction were 14%, 15% and 12%; fluoranthene fraction were 14%, 18% and 23%; benzo(k)fluoranthene contributed 7%, 4% and 6% and benz(a)anthracene contributed 6%, 6% and 2%. Among the LMW PAHs, phenanthrene contributed 86%, 93% and 100% in 2010, 2013 and 2014 respectively. The similar ratios of HMW and LMW PAHs suggests that the mechanism for ebullition facilitated PAH transport is similar pre and post-capping.

Similarly, the order of increasing sediment HMW PAH concentration were as follows: Pyrene > Chrysene >Fluoranthene>Benz(a)anthracene> Benzo(b)fluoranthene> Benzo(a)pyrene> Benzo(k)fluoranthene. It was observed that the increasing order of post-cap HMW PAH flux follows a similar order: Pyrene > Chrysene > Fluoranthene> Benzo(b)fluoranthene> Benzo(a)pyrene> Benzo(k)fluoranthene> Benz(a)anthracene with Benz(a)anthracene being the only exception. A similar trend was also observed for LMW PAHs (Figure 4.2). These trends further suggest that the post-cap PAH fluxes originate from the underlying contaminated sediment. A combination of factors including sediment concentrations and partitioning properties ($\log K_{oc}$ between 4.7-6.3 for HMWPAHs and 3.1 - 4.5 for LMWPAHs) dictates the magnitude of observed post-cap fluxes.

The observed ratios of individual PAHs to TPAH in glass wool were compared to that in the gas phase (EPT-Air, C_a) and water phase (EPT-Water, C_w) predicted by an equilibrium partition model (EPM) (Eq 4.1 and 4.2) Literature values of K_{oc}, Henry's constant (K_H) and measured values of sediment concentration (C_{sed}, mg/kg-dry) and sediment f_{oc} values (data presented in Table 4.14) were used. The observed and equilibrium model predicted fraction of individual PAHs is presented in Figure 4.3.

$$C_w = \frac{C_{sed}}{K_{oc} \times f_{oc}} \tag{0.1}$$

$$C_a = \frac{C_{sed} \times K_H}{K_{oc} \times f_{oc}} \tag{0.2}$$

The EPM predicted a higher fraction of LMW PAHs and lower fractions of HMW PAHs in the air phase, contrary to the trend observed in the ebullition facilitated flux data. This is expected considering the higher affinity of HMW PAHs to organic carbon fraction and low K_{oc} values of LMW PAHs such as naphthalene. Similarly pore water concentrations predicted by EPM model showed greater fraction of LMW PAHs compared to HMW PAHs. The measured post-cap flux represents the PAH fraction that has partitioned from the gas phase to the glass wool and the higher HMW fractions reflect the greater affinity of HMW PAHs to the glass wool. Also the lower affinity of LMW PAHs and losses to water column account for lower fraction of LMW PAHs observed in the glass wool.

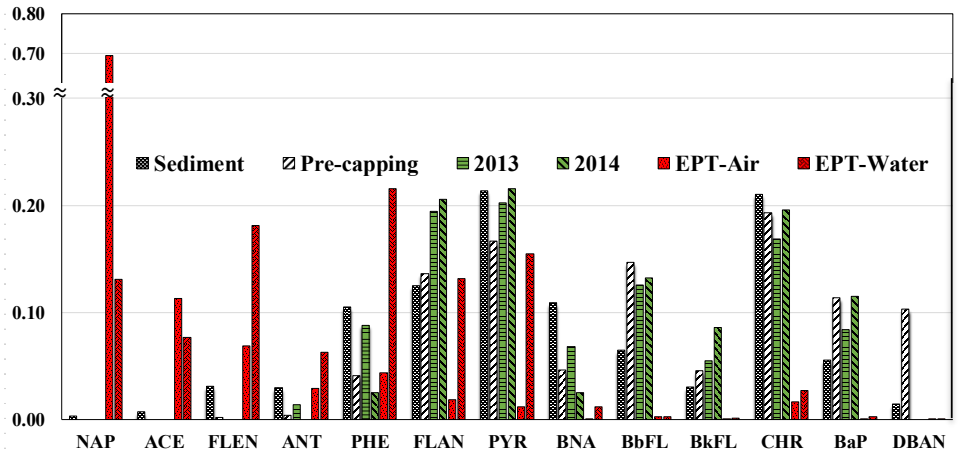

Figure 0.3 Comparison of fractional contribution of individual PAHs to total PAHs in the sediment, pre-cap, 2013 and 2014 glass wool (GW) measured fluxes along with the predicted fractional contribution in the air and water phase using an equilibrium-partitioning model. Data for 2012 GW is not presented, as Chrysene was the only detectable PAH flux measured only at GCR6.

Figure 4.3 clearly shows that the ratios observed in post-capping glass wool is similar to that observed in post-capping and the pre-capping contaminated sediment. Further emphasizing the similar transport mechanisms in both scenarios. It is postulated that pre-capping PAH transport involves a multimodal transport mechanism (involving sediment re-suspension and gas phase transport) and explains the higher fluxes observed in pre-cap dataset. Alternatively, post-capping PAH transport is primarily through gas bubble partitioning as capping eliminates contaminated sediment re-suspension thereby explaining the lower post-capping PAH fluxes. Also the similar order of dominant PAHs in glass wool and the contaminated sediment suggest that PAHs originate from the contaminated sediment zone below the cap. The effect of surficial recontamination could not be ascertained; as post-capping sediment contaminant levels were not measured in this study. It is important to note that the measured post-capping flux does not capture 100% of bubble transported PAHs as some of the bubble bound particles can adhere to

the walls of the funnel or can be lost to the water column.

4.5 Conclusions:

The extensive monitoring data suggest that the cap performs well in controlling ebullition facilitated PAH and metal fluxes to the water column. Post-capping metal fluxes showed significant reduction with mean flux ranging between 0.8 – 3.2 mg/m^2/d compared to a mean pre-capping flux of 58 mg/m^2/d. Post-cap PAH fluxes in 2012 and 2014 also showed significant reductions with mean fluxes of 0.001 and 0.004 mg/m^2/d respectively. Although 2013 PAH fluxes were relatively higher at 0.14 mg/m^2/d, the fluxes were still below than the pre-capping flux of 0.22 mg/m^2/d. Flux reductions were between 94 – 97% for metals and around 98% for PAHs except for 2013 with a 38% PAH reduction. The comparison of field-measured fluxes to literature models revealed that the Fendinger EP model does not capture the multimodal mechanism involved in PAH transport and greatly under predicts measured values. The regression models for metal and PAH fluxes developed by Viana et al are derived from a data set with high gas flux rates and sediment concentrations and should only be used for sites with similar gas fluxes. Yuan et al model is a better predictor of ebullition facilitated PAH fluxes. However, mass transfer coefficients for all PAHs are not available in the range of field observed gas ebullition rates, restricting their use to a limited number of PAHs. This study corroborated previous findings (Viana, Yin, and Rockne 2012) that metal flux contributions are primarily from sediment re-suspension with limited advective and diffusive migration from the underlying contaminated sediment. Post-capping PAH transport is primarily by partitioning into gas phase followed by bubble migration across the cap material. Observations during field visits suggested two modes of gas bubble

release: 1) Gas-bubbles released from the surficial zone were characterized by smaller bubbles spread across a larger streambed area and were released by minor disturbances in the water column, 2) Distinct gas-seeps characterized by continuous release of trapped gases for 1- 2 minutes from deeper sediment through fissures in the cap material. The latter mode of gas release is expected to contribute significantly to the PAH fluxes to the water column. The ebullition facilitated fluxes reported here are an estimate of the actual as the trap does not capture 100% of the contaminants. PAH transport is expected to continue as long as the contaminated sediment zone is ebullition active at magnitudes much lower than that observed during the pre-cap monitoring campaign. The rise and fall in PAH fluxes in 2013 and 2014 clearly showed that PAHs transport via gas ebullition can be a significant source of pollution if the contaminated sediment zone continues to be ebullition active. Higher sediment temperatures in 2013 increased gas production in the contaminated sediment thereby increasing PAH transport to the water column and atmosphere. The lower temperature normally expected in the late fall season suggests that the fluxes reported here fall in the lower spectrum of expected fluxes. Also, as sediment temperatures peak in the summer months, ebullition facilitated PAH transport can be significantly higher and repeating this study in the summer could provide a better range of post-capping flux estimates. It is not clear if the underlying contaminated sediment will continue to be ebullition active although the gas flux is expected to decrease over time from the depletion of OM. These findings warrant further monitoring to understand the long-term effectiveness of capping and PAH transport from the underlying contaminated sediment.

4.5 Supporting Information

Table 0.1 Ebullition facilitated metal fluxes during the pre-capping sampling campaign in 2010. Non-detects are reported as zero. Gas flux data from GCR 13 was not included in mean calculation as one week of sampling was obtained due to low water levels. ND= No data available.

Site	Metal Flux, mg/m^2/d								GasFlux, mmol/m^2/d
	As	Ba	Cd	Cr	Cu	Pb	Hg	ΣMetals	
GCR1	0.32	4.40	0.20	5.21	4.8	12.0	0.02	26.9	57.6
GCR2	0.60	6.01	0.13	7.85	9.70	18.0	6.01	48.3	11.2
GCR3	ND	ND	ND	ND	ND	ND	ND	ND	44.3
GCR4	0.00	2.04	0.00	2.39	2.13	5.76	0.01	12.3	30.5
GCR5	ND	ND	ND	ND	ND	ND	ND	ND	81.7
GCR6	ND	ND	ND	ND	ND	ND	ND	ND	41.3
GCR8	0.68	6.83	0.24	7.88	7.88	25.7	0.03	49.3	49.4
GCR9	ND	ND	ND	ND	ND	ND	ND	ND	40.1
GCR10	ND	ND	ND	ND	ND	ND	ND	ND	58.3
GCR11	0.00	1.70	0.00	1.02	1.92	4.13	0.12	8.90	27.6
GCR12	0.00	6.60	0.00	3.63	8.81	6.74	0.03	25.8	67.9
GCR13	0.00	7.23	0.00	2.46	10.8	5.69	0.03	26.2	299
Mean	**0.23**	**4.97**	**0.08**	**4.35**	**6.57**	**11.2**	**0.89**	**0.23**	**46.3**

SE	**0.12**	**0.87**	**0.04**	**1.03**	**1.37**	**3.04**	**0.85**	**0.12**	**5.95**

Table 0.2 Ebullition facilitated metal fluxes during the post-capping sampling campaign in 2012.

2012 Post-cap Metal Flux, mg/m^2/d									
Site	**As**	**Ba**	**Cd**	**Cr**	**Cu**	**Pb**	**Hg**	**ΣMetals**	**GasFlux, mmol/m^2/d**
GCR1	0.00	0.22	0.00	0.11	0.00	0.36	0.00	0.68	8.61
GCR2	0.00	1.04	0.00	0.59	0.58	1.89	0.00	4.10	2.73
GCR3	0.11	0.78	0.00	0.57	0.57	1.61	0.00	3.65	3.23
GCR4	0.00	0.85	0.00	0.49	0.00	1.44	0.00	2.79	1.89
GCR5	0.00	0.32	0.00	0.16	0.00	0.39	0.00	0.86	1.56
GCR6	0.00	0.71	0.00	0.47	0.33	1.48	0.00	2.98	21.39
GCR8	0.00	0.71	0.00	0.49	0.36	1.32	0.01	2.88	3.65
GCR9	0.00	0.17	0.00	0.00	0.00	0.12	0.00	0.28	10.33
GCR10	0.00	0.16	0.00	0.00	0.00	0.11	0.00	0.28	7.72
GCR11	0.00	0.47	0.00	0.14	0.00	0.33	0.00	0.94	6.87
GCR12	0.00	0.29	0.00	0.00	0.00	0.17	0.00	0.46	0.79
GCR13	0.00	0.38	0.00	0.00	0.00	0.24	0.00	0.62	21.56
Mean	**0.01**	**0.51**	**0.00**	**0.25**	**0.15**	**0.79**	**0.00**	**1.71**	**7.53**
SE	**0.01**	**0.09**	**0.00**	**0.07**	**0.07**	**0.20**	**0.00**	**0.42**	**2.07**

Table 0.3 Ebullition facilitated metal fluxes during the post-capping sampling campaign in 2013. Data from GCR 6 was not included in mean and SE calculation as it was an outlier.

2013 Post-cap Metal Flux, mg/m^2/d									
Site	**As**	**Ba**	**Cd**	**Cr**	**Cu**	**Pb**	**Hg**	**ΣMetals**	**GasFlux, mmol/m^2/d**
GCR1	0.08	1.16	0.03	0.56	0.72	1.67	0.00	4.21	10.50
GCR2	0.02	0.60	0.01	0.32	0.36	0.87	0.00	2.19	4.84
GCR3	0.06	1.09	0.00	0.54	0.50	1.09	0.00	3.27	6.38
GCR4	0.06	1.12	0.03	0.52	0.71	1.34	0.00	3.78	4.75
GCR5	0.09	1.57	0.03	0.69	1.02	1.89	0.00	5.30	4.58
GCR6	0.06	0.80	0.03	0.59	0.59	1.47	0.00	3.55	359
GCR8	0.13	1.63	0.05	0.90	1.06	2.43	0.00	6.18	5.13
GCR9	0.00	0.24	0.00	0.08	0.14	0.12	0.00	0.57	9.97
GCR10	0.00	0.19	0.00	0.06	0.10	0.09	0.00	0.45	25.11
GCR11	0.04	0.99	0.00	0.28	0.89	0.82	0.00	3.01	48.44
GCR12	0.06	1.19	0.00	0.32	1.41	0.82	0.00	3.79	23.68
GCR13	0.00	0.62	0.00	0.17	0.73	0.45	0.00	1.98	71.80
Mean	**0.05**	**0.93**	**0.01**	**0.42**	**0.68**	**1.09**	**0.00**	**3.19**	**19.56**
SE	**0.01**	**0.13**	**0.01**	**0.07**	**0.11**	**0.21**	**0.00**	**0.49**	**6.63**

Table 0.4 Ebullition facilitated metal fluxes during the post-capping sampling campaign in 2014.

2014 Post cap Metal Flux, mg/m^2/d									
Site	**As**	**Ba**	**Cd**	**Cr**	**Cu**	**Pb**	**Hg**	**ΣMetals**	**GasFlux, mmol/m^2/d**
GCR1	0.00	0.54	0.00	0.22	0.25	0.77	0.00	1.79	11.3
GCR2	0.00	0.34	0.00	0.12	0.08	0.39	0.00	0.92	6.80
GCR3	0.00	0.29	0.00	0.09	0.00	0.32	0.00	0.70	18.9
GCR4	0.00	0.20	0.00	0.09	0.00	0.14	0.00	0.43	6.25
GCR5	0.00	0.34	0.00	0.13	0.15	0.31	0.00	0.91	4.41
GCR6	0.00	0.38	0.00	0.15	0.16	0.38	0.00	1.06	67.6
GCR8	0.00	0.65	0.00	0.13	0.21	0.47	0.00	1.46	0.84
GCR9	0.00	0.23	0.00	0.05	0.00	0.15	0.00	0.44	4.72
GCR10	0.00	0.19	0.00	0.00	0.00	0.11	0.00	0.30	26.2
GCR11	0.00	0.46	0.00	0.13	0.21	0.29	0.00	1.09	3.42
GCR12	0.00	0.30	0.00	0.08	0.16	0.16	0.00	0.70	39.4
GCR13	0.00	0.11	0.00	0.05	0.00	0.06	0.00	0.22	133.5
Mean	**0.00**	**0.34**	**0.00**	**0.10**	**0.10**	**0.30**	**0.00**	**0.84**	**26.96**

SE	**0.00**	**0.05**	**0.00**	**0.02**	**0.03**	**0.06**	**0.00**	**0.14**	**11.20**

Table 0.5 Metal concentrations in pre-capping surficial sediment obtained using a Ponar dredge sampler during the 2010 sampling campaign.

	Sediment Metal Concentration (C_{sed}), mg/kg-dry							
Site	**As**	**Ba**	**Cd**	**Cr**	**Cu**	**Pb**	**Hg**	**ΣMetals**
GCR1	33	340	24.5	430	320	680	1.02	1829
GCR2	23	230	16	240	220	520	1.2	1250
GCR 3	94	330	26	790	370	1300	7.6	2918
GCR 4	77	600	65	1300	710	1500	3	4255
GCR 5	25	310	11	260	300	970	1.8	1878
GCR 6	42	1200	27	700	1100	1500	5.2	4574
GCR 8	140	620	59	2300	430	1500	2.5	5052
GCR 9	180	370	55	790	520	2700	5	4620
GCR 10	29	205	18	315	225	740	0.9	1533
GCR11	97	540	72	730	590	1100	3.2	3132
GCR12	25	580	20	450	770	780	2.8	2628
GCR 13	23	320	6.1	170	740	360	0.87	1620
Mean	65.7	470.4	33.3	706.3	524.6	1137.5	2.92	2941

SE	15.2	78.4	6.6	172	77.1	182	0.6	397

Table 0.6 Ebullition facilitated PAH fluxes during the pre-capping sampling campaign in 2010. Non-detects are reported as zero. ND= No data available.

2010 Pre-cap PAH flux, mg/m^2/d																	
Site	ACE	ANT	BNA	BaP	BbFL	BkFL	CHR	DBAN	FLAN	FLEN	INP	NAP	PHE	PYR	**∑LMW**	**∑HMW**	**∑PAHs**
GCR1	0.00	0.00	0.01	0.02	0.02	0.01	0.03	0.02	0.01	0.00	0.00	0.00	0.00	0.02	0.00	0.12	0.12
GCR2	0.00	0.00	0.01	0.03	0.02	0.02	0.04	0.01	0.02	0.00	0.01	0.00	0.01	0.02	0.02	0.17	0.19
GCR3	ND	ND	ND	ND	ND	ND	ND	ND	ND	ND	ND	ND	ND	ND	ND	ND	ND
GCR4	0.00	0.00	0.01	0.02	0.02	0.01	0.02	0.01	0.01	0.00	0.01	0.00	0.01	0.01	0.01	0.10	0.11
GCR5	ND	ND	ND	ND	ND	ND	ND	ND	ND	ND	ND	ND	ND	ND	ND	ND	ND
GCR6	ND	ND	ND	ND	ND	ND	ND	ND	ND	ND	ND	ND	ND	ND	ND	ND	ND
GCR8	0.00	0.00	0.00	0.07	0.07	0.00	0.10	0.08	0.00	0.00	0.00	0.00	0.00	0.05	0.00	0.37	0.37
GCR9	ND	ND	ND	ND	ND	ND	ND	ND	ND	ND	ND	ND	ND	ND	ND	ND	ND
GCR10	ND	ND	ND	ND	ND	ND	ND	ND	ND	ND	ND	ND	ND	ND	ND	ND	ND
GCR11	0.00	0.00	0.01	0.02	0.02	0.01	0.02	0.01	0.02	0.00	0.01	0.00	0.02	0.02	0.02	0.14	0.16
GCR12	0.00	0.00	0.01	0.00	0.06	0.00	0.06	0.01	0.09	0.00	0.00	0.00	0.00	0.08	0.00	0.31	0.31
GCR13	0.00	0.00	0.02	0.03	0.04	0.02	0.04	0.03	0.06	0.00	0.02	0.00	0.03	0.05	0.03	0.28	0.31
Mean	**0.00**	**0.00**	**0.01**	**0.03**	**0.03**	**0.01**	**0.04**	**0.02**	**0.03**	**0.00**	**0.01**	**0.00**	**0.01**	**0.04**	**0.01**	**0.21**	**0.22**
SE	**0.00**	**0.00**	**0.00**	**0.01**	**0.01**	**0.00**	**0.01**	**0.01**	**0.01**	**0.00**	**0.00**	**0.00**	**0.00**	**0.01**	**0.00**	**0.04**	**0.04**

Table 0.7 Ebullition facilitated PAH fluxes during the post-capping sampling campaign in 2012.

2012 Post-cap PAH flux, mg/m^2/d																	
Site	ACE	ANT	BNA	BaP	BbFL	BkFL	CHR	DBAN	FLAN	FLEN	INP	NAP	PHE	PYR	**∑LMW**	**∑HMW**	**∑PAHs**
GCR1	0	0	0	0	0	0	0	0	0	0	0	0	0	0	0	0	0
GCR2	0	0	0	0	0	0	0	0	0	0	0	0	0	0	0	0	0
GCR3	0	0	0	0	0	0	0	0	0	0	0	0	0	0	0	0	0
GCR4	0	0	0	0	0	0	0	0	0	0	0	0	0	0	0	0	0
GCR5	0	0	0	0	0	0	0	0	0	0	0	0	0	0	0	0	0
GCR6	0	0	0	0	0	0	0.003	0	0	0	0	0	0	0	0	0.003	0.003
GCR8	0	0	0	0.002	0.002	0	0.004	0	0	0	0	0	0	0.002	0	0.011	0.011
GCR9	0	0	0	0	0	0	0	0	0	0	0	0	0	0	0	0	0
GCR10	0	0	0	0	0	0	0	0	0	0	0	0	0	0	0	0	0
GCR11	0	0	0	0	0	0	0	0	0	0	0	0	0	0	0	0	0
GCR12	0	0	0	0	0	0	0	0	0	0	0	0	0	0	0	0	0
GCR13	0	0	0	0	0	0	0	0	0	0	0	0	0	0	0	0	0
Mean	**0**	**0**	**0**	**0**	**0**	**0**	**0**	**0**	**0**	**0**	**0**	**0**	**0**	**0**	**0**	**0.0003**	**0.0003**
SE	**0**	**0**	**0**	**0**	**0**	**0**	**0**	**0**	**0**	**0**	**0**	**0**	**0**	**0**	**0**	**0.0003**	**0.0003**

Table 0.8 Ebullition facilitated PAH fluxes during the post-capping sampling campaign in 2013.

	2013 Post-cap PAH flux, mg/m^2/d																
Site	ACE	ANT	BNA	BaP	BbFL	BkFL	CHR	DBAN	FLAN	FLEN	INP	NAP	PHE	PYR	**∑LMW**	**∑HMW**	**∑PAHs**
GCR1	0.00	0.00	0.00	0.00	0.00	0.00	0.02	0.00	0.00	0.00	0.00	0.00	0.00	0.02	0.00	0.04	0.04
GCR2	0.00	0.00	0.00	0.01	0.01	0.00	0.01	0.00	0.01	0.00	0.00	0.00	0.00	0.01	0.00	0.05	0.05
GCR3	0.00	0.00	0.00	0.00	0.00	0.00	0.00	0.00	0.00	0.00	0.00	0.00	0.00	0.00	0.00	0.00	0.00
GCR4	0.00	0.00	0.01	0.02	0.02	0.00	0.02	0.00	0.02	0.00	0.00	0.00	0.00	0.02	0.00	0.11	0.11
GCR5	0.00	0.00	0.00	0.00	0.02	0.00	0.02	0.00	0.02	0.00	0.00	0.00	0.00	0.02	0.00	0.08	0.08
GCR6	0.00	0.00	0.01	0.02	0.02	0.00	0.03	0.00	0.01	0.00	0.00	0.00	0.00	0.02	0.00	0.11	0.11
GCR8	0.00	0.00	0.04	0.04	0.05	0.02	0.11	0.02	0.05	0.00	0.02	0.00	0.03	0.08	0.03	0.41	0.44
GCR9	0.00	0.00	0.00	0.00	0.00	0.00	0.00	0.00	0.00	0.00	0.00	0.00	0.00	0.00	0.00	0.00	0.00
GCR10	0.00	0.00	0.00	0.00	0.00	0.00	0.00	0.00	0.00	0.00	0.00	0.00	0.00	0.00	0.00	0.00	0.00
GCR11	0.00	0.00	0.02	0.02	0.03	0.02	0.03	0.00	0.04	0.00	0.01	0.00	0.01	0.04	0.01	0.19	0.21
GCR12	0.00	0.02	0.03	0.03	0.04	0.04	0.05	0.00	0.11	0.00	0.02	0.00	0.07	0.09	0.09	0.38	0.47
GCR13	0.00	0.00	0.01	0.01	0.02	0.01	0.02	0.00	0.04	0.00	0.01	0.00	0.03	0.03	0.03	0.14	0.17
Mean	**0.00**	**0.00**	**0.01**	**0.01**	**0.01**	**0.01**	**0.02**	**0.00**	**0.02**	**0.00**	**0.00**	**0.00**	**0.01**	**0.02**	**0.01**	**0.10**	**0.11**
SE	**0.00**	**0.00**	**0.00**	**0.00**	**0.00**	**0.00**	**0.01**	**0.00**	**0.01**	**0.00**	**0.00**	**0.00**	**0.01**	**0.01**	**0.01**	**0.03**	**0.04**

Table 0.9 Ebullition facilitated PAH fluxes during the post-capping sampling campaign in 2014.

	2014 Post-cap PAH flux, mg/m^2/d																
Site	ACE	ANT	BNA	BaP	BbFL	BkFL	CHR	DBAN	FLAN	FLEN	INP	NAP	PHE	PYR	**∑LMW**	**∑HMW**	**∑PAHs**
GCR1	0	0	0	0	0	0	0	0	0	0	0	0	0	0	0	0	0
GCR2	0	0	0	0	0	0	0	0	0	0	0	0	0	0	0	0	0
GCR3	0	0	0	0	0	0	0	0	0	0	0	0	0	0	0	0	0
GCR4	0	0	0	0	0	0	0	0	0	0	0	0	0	0	0	0	0
GCR5	0	0	0	0	0	0	0	0	0	0	0	0	0	0	0	0	0
GCR6	0	0	0	0.001	0.001	0	0.002	0	0.001	0	0	0	0	0.001	0	0.006	0.006
GCR8	0	0	0	0.002	0.002	0	0.003	0	0.002	0	0	0	0	0.002	0	0.011	0.011
GCR9	0	0	0	0	0	0	0.001	0	0.001	0	0	0	0	0.001	0	0.004	0.004
GCR10	0	0	0	0	0	0	0	0	0	0	0	0	0	0	0	0	0
GCR11	0	0	0.001	0.001	0.002	0.001	0.002	0	0.002	0	0.001	0	0.001	0.002	0.001	0.010	0.011
GCR12	0	0	0	0.002	0.002	0.002	0.002	0	0.002	0	0.001	0	0	0.002	0	0.011	0.011
GCR13	0	0	0	0	0	0	0	0	0	0	0	0	0	0	0	0	0
Mean	**0**	**0**	**0**	**0**	**0.001**	**0**	**0.001**	**0**	**0.001**	**0**	**0**	**0**	**0**	**0.001**	**0**	**0.003**	**0.003**
SE	**0**	**0**	**0**	**0**	**0**	**0**	**0**	**0**	**0**	**0**	**0**	**0**	**0**	**0**	**0**	**0.001**	**0.001**

Table 0.10 PAH concentrations in pre-capping surficial sediment obtained using a Ponar dredge sampler during the 2010 sampling campaign.

	Sediment PAH Concentration (C_{sed}), mg/kg-dry																
Site	ACE	ANT	BNA	BaP	BbFL	BkFL	CHR	DBAN	FLAN	FLEN	INP	NAP	PHE	PYR	**∑LMW**	**∑HMW**	**∑PAHs**
GCR1	0.1	0.5	2.2	1.9	2.7	1.0	3.6	0.6	3.3	0.2	0.1	1.7	3.7	2.6	18.9	21.4	0.1
GCR2	0.2	0.5	2.9	2.2	2.7	1.3	4.7	0.6	3.8	0.3	0.1	2.5	4.6	3.6	22.8	26.3	0.2
GCR3	0.8	4.7	7.3	4.4	5.5	2.4	14.0	1.3	9.0	5.9	0.6	23.0	14.0	35.0	57.9	92.9	0.8
GCR4	0.6	2.7	11.0	4.4	5.5	2.6	18.0	1.1	12.0	2.6	0.4	33.0	18.0	39.3	72.6	111.9	0.6
GCR5	1.0	1.7	9.7	5.4	7.4	3.6	20.0	1.7	8.9	1.1	0.6	4.2	14.0	8.5	70.7	79.2	1.0
GCR6	0.3	0.6	2.7	1.7	2.1	0.8	5.3	0.6	2.4	0.5	0.1	1.1	4.3	2.5	19.9	22.4	0.3
GCR8	1.0	2.5	13.0	5.4	5.1	4.7	25.0	1.2	13.0	1.9	0.2	2.1	25.0	7.6	92.4	100.0	1.0
GCR9	2.2	11.0	37.0	12.0	13.0	6.0	73.0	3.4	39.0	14.0	0.4	2.3	82.0	29.9	265.4	295.3	2.2
GCR10	0.3	1.2	5.7	5.4	4.2	2.1	13.5	1.3	5.2	0.6	0.1	1.1	10.1	3.2	47.5	50.7	0.3
GCR11	0.5	2.3	6.3	4.9	4.8	1.1	16.0	0.9	9.2	2.5	0.4	23.0	17.0	28.6	60.2	88.8	0.5
GCR12	0.2	0.5	2.4	2.2	3.7	1.4	3.5	0.6	5.2	0.3	0.1	2.8	4.4	3.8	23.4	27.2	0.2
GCR13	0.1	0.8	4.0	3.1	5.2	2.0	4.9	0.8	8.9	0.2	0.1	3.9	7.2	5.1	36.1	41.2	0.1
Mean	**0.6**	**2.4**	**8.7**	**4.4**	**5.2**	**2.4**	**16.8**	**1.2**	**10.0**	**2.5**	**0.3**	**8.4**	**17.0**	**14.1**	**65.6**	**79.8**	**0.6**
SE	**0.2**	**0.8**	**2.6**	**0.7**	**0.8**	**0.4**	**5.1**	**0.2**	**2.6**	**1.1**	**0.1**	**3.0**	**5.7**	**3.8**	**17.9**	**20.1**	**0.2**

Table 0.11 PAH flux reduction for all three post-cap monitoring years. Cases with negative values represent increase in post-capping PAH flux. The negative reductions observed for anthracene and phenanthrene is attributed to negligible fluxes observed in the pre-capping data.

	Post-cap flux reduction, %															
Year	**ACE**	**ANT**	**BNA**	**BaP**	**BbFL**	**BkFL**	**CHR**	**DBAN**	**FLAN**	**FLEN**	**INP**	**NAP**	**PHE**	**PYR**	**∑LMW**	**∑HMW**	**∑PAHs**
2012	-	100	100	99	99	100	99	100	100	100	100	-	100	100	100	99	99
2013	-	-64	-1	53	49	27	40	93	20	100	26	-	-22	26	-19	38	41
2014	-	100	99	98	98	98	98	100	98	100	98	-	99	98	99	98	98

Table 0.12 Metal flux reduction for all three post-cap monitoring years.

	Post-cap flux reduction, %							
Year	**As**	**Ba**	**Cd**	**Cr**	**Cu**	**Pb**	**Hg**	**ΣMetals**
2012	96	90	100	94	98	93	100	94
2013	79	81	83	90	90	90	100	89
2014	100	93	100	98	98	97	100	97

Table 0.13 Chemical properties of PAHs including molecular weight, organic carbon water partitioning coefficient (K_{oc}) and Henry's constant (K_H) of PAHs used in equilibrium partition model (USEPA 1996).

Parameter	**NAP**	**ACE**	**FLEN**	**ANT**	**PHE**	**FLAN**	**PYR**	**BNA**	**BbFL**	**BkFL**	**CHR**	**BaP**	**DBAN**
	LMW	LMW	LMW	LMW	LMW	HMW	HMW	HMW	HMW	HMW	HMW	HMW	HMW
Number of Rings	2	2	2	3	3	3	4	4	4	4	4	5	5
MW, g/mol	128.2	154.2	166.2	178.2	178.2	202.3	202.3	228.3	252.3	252.3	228.3	252.3	278.3
logK_{oc}, L/kg	3.09	3.7	3.95	4.39	4.4	4.69	4.85	5.66	6.09	6.09	5.6	6.07	6.31
K_H , atm-m3/mol	5E-04	2E-04	6E-05	7E-05	3E-05	2E-05	1E-05	3E-06	1E-04	8E-07	9E-05	1E-06	1E-08

Table 0.14 Pore-water concentration of PAHs predicted by the equilibrium partition model (EPT), C_w (mg/L).

Concentration in Water, C_w, mg/L													
Site	**NAP**	**ACE**	**FLEN**	**ANT**	**PHE**	**FLAN**	**PYR**	**BNA**	**BbFL**	**BkFL**	**CHR**	**BaP**	**DBAN**
GCR1	1E-03	5E-04	4E-04	4E-04	1E-03	1E-03	1E-03	9E-05	4E-05	2E-05	2E-04	3E-05	5E-06
GCR2	2E-03	6E-04	6E-04	4E-04	2E-03	1E-03	1E-03	1E-04	4E-05	2E-05	2E-04	3E-05	5E-06
GCR3	4E-03	1E-03	6E-03	2E-03	8E-03	2E-03	2E-03	1E-04	4E-05	2E-05	3E-04	3E-05	5E-06
GCR4	3E-03	1E-03	3E-03	1E-03	1E-02	2E-03	2E-03	2E-04	4E-05	2E-05	4E-04	3E-05	5E-06
GCR5	1E-02	4E-03	3E-03	2E-03	4E-03	4E-03	4E-03	5E-04	1E-04	7E-05	1E-03	1E-04	2E-05
GCR6	4E-04	4E-04	4E-04	1E-04	3E-04	3E-04	4E-04	4E-05	1E-05	4E-06	9E-05	9E-06	2E-06
GCR8	1E-03	2E-03	2E-03	1E-03	9E-04	3E-03	4E-03	3E-04	4E-05	4E-05	7E-04	5E-05	6E-06
GCR9	3E-03	4E-03	2E-02	4E-03	9E-04	8E-03	1E-02	8E-04	1E-04	5E-05	2E-03	1E-04	2E-05
GCR10	1E-03	9E-04	1E-03	7E-04	7E-04	2E-03	2E-03	2E-04	5E-05	3E-05	5E-04	7E-05	1E-05
GCR11	3E-03	9E-04	3E-03	9E-04	9E-03	2E-03	2E-03	1E-04	4E-05	9E-06	4E-04	4E-05	4E-06
GCR12	4E-04	3E-04	3E-04	2E-04	9E-04	9E-04	5E-04	4E-05	3E-05	1E-05	7E-05	2E-05	2E-06
GCR13	5E-04	3E-04	3E-04	3E-04	2E-03	2E-03	1E-03	1E-04	5E-05	2E-05	1E-04	3E-05	4E-06

Table 0.15 Partial pressure of PAHs in the gaseous phase as predicted by the equilibrium partitioning model (EPT), C_a (atm)

	Partial pressure in gaseous phase, Ca, atm												
Site	**NAP**	**ACE**	**FLEN**	**ANT**	**PHE**	**FLAN**	**PYR**	**BNA**	**BbFL**	**BkFL**	**CHR**	**BaP**	**DBAN**
GCR1	5E-09	5E-10	1E-10	1E-10	2E-10	1E-10	5E-11	1E-12	2E-11	5E-14	7E-11	1E-13	3E-16
GCR2	7E-09	6E-10	2E-10	1E-10	3E-10	1E-10	7E-11	2E-12	2E-11	6E-14	9E-11	2E-13	3E-16
GCR3	1E-08	1E-09	2E-09	6E-10	1E-09	1E-10	9E-11	2E-12	2E-11	5E-14	1E-10	1E-13	3E-16
GCR4	1E-08	1E-09	1E-09	4E-10	2E-09	2E-10	1E-10	3E-12	2E-11	6E-14	2E-10	2E-13	3E-16
GCR5	4E-08	4E-09	1E-09	6E-10	5E-10	3E-10	2E-10	7E-12	6E-11	2E-13	5E-10	5E-13	1E-15
GCR6	1E-09	4E-10	1E-10	5E-11	4E-11	3E-11	2E-11	6E-13	5E-12	1E-14	4E-11	4E-14	1E-16
GCR8	5E-09	2E-09	9E-10	4E-10	1E-10	2E-10	2E-10	5E-12	2E-11	1E-13	3E-10	2E-13	3E-16
GCR9	1E-08	4E-09	6E-09	2E-09	1E-10	6E-10	6E-10	1E-11	4E-11	2E-13	7E-10	4E-13	8E-16
GCR10	5E-09	9E-10	4E-10	3E-10	1E-10	1E-10	1E-10	3E-12	2E-11	9E-14	2E-10	3E-13	5E-16
GCR11	1E-08	9E-10	1E-09	3E-10	1E-09	1E-10	1E-10	2E-12	2E-11	3E-14	2E-10	2E-13	2E-16
GCR12	2E-09	3E-10	1E-10	6E-11	1E-10	7E-11	3E-11	7E-13	1E-11	3E-14	3E-11	7E-14	1E-16
GCR13	2E-09	3E-10	1E-10	1E-10	2E-10	2E-10	6E-11	1E-12	2E-11	6E-14	6E-11	1E-13	2E-16

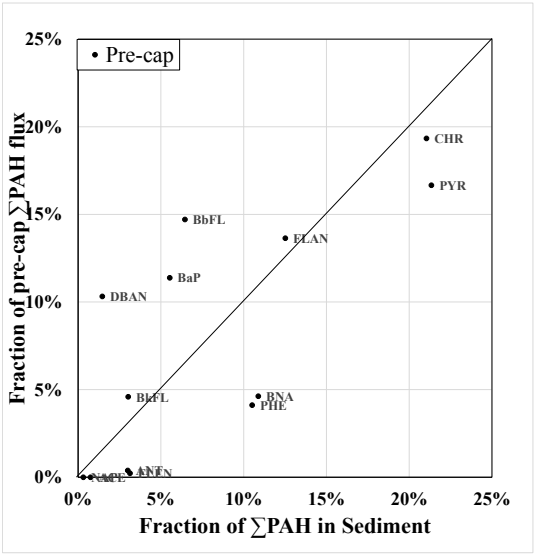

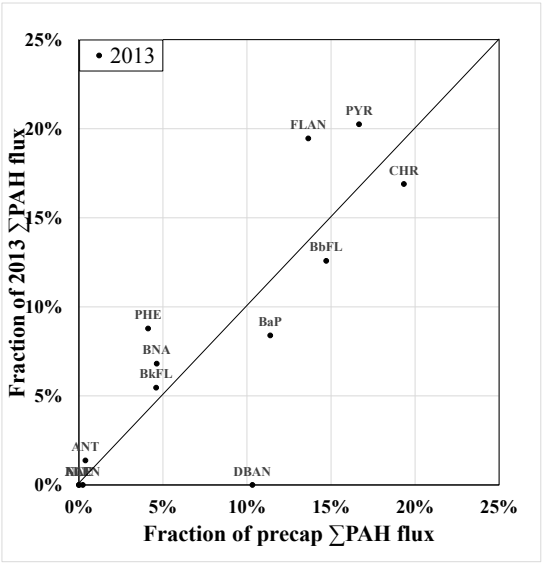

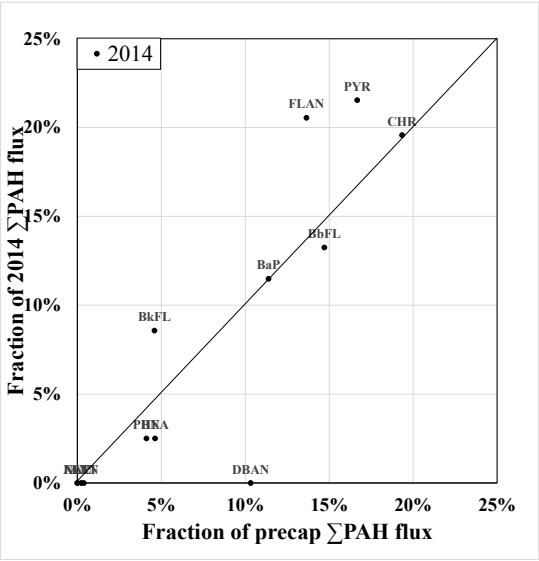

Figure 0.4 Comparison plot of fraction of individual PAHs to total PAHs in glass wool and contaminated sediment for A) pre-capping B) 2013 and C) 2014

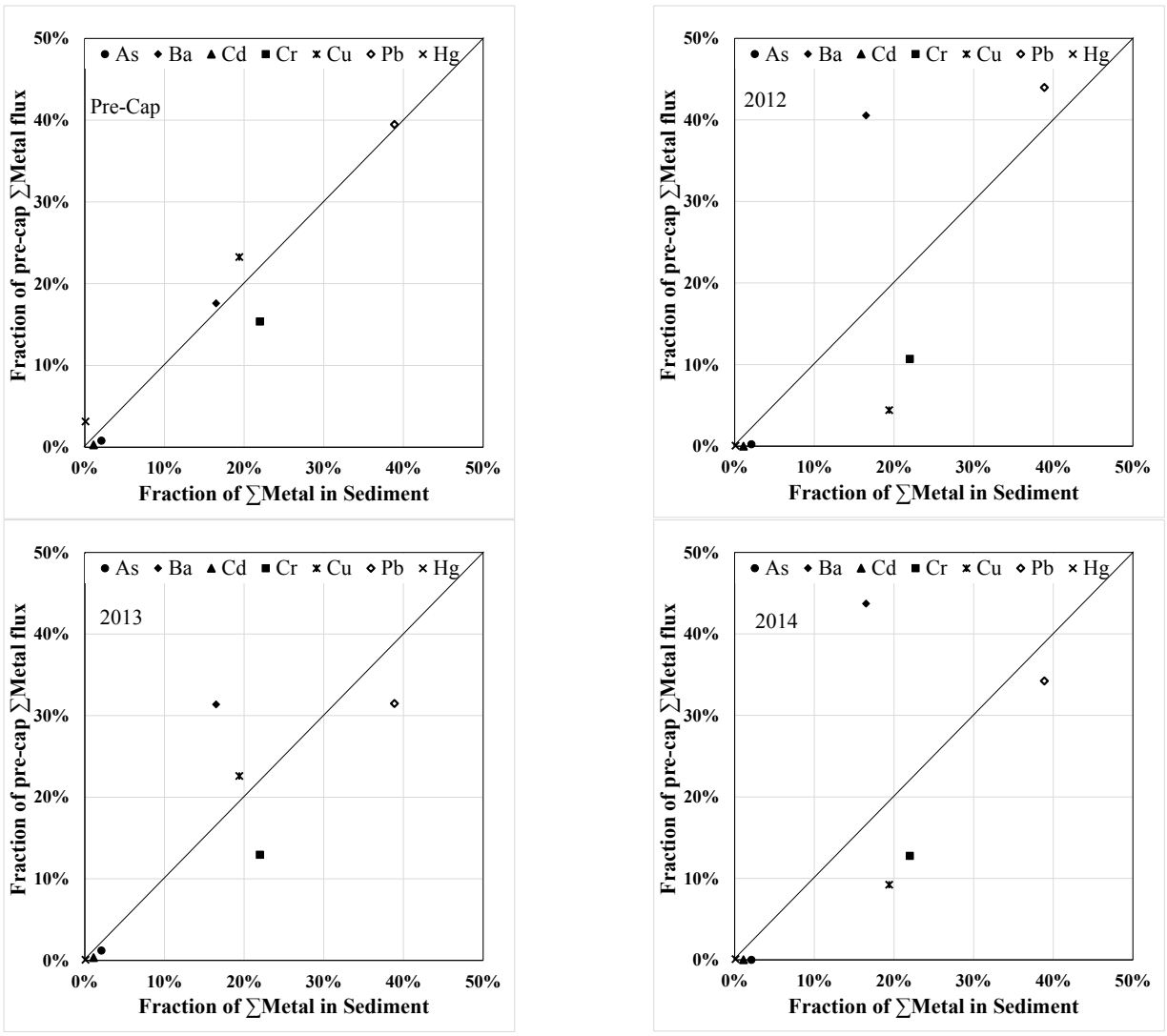

Figure 0.5 Comparison plot of fraction of individual metals to total metals in glass wool and contaminated sediment for A) pre-capping B) 2012 C) 2013 and D)2014.

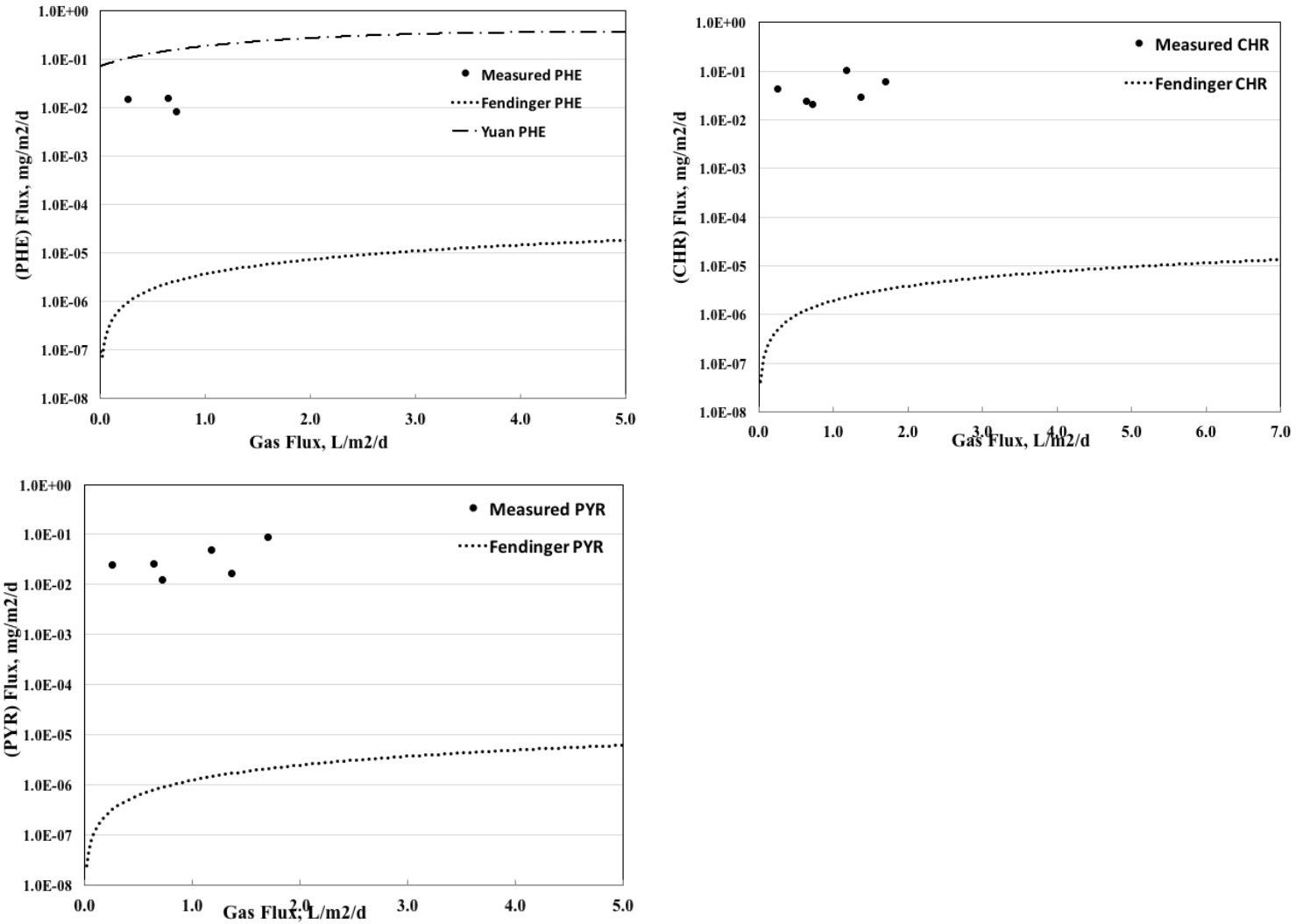

Figure 0.6 Predicted ebullition facilitated PAH fluxes for A)Pyrene (PYR), B)Chrysene (CHR) C)Phenathrene (PHE) plotted as a function of gas flux and compared with field measured fluxes.

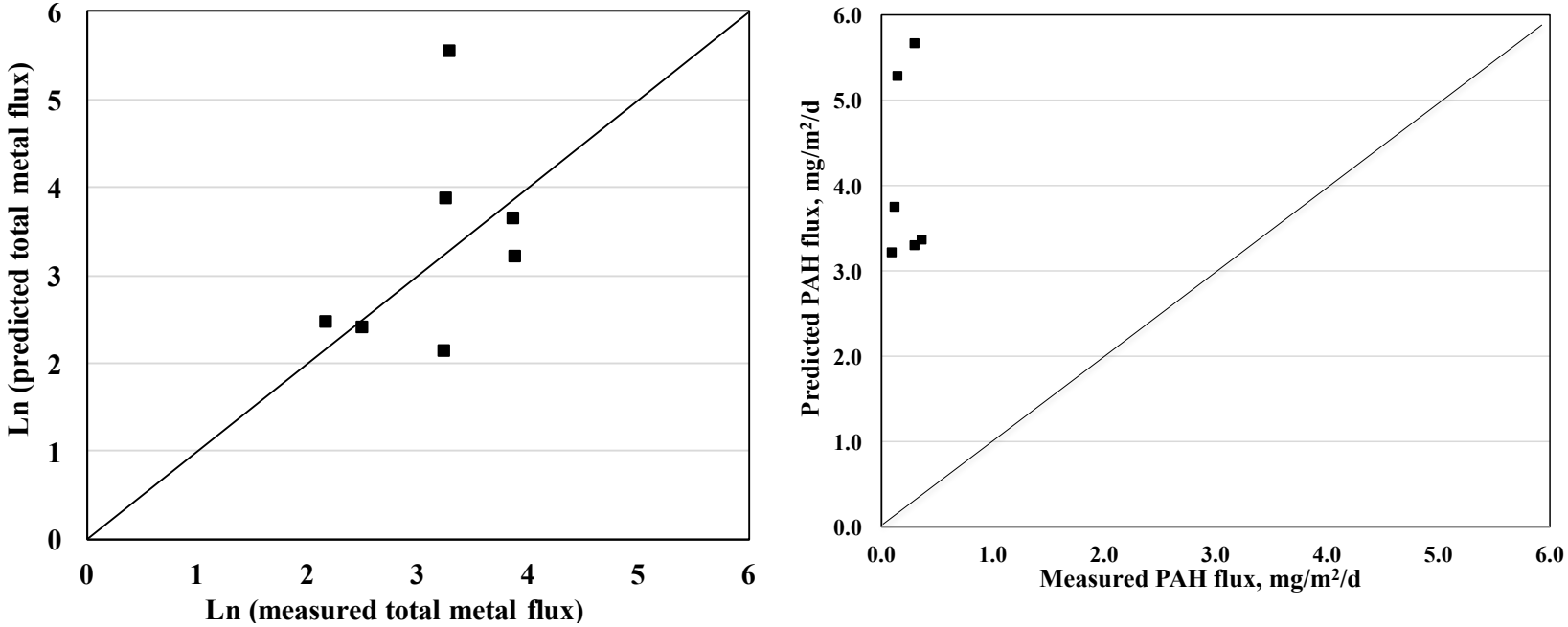

Figure 0.7 Comparison plot of Viana et al predicted metal and PAH flux and field measured ebullition facilitated flux.

Viana et al Regression equation for Individual and Total Metals:

$$\ln CF_{Tmetal} = 2.64 + 0.0072GF_m + 0.20T - 0.099\theta + 0.056CoreOM + 6.9S_{labile} - 0.71C_{sed} - 0.79D_w \quad (0.3)$$

Viana et al Regression equation for ebullition facilitated Total PAH flux:

$$\ln CF_{TPAH} = 13 - 0.676 \ln C_{Sed} + 0.0075GF_m - 0.017 \rho_b + 0.744 SGOC + 0.17 CoreOM - 0.51CoreOC + 18.3 S_{labile} \quad (0.4)$$

Where $\ln CF_{metal}$ = Ebullition facilitated individual metal flux, $mg/m^2/d$

$\ln CF_{Tmetal}$ = Ebullition facilitated total metal flux, $mg/m^2/d$

$\ln CF_{TPAH}$ = Ebullition facilitated total PAH flux, $mg/m^2/d$

K_d = Sediment water partitioning coefficient, L kg^{-1}

GF_m = Molar gas flux, $mmol/m^2/d$

Φ = percent solids, %

S_{labile} = SGCOD/SG OC

D_{sed} = sediment depth to hard clay pan

C_{sed} = sediment concentration in mg/kg

T = sediment temperature, °C

θ = sediment porosity, %

ρ_b = sediment bulk densitu, g/cm^3

CoreOM = Mean core organic mater content, %

CoreOC = Mean core organic carbon content, %

SGO= Sediment grab organic carbon content,

SGCOD = Sediment grab chemical oxygen demand, mg/kg

Fendinger contaminant flux model:

Contaminat Flux $(mg/m^2/d) = (K_H * C_{sed} * GF_m) / (K_{oc} * f_{oc})$

Where K_H – Henry's law Constant

f_{oc} – fraction organic carbon

K_{oc} – Organic carbon water partition coefficeint

CHAPTER V ARCHAEAL COMMUNITY STRUCTURE IN PRE AND POST CAP WEST BRANCH GRAND CALUMET RIVER SEDIMENTS

5.1 Introduction

Fine-grained river sediments are rich in organic matter and represent an important component of this biogeochemical and microbial cycles in fluvial ecosystems (Meyers and Eadie 1993). Organic matter is degraded by a consortium of microbial groups typically following a specific order of substrate consumption reflecting the decreasing order of free energy change ($\Delta G^{\circ\prime}$) associated with the biochemical redox reactions. The end products of OM breakdown are sediment gases that are composed primarily of CH_4, CO_2, and N_2. An overview of the different stages of carbon metabolism and factors influencing sedimentary gas production is discussed in detail in chapter two with methanogenesis being the last step in anaerobic degradation of OM to produce CH_4. Methanogenesis typically follows a four-stage process of hydrolysis, acidogenesis, acetogenesis and methanogenesis that involves a complex group of bacteria and *Archaea*. Methanogenesis is performed by two main groups of *Archaea*; hydrogenotrophs and acetoclasts. The contribution of different archaeal groups to CH_4 production varies with substrate availability and sediment temperature, with acetoclastic methanogens dominating at lower temperatures and hydrogenotrophs dominating at higher temperature ranges (Glissman et al. 2004).

The release of accumulated gases in the sediment to the atmosphere is referred to as gas ebullition and occurs when the buoyant force of gas bubbles exceeds the combined cohesive forces in the sediment and the hydrostatic pressure exerted by the water column. In capping of contaminated streambeds, post-cap gas production has the potential to significantly impact the effectiveness of the cap in isolating the contaminated sediments from the water column and

adsorbing migrating contaminants by sequestration. Gas ebullition events form preferential pathways that allow transport of hydrophobic organic contaminants (HOCs) such as PAHs and PCBs in vapor or non-aqueous phase to the atmosphere and also result in the deterioration of the surface water quality due to re-suspension of contaminated surficial sediments (Yuan et al. 2007). Furthermore, the formation of sediment fractures can facilitate transport across the cap.

Although gas production from underneath the cap material is expected to decrease over time due to the cessation of new OM input to the originally bioactive zone, significant post-cap gas ebullition have been reported at Anacostia River (Reible et al. 2006) and West Branch Grand Calumet River (WBGCR) (Rockne and Kaliappan 2013). Field monitoring of ebullition rates at WBGCR revealed high seasonal variability in gas fluxes but failed to identify the primary zone of gas production. Physical characterization of post-cap sediment cores showed sufficient availability of labile organic matter (15 – 25% OM) in the contaminated sediment zone (>45 cm depth) at fractions much higher than that observed in new surficial deposits (1 – 3%). Incubation studies with sediment from core sections provided evidence of sustained gas production even after one year of incubation (Chapter 3). As expected the post-cap ebullition rates were significantly correlated with sediment temperature, and gas production rate constant data suggested that the underlying CSed could be the primary gas producing zone. To further ascertain the contribution of different layers of the streambed to total gas production, phylogenetic analysis of 16sRNA from four sections (ND, GAL, OrgC, CSed) of the sediment core were investigated to evaluate the archaeal community structure and abundance of methanogenic *Archaea*. *Archaea* and *Bacteria* are both single celled Prokaryotes organism. *Archaea* have a longer evolutionary history with adaptation for extreme environments and are closely related to *Ekarya* than *Bacteria*. *Archaea* are harder to culture with methanogenic

archaea primarily responsible for methane production in the environment. PCR based amplification of 16sRNA genes provide the ability to assess microbial diversity and its environmental significance without culture-based studies, which can result in a well-known culturability bias. With the advent of bioinformatics tools for the analysis of large quantities of sequencing data has simplified the investigation of the microbial community structure to provide a better understanding of site-specific biochemical processes.

5.2 Objectives

There are three objectives for the investigation presented here. The first objective was to investigate the archaeal community structure in the surficial sediments prior to the dredging and placement of an active sediment cap in the WGCR. These data were evaluated to compare variations in abundance of methanogenic *Archaea*, compared with sediment physio-chemical characteristics to assess their impact on the methanogen distribution and field measured gas production rates.

The second objective was to investigate the stratification of the archaeal community in four layers of the sediment following capping to understand the specific microbial gas production mechanism and the predominant group of microorganisms involved its production. The distribution of microorganisms with depth will be used to assess the microbial organisms capable of degrading more recalcitrant organic matter.

The final objective was to assess the impact of capping on the archaeal microbial community structure and to determine if there were any changes in the primary methanogenic pathway from/to acetoclasty or hydrogenotrophy.

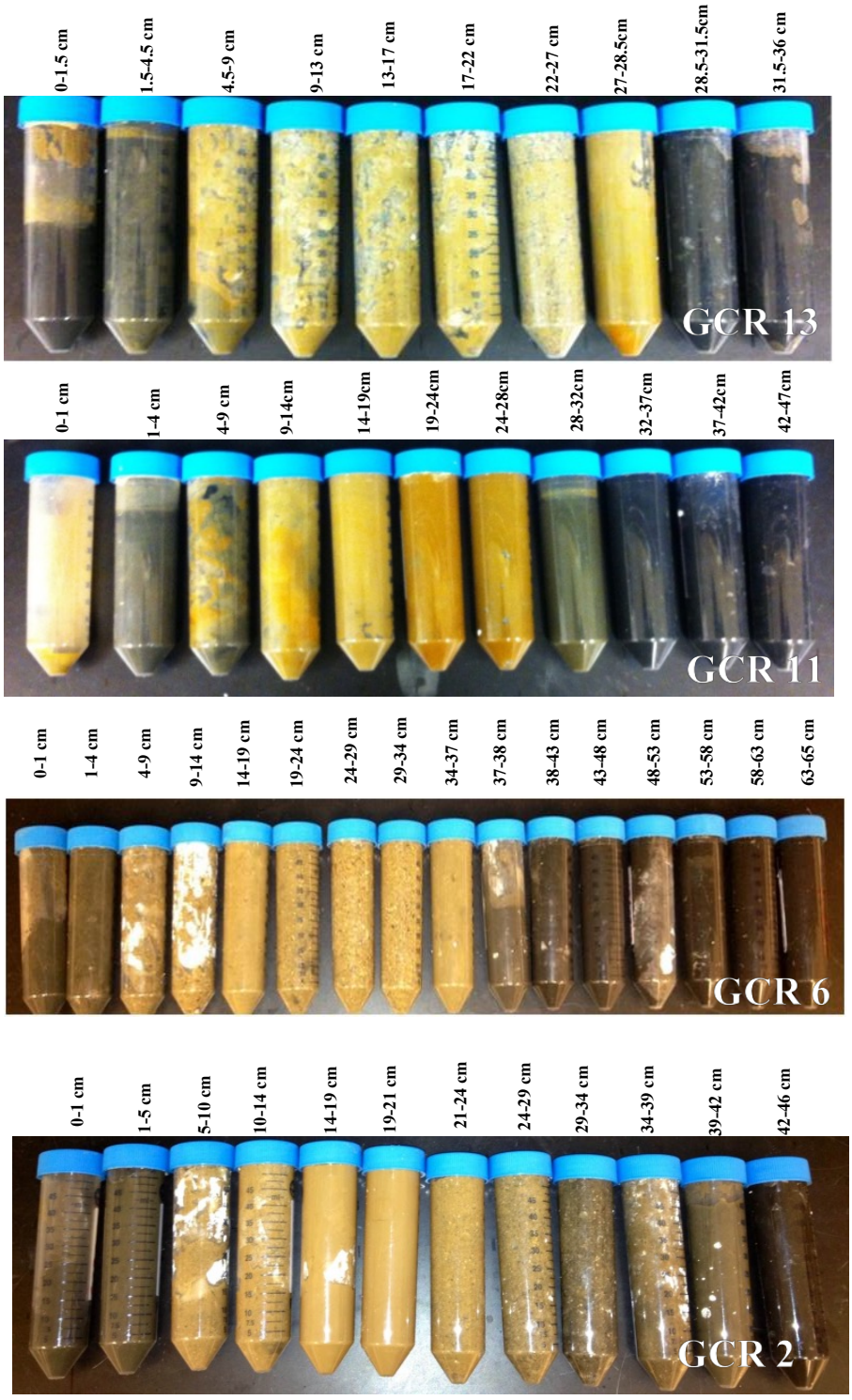

Figure 0.1 Sediment samples obtained from four cores in the WBGCR The dark grey material (1-5 cm) represents new sediment. Brown material (5-25cm) represents the armoring layer, greyish material (25-35cm) represents the organoclay cap and the black material represents the underlying contaminated sediment.

5.3 Materials and Methods

Surficial sediment grabs were obtained at all 13 monitoring locations and post-capping sediment cores were obtained for sites GCR2, 6, 11 and 13. Four sections of the post-cap sediment cores were selected for investigation of the microbial community structure at depths corresponding to the new sediment deposition (ND layer) on top of the cap, the gravel armoring layer (GAL), the organoclay (OrgC) clay layer and the underlying contaminated sediment layer (CSed). Figure 5.1 shows sectioning depths for post-cap sediment cores. OM, OC and BC were analyzed using methods described in Borrel et al (Borrel et al. 2012). Sediment characteristics and depths chosen for DNA sequencing and incubation studies are shown in Table 5.1. The OM content in the OrgC layer is in the range of values observed in the ND layer probably due to mixing of contaminated sediment and organoclay during cap placement.

Table 0.1 Properties and DNA content of sediment core sections chosen for analysis.

Site	Sample ID	Depth	Layer	DNA Conc	Organic Matter (OM)	Organic Carbon (OC)	Black Carbon (BC)
		(cm)		(ng/uL)	%	%	%
GCR2	GCR 2-1	0-5	ND	74.1	1.29	0.44	0.07
	GCR 2-3	14-19	GAL	6.3	0.65	0.29	0.07
	GCR 2-5	39-42	OrgC	8.2	1.29	0.75	0.12
	GCR 2-6	42-45	CSed	26.9	10.94	14.43	1.38
GCR6	GCR 6-1	0-4	ND	69	2.46	1.13	0.07
	GCR 6-2	9-14	GAL	7.4	0.27	0.05	0.01
	GCR 6-5	34-37	OrgC	5.9	1.06	1.23	0.10
	GCR 6-6	43-48	CSed	24.2	23.59	18.20	1.36
GCR11	GCR 11-1	0-4	ND	51	3.50	2.26	0.29
	GCR 11-2	9-14	GAL	10.3	0.55	0.11	0.04
	GCR 11-4	19-24	OrgC	10.5	1.33	0.91	0.18
	GCR 11-6	32-37	CSed	25.5	26.15	21.01	1.40
GCR13	GCR 13-1	0-4.5	ND	63.7	2.26	2.10	0.07
	GCR 13-2	13-17	GAL	19.3	0.28	0.08	0.01
	GCR 13-4	22-27	OrgC	9.6	0.94	0.53	0.06
	GCR 13-6	31.5-36	CSed	22.5	14.75	5.03	0.82

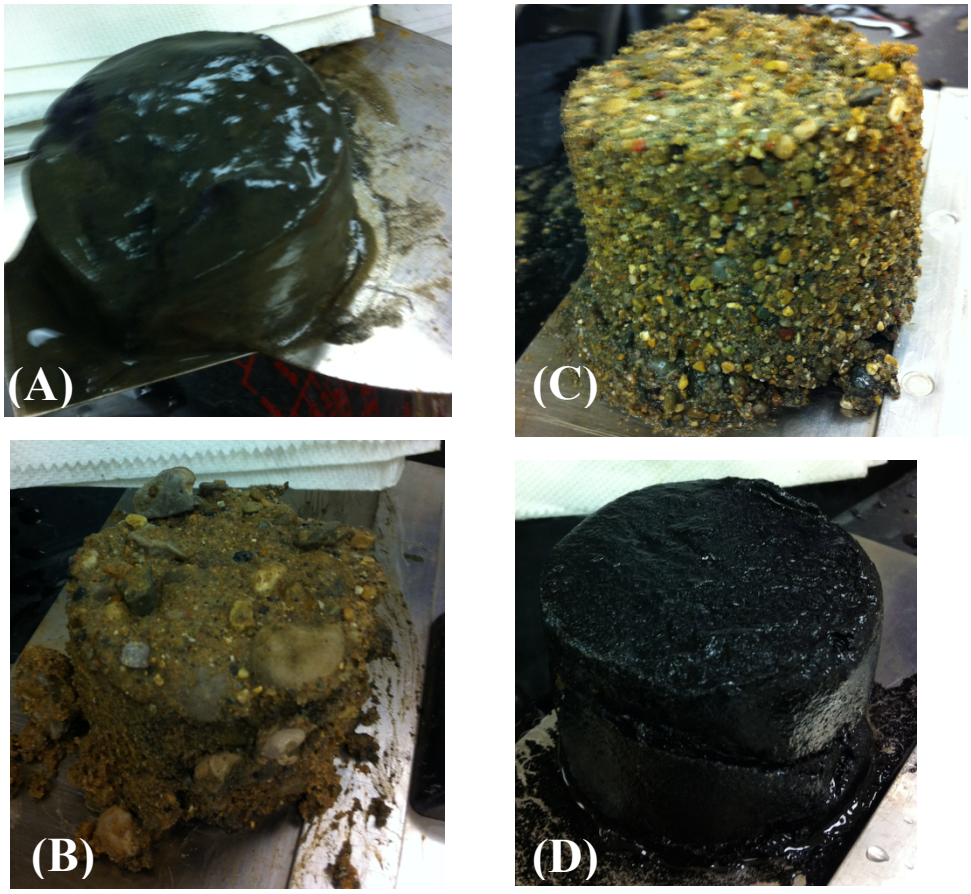

Figure 0.2 Texture of the sediment core sections from the A) new sediment deposit, B) armor layer (gravel-sand mixture with high percentage of gravel), C) organoclay layer (sandy texture), and the D) underlying contaminated sediment (clayey texture).

5.3.1 DNA extraction

The Mobio PowerSoil® DNA isolation kit was used to extract DNA from the contaminated samples following the manufacturer's instruction (Mo Bio Laboratories, Carlsbad, CA). The kit consists of PowerBead Tubes, 2ml collection tubes, proprietary solutions C1-C6 and spin filters. The sediment sample was processed through a series of steps as described in the instruction manual with all centrifugation steps performed at 10,000 g for 1 minute.

In the first step, wet sediment weighing 0.25g and 60µL of solution C1 were added to a PowerBead tube provided with the kit. The tube was vortexed for 15 minutes to ensure cell lysis

and release of nucleic acids in the cell. The sample was centrifuged and the supernatant transferred to a new 2 ml collection tube. In the second step, 250µL of solution C2 was added followed by vortexing for 5sec and incubation at 4 °C for 5 minutes. This precipitates non-DNA organic and inorganic material in the solution. The sample was centrifuged and the supernatant transferred to a new 2ml collection tube. In the third step, 200µL of solution C3 was added to the supernatant followed by vortexing and incubation at 4 °C for 5 minutes. Solution C3 contains proprietary inhibitor removal technology to precipitate additional non-DNA organic and inorganic material. Following incubation, the collection tubes was centrifuged and up to 750 µL of supernatant was transferred to a new collection tube. In the fourth step, 1.2ml of solution C4 was added to supernatant and vortexed for 5 seconds. Solution C4 is a high concentration salt solution that promotes binding of DNA to the silica spin filter provided with the kit. In the fifth step, a spin filter was placed inside a 2ml collection tube and up to 675 µL of the supernatant from previous step was loaded onto it. The collection tube with spin filter was centrifuged at 10,000 g for 1 minute and flow through was discarded. DNA in the solution binds to silica in the spin filter as it passes through the filter. In the sixth step, the DNA bound spin filter was transferred to a new 2ml collection tube and 500 µL of wash solution C5 was added. Solution C5 is an ethanol-based solution that further purifies the DNA in the spin filter and removes residual salt and humic in the filter. The spin filter with solution C5 was centrifuged and the flow through was discarded. In the seventh step, cleaned spin filter was again transferred to a new 2ml collection tube and 50 µL of solution C6 was added. Solution C6 is a sterile DNA-free elution buffer that releases DNA bound to the spin filter. The DNA in the flow through from step seven was stored at -40 °C until further processing. DNA extracts were analyzed in a Nanodrop to ensure sufficient DNA concentration for sequencing purposes.

5.3.2 16S rRNA sequencing

Sequencing was performed at the W.M. Keck Center for Comparative and Functional Genomics at the University of Illinois at Urbana-Champaign. DNA samples were prepared for two-step PCR protocol, as described previously (Green, Venkatramanan, and Naqib 2015). DNA was PCR amplified with two primer sets, targeting the small subunit ribosomal RNA (SSU rRNA) gene of Archaea using primers forward primer Ar915aF (AGG AAT TGG CGG GGG AGC AC) and reverse primer Ar1386R (GCG GTG TGT GCA AGG AGC), targeting the V6-V8 variable region (Kittelmann et al. 2013). PCR amplifications were performed as described in Earley et al (Earley et al. 2015). The sample was loaded on a MiSeq System (Model v3, Illumina Inc, San Diego, CA) flow cell at a concentration of 5.5pM and sequenced in 2x300bp paired end format using a 600-cycle MiSeq v3 reagent cartridge.

5.3.3 MGRAST Pipeline

MGRAST is an open source web application server that can be used for sequence annotation and comparative analysis of metagenomes. MGRAST allows upload of sequence data in raw formats such as "*.fasta" and "*.fastq", which are normalized by the pipeline, processed and outputs detailed information on the metagenome. The Illumina sequencer used in this analysis produces two reads (R1 and R2) corresponding to the forward and reverse reads of the 16S rRNA genes, respectively. The raw reads were uploaded to the MGRAST. The joined paired ends option was used during the upload process to join the forward and reverse reads R1 and R2 for each sequence pair. Once paired, the sequences were submitted to the MGRAST pipeline without de-replication as it is not suitable for amplicon sequences in the removal of artificial duplicate reads (ADR). The option for dynamic trimming was left checked. The MGRAST pipeline utilizes DRISEE (Duplicate Read Inferred Sequencing Error Estimation) to analyze for ADRs and has screening tools to remove genomes for fly, cow, mouse and human. MGRAST also provides rRNA clustering of sequences at a 97% identity cutoff (adjustable) and the longest sequence was chosen as the cluster representative. Low quality sequences of less than 300 bp were removed from the MGRAST pipeline and representative rRNA sequences were compared against the M5RNA database using the BLAST alignment algorithm for similarity search (Wilke et al. 2014). M5RNA is a comprehensive rRNA database that combines SILVA (Pruesse et al. 2007), Greengenes (DeSantis et al. 2006) and the RDP (Cole et al. 2003) rRNA databases that contain annotated bacterial and archaeal16srRNA sequences. MGRAST provides user defined threshold parameters for annotation transfer by specifying e-value, percent identity and alignment length during sequence analysis. In this analysis an e-value cutoff of 1E-5, identity cutoff of 80%, and a minimum alignment length cutoff of 15 were used for annotation transfer.

Table 0.2 Statistics for pre- and post-quality control of post-capping DNA sequences submitted to MGRAST.

Post-cap sequences			Pre-quality Control				Post-quality Control			
Site	**Depth (cm)**	**Sample ID**	**bp[(1)]**	**Sequence Count**	**Mean Length**	**G+C%**	**bp[(1)]**	**Sequence Count**	**Mean Length**	**G+C%[(2)]**
GCR2	0-5 cm	GCR 2-1	35,601,535	84,941	419 ± 61	53 ± 2	31,783,093	82,478	385 ± 158	53 ± 3
	14-19 cm	GCR 2-3	11,544,229	27,426	420 ± 60	55 ± 1	10,356,031	26,728	387 ± 158	55 ± 4
	39-42 cm	GCR 2-5	33,207,491	78,677	422 ± 58	55 ± 1	30,007,007	76,831	390 ± 157	55 ± 3
	42-45 cm	GCR 2-6	41,218,693	101,236	407 ± 65	56 ± 2	36,233,987	98,678	367 ± 157	56 ± 3
GCR6	0-4 cm	GCR 6-1	44,237,107	104,453	423 ± 58	54 ± 1	39,856,889	101,794	391 ± 159	54 ± 3
	9-14 cm	GCR 6-2	30,188,161	70,977	425 ± 56	54 ± 1	27,420,666	69,374	395 ± 156	54 ± 3
	34-37 cm	GCR 6-5	36,438,552	86,581	420 ± 59	55 ± 1	32,657,710	84,268	387 ± 159	54 ± 3
	43-48 cm	GCR 6-6	39,062,630	91,944	424 ± 56	54 ± 1	35,334,267	89,849	393 ± 158	54 ± 3
GCR11	0-4 cm	GCR 11-1	33,947,126	80,837	419 ± 59	54 ± 2	30,369,373	78,529	386 ± 159	54 ± 3
	9-14 cm	GCR 11-2	21,655,730	51,343	421 ± 59	55 ± 2	19,404,912	49,906	388 ± 160	54 ± 3
	19-24 cm	GCR 11-4	57,302,560	135,604	422 ± 58	55 ± 1	51,741,315	132,301	391 ± 157	55 ± 3
	32-37 cm	GCR 11-6	81,202,351	192,132	422 ± 58	55 ± 1	73,235,052	187,304	390 ± 162	54 ± 3
GCR13	0-4.5 cm	GCR 13-1	42,510,137	101,346	419 ± 61	54 ± 2	38,002,995	98,730	384 ± 157	54 ± 3
	13-17 cm	GCR 13-2	13,190,331	31,211	422 ± 58	55 ± 1	11,928,386	30,423	392 ± 155	55 ± 3
	22-27 cm	GCR 13-4	40,184,321	94,809	423 ± 57	55 ± 1	36,328,875	92,465	392 ± 159	55 ± 4
	31.5-36 cm	GCR 13-6	56,896,912	138,260	411 ± 64	56 ± 2	50,165,706	134,720	372 ± 160	55 ± 4

(1) Number of basepairs. (2) Guanine and Cytosine percentage

5.4 Results and Discussion

5.4.1 Sequence Statistics

To ensure high quality classification of the indigenous microbial community, the amplicon sequences were subject to quality control using the MGRAST pipeline as described above. A total of 29 metagenomes were submitted to MGRAST and the quality control process removed between 2.2% to 2.9% of the sequences in each metagenome with 100% of the quality-controlled sequences identified as ribosomal RNA genes. The G+C content ranged between 53 to 55%, indicating a lack of bias and good quality of sequencing data (Che Aziz 2014).

Table 0.3 Sequence statistics for pre-capping DNA sequencing data from sediment surface grabs.

	Pre-quality Control				Post-quality Control			
Site	**bp**	**Count**	**Length**	**GC%**	**bp**	**Count**	**Length**	**GC%**
GCR1	36,449,470	87,227	417 ± 61	55 ± 2	32,486,527	84,920	382 ± 159	55 ± 3
GCR2	26,646,733	63,624	418 ± 60	55 ± 2	23,838,740	61,974	384 ± 159	55 ± 3
GCR3	25,454,556	60,507	420 ± 59	55 ± 1	22,882,690	59,173	386 ± 156	55 ± 3
GCR4	25,113,954	60,121	417 ± 61	55 ± 2	22,440,783	58,530	383 ± 157	55 ± 3
GCR5	22,890,999	54,723	418 ± 61	55 ± 2	20,441,800	53,270	383 ± 159	55 ± 3
GCR6	23,489,160	55,193	425 ± 56	55 ± 1	21,280,644	53,949	394 ± 160	54 ± 3
GCR7	25,094,795	60,489	414 ± 62	56 ± 2	22,390,357	59,164	378 ± 155	55 ± 3
GCR8	31,917,444	76,552	416 ± 61	55 ± 2	28,381,340	74,370	381 ± 157	54 ± 3
GCR9	48,332,154	115,813	417 ± 61	55 ± 2	43,169,372	112,677	383 ± 161	55 ± 3
GCR10	40,207,930	95,651	420 ± 59	55 ± 2	36,166,691	93,369	387 ± 156	55 ± 3
GCR11	38,445,043	90,660	424 ± 57	55 ± 1	34,830,768	88,617	393 ± 156	54 ± 3
GCR12	32,423,782	76,300	424 ± 56	55 ± 1	29,370,540	74,524	394 ± 160	54 ± 3
GCR13	37,042,634	87,890	421 ± 59	55 ± 1	33,192,708	85,557	387 ± 159	54 ± 3

Sequence statistics for pre-capping metagenomes from surficial sediment are shown in Table 5.3. More than 95% of the pre-capping sequences were classified as *Archaea* by the M5RNA database with only a small (<0.01%) fraction of unidentified sequences. Sites GCR 9 and 10 had higher number of bacterial sequences at around 10%, whereas other sites were in the range of 1-5%. A negligible fraction (0.03 – 0.1%) of the sequences were assigned to the domain viruses (Table 5.4).

It is worth noting that sequence counts were similar to that from 0-5cm depths in the post-capping ND layer. Sequence counts were higher at sites GCR13 to GCR8 (i.e. Reach 2), with the highest sequence count of 115,000 recorded at GCR9. This may be attributed to deposition of organic-rich sediment scoured by the HSD outfall. The outfall was deepened and reinforced with rip-rap to prevent sediment scouring, preventing downstream deposition. Lower sequence counts were observed at sites GCR6 - 2 (i.e. Reach 1). GCR1 located at the edge of the cap had higher sequence counts compared to other sites in Reach 1. The G+C count and sequence length (>400bp) were in the range of values suggestive of good quality of sequence data (Che Aziz 2014).

In post-cap cores, the sequence counts in the CSed layers were higher for Reach 2 sites GCR 11 and 13 located west of the Hammond Sanitary District (HSD) outfall; 138,000 and 192,000 respectively (Table 5.5). Sequence count in the surficial zone was also higher at GCR13 (101,000) compared to GCR11 (81,000). The water quality at these sites was comparatively poor with a stagnant water column and anaerobic conditions. GCR13 and 11 are located closer to HSD outfall, which is a potential source of new OM and nutrient input to the reach. The OrgC layer at sites GCR 11 and 13 had elevated sequence counts (135,000 and 94,000) compared to the GAL layer. This can be due to the shorter depth of the cap at these sites and greater mixing

with the CSed, layer as evidenced by higher OM content (Table 5.2). GCR 6 and 2 located in Reach 1 were marked by comparatively lower sequence counts in the CSed layer 91, 000 and 101,000 sequences respectively. At GCR6 the sequence count in the ND layer was comparable to that at GCR13. It is interesting to note that the GCR 6 had higher gas production rates and higher sequence counts throughout the core depth. GCR 2 exhibited the lowest sequence count for the GAL and OrgC layer among the four post-cap sites, although sequence counts in the ND and CSed layers were comparable to other sites.

5.4.2 Species Richness and Diversity in Pre-Capping Sediments

Rarefaction curves and the alpha diversity of the pre-capping sequences were analyzed to evaluate the diversity of *Archaea* and species richness captured by sequencing. The rarefaction curve is a plot of total number of distinct species as a function of the cumulative number of sequences. The curve is characterized by a steep slope to the left with a flatter slope to the right representing progressively rarer species. The curve becomes asymptotic to the right as fewer distinct species are identified, indicating that majority of the organisms are characterized and more intense sequencing will result in only few additional species. MGRAST also computes the α-diversity representing the species richness in a sequence. A higher α-diversity number signifies a greater number of species in the samples with similar abundance. A higher species count with lower abundance will result in a lower α-diversity score.

The rarefaction curves for pre-capping sites in reach 1 and reach 2 are shown in Figure 5.3. It is interesting to note that the site GCR1 and 9 close to the HSD outfall has the highest species count and reach a plateau indicating good representation of the indigenous microbial community. Sites GCR 2 and 6 in Reach-1 and sites GCR 8, 10, 12 and 13 in Reach-2 also reach a plateau with similar slope to sites GCR 1 and 9.

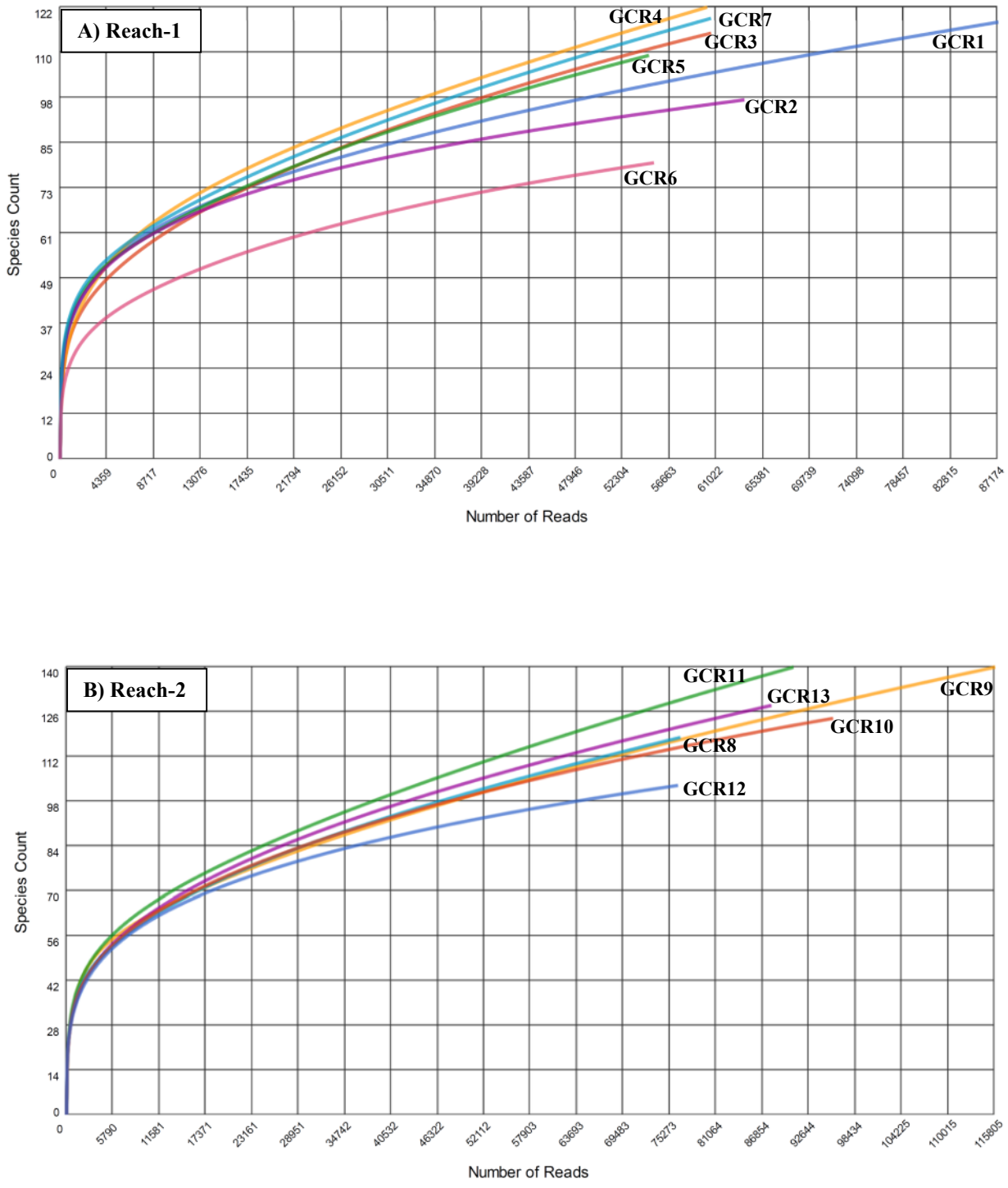

Figure 0.3 Rarefaction curves depicting species richness in pre-capping surficial sediments in A) Reach-1 and B) Reach-2.

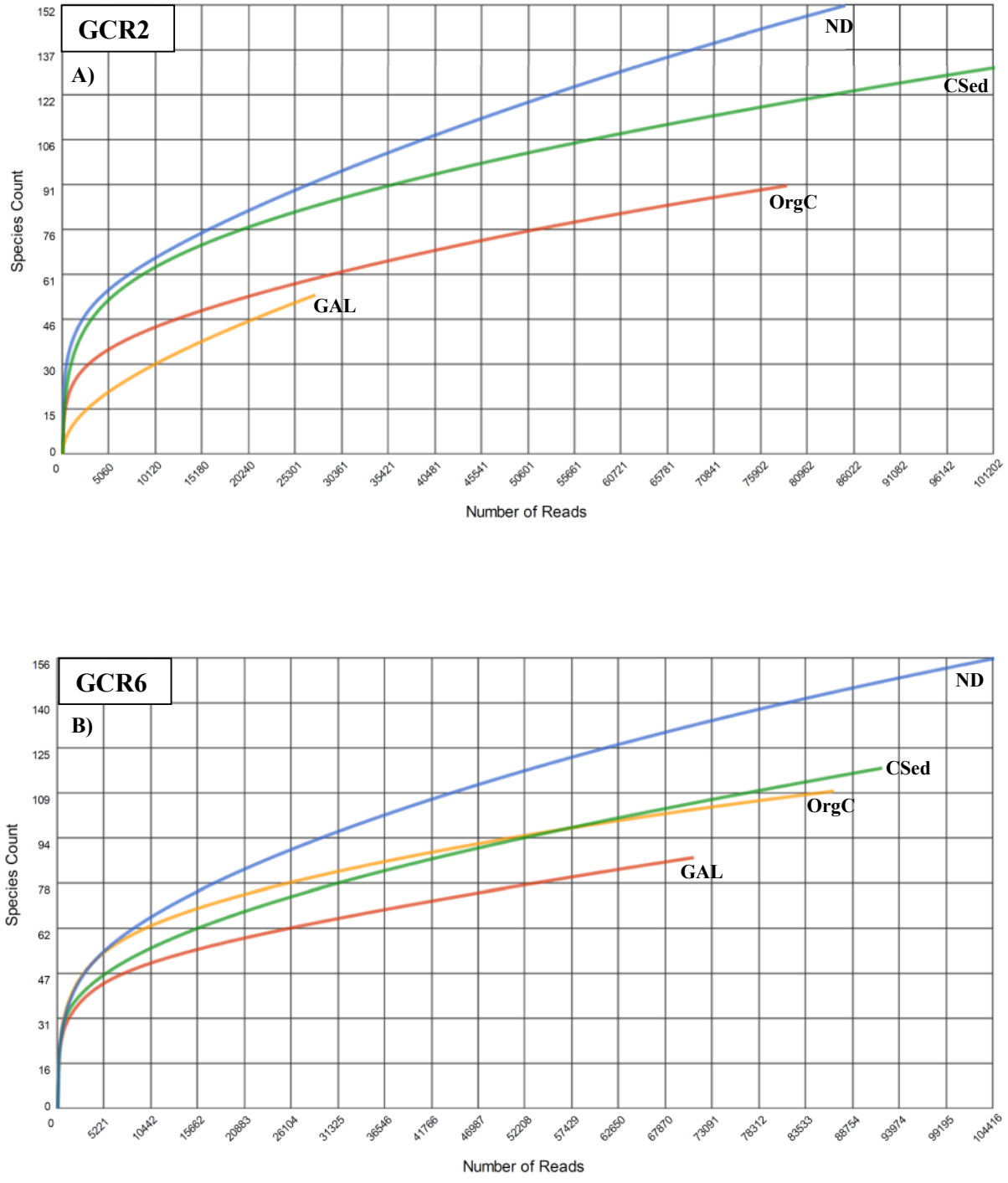

Figure 0.4 Rarefaction curves for archaeal sequences in new deposit (ND), gravel armor layer (GAL), organo-clay layer (OrgC) and contaminated sediment (CSed) layers in sediment cores from Reach-1 sites A) GCR2 and B) GCR6.

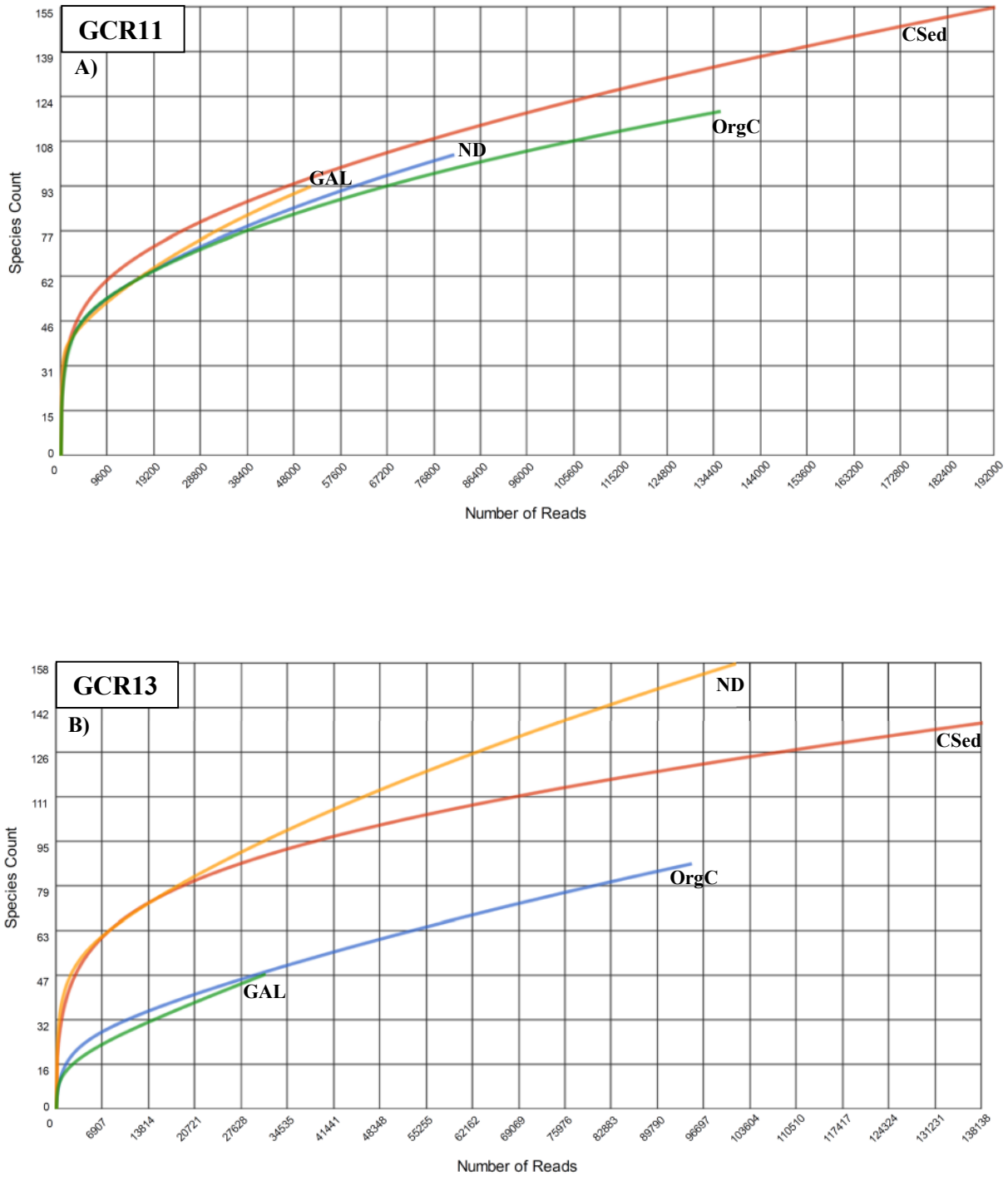

Figure 0.5 Rarefaction curves for archaeal sequences in new deposit (ND), gravel armor layer (GAL), organo-clay layer (OrgC) and contaminated sediment (CSed) layers in sediment cores from Reach-2 sites A) GCR11 and B) GCR13.

Table 0.4 Pre-capping domain level distribution of sequences expressed as percentage and number of sequences.

	GCR1	GCR2	GCR3	GCR4	GCR5	GCR6	GCR7	GCR8	GCR9	GCR10	GCR11	GCR12	GCR13
Percentage (%)													
Archaea	98.51	98.58	95.86	95.75	98.65	99.74	94.63	96.30	90.68	90.05	94.85	94.07	96.49
Bacteria	1.43	1.38	4.08	4.20	1.30	0.21	5.29	3.63	9.26	9.89	5.04	5.86	3.45
Viruses	0.05	0.03	0.06	0.03	0.05	0.04	0.07	0.06	0.05	0.05	0.10	0.06	0.05
Unclassified	0.002	-	-	0.005	-	-	0.002	-	-	0.003	-	0.002	0.001
Number of Sequences													
Archaea	58379	40422	39829	41772	38021	41221	38099	50433	69123	62359	65306	50887	73232
Bacteria	850	565	1696	1834	502	87	2128	1901	7060	6849	3472	3171	2618
Viruses	32	14	23	13	18	18	29	32	36	35	66	32	39
Unclassified	1	-	-	2	-	-	1	-	-	2	-	1	1

Table 0.5 Post-capping domain level distribution of sequences expressed as percentage and number of sequences.

Site	**GCR2**				**GCR6**				**GCR11**				**GCR13**			
Layer	ND	GAL	OrgC	CSed	ND	GAL	OrgC	CSed	ND	GAL	OrgC	CSed	ND	GAL	OrgC	CSed
Percentage (%)																
Archaea	95.95	92.74	88.25	77.76	92.88	92.73	88.06	93.98	94.52	89.85	90.85	92.89	94.58	91.38	94.70	81.86
Bacteria	3.98	5.44	11.67	22.11	7.05	7.23	11.88	5.96	5.43	10.06	9.11	7.07	5.36	7.52	4.92	18.08
Viruses	0.05	1.68	0.08	0.13	0.07	0.04	0.05	0.06	0.06	0.07	0.04	0.04	0.05	0.92	0.3	0.06
Unclassified	0.002	0.044		0.002	0.001			0.001		0.003	0.001		0.003			
Number of Sequences																
Archaea	43431	2095	21313	33725	67347	44543	54217	63591	41176	26283	92952	136366	59851	1494	7502	64898
Bacteria	1803	123	2818	9590	5112	3473	7313	4032	2364	2944	9322	10381	3392	123	390	14337
Viruses	23	38	19	55	50	18	30	40	24	21	37	55	33	15	26	45
Unclassified	1	1	-	1	1	-	-	1	-	1	1	-	2	-	-	-

The rarefaction curve for sites GCR 3, 4, 5, 7 and 11 has a higher slope to the right compared to other sites indicating that more species may be captured by the sequencing. However, the rarefaction curve at all sites reached sufficiently broad plateaus for characterization of the microbial community structure.

5.4.3 Species Richness and Diversity in post-cap sections

Rarefaction curves of archaeal diversity in core sections from to the four distinct layers are shown in Figures 5.3 and 5.4. The CSed layer and OrgC layers at all sites reached a sufficient plateau to capture most of the diversity, whereas samples from the GAL layer had a higher slope indicating a more diverse microbial community. It is worth noting that, the rarefaction curve for CSed at GCR11 has the highest slope and sequence count among all layers, suggesting that proximity to the HSD outfall might support diverse functional communities even in deeper sediments. The ND layer at all four sites was not completely plateaued, indicating that some of the species diversity was not completely captured.

The species diversity was compared to sediment chemical characteristics such as Organic Matter (OM), Total Organic Carbon (TOC), Black Carbon (BC) and the COD/TOC ratios to examine whether there was any dependence of the microbial diversity on nutrient and carbon levels (Table 5.6). The COD/TOC ratio is a measure of the lability of the organic carbon to degradation, with low values indicating more recalcitrant OM as demonstrated in our previous studies in Bubbly Creek in Chicago, IL (Rockne, Viana, and Yin 2010, Viana, Yin, and Rockne 2012). COD is a measure of the ability of a strong oxidant (chromate) to break down organic matter and lower COD values normalized to TOC will result in lower ratios reflecting higher fraction of refractory organic matter. The α-diversity was found to have a highly significant ($R=0.66$, $p=0.01$) positive correlation with COD/TOC ratio and a significant negative correlation

with TOC (R=0.72, p=0.006). The increase in α-diversity with COD/TOC ratio suggests that the labile nature of the sediment OM supports a diverse archaeal community. The negative correlation with OC is puzzling as greater OC content is expected to result in an increase in archaeal diversity as the fraction of recalcitrant OM remains relatively constant as revealed by a negative correlation between OC and COD/TOC ratio. The negative correlation can be attributed to the way alpha diversity is calculated. Although a higher OC content may be expected to support a diverse microbial community, the α-diversity can still be low if the abundance of the individual species is low. In marked contrast to the post-capping environment, sequences from surface grabs prior to capping did not exhibit any significant relationship with distance from the treatment plant outfall; although elevated α-diversity values were observed at sites GCR9 and GCR1 located closer to the HSD outfall.

Table 0.6 Chemical characteristics of pre-capping surface sediment and α-diversity of archaeal sequences.

Site	α-diversity	Average Porosity	Average OM (%)	Average OC (%)	Average BC (%)	BOD/COD Ratio	COD/TOC ratio
GCR1	10.58	51.0	5.9	5.2	3.3	0.02	0.62
GCR2	8.85	48.2	5.2	5.4	3.5	0.04	0.36
GCR3	7.94	58.1	17.3	12.0	5.0	0.05	0.41
GCR4	8.41	57.1	15.8	11.1	5.2	0.05	0.29
GCR5	10.58	55.9	7.4	4.5	4.0	0.03	0.59
GCR6	6.44	55.5	25.1	15.2	5.7	0.07	0.37
GCR7	11.46	46.2	4.9	3.3	1.0	0.04	0.58
GCR8	7.79	54.3	16.3	9.3	1.9	0.04	0.40
GCR9	10.41	58.8	19.8	10.5	1.8	0.14	0.43
GCR10	8.96	52.3	12.2	6.5	1.0	0.06	0.75
GCR11	8.36	54.7	19.2	10.4	2.5	0.09	0.36
GCR12	7.94	56.7	20.2	11.8	3.4	0.05	0.30
GCR13	5.95	53.6	15.7	9.1	5.7	0.10	0.27

Table 0.7 Comparison of **s**ediment chemical characteristics and Archaeal α-diversity for the ND, GAL, OrgC and CSed layers for sediment cores sampled in 2012 at sites GCR 2, 6, 11 and 13.

Site	Depth (cm)	Layer	α-diversity	Average Porosity	Average OM (%)	Average OC (%)	Average BC (%)
GCR2	0-5 cm	ND	20	47.66	1.29	0.44	0.07
	14-19 cm	GAL	3.29	35.34	0.46	0.17	0.05
	39-42 cm	OrgC	9.4	40.59	1.03	0.69	0.1
	42-45 cm	CSed	9.58	67.48	10.94	7.02	1.38
GCR6	0-4 cm	ND	6.78	55.33	2.46	1.13	0.07
	9-14 cm	GAL	9.65	36.82	0.47	0.79	0.03
	34-37 cm	OrgC	8.35	41.44	1.6	1.12	0.13
	43-48 cm	CSed	6.47	81.8	22.12	18.46	1.39
GCR11	0-4 cm	ND	19.55	66.47	2.96	2.2	0.19
	9-14 cm	GAL	18.09	38.23	0.98	0.37	0.07
	19-24 cm	OrgC	8.01	37.25	1.55	1.45	0.12
	32-37 cm	CSed	5.96	86.09	27.61	21.13	1.73
GCR13	0-4.5 cm	ND	12.76	61.95	2.26	2.1	0.07
	13-17 cm	GAL	8.21	36.18	0.54	0.2	0.02
	22-27 cm	OrgC	5.93	37.66	1.54	1.11	0.1
	31.5-36 cm	CSed	9.8	73.99	17.81	9.09	0.86

The archaeal α-diversity in the ND layer was similar to those observed in the pre-capping surficial sediments. Lower species diversity was observed in the GAL layer at GCR 2 and 13, sites that were also characterized by steep rarefaction curves. It is worth noting that site GCR 11 located immediately west of the HSD outfall had the highest α-diversity with highest diversity in the GAL layer; as much as twice that of other sites (Table 5.7). GCR 6 exhibited lower α-diversity in the CSed and ND layer and elevated diversity in the GAL layer.

5.4.4 Indigenous Archaeal Community Structure in Pre-Capping Sediment

Organism abundance was evaluated using the Lowest Common Ancestor (LCA) method (Huson et al. 2007). The LCA method assigns a bit score to all matches that are closest to the best hit in the collection. The collection is later assigned annotation at a single higher level of all species in the collection. The primary advantage of the method is that it avoids any ambiguity in assigning annotations in the taxonomy tree (Wilke et al. 2014).

The section below provides an overview of the composition of the archaeal community in the pre-capping surface sediment. An abundance table was generated for each site using the M5RNA database, and the top 15 organisms of numerical abundance are presented in Appendix. For discussion purposes, only sequences representing >1% of total archaeal community structure are considered. Visualization of the archaeal community structure were also generated at the family level using the KRONA data visualization package (Ondov, Bergman, and Phillippy 2011), which are presented in Figures 5.9 – 21. Primarily the distribution of methanogenic *Archaea* is discussed below with complete breakdown provided in the Appendix (Tables A9.1-13).

GCR1: More than 91% of the *Archaea* were comprised of *Methanomicrobia* (50%) and *Methanobacteria* (41%), along with 5% unclassified *Euryarchaeota* and 2% unclassified *Archaea*. The *Methanomicrobia* were composed of 40% *Methanosaeta*, 2% *Methanolinea*, 1% *Methanomethylovorans*, 1% unclassified *Methanosarcinales*, 1% *Methanocella* and 5% unclassified *Methanomicrobia*. The *Methanobacteria* were further classified into 36% *Methanobacterium*, 2% *Methanobrevibacter* and 3%unclassified *Methanobacteriaceae* at the genus level.

GCR2: Similar to GCR1, the archaeal community was dominated by the class *Methanomicrobia* (54%) and *Methanobacteria* (36%). Unclassified *Euryarchaeota* and unclassified *Archaea* were represented at 3% each along with 1% of *Desulfurococcaceae* belonging to the Class *Thermoprotei*. At the genus level the *Methanomicrobia* were further classified in increasing order of representation as *Methanosaeta* (48%), unclassified *Methanomicrobia* (3%), *Methanomethylovorans* (2%) and *Methanocella* (1%). *Methanobacteria* was classified into *Methanobacterium* (29%), *Methanobrevibacter* (6%) and unclassified *Methanobacteriaceae* (1%).

GCR3: *Methanomicrobia* and *Methanobacteria* represented 68% and 20%, respectively, with 7% unclassified *Euryarchaeota* and 1% unclassified *Archaea*. Genus level composition of *Methanomicrobia* in decreasing order of representation were *Methanosaeta* (55%), unclassified *Methanomicrobia* (8%), *Methanolinea* (2%), *Methanocorpusculum* (1%), *Methanomethylovorans* (1%) and unclassified *Methanosarcinales* (1%). The class *Methanobacteria* included the genera *Methanobacteria* (17%), *Methanobrevibacter* (2%) and 1% of unclassified *Methanobacteriaceae*.

GCR4: *Methanomicrobia* and *Methanobacteria* represented 56% and 27%, respectively, with 13% unclassified *Euryarchaeota* and 2% unclassified *Archaea*. *Methanomicrobia* (56%) were composed of the genera *Methanosaeta* (51%), *Methanospirillum* (1%), *Methanolinea* (1%) and *Methanomethylovorans* (0.5%) along with 3% of unclassified *Methanomicrobiales*. *Methanobacteria* (27%) were classified into *Methanobacterium* (21%), *Methanobrevibacter* (5%) and the *Methanobacteriaceae* (1%).

GCR5: *Methanomicrobia* and *Methanobacteria* represented 60% and 26%, respectively, along with 4% of unclassified *Euryarchaeota* and 4% unclassified sequences derived from domain

Archaea. In addition to the aforementioned structure the genus *Candidatus Nitrosocaldus* represented 4% of the sequences belonging to the Phylum *Crenarchaeota*. *Methanomicrobia* (60%) were characterized into *Methanosaeta* (55%), *Methanomethylovorans* (1%), *Methanospirillum* (1%), *Methanosarcina* (1%) and 2% belonging to the order *Methanomicrobiales*. *Methanobacteria* were composed of the genera *Methanobacterium* (19%) and *Methanobrevibacter* (7%) with 1% of the family *Methanobacteriaceae*.

GCR6: *Methanomicrobia* and *Methanobacteria* represented 76% and 6% of the total Archaeal sequences respectively. *Methanomicrobia* were primarily composed of the genera *Methanosaeta* (67%) and *Methanocella* (1%) along with 8% of sequences in the order *Methanomicrobiales*. Similarly, *Methanobacteria* were composed of the genera *Methanobacterium* (5%) and *Methanobrevibacter* (1%). The archaeal consortium also contained 13% of unclassified *Euryarchaeota* and 4% unclassified *Archaea*.

GCR7: *Methanomicrobia* represented 67% of the total sequences that included the genera *Methanosaeta* (45%), *Methanomethylovorans* (1%) and *Methanocella* (1%), along with 15% of the family *Methanosarcinaceae* and 5% of unclassified *Methanomicrobia*. *Methanobacteria* represented 20% of total sequences composed of the genera *Methanobacterium* (15%), *Methanobrevibacter* (3%) and the family *Methanobacteriaceae* (2%). The remaining sequences were composed of 3% of unclassified *Archaea*, 5% unclassified *Euryarchaeota*, 1% of the family *Desulfurococcaceae* in Class *Thermoprotei* and 1% of the genera *Candidatus Nitrososphaera* in the phylum *Thaumarchaeota*.

GCR8: *Methanomicrobia* represented 79% of the sequences dominated by the genus *Methanosaeta* (67%), *Methanomethylovorans* (3%), *Methanocella* (1%), *Methanolinea* (1%), the order *Methanomicrobiales* (2%) and unclassified *Methanomicrobia* (3%). *Methanobacteria*

represented 18% of the sequences, which included the genera *Methanobacterium* (15%), *Methanobrevibacter* (2%) and *Methanobacteriaceae* (1%). The *Archaea* also included 2% unclassified *Archaea* and 1% *Euryarchaeota*.

GCR9: *Methanomicrobia* represented 75% of the total Archaeal sequences including the genera *Methanosaeta* (56%), *Methanomethylovorans* (2%), *Methanospirillum* (1%), *Methanocella* (1%), *Methanosarcina* (1%), the order *Methanomicrobiales* (13%) and unclassified *Methanomicrobia* (1%). The class *Methanobacteria* accounted for 17% of the sequences and were comprised of *Methanobacterium* (16%) and *Methanobrevibacter* (1%). Unclassified sequences derived from *Archaea* and *Euryarchaeota* represented 6% and 1% respectively.

GCR10: *Methanomicrobia* represented 72% of the archaeal community that included the genera *Methanosaeta* (59%), *Methanolinea* (1%), *Methanomethylovorans* (1%), *Methanospirillum* (1%), the order *Methanomicrobiales* (7%) and unclassified *Methanomicrobia* (3%). Nearly 18% of the Archaeal sequences were composed of *Methanobacteria* which were further classified into *Methanobacterium* (14%) and *Methanobrevibacter* (4%). Unclassified sequences derived from *Archaea* and *Euryarchaeota* accounted for 3% each.

GCR11: *Methanomicrobia* represented 67% of the archaeal sequences including *Methanosaeta* (58%), *Methanocorpusculum* (2%), *Methanospirillum* (2%), the order *Methanomicrobiales* (1%) and unclassified *Methanomicrobia* (4%). *Methanobacteria* accounted for 26% of the sequences comprising of the genera *Methanobacterium* (22%), *Methanobrevibacter* (2%) and the family *Methanobacteriaceae* (2%). Unclassified sequences derived from *Archaea* and *Euryarchaeota* accounted for 2% each.

GCR12: *Methanomicrobia* represented 75% of *Archaea* comprised of *Methanosaeta* (62%), *Methanolinea* (2%), *Methanospirillum* (1%), *Methanosphaerula* (1%) the order *Methanomicrobiales* (2%) and unclassified *Methanomicrobia* (7%). *Methanobacteria* accounted for 17% of the sequences composed of the genera *Methanobacterium* (16%) and *Methanobrevibacter* (1%). Unclassified sequences derived from *Archaea* and *Euryarchaeota* represented 3% and 5% respectively.

GCR13: *Methanomicrobia* represented 73% of the archaeal community including *Methanosaeta* (68%), *Methanocorpusculum* (1%), *Methanosarcina* (1%), *Methanosphaerula* (1%), and unclassified *Methanomicrobia* (2%). *Methanobacteria* accounted for 12% of the sequences composed of the genera *Methanobacterium* (11%) and *Methanobrevibacter* (1%). Unclassified sequences derived from *Archaea* and *Euryarchaeota* represented 12% and 3% respectively.

5.4.5 Trends in distribution of Archaea in pre-capping surficial sediment

Methanomicrobia and *Methanobacteria* were the most dominant class of *Archaea* with abundance ranging between 54 - 79% and 6 - 38%, respectively, and a mean of 68% and 22%, respectively for all sites. Sites GCR 1 -5 in Reach 1 had a higher abundance of *Methanobacteria* (26 – 38%), whereas Reach 2 abundance varied between 12 – 26%. An opposite trend was observed for *Methanomicrobia*, with higher levels in Reach 2, suggesting a shift in archaeal community structure between the two groups in response to changes in environmental conditions. At the genus level *Methanosaeta* was the most abundant archaeal genera of 40±8.7% (mean±SEM) followed by *Methanobacterium* (18±8%), *Methanobrevibacter* (2.8±2.1%), *Methanomethylovorans* (1±0.8%), *Methanolinea* (0.8±0.7%), *Methanospirillum* (0.7±0.4%), *Methanocorpusculum* (0.5±0.6%), *Methanocella* (0.5±0.5%), *Methanosarcina* (0.3±0.2%) and *Methanosphaerula* (0.2±0.2%). Genus level distribution of the archaeal sequences is presented in

Table 5.8 and Figure 5.6. GCR 6 exhibited significantly lower abundance of *Methanobacterium* (5%) compared to other sites and was dominated by *Methanosaeta.* This result is consistent with the low α-diversity value of 6.44 observed at GCR6 discussed above in section 5.4.2 (Table 5.6). The genera *Methanomethylovorans* and *Methanocella* exhibited an increase in abundance with distance from the HSD outfall up to site GCR8. In contrast *Methanospirillum* had higher abundances at sites closer to the HSD outfall, with the highest abundance occurring at GCR11. The observed trend relative to the HSD outfall is suggestive of the effluent influencing the archaeal community structure.

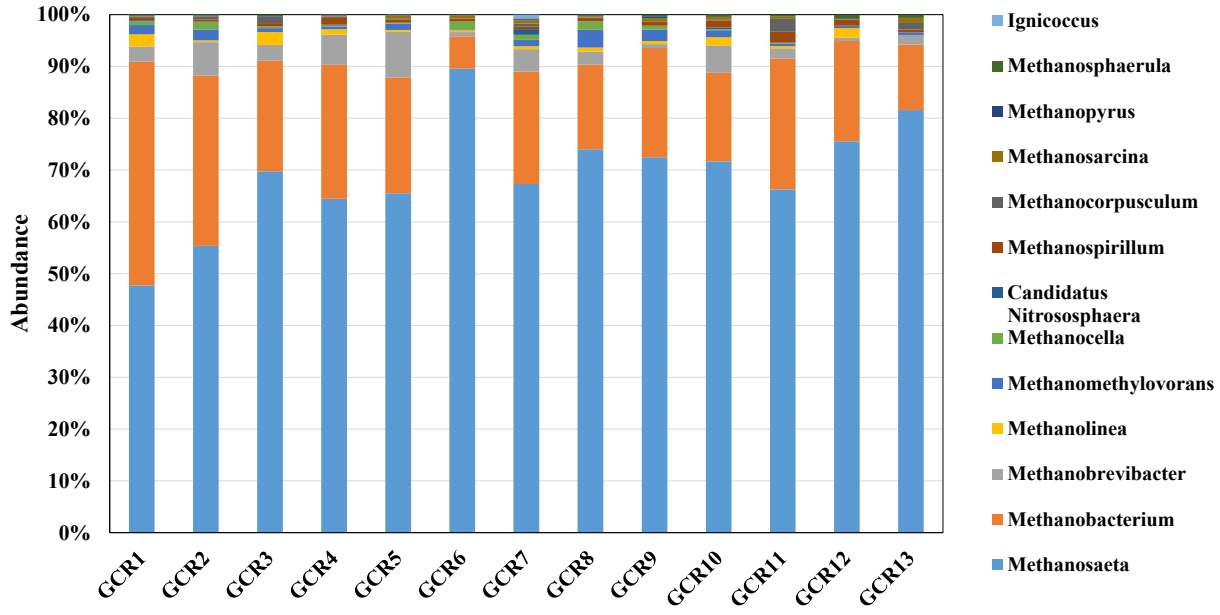

Figure 0.6 Composition of the most abundant archaeal genera for all pre-capping sites as revealed by the M5RNA database. Detailed classification at the Family and Order level can be found in Tables A4.1 – 13.

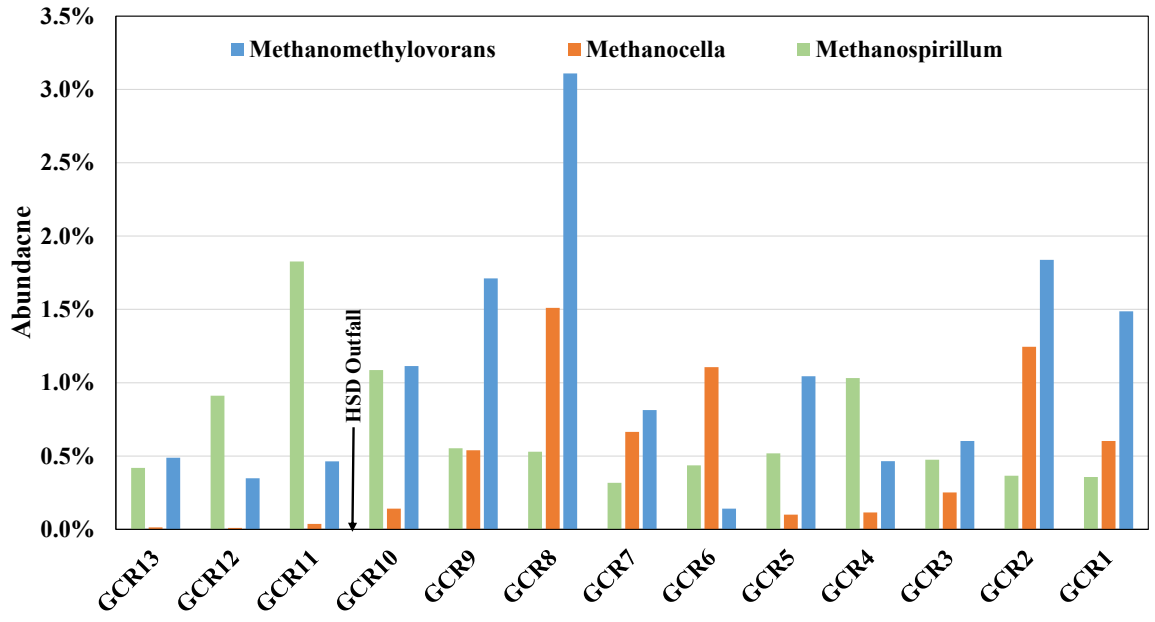

Figure 0.7 Trend in *Methanomethylovorans*, *Methanocella* and *Methanospirillum* abundance relative to proximity to the HSD outfall.

Heat-map analysis (Eisen et al. 1998) was performed using ward clustering and Bray-Curtis distance method, to further analyze inter-site genome similarities based on location. The heat-map analysis (Figure 5.8) provides evidence of archaeal biome similarities based on distance from the HSD outfall location. The y-axis dendrogram shows grouping of Archaea at the class level. The figure shows grouping of methanogenic *Archaea* primarily dominated by *Methanomicrobia*, *Methanobacteria*, unclassified *Archaea* and unclassified *Euryarchaeaota*. Similarly, extreme thermophiles belonging to the class Thermoprotei and unclassified *Crenarchaeaota* are grouped together. Also, *Methanopyri* and unclassified *Thaurmarchaeota*, primarily composed of Ammonia Oxidizing Archaea (AOA) are grouped together. The rest of the grouping in y-axis represent viruses and bacteria with insignificant sequences counts and are not discussed here. The x-axis dendrogram identified two main groups, which included sites GCR6, 10, 11, 12 and 13 in Group-I and sites GCR1, 2, 3, 4, 5, 7, 8 and 9 in Group-II. Metagenomic grouping was compared with α-diversity, OM, OC, COD/TOC (Table 5.6) and gas

production rates (Table 3.6, Chapter 3). The grouping did not reveal any significant relationship with gas production rates or any of the aforementioned sediment chemical characteristics. As discussed in Chapter 3, the pre-capping gas production rates did not vary with reach or distance from HSD outfall. However, it is evident that Group I is composed of sites closer to the HSD outfall (except for site GCR6). This suggests that the outfall might play a role in the relative abundance of the archaeal consortium as the nutrient availability is expected to be similar at sites closer to the outfall. A second possibility is that temperature plays a role. Recall from Chapter 3 that sediment temperatures were quite variable in the two reaches.

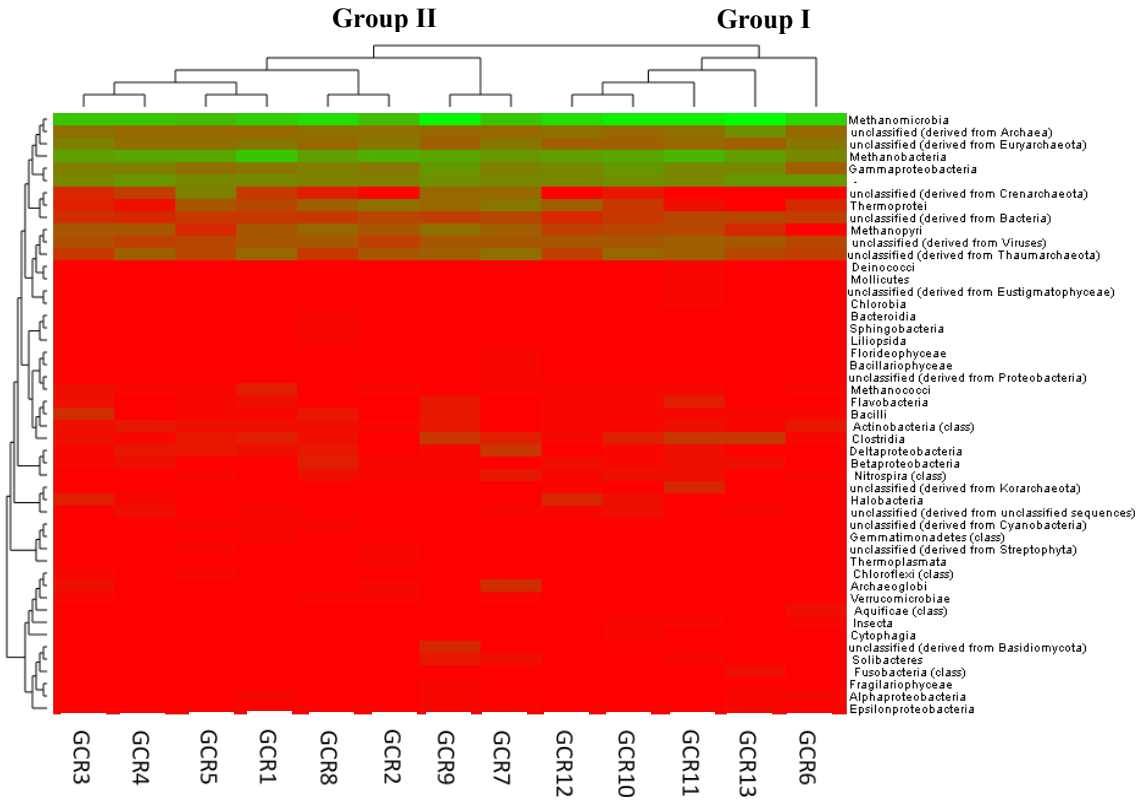

Figure 0.8 Heat map analysis of pre-capping surficial sediment. The dendrogram in x-axis depicts similarity in the genomes with similar samples clustered in the dendrogram. Transition in colors from red to green represents increasing abundance of sequences.

It is also worth noting that GCR6 is at highest order of grouping among sites in Group I. This suggests GCR6 has a distinct metagenome, in line with evidence of highly labile OM and gas

production at this site. Also the subgrouping of metagenomes in each group closely followed the α-diversity values. For example, the subgrouping in Group-II followed an increasing order of α-diversity from sites GCR 3 and GCR4 with lower α-diversity values (7.94 and 8.41 respectively) to sites GCR7 and GCR9 with the highest observed α-diversity of 11.46 and 10.4 respectively. In contrast, the subgrouping between metagenomes in Group-I followed a decreasing order of α-diversity.

5.4.6 Relationship between field-measured gas production rates, sediment physical characteristics and distribution of archaeal community structure

Correlation analysis was performed to evaluate relationship between gas ebullition (G_{ebu}) rates and relative abundance of archaeal genera found in GCR sediment. The analysis revealed significant correlations between gas production rates and the most abundant genera, *Methanosaeta* (abundance = 56±9%) with (R=0.62, p=0.02). *Methanosarcina* (R=0.67, p=0.01) and *Methanosphaerula* (R=0.64, p=0.01) were also positively correlated with G_{ebu}. Neither *Methanobacterium* (the second most abundant genera) nor *Methanobrevibacter* exhibited significant correlations with G_{ebu}.

Organism abundance was also compared with a more complete set of bulk and micropollutant characteristics including OM, OC, COD/TOC ratio, BOD/COD ratio, total PAHs (TPAH) and total metals. A significant correlation exists for both *Methanosaeta* and *Methanosarcina* abundance and BOD/COD ratio (R= 0.7, p<0.007). BOD/COD ratio is a specific indicator of biodegradability of the OM (Viana, Yin, and Rockne 2012, Rockne, Kaliappan, and Bourgon 2011) and higher abundance of the aforementioned organisms were observed for sites with higher biodegradability. A negative correlation existed between *Methanobrevibacter* and BOD/COD ratio (R=-0.5, p=0.04) suggesting that the genera is more dominant at sites with

higher levels of recalcitrant OM. In the case of COD/TOC ratio, which is a measure of degradation recalcitrance of the organic carbon (Viana, Yin, Zhao, et al. 2007, Rockne, Viana, and Yin 2010), with lower values indicating more recalcitrant organic fraction, *Candidatus Nitrososphaera* had a significant positive correlation ($R=0.64$, $p=0.02$). Summary of Pearson's correlation between archaeal abundance and sediment chemical parameters is shown in Table A30, Appendix.

Methanobrevibacter was also negatively correlated (both $p<0.05$) with OC and OM ($R=-0.65$ and -0.67 respectively) consistent with the hypothesis that the organism is dominant in sites with low levels of OM and recalcitrant sediment. The positive correlations of *Methanosaeta*, *Methanosarcina* and *Candidatus Nitrososphaera* with BOD/COD ratio and COD/TOC ratios suggest that these organisms are more dominant in highly labile organic rich sediments. Comparison of archaeal species abundance with bulk sediment concentration of micro-pollutants revealed a strong positive correlation between *Methanopyrus* abundance and TPAHs ($R=0.87$, $p<0.008$) and heavy metals ($R=0.72$, $p<0.008$), suggesting that *Methanopyrus* has more toxicity tolerance and could play an important role in heavily contaminated sediment.

Among the dominant archaeal groups identified in this study, a significant pairwise correlation existed between *Methanosaeta* and the genera *Methanosarcina* ($R=0.79$), *Methanosphaerula* ($R=0.79$) and *Methanospirillum* ($R=0.49$) all with $p<0.001$, with all genera classified under the class *Methanomicrobia*. The shared metabolic pathways of acetoclastic methanogens in the genera *Methanosaeta* and *Methanosarcina* can be attributed to this correlation. The other dominant class, *Methanobacteria* did not have statistically significant correlations with organisms in the class. The functional significance of each methanogenic genus to gas production will be discussed in the next section.

Table 0.8 Dominant archaeal genera and sequence count in pre-capping sediment. Sequence count is shown in parenthesis.

Genera	GCR1	GCR2	GCR3	GCR4	GCR5	GCR6	GCR7	GCR8	GCR9	GCR10	GCR11	GCR12	GCR13
Methanosaeta	39.8%	48.4%	54.6%	51.3%	54.5%	67.4%	45.2%	67.0%	56.2%	59.1%	58.4%	62.5%	68.0%
	(23236)	*(19555)*	*(21752)*	*(21415)*	*(20734)*	*(27768)*	*(17211)*	*(33781)*	*(38880)*	*(36834)*	*(38151)*	*(31786)*	*(49784)*
Methanobacterium	36.0%	28.7%	16.7%	20.6%	18.6%	4.7%	14.6%	14.8%	16.4%	14.1%	22.2%	16.0%	10.5%
	(21038)	*(11597)*	*(6650)*	*(8594)*	*(7081)*	*(1938)*	*(5558)*	*(7457)*	*(11322)*	*(8795)*	*(14523)*	*(8147)*	*(7704)*
Methanobrevibacter	2.4%	5.7%	2.4%	4.6%	7.3%	0.6%	2.9%	2.3%	0.6%	4.4%	1.7%	0.5%	1.5%
	(1416)	*(2290)*	*(947)*	*(1932)*	*(2782)*	*(257)*	*(1097)*	*(1149)*	*(402)*	*(2720)*	*(1142)*	*(259)*	*(1092)*
Methanolinea	2.0%	0.3%	1.9%	0.8%	0.3%	0.3%	0.4%	0.7%	0.5%	1.3%	0.4%	1.5%	0.0%
	(1140)	*(118)*	*(774)*	*(346)*	*(114)*	*(105)*	*(151)*	*(352)*	*(316)*	*(810)*	*(252)*	*(783)*	*(10)*
Methanomethylovorans	1.5%	1.8%	0.6%	0.5%	1.0%	0.1%	0.8%	3.1%	1.7%	1.1%	0.5%	0.3%	0.5%
	(868)	*(743)*	*(240)*	*(194)*	*(397)*	*(58)*	*(310)*	*(1568)*	*(1183)*	*(694)*	*(303)*	*(177)*	*(358)*
Methanocella	0.6%	1.2%	0.3%	0.1%	0.1%	1.1%	0.7%	1.5%	0.5%	0.1%	0.0%	0.0%	0.0%
	(352)	*(503)*	*(100)*	*(48)*	*(38)*	*(456)*	*(253)*	*(762)*	*(373)*	*(88)*	*(24)*	*(5)*	*(10)*
Methanospirillum	0.4%	0.4%	0.5%	1.0%	0.5%	0.4%	0.3%	0.5%	0.6%	1.1%	1.8%	0.9%	0.4%
	(208)	*(148)*	*(189)*	*(431)*	*(197)*	*(180)*	*(121)*	*(267)*	*(382)*	*(677)*	*(1193)*	*(464)*	*(307)*
Methanocorpusculum	0.2%	0.4%	1.0%	0.2%	0.1%	0.0%	0.4%	0.1%	0.0%	0.1%	2.2%	0.1%	1.2%
	(108)	*(169)*	*(389)*	*(99)*	*(33)*	*(15)*	*(159)*	*(41)*	*(10)*	*(88)*	*(1419)*	*(58)*	*(859)*
Methanosarcina	0.1%	0.1%	0.0%	0.1%	0.5%	0.4%	0.4%	0.2%	0.5%	0.4%	0.4%	0.1%	0.7%
	(64)	*(49)*	*(7)*	*(60)*	*(183)*	*(168)*	*(149)*	*(106)*	*(357)*	*(275)*	*(244)*	*(27)*	*(491)*
Candidatus Nitrososphaera	0.2%	0.1%	0.0%	0.1%	0.0%	0.0%	0.7%	0.0%	0.1%	0.3%	0.1%	0.0%	0.0%
	(115)	*(37)*	*(11)*	*(56)*	*(14)*	*(11)*	*(280)*	*(9)*	*(45)*	*(178)*	*(81)*	*(10)*	*(17)*
Methanosphaerula	0.1%	0.2%	0.2%	0.0%	0.1%	0.1%	0.1%	0.1%	0.2%	0.3%	0.3%	0.7%	0.5%
	(87)	*(67)*	*(81)*	*(20)*	*(44)*	*(41)*	*(40)*	*(53)*	*(171)*	*(217)*	*(216)*	*(341)*	*(381)*
Methanopyrus	0.1%	0.1%	0.1%	0.1%	0.0%	-	0.2%	0.2%	0.3%	0.0%	0.0%	0.0%	0.0%
	(39)	*(35)*	*(35)*	*(33)*	*(6)*	-	*(60)*	*(84)*	*(217)*	*(15)*	*(17)*	*(13)*	*(5)*

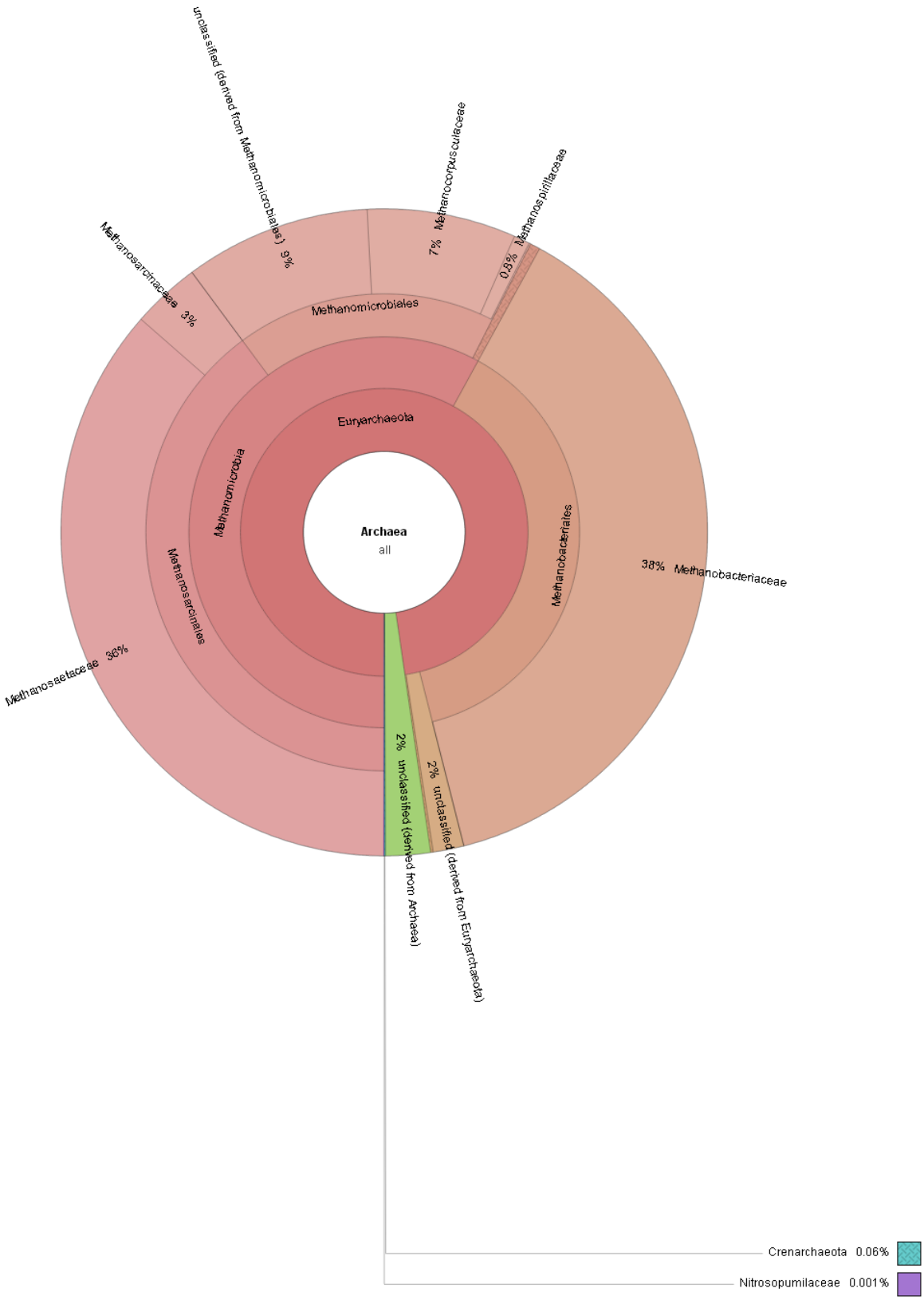

Figure 0.9 Distribution of archaeal community structure in pre-capping sediment at site GCR1.

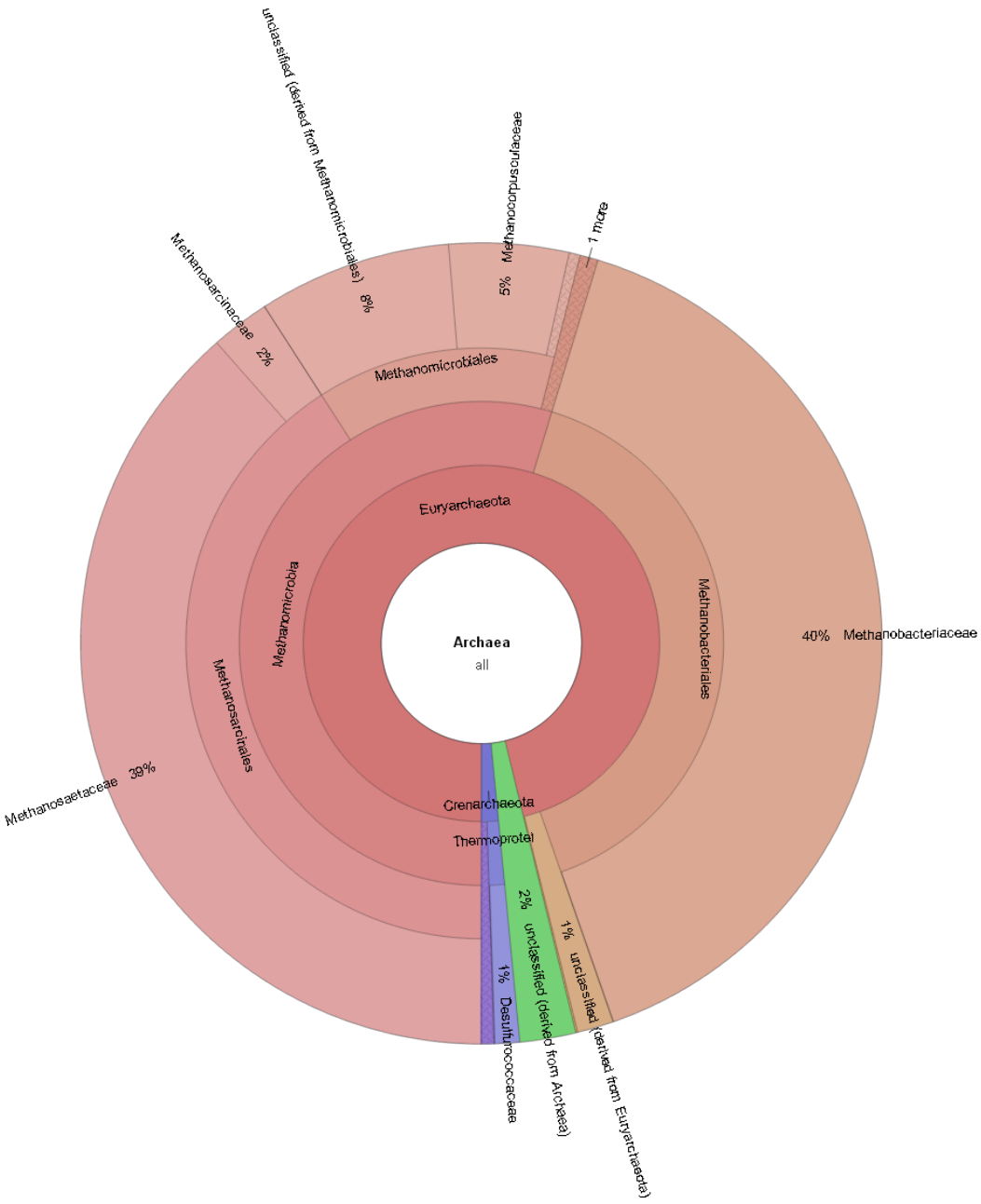

Figure 0.10 Distribution of archaeal community structure in pre-capping sediment at site GCR2.

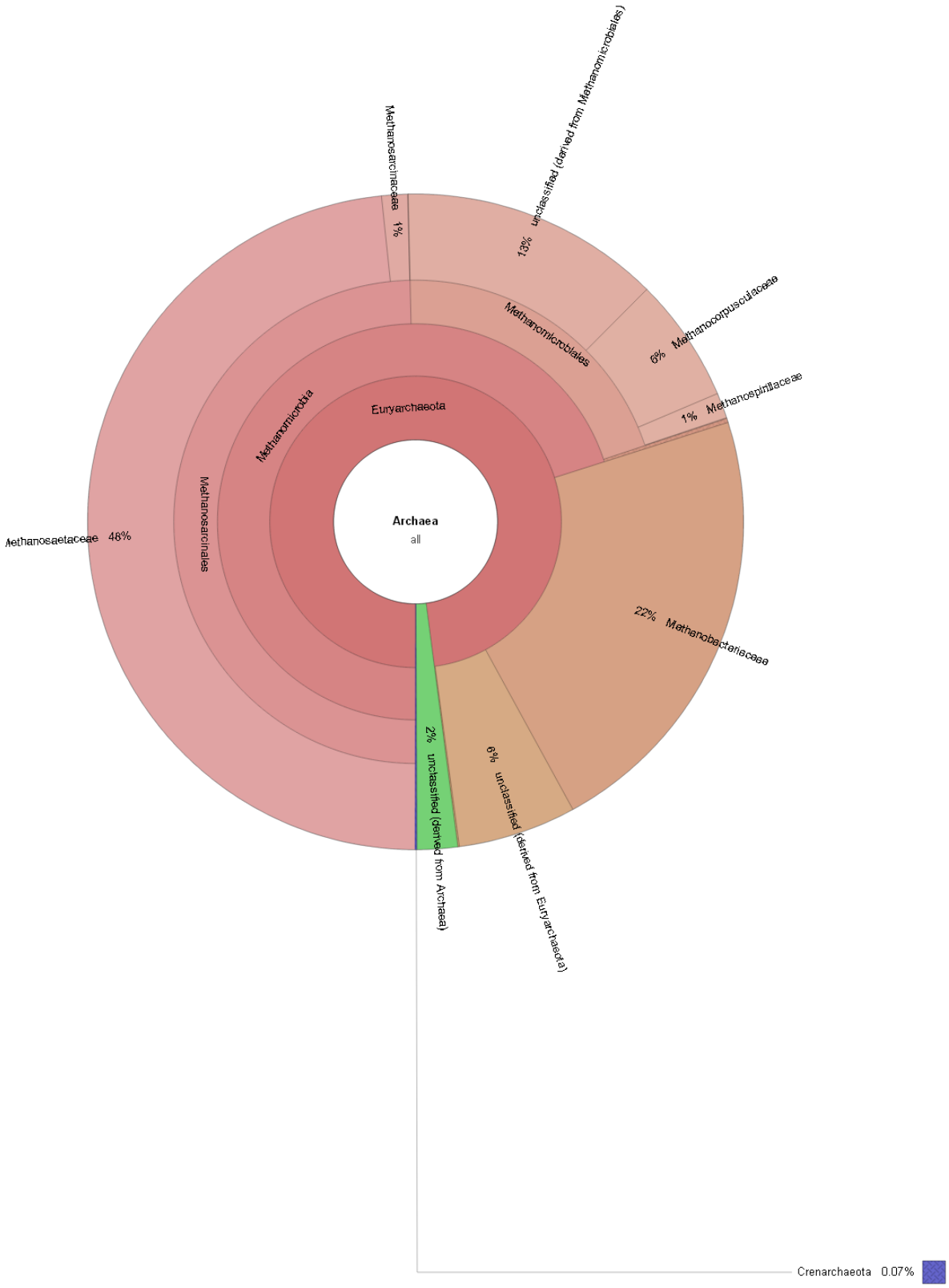

Figure 0.11 Distribution of archaeal community structure in pre-capping sediment at site GCR3.

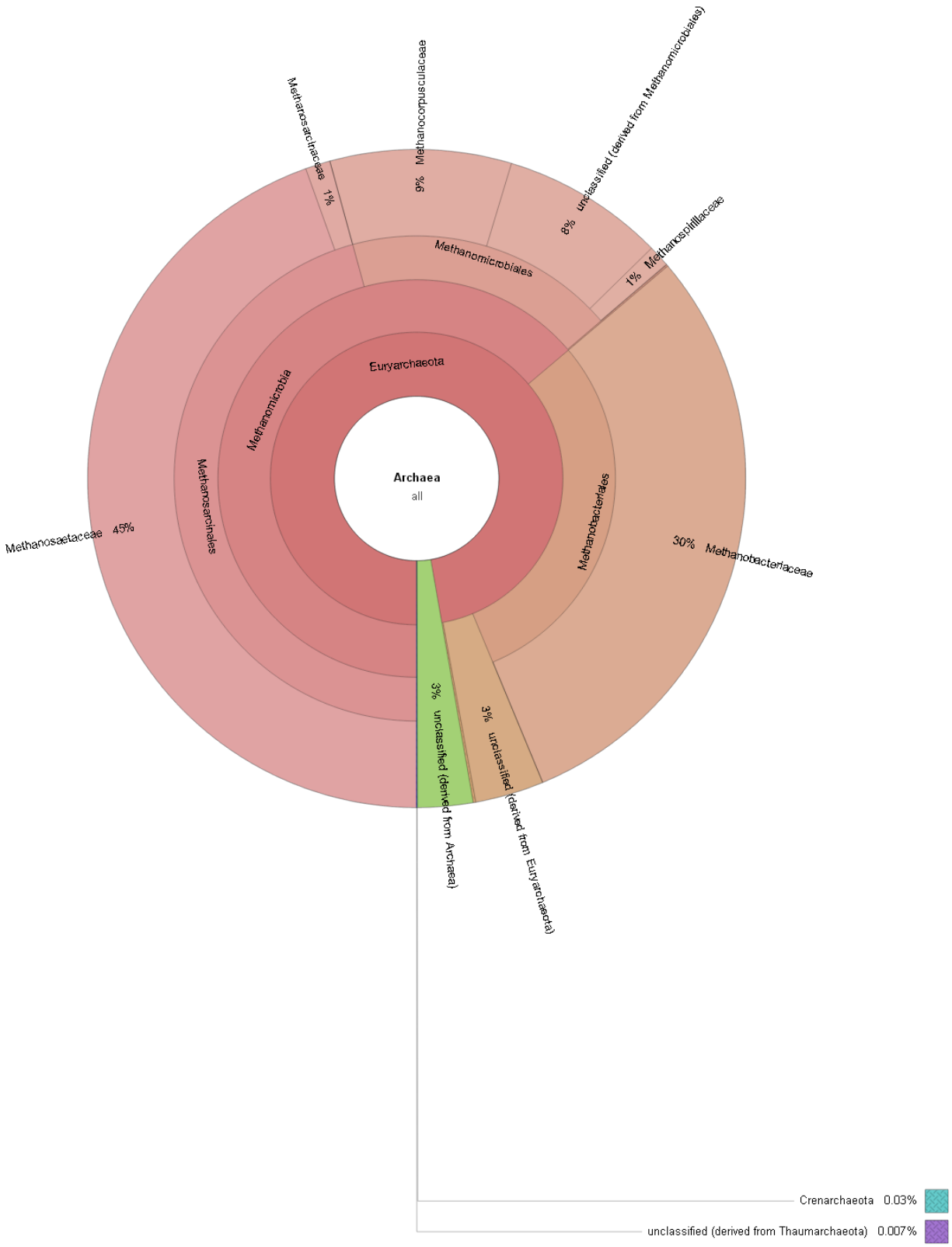

Figure 0.12 Distribution of archaeal community structure in pre-capping sediment at site GCR4.

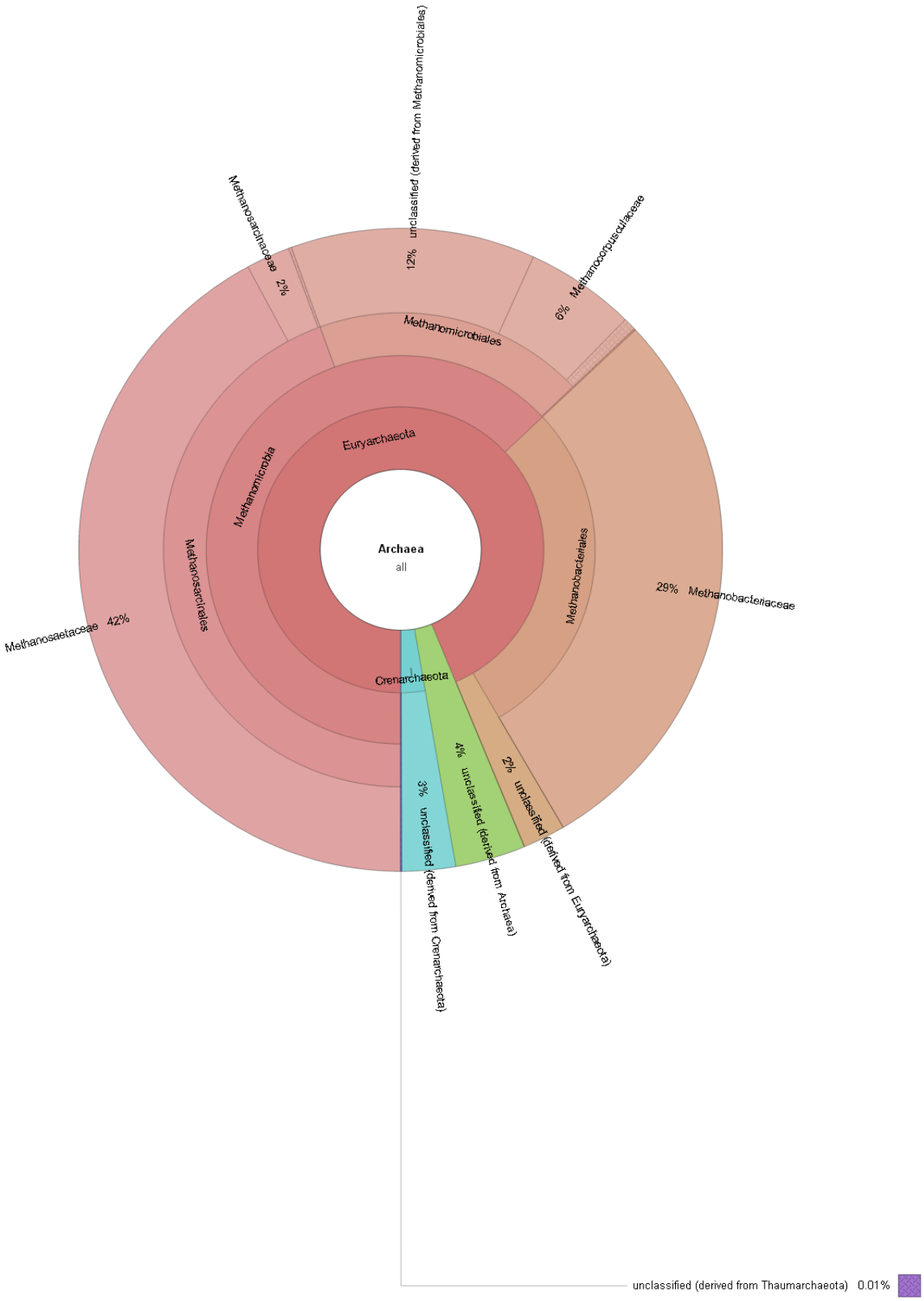

Figure 0.13 Distribution of archaeal community structure in pre-capping sediment at site GCR5.

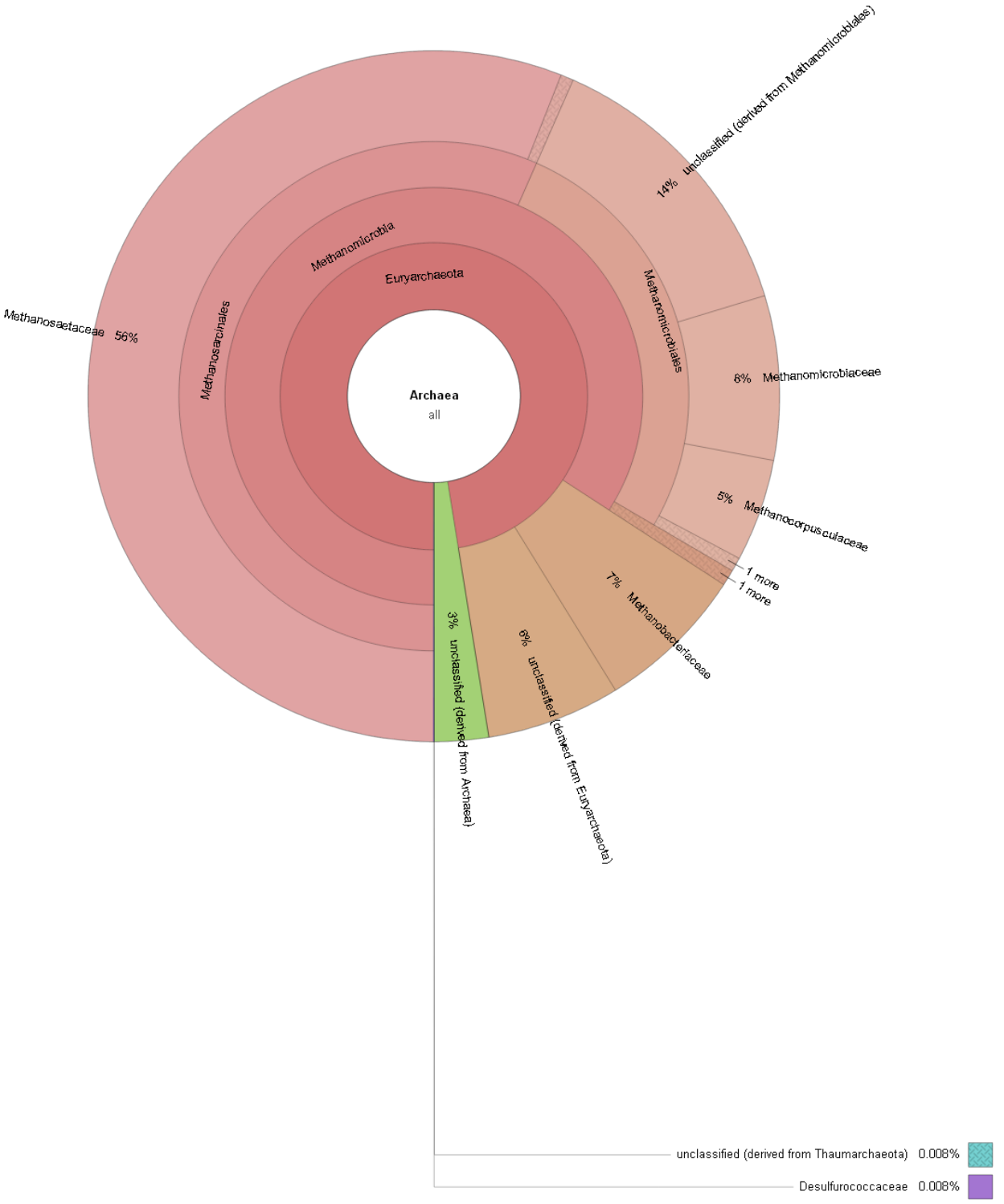

Figure 0.14 Distribution of archaeal community structure in pre-capping sediment at site GCR6.

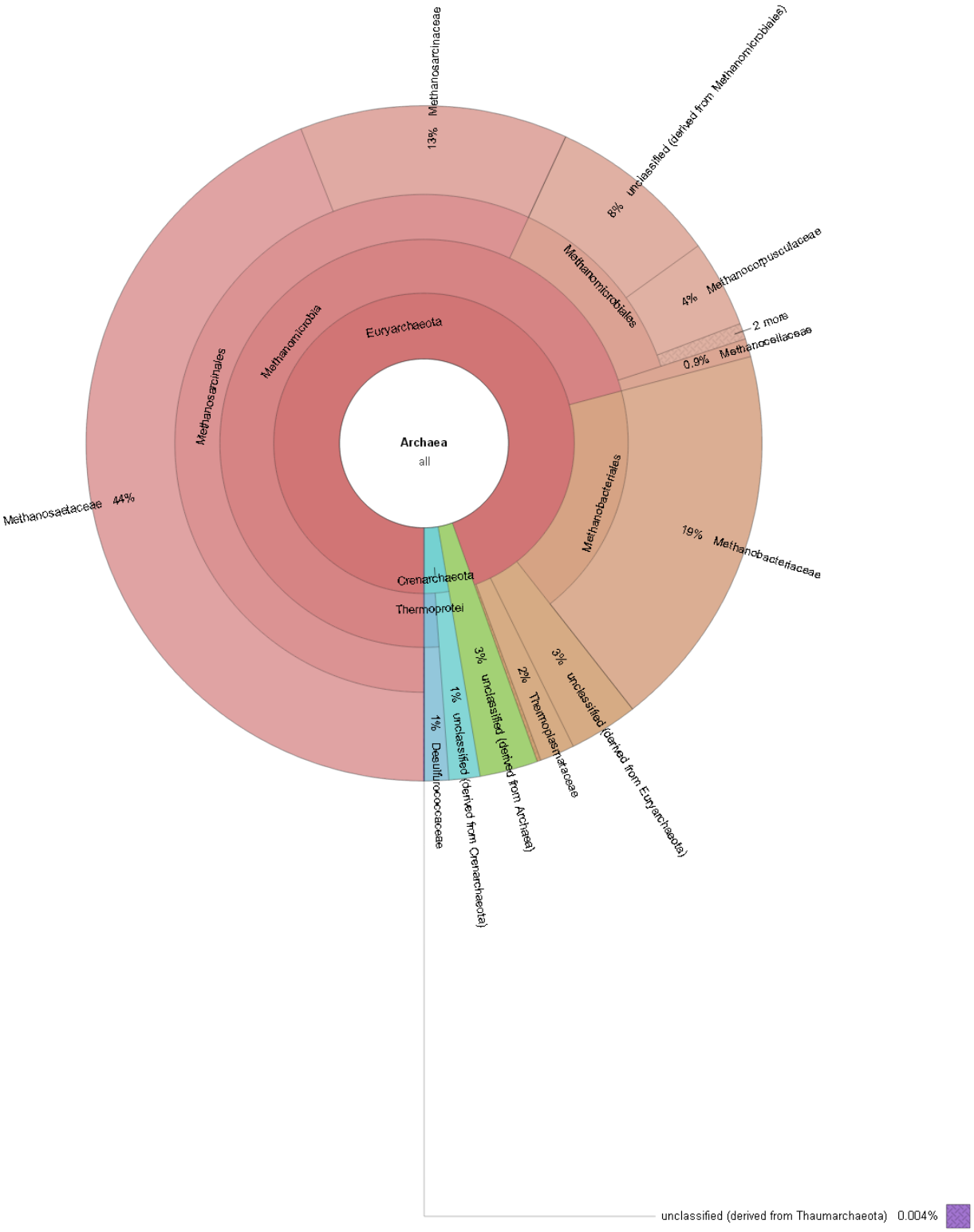

Figure 0.15 Distribution of archaeal community structure in pre-capping sediment at site GCR7.

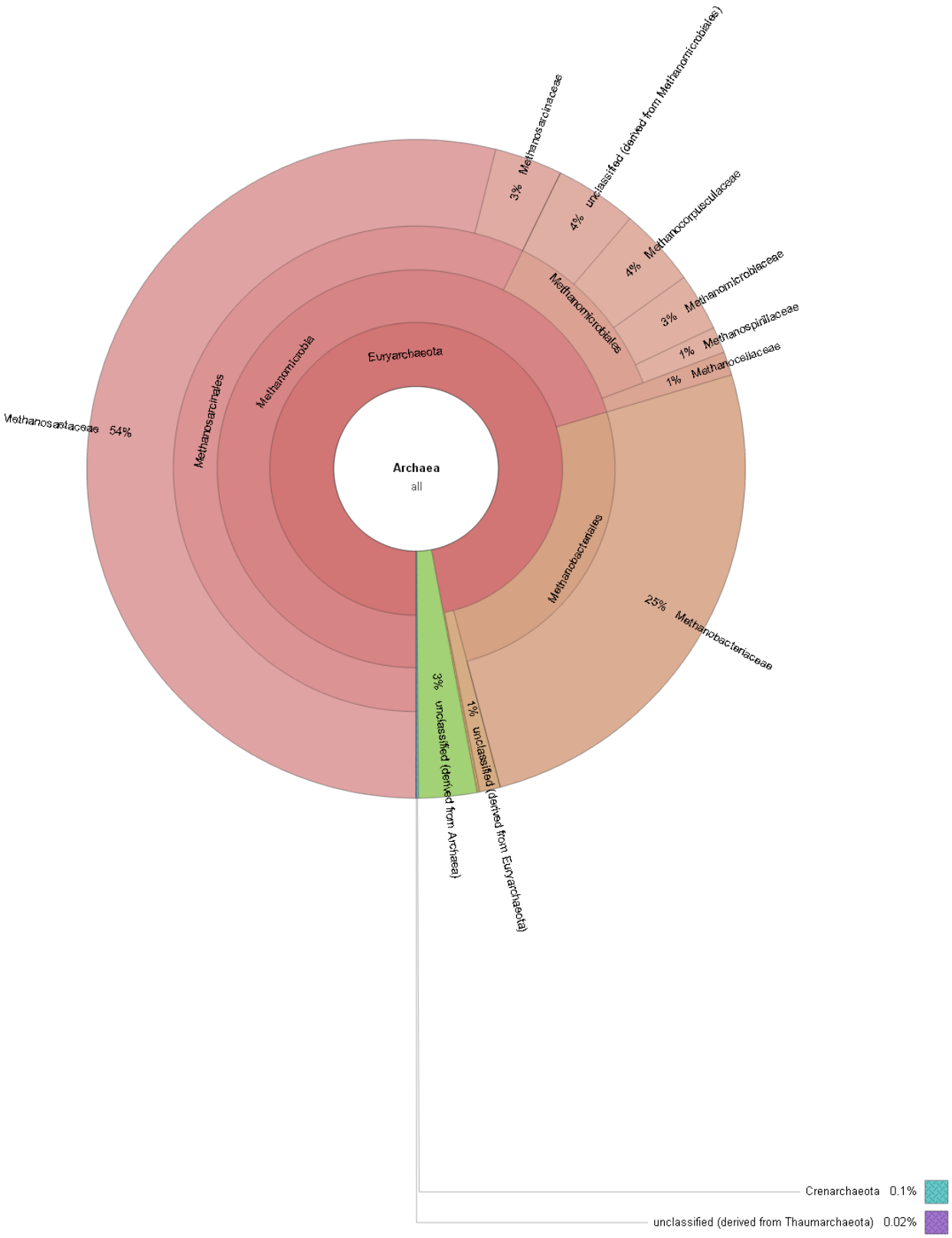

Figure 0.16 Distribution of archaeal community structure in pre-capping sediment at site GCR8.

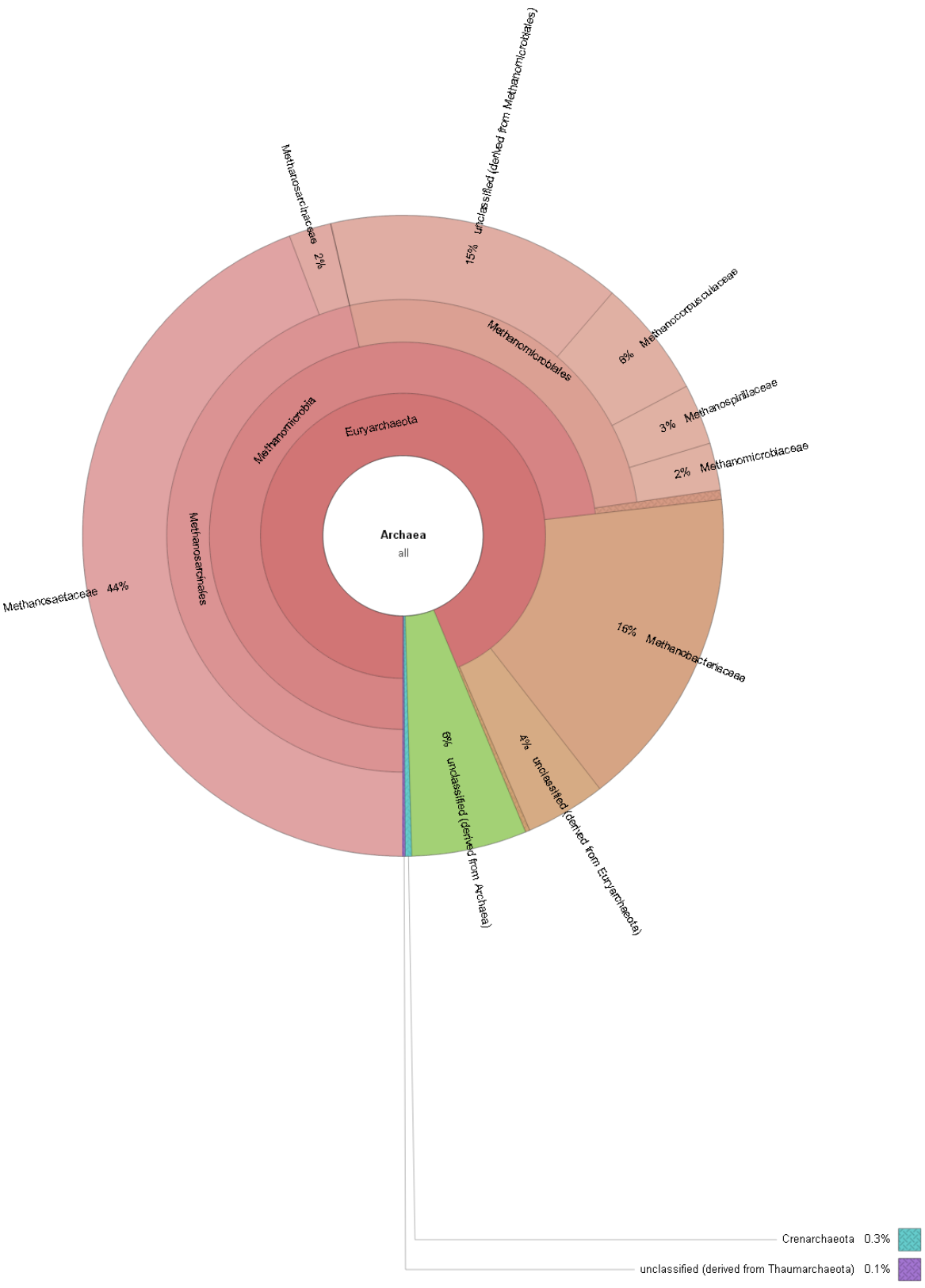

Figure 0.17 Distribution of archaeal community structure in pre-capping sediment at site GCR9.

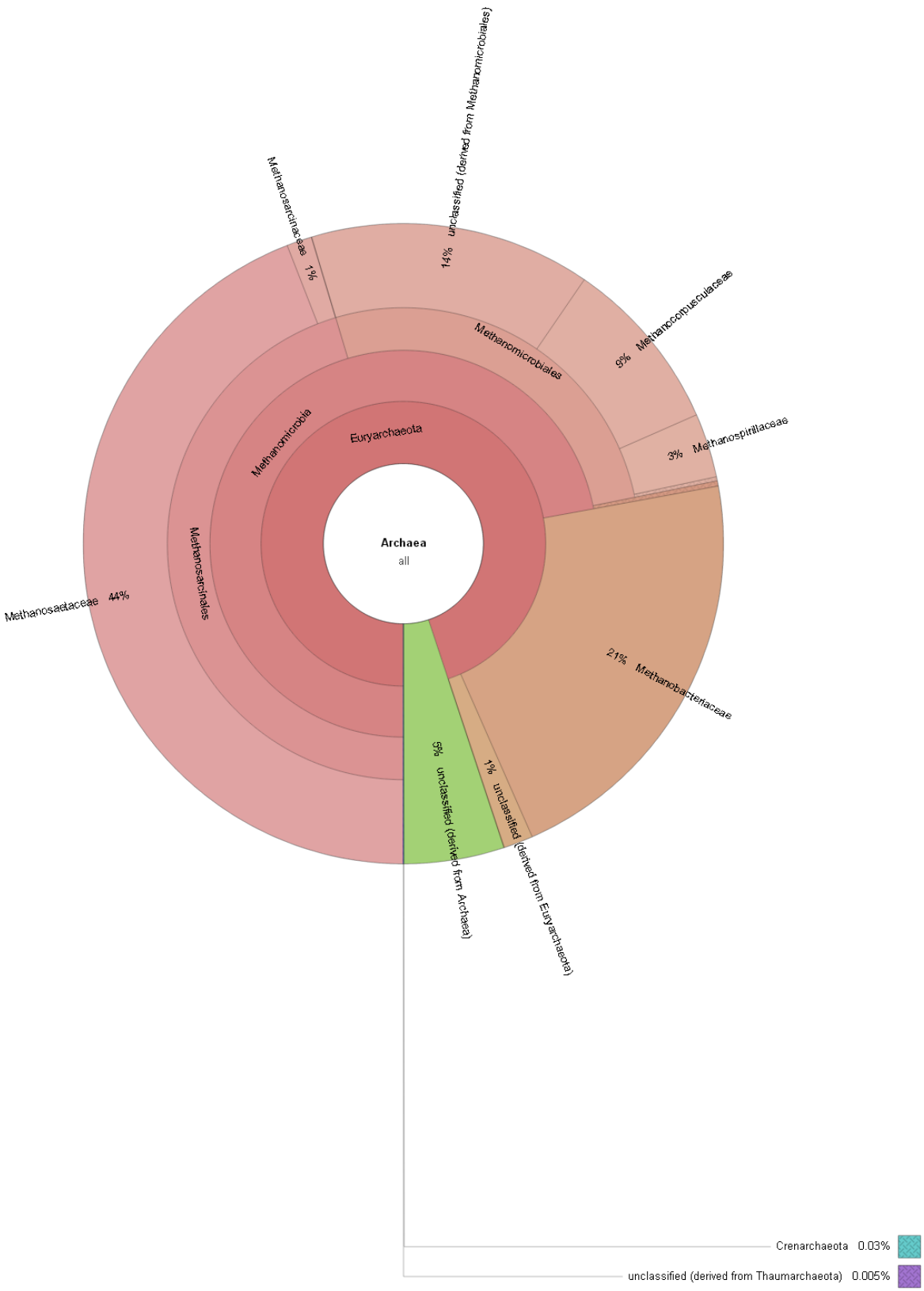

Figure 0.18 Distribution of archaeal community structure in pre-capping sediment at site GCR10.

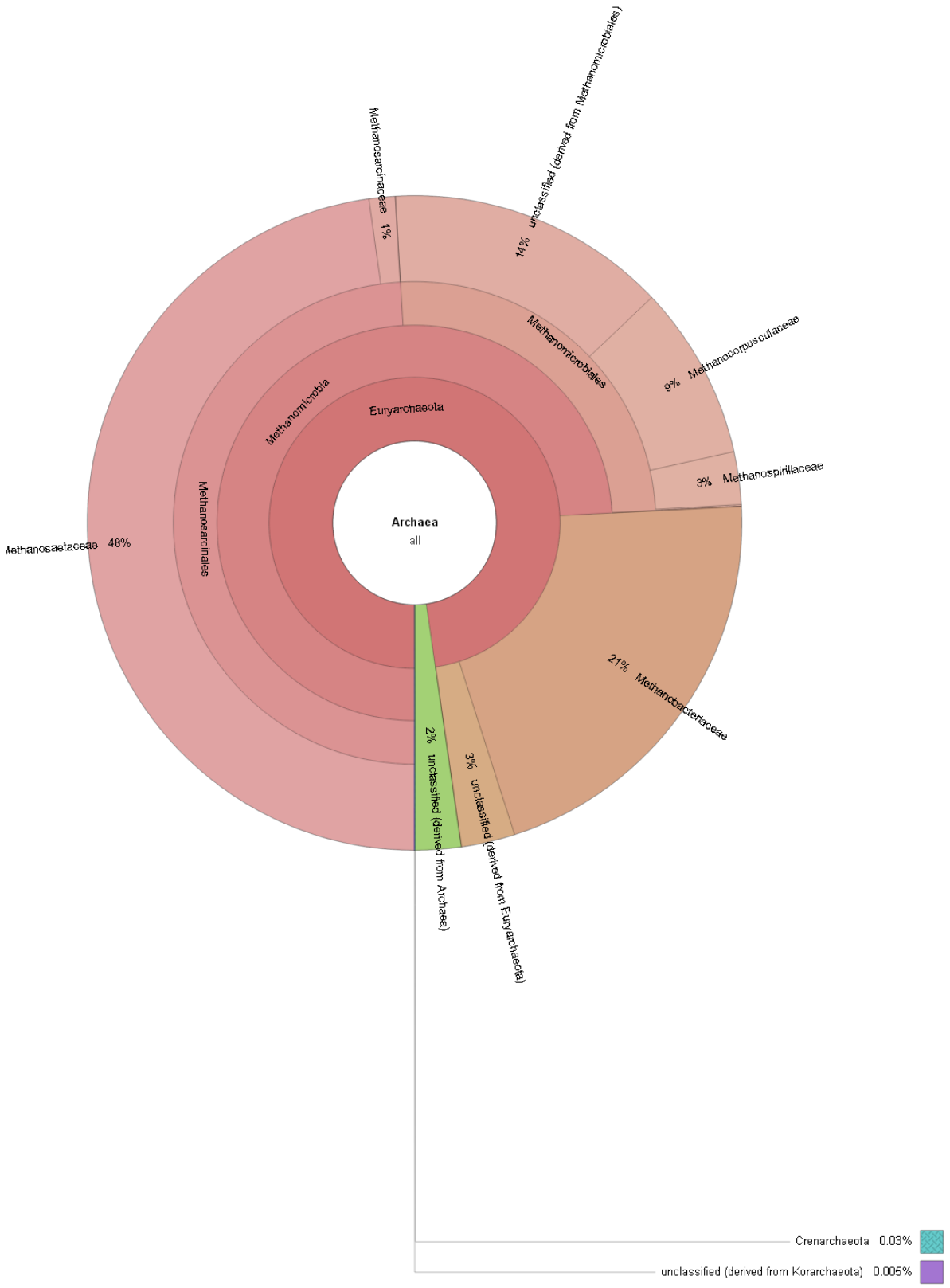

Figure 0.19 Distribution of archaeal community structure in pre-capping sediment at site GCR11.

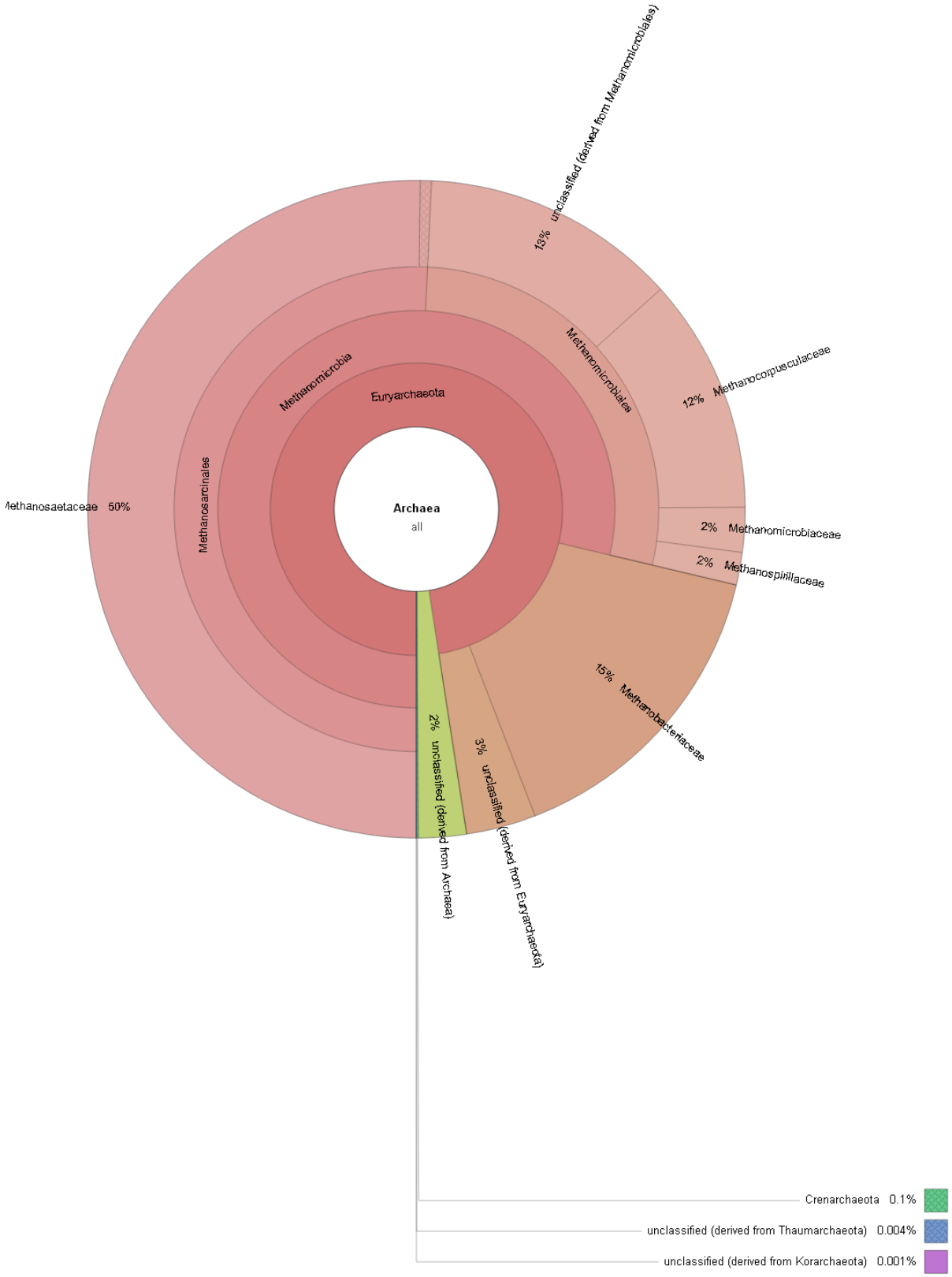

Figure 0.20 Distribution of archaeal community structure in pre-capping sediment at site GCR12.

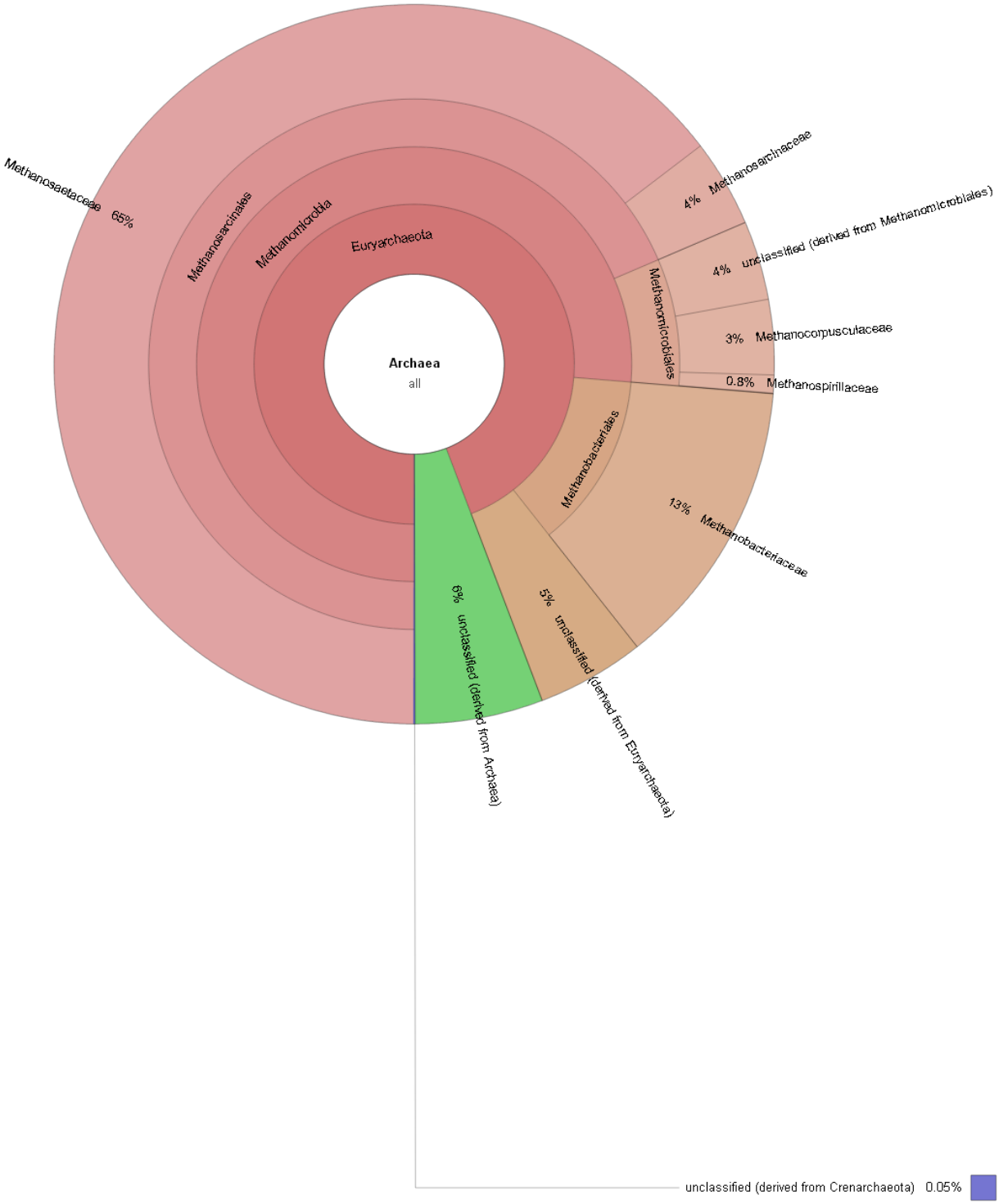

Figure 0.21 Distribution of archaeal community structure in pre-capping sediment at site GCR13.

5.4.7 Functional significance of Methanoarchaea in Pre-cap GCR Sediments

Approximately two-thirds of methane emissions in the natural environment originate from acetate (Jobbágy and Jackson 2000) which are produced by acetoclastic methanogens that include only two genera *Methanosaeta* and *Methanosarcina*. *Methanosarcina* utilize both C1 compounds such as methanol and methylamines along with the C2 acetate, whereas *Methanosaeta* utilizes only C2 acetate as a substrate for methanogenesis (Dubey et al. 2014). *Methanosarcina* requires a relatively high acetate threshold of ~1mM for the reaction to proceed, whereas *Methanosaeta* has a lower threshold of 5-20 μM (Tarnocai et al. 2009). This allows *Methanosaeta* to outcompete *Methanosarcina* in low acetate environments, which seems to be the case in GCR sediments. *Methanosaeta* were the most dominant archaeal group in the upper sediment layers of a fresh water meromictic lake in France (Borrel et al. 2012), suggesting *Methanosaeta* may dominate in the surficial zone. The metabolic pathway used in methane generation is essentially the same in both genera, with the exception of the enzymes used in the first step of acetate cleavage to form acetyl-CoA. *Methanosaeta* utilizes acetyl-CoA synthase (ACS), whereas *Methanosarcina* uses the combined action of acetate kinase (AK) and phospotransacetylase (PTA) (Smith and Ingram-Smith 2007). More recent research has revealed exciting new information on the role of *Methanosaeta*. The genera has been identified to be more metabolically diverse than previously assumed with new findings in regards to the presence of Ady2 homologs that can transport un-dissociated acetate across the cytoplasm (Paiva et al. 2004, Smith and Ingram-Smith 2007). Further a recent study demonstrated the existence of Direct Interspecies Electron Transfer (DIET) in *Methanosaeta* where the organism can make a direct electrical connection with *Geobacter* spp using electrically conductive pili (MallaáShrestha 2014). The electron transferred in the process can be used in the direct reduction of CO_2 to

methane, the metabolic pathway for which was previously unknown to exist in *Methanosaeta*. More recently, full genome sequences of *Methanosaeta* species have shown the presence of the genes for CO_2 reduction (Zhu et al. 2012, Barber et al. 2011). In GCR, the low abundance of *Methanosarcina* (0.3%) and dominance of *Methanosaeta* (typically greater than 50%) suggests that the majority of methane production occurs from acetate produced as intermediate in the anaerobic consortium in the sediments. This is further supported by sediment temperature data observed at GCR (between 5 – 20℃) where *Methanosaeta* is expected to outcompete hydrogenotrophic methanogens which are known to thrive at higher temperatures (>35ºC). Previous reports suggests that methanogenesis in freshwater sediments is primarily produced via the hydrogenotrophic and acetoclastic pathways (Bae et al. 2015), and the natural distribution of the two pathways is 33% and 67% respectively following the stoichiometry of glucose fermentation (Conrad 1999). The mean abundance of *Methanosaeta* (56%) and *Methanobacterium* (18%) is also fairly similar to the natural distribution, if other archaeal genera that use the acetate and H_2/CO_2 are accounted for. Hydrogenotrophic methanogens (Demirel and Scherer 2008, Sarmiento, Leigh, and Whitman 2011) identified in GCR include *Methanobacterium*, *Methanobrevibacter* and *Methanolinea* totaling 24% of the archaeal abundance. Hydrogenotrophs use primarily CO_2 as carbon source (Daniels et al. 1980) and eleven species have been described in the *Methanobacterium* genus (Garrity, Bell, and Lilburn 2004) which are mesophilic and thermophilic obligate autotrophs with some species capable of utilizing formate as carbon source (Smith et al. 1997). *Methanomethylovorans* (1%) and *Methanosarcina* (0.3%) are members of the family *Methanosarcinaceae* that contain a versatile group of *Archaea* that use H_2/CO_2, acetate and C1 compounds such as methanol, methylamines and methylated sulfides for methanogenesis (Boone, Whitman, and Rouvière 1993). The genus

Methanomethylovorans isolated in 1999 (Lomans et al. 1999) is a freshwater obligate methylotroph that can metabolize methanol, methylated amines, dimethyl sulfide and methane-thiol for CH_4 production (Jiang et al. 2005). The low presence of this genus at all sites suggests the presence of methane-thiol, dimethyl sulfide and/or methoxylated aromatic compounds produced from lignin degradation (Lomans et al. 1997). The low abundance of *Methanomethylovorans* can be attributed to the presence of sulfate reducing bacteria that outcompete methanogens for sulfur containing C1 compounds (Lomans et al. 1997, Bae et al. 2015). Other genera in limited abundance include *Methanocella*, *Methanospirillum*, *Methanosphaerula*, *Methanocorpusculum* and *Methanopyrus*; all of which utilize H_2/CO_2 for methane synthesis (Anderson et al. 2009, Sakai et al. 2008, Ferry, Smith, and Wolfe 1974, Slesarev et al. 2002, Cadillo-Quiroz, Yavitt, and Zinder 2009). *Methanopyrus* is a primitive hyperthermophilic *Archaea* (Brochier, Forterre, and Gribaldo 2004) placed closed to root of *Euryarchaeota* in the phylogenetic tree with no close affinity to other methanogens discussed earlier (Slesarev et al. 2002, Kurr et al. 1991). *Methanopyrus kandleri*, the only species in this genera, contains high concentration of the intracellular anion cyclic 2,3 diphosphoglycerate which is responsible for enzyme stability at high temperature (Shima et al. 1998). The statistically significant correlation of *Methanopyrus* abundance with sediment PAHs and heavy metals suggests the organism may be adapted to polluted environmental conditions.

Among the non-methanogenic *Archaea* found in GCR are various *Candidatus* spp. *Candidatus Nitrososphaera* is a member of the recently discovered Ammonia Oxidizing Archaea (AOA) group (Treusch et al. 2005, Könneke et al. 2005) which is part of the newly identified phylum *Thaumarchaeota* (Brochier-Armanet et al. 2008). The members of this genera oxidize ammonia to nitrite and fix inorganic carbon (Spang et al. 2012). The presence of AOA suggests that

ammonia must be present in GCR sediments. The HSD practices Nitrifications, so Ammonia levels would be expected to be low. A second possible source of ammonia is the presence of Dissimilatory Nitrate Reduction to Ammonia (DNRA) (Koike and Hattori 1978, Dong et al. 2009) where the nitrate in HSD effluent is converted to ammonia in the anaerobic sediment. This was further confirmed by presence of high levels of ammonia in the water column at sites upstream of the outfall (GCR11-13) (Figure 5.22). Finally, ammonia can be produced by decomposition of amino acids in the sediment (MOLONGOSKI and KLUG 1980, McKew et al. 2013). The observed trend in *Candidatus Nitrososphaera* abundance in Reach-2 peaks at site GCR10, with values decreasing at sites further away from the HSD outfall. This would be consistent with DNRA or HSD derived ammonia driving AOA at sites closer to the outfall in the surficial sediment.

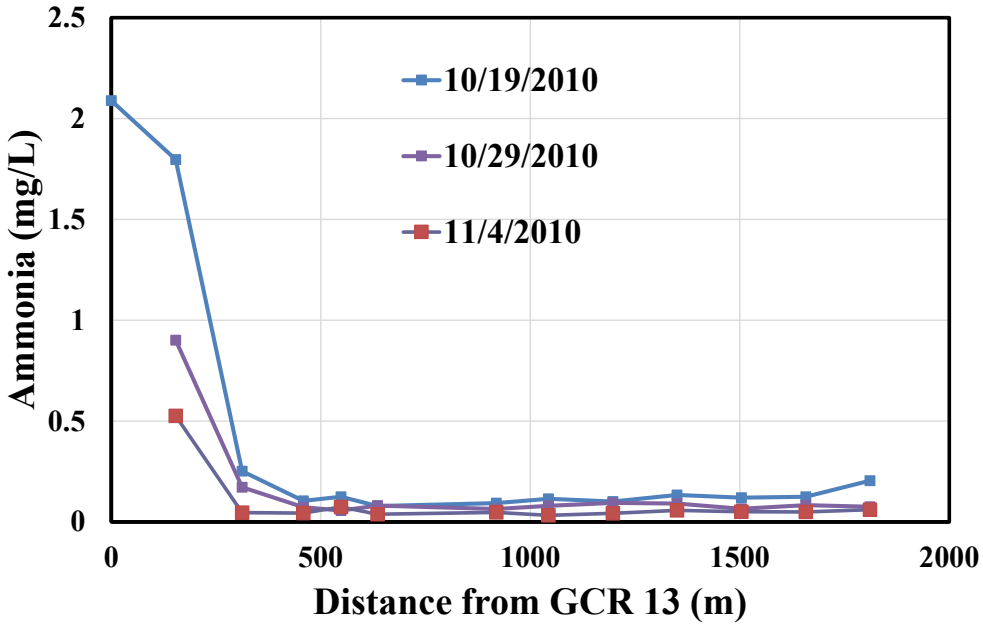

Figure 0.22 Water column ammonia levels during pre-cap monitoring at sites GCR 13 to GCR1 (Site GCR13 is marked as origin on x-axis).

5.4.8 Archaeal Community Structure in Post-capping Sediment

Similar to the previous discussion in section 5.4.4, only taxonomic classifications with abundances greater than 1% are discussed. The KRONA plots of metagenomes from individual sites are presented in Figures 5.24 -39.

GCR2-ND: The new deposit layer in GCR 2 was dominated by the Class *Methanomicrobia* accounting for 39% of the sequences, with unclassified *Archaea* and *Methanobacteria* accounting for 24% and 19%, respectively. *Methanomicrobia* was further classified into *Methanosarcinaceae* (16%) family, *Methanomethylovorans* (9%), *Methanosaeta* (9%), *Methanocella* (5%) and unclassified *Methanomicrobia* (1%). *Methanobacteria* was entirely composed of the Genus *Methanobacterium*. The remaining sequences were classified primarily into class Thermoprotei (10%) and the genera *Methanopyrus* (3%) and *Candidatus Nitrososphaera* (1%).

GCR2-GAL: Over 80% of the sequences in the gravel armor layer were unclassified *Archaea*, followed by *Methanomicrobia* comprising of *Methanosaeta* (5%), *Methanomethylovorans* (2%) and *Methanosarcinaceae* (2%). The genera *Candidatus Nitrososphaera* belonging to *Thaumarchaeota* accounted for 8% of the sequences.

GCR2-OrgC: Methanomicrobia accounted for 71% of the sequences dominated the organoclay layer. The class was further classified into genera *Methanosaeta* (39%), *Methanocorpusculum* (21%) *Methanoculleus* (1%) and *Methanolinea* (1%). The orders *Methanosarcinales*, *Methanomicrobiales* and *Methanomicrobia* accounted 4%, 2% and 3%, respectively. *Candidatus Nitrososphaera* accounted for 15%. Unclassified *Archaea* and *Methanobacteria* accounted for 5% and 8% respectively with *Methanobacteria* further classified into *Methanobrevibacter* and *Methanobacterium* in equal proportion.

GCR2-CSed: *Methanomicrobia* accounted for 59% of the sequences and included of the genera *Methanosaeta* (41%), *Methanolinea* (3%), *Methanoculleus* (1%) and unclassified *Methanomicrobiales* (17%). *Methanobacteria* accounted for 14% of archaeal abundance that included the genera *Methanobacterium* (8%) and *Methanobrevibacter* (6%). The phylum *Crenarchaeota* represented 13% of the sequences that were classified into *Desulfurococcaceae* (4%) and unclassified *Crenarchaeota* (9%). Unclassified *Archaea* together contributed 8% of the total.

GCR6-ND: *Methanomicrobia* contributed to 80% of the archaeal abundance in GCR6-ND sediment and were classified into *Methanosaeta* (65%), *Methanospirillum* (2%), *Methanolinea* (1%), *Methanomethylovorans* (1%), *Methanosphaerula* (1%) and unclassified *Methanomicrobia* (10%). Methanobacteria represented 8% of the total comprising of *Methanobacterium* (5%) and *Methanobrevibacter* (3%). The genus *Methanopyrus* in class *Methanopyri* accounted for 1% and unclassified sequences derived from *Archaea* accounted for 8% of the total archaeal sequences.

GCR6-GAL: The GAL layer was dominated by *Methanomicrobia* accounting to 81% of the sequences in this sediment and included the genera *Methanosaeta* (45%), *Methanomethylovorans* (5%), *Methanospirillum* (3%), *Methanosphaerula* (1%), the family *Methanosarcinaceae* (24%) and unclassified *Methanomicrobia* (3%). Class *Methanobacteria* accounted for 12% of the sequences that included the genera *Methanobacterium* (11%) and *Methanobrevibacter* (1%). The remaining sequences included genera *Candidatus Nitrososphaera* (2%), *Thermoprotei* (1%), unclassified *Euryarchaeota* (1%) and unclassified *Thaumarchaeota* (2%).

GCR6-OrgC: The archaeal community structure in GCR6-OrgC included 83% of sequences categorized under *Methanomicrobia* comprising of the genera *Methanosaeta* (67%),

Methanospirillum (2%), *Methanomethylovorans* (1%), *Methanosphaerula* (1%), *Methanolinea* (1%) and *Methanosarcina* (1%). The remaining *Methanomicrobia* were composed of the family *Methanosarcinaceae* (1%) and unclassified *Methanomicrobia* (10%). *Methanobacteria* accounted for 10% comprising of the genera *Methanobacterium* (7%) and *Methanobrevibacter* (3%). Unclassified *Thaumarchaeota* and *Euryarchaeota* comprised of 2% and 1% of the sequences along with 3% of unclassified sequences derived from *Archaea*.

GCR6-CSed: The genera *Methanosaeta* (68%), *Methanospirillum* (1%), *Methanosphaerula* (1%) and the order *Methanomicrobiales* (8%) accounted for 80% of the archaeal sequences in the Class *Methanomicrobia*. *Methanobacteria* was entirely composed of the genera *Methanobacterium* (14%) with the remaining sequences primarily composed of unclassified *Euryarchaeota* (3%) and unclassified *Archaea* (2%).

GCR11-ND: The genera *Methanosaeta* (26%), *Methanomethylovorans* (10%), *Methanospirillum* (5%), *Methanosarcina* (4%), *Methanosphaerula* (3%) and *Methanocorpusculum* (1%) accounted for 49% of the archaeal sequences in the class *Methanomicrobia*. *Methanobacteria* were primarily composed of the genera *Methanobacterium* (19%) and 1% of unclassified *Methanobacteriaceae*. The rest of the archaeal sequences were categorized under the genera *Methanopyrus* (6%), *Candidatus Nitrososphaera* (5%) and *Nitrosopumilus* (5%) along with 5% of unclassified *Archaea* and 1% of unclassified sequences derived from *Euryarchaeota*.

GCR11-GAL: Similar to other sites, a majority of the archaeal sequences were categorized under *Methanomicrobia* that included the genera *Methanosaeta* (39%), *Methanosphaerula* (9%), *Methanomethylovorans* (8%), *Methanospirillum* (4%), *Methanosarcina* (4%), *Methanocorpusculum* (1%) and unclassified *Methanosarcinaceae* (1%). The layer also had a

significant percentage of unclassified sequences derived from *Archaea* (17%) and 2% of unclassified Euryarchaeota. The genera *Methanobacterium* and *Methanobrevibacter*, which fall under the class Methanobacteria, accounted for 9% and 1% respectively. *Methanopyrus* and *Candidatus Nitrososphaera* contributed to 1% each.

GCR11-OrgC: *Methanomicrobia* represented 83% of the archaeal sequences with 51% of the sequences categorized as unclassified *Methanosarcinaceae*. Other genera in *Methanomicrobia* included *Methanosaeta* (26%), *Methanomethylovorans* (1%) and unclassified *Methanomicrobia* (5%). *Methanomicrobia* was the second dominant class that included the genera *Methanobacterium* (6%) and *Methanobrevibacter* (4%). Other archaeal groups in the sediment included *Candidatus Nitrososphaera* (1%), *Thermoproteaceae* (1%) and unclassified *Archaea* (4%).

GCR11-CSed: *Methanomicrobia* accounted for 84% of the archaeal consortium in GCR11-CSed that included the genera Methanosaeta (57%), *Methanolinea* (2%), *Methanocorpusculum* (1%), *Methanospirillum* (1%), unclassified sequences of the order *Methanomicrobiales* (22%) and unclassified *Methanomicrobia* (1%). *Methanobacteria* accounted for 11% of the sequences and classified into the genera *Methanobacterium* (7%) and *Methanobrevibacter* (2%) with 2% of sequences identified as unclassified *Methanobacteriaceae*. Unclassified *Archaea* and *Euryarchaeota* sequences represented 3% and 1% of the archaeal consortium in this sediment.

GCR13-ND: *Methanomicrobia* accounted for 61% of the archaeal consortium in GCR13-ND and included the genera *Methanosaeta* (40%), *Methanospirillum* (4%), *Methanocella* (2%), *Methanolobus* (1%) and *Methanolinea* (1%). The remaining sequences in *Methanomicrobia* were classified under the family *Methanosarcinaceae* (3%), *Methanomicrobiales* (7%) and unclassified *Methanomicrobia* (3%). *Methanobacteria* accounted for 20% of the sequences that

included the genera *Methanobacterium* (17%), *Methanobrevibacter* (1%) and the family *Methanobacteriaceae* (2%). The genera *Methanopyrus* and *Candidatus Nitrososphaera* that falls under the class *Methanopyri* and unclassified *Thaumarchaeota* represented 2% and 5% of the sequences respectively.

GCR13-GAL: The distribution of *Methanomicrobia* consisted of the genera *Methanosaeta* (64%), *Methanomethylovorans* (16%) and *Methanocella* (7%). *Methanobacteria* was completely absent in this armor layer. The remaining sequences were classified into *Methanopyrus* (2%) and unclassified *Archaea* (10%).

GCR13-OrgC: In contrast to all other sites that were dominated by *Methanomicrobia*, *Methanobacteria* was the most dominant class in GCR13-CSed representing 72% of the sequences. This family included the genera *Methanobacterium* (67%) and *Methanobrevibacter* (5%). *Methanomicrobia* accounted for 17% of the sequences that were further classified into the genera *Methanosaeta* (10%), family *Methanosarcinaceae* (2%) and order *Methanomicrobiales* (5%). The remaining sequences consisted of *Candidatus Nitrososphaera* (8%), *Crenarchaeota* (1%) and unclassified *Archaea* (1%).

GCR13-CSed: *Methanomicrobia* represented 63% of the archaeal consortium that included the genera *Methanosaeta* (47%), *Methanospirillum* (2%), *Methanocorpusculum* (1%) and *Methanoculleus* (1%). The remaining sequences in *Methanomicrobia* were consisted of the order *Methanomicrobiales* (6%) and unclassified *Methanomicrobia* (6%). Class *Crenarchaeota* accounted for 18% of the archaeal consortium, which included the genera *Candidatus Nitrosocaldus* (13%), *Ignicoccus* (1%) and the family *Desulfurococcaceae* (4%). *Methanobacteria* comprising of the genera *Methanobacterium* and *Methanobrevibacter* accounted for 4% each. A small fraction of the sequences were classified under the phylum

Thaumarchaeota that including the genus *Nitrosopumilus* (1%) and unclassified *Thaumarchaeota* (1%). Unclassified sequences derived from *Archaea* accounted for 4% of the archaeal abundance.

Table 0.9 Archaeal abundance in new deposit (ND) layer sediments at sites GCR2, 6, 11 and 13.

Phylum	Class	Order	Family	Genus	GCR2	GCR6	GCR11	GCR13
Unclassified	*Unclassified*	*Unclassified*	*Unclassified*	*Unclassified*	24%	6%	5%	6%
Euryarchaeota	*Unclassified*	*Unclassified*	*Unclassified*	*Unclassified*	1%	2%	-	1%
Crenarchaeota	*Thermoprotei*	*Unclassified*	*Unclassified*	*Unclassified*	10%	-	-	-
Euryarchaeota	*Methanomicrobia*	*Unclassified*	*Unclassified*	*Unclassified*	1%	6%	-	3%
Euryarchaeota	*Methanomicrobia*	*Methanomicrobiales*	*Unclassified*	*Unclassified*	-	4%	-	7%
Euryarchaeota	*Methanomicrobia*	*Methanosarcinales*	*Methanosarcinaceae*	*Unclassified*	16%	-	7%	3%
Euryarchaeota	*Methanobacteria*	*Methanobacteriales*	*Methanobacteriaceae*	*Unclassified*	-	-	1%	2%
Euryarchaeota	*Methanomicrobia*	*Methanosarcinales*	*Methanosaetaceae*	*Methanosaeta*	8.7%	65.3%	25.7%	39.9%
Euryarchaeota	*Methanobacteria*	*Methanobacteriales*	*Methanobacteriaceae*	*Methanobacterium*	18.9%	5.4%	18.7%	17.4%
Euryarchaeota	*Methanobacteria*	*Methanobacteriales*	*Methanobacteriaceae*	*Methanobrevibacter*	0.5%	2.5%	0.4%	1.3%
Euryarchaeota	*Methanomicrobia*	*Methanomicrobiales*	*Methanospirillaceae*	*Methanospirillum*	0.4%	1.7%	4.9%	3.7%
Euryarchaeota	*Methanomicrobia*	*Methanomicrobiales*	*Unclassified (derived from Methanomicrobiales)*	*Methanolinea*	0.0%	1.3%	0.2%	1.2%
Euryarchaeota	*Methanopyri*	*Methanopyrales*	*Methanopyraceae*	*Methanopyrus*	3.2%	1.0%	5.8%	1.8%
Euryarchaeota	*Methanomicrobia*	*Methanosarcinales*	*Methanosarcinaceae*	*Methanomethylovorans*	8.7%	0.7%	9.9%	0.9%
Euryarchaeota	*Methanomicrobia*	*Methanomicrobiales*	*Unclassified (derived from Methanomicrobiales)*	*Methanosphaerula*	0.2%	0.5%	3.3%	0.0%
Thaumarchaeota	*Unclassified (derived from Thaumarchaeota)*	*Unclassified (derived from Thaumarchaeota)*	*Unclassified (derived from Thaumarchaeota)*	*Candidatus Nitrososphaera*	0.7%	0.4%	5.1%	5.3%
Euryarchaeota	*Unclassified (derived from Euryarchaeota)*	*Unclassified (derived from Euryarchaeota)*	*Unclassified (derived from Euryarchaeota)*	*Unclassified (derived from Euryarchaeota)*	0.7%	0.4%	1.0%	0.7%
Euryarchaeota	*Methanomicrobia*	*Methanosarcinales*	*Methanosarcinaceae*	*Methanosarcina*	0.2%	0.2%	4.3%	0.1%
Euryarchaeota	*Methanomicrobia*	*Methanocellales*	*Methanocellaceae*	*Methanocella*	5.5%	0.2%	0.2%	2.5%
Euryarchaeota	*Methanomicrobia*	*Methanomicrobiales*	*Methanocorpusculaceae*	*Methanocorpusculum*	0.0%	0.1%	0.8%	0.1%
Euryarchaeota	*Methanomicrobia*	*Methanomicrobiales*	*Methanomicrobiaceae*	*Methanoculleus*	0.0%	0.0%	-	0.6%

Table 0.10 Archaeal abundance in new deposit (GAL) layer sediments at sites GCR2, 6, 11 and 13.

Phylum	Class	Order	Family	Genus	GCR2	GCR6	GCR11	GCR13
Unclassified	*Unclassified*	*Unclassified*	*Unclassified*	*Unclassified*	81.0%	1.1%	17.3%	10.2%
Euryarchaeota	*Unclassified*	*Unclassified*	*Unclassified*	*Unclassified*	-	-	-	-
Crenarchaeota	*Thermoprotei*	*Unclassified*	*Unclassified*	*Unclassified*	-	0.7%	-	-
Euryarchaeota	*Methanomicrobia*	*Unclassified*	*Unclassified*	*Unclassified*	-	2.1%	-	-
Euryarchaeota	*Methanomicrobia*	*Methanomicrobiales*	*Unclassified*	*Unclassified*	-	1.3%	0.9%	-
Euryarchaeota	*Methanomicrobia*	*Methanosarcinales*	*Methanosarcinaceae*	*Unclassified*	-	24.1%	1.0%	0.3%
Euryarchaeota	*Methanomicrobia*	*Methanosarcinales*	*Methanosaetaceae*	*Methanosaeta*	4.7%	45.0%	39.3%	64.1%
Euryarchaeota	*Methanobacteria*	*Methanobacteriales*	*Methanobacteriaceae*	*Methanobacterium*	0.1%	10.7%	9.3%	-
Euryarchaeota	*Methanomicrobia*	*Methanosarcinales*	*Methanosarcinaceae*	*Methanomethylovorans*	2.0%	4.5%	7.9%	15.6%
Euryarchaeota	*Methanomicrobia*	*Methanomicrobiales*	*Methanospirillaceae*	*Methanospirillum*	-	2.6%	3.8%	-
Thaumarchaeota	*Unclassified (derived from Thaumarchaeota)*	*Unclassified (derived from Thaumarchaeota)*	*Unclassified (derived from Thaumarchaeota)*	*Candidatus Nitrososphaera*	7.7%	2.5%	0.8%	-
Euryarchaeota	*Unclassified (derived from Euryarchaeota)*	*Unclassified (derived from Euryarchaeota)*	*Unclassified (derived from Euryarchaeota)*	*Unclassified (derived from Euryarchaeota)*	-	1.4%	2.4%	-
Euryarchaeota	*Methanobacteria*	*Methanobacteriales*	*Methanobacteriaceae*	*Methanobrevibacter*	-	0.9%	0.9%	-
Euryarchaeota	*Methanomicrobia*	*Methanomicrobiales*	*Unclassified (derived from Methanomicrobiales)*	*Methanosphaerula*	-	0.8%	9.1%	0.1%
Euryarchaeota	*Methanopyri*	*Methanopyrales*	*Methanopyraceae*	*Methanopyrus*	0.2%	0.8%	0.9%	2.5%
Euryarchaeota	*Methanomicrobia*	*Methanosarcinales*	*Methanosarcinaceae*	*Methanosarcina*	-	0.5%	3.7%	-
Euryarchaeota	*Methanomicrobia*	*Methanomicrobiales*	*Methanocorpusculaceae*	*Methanocorpusculum*	-	0.0%	0.8%	-

Table 0.11 Archaeal abundance in new deposit (OrgC) layer sediments at sites GCR2, 6, 11 and 13

Phylum	Class	Order	Family	Genus	GCR2	GCR6	GCR11	GCR13
Unclassified	*Unclassified*	*Unclassified*	*Unclassified*	*Unclassified*	4.3%	2.9%	4.7%	1.1%
Euryarchaeota	*Unclassified*	*Unclassified*	*Unclassified*	*Unclassified*	-	1.2%	-	-
Euryarchaeota	*Methanomicrobia*	*Unclassified*	*Unclassified*	*Unclassified*	2.7%	4.2%	2.1%	-
Euryarchaeota	*Methanomicrobia*	*Methanomicrobiales*	*Unclassified*	*Unclassified*	1.1%	5.5%	2.8%	4.9%
Euryarchaeota	*Methanomicrobia*	*Methanosarcinales*	*Unclassified*	*Unclassified*	0.7%	-	-	-
Euryarchaeota	*Methanomicrobia*	*Methanosarcinales*	*Methanosarcinaceae*	*Unclassified*	4.4%	1.1%	51.5%	1.9%
Crenarchaeota	*Thermoprotei*	*Thermoproteales*	*Thermoproteaceae*	*Unclassified*	-	-	-	0.9%
Euryarchaeota	*Methanomicrobia*	*Methanosarcinales*	*Methanosaetaceae*	*Methanosaeta*	39.5%	66.7%	26.4%	9.5%
Euryarchaeota	*Methanomicrobia*	*Methanomicrobiales*	*Methanocorpusculaceae*	*Methanocorpusculum*	20.6%	0.5%	0.0%	0.0%
Thaumarchaeota	*Unclassified (derived from Thaumarchaeota)*	*Unclassified (derived from Thaumarchaeota)*	*Unclassified (derived from Thaumarchaeota)*	*Candidatus Nitrososphaera*	15.0%	2.3%	1.2%	7.7%
Euryarchaeota	*Methanobacteria*	*Methanobacteriales*	*Methanobacteriaceae*	*Methanobrevibacter*	4.3%	2.8%	2.0%	5.5%
Euryarchaeota	*Methanobacteria*	*Methanobacteriales*	*Methanobacteriaceae*	*Methanobacterium*	3.9%	7.0%	5.7%	67.4%
Euryarchaeota	*Methanomicrobia*	*Methanomicrobiales*	*Unclassified (derived from Methanomicrobiales)*	*Methanolinea*	1.2%	0.6%	0.3%	0.5%
Euryarchaeota	*Methanomicrobia*	*Methanomicrobiales*	*Methanomicrobiaceae*	*Methanoculleus*	0.5%	0.0%	0.0%	-
Euryarchaeota	*Methanomicrobia*	*Methanosarcinales*	*Methanosarcinaceae*	*Methanomethylovorans*	0.3%	0.7%	0.7%	0.0%
Euryarchaeota	*Methanomicrobia*	*Methanomicrobiales*	*Methanospirillaceae*	*Methanospirillum*	0.2%	2.3%	0.2%	-
Euryarchaeota	*Methanomicrobia*	*Methanomicrobiales*	*Unclassified (derived from Methanomicrobiales)*	*Methanosphaerula*	0.0%	0.6%	0.2%	-
Euryarchaeota	*Methanomicrobia*	*Methanosarcinales*	*Methanosarcinaceae*	*Methanosarcina*	0.0%	0.5%	0.3%	0.0%
Euryarchaeota	*Methanomicrobia*	*Methanomicrobiales*	*Unclassified (derived from Methanomicrobiales)*	*Methanoregula*	0.1%	0.2%	0.0%	-

Table 0.12 Archaeal abundance in new deposit (CSed) layer sediments at sites GCR2, 6, 11 and 13

Phylum	Class	Order	Family	Genus	GCR2	GCR6	GCR11	GCR13
Unclassified	*Unclassified*	*Unclassified*	*Unclassified*	*Unclassified*	7.7%	2.8%	3.2%	5.0%
Euryarchaeota	*Unclassified*	*Unclassified*	*Unclassified*	*Unclassified*	1.8%	1.7%	1.4%	1.2%
Euryarchaeota	*Methanomicrobia*	*Unclassified*	*Unclassified*	*Unclassified*	2.6%	1.0%	0.9%	5.5%
Euryarchaeota	*Methanomicrobia*	*Methanomicrobiales*	*Unclassified*	*Unclassified*	14.1%	7.7%	21.6%	5.6%
Euryarchaeota	*Methanobacteria*	*Methanobacteriales*	*Methanobacteriaceae*	*Unclassified*	-	0.5%	1.6%	-
Crenarchaeota	*Thermoprotei*	*Desulfurococcales*	*Desulfurococcaceae*	*Unclassified*	3.9%	-	-	-
Euryarchaeota	*Methanomicrobia*	*Methanosarcinales*	*Methanosaetaceae*	*Methanosaeta*	40.7%	68.2%	57.1%	47.2%
Crenarchaeota	*Unclassified (derived from Crenarchaeota)*	*Unclassified (derived from Crenarchaeota)*	*Unclassified (derived from Crenarchaeota)*	*Candidatus Nitrosocaldus*	8.7%	0.0%	0.0%	13.0%
Euryarchaeota	*Methanobacteria*	*Methanobacteriales*	*Methanobacteriaceae*	*Methanobacterium*	8.0%	13.5%	7.4%	4.1%
Euryarchaeota	*Methanobacteria*	*Methanobacteriales*	*Methanobacteriaceae*	*Methanobrevibacter*	5.6%	0.3%	1.5%	4.0%
Euryarchaeota	*Methanomicrobia*	*Methanomicrobiales*	*Unclassified (derived from Methanomicrobiales)*	*Methanolinea*	2.5%	0.3%	1.6%	0.6%
Euryarchaeota	*Methanomicrobia*	*Methanomicrobiales*	*Methanomicrobiaceae*	*Methanoculleus*	1.3%	0.0%	0.0%	0.9%
Euryarchaeota	*Methanomicrobia*	*Methanomicrobiales*	*Methanocorpusculaceae*	*Methanocorpusculum*	0.5%	0.1%	0.6%	1.4%
Euryarchaeota	*Methanomicrobia*	*Methanocellales*	*Methanocellaceae*	*Methanocella*	0.3%	0.0%	0.1%	0.2%
Euryarchaeota	*Methanomicrobia*	*Methanomicrobiales*	*Unclassified (derived from Methanomicrobiales)*	*Methanosphaerula*	0.2%	1.0%	0.2%	0.0%
Euryarchaeota	*Methanomicrobia*	*Methanomicrobiales*	*Methanospirillaceae*	*Methanospirillum*	0.2%	1.0%	0.5%	2.0%
Crenarchaeota	*Thermoprotei*	*Desulfurococcales*	*Desulfurococcaceae*	*Ignicoccus*	0.2%	-	0.0%	0.8%
Euryarchaeota	*Methanomicrobia*	*Methanomicrobiales*	*Unclassified (derived from Methanomicrobiales)*	*Methanoregula*	0.1%	0.2%	0.0%	0.1%
Thaumarchaeota	*Unclassified (derived from Thaumarchaeota)*	*Unclassified (derived from Thaumarchaeota)*	*Unclassified (derived from Thaumarchaeota)*	*Candidatus Nitrososphaera*	0.1%	0.2%	0.2%	0.1%
Euryarchaeota	*Methanomicrobia*	*Methanosarcinales*	*Methanosarcinaceae*	*Methanosarcina*	0.1%	0.0%	0.1%	0.2%

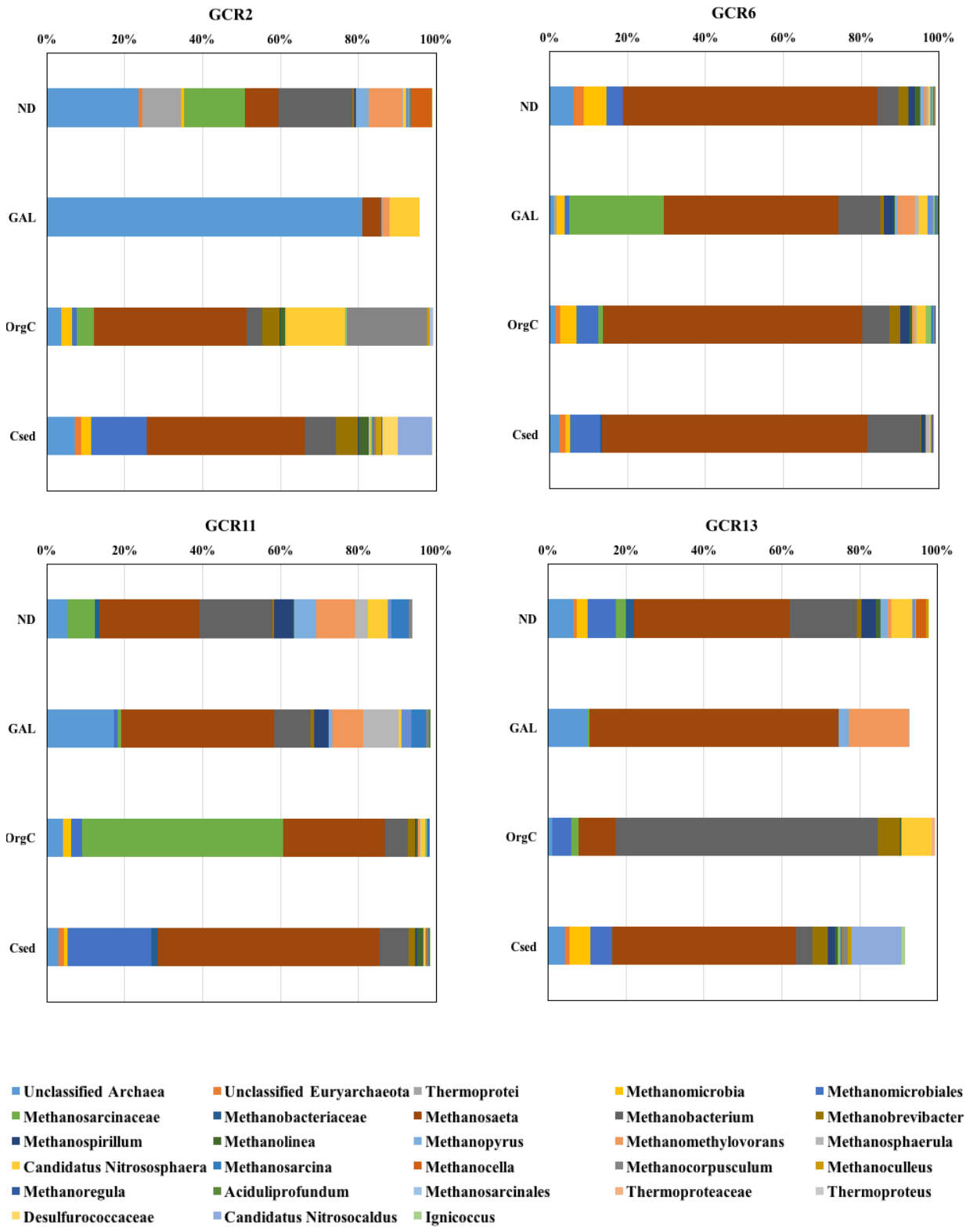

Figure 0.23 Dominant archaeal groups in the ND, GAL, OrgC and CSed layers. *Methanosaeta* dominates at most sites.

5.4.9 Trends in post-capping distribution of Archaeal community structure, sediment physical characteristics and field gas ebullition rates

Archaeal abundance was compared to field measured gas ebullition rates and sediment characteristics. *Methanosaeta* was the only *Archaea* statistically significantly correlated with field gas ebullition rates with ($R= 0.53$, $p<0.05$) in both 2012 and 2013. This provides further support for the findings that acetoclastic methanogenesis is the dominant methanogenesis pathway. Correlation analysis with sediment physical characteristics was limited to OM, OC and BC as other parameters such as sediment chemical concentration, BOD/COD and COD/TOC ratios are not available or relevant in all layers. Statistically significant ($p<0.05$) positive correlations were observed between OM and *Methanomicrobiales* ($R=0.74$), *Methanosaeta* ($R=0.73$) and *Methanopyrus* ($R=0.77$) (Table A9.31). Similar correlations were also observed for these *Archaea* and OC ($R=0.78$). BC content in the corresponding layers were significantly correlated with *Methanopyrus* ($R=0.88$, $p=0.004$). BC is known to have high affinity for hydrophobic organic contaminants such as PAHs and PCBs (Cornelissen et al. 2005, Li et al. 2009) and the previous finding of a statistically significant correlation between *Methanopyrus* and TPAHs in pre-capping sediments is consistent with the BC data here.

In the New Deposit layer, *Methanosaeta* was the most dominant genera with abundance ranging between 8 – 65% among the four sites. The lowest abundance of 8% was observed at the low gas producing site GCR2 and the highest abundance at GCR6, which had the highest post-capping gas ebullition rates (Table 5.9). Similar to pre-capping findings, *Methanobacterium* was the second dominant *Archaea* in the ND layers with abundances in the range of 5.4 – 19%. It is interesting to note that GCR6 has a very high *Methanosaeta* abundance of 65% and also one of the lowest *Methanobacterium* abundance of 5.4%, signifying the importance of acetoclastic

pathway in the ND layer. The distribution of *Archaea* at GCR2 demonstrates that this sites is more diverse than other sites, and is composed primarily of *Methanosarcinaceae* (25%) that utilize a wide range of methyl compounds including acetate. The family *Methanosarcinaceae* has eight genera including *Methanomethylovorans*, which represented 9% of the sequences at GCR2. The site was also characterized by higher abundance of *unclassified Archaea* (24%), *Thermoprotei* (10%) and the hydrogenotroph *Methanocella* (5.5%). The class *Thermoprotei* is mainly composed of thermophilic *Archaea* that are typically found in extreme environments but have also been reported in non-extreme conditions like freshwater sediments (Graças et al. 2011). Organisms in *Thermoprotei* are primarily acidophilic-sulfur reducing species that do not produce methane (Itoh and Iino 2013). The low gas production at GCR2 may be attributed to the lower abundance of *Methanosaeta* and higher diversity of other methanogenic *Archaea* that use methylated compounds for gas production. In contrast, GCR6 was dominated by the obligate acetoclast *Methanosaeta* (65%) with a lower abundance of hydrogenotrophic methanogens *Methanomicrobiales* (4%) and *Methanobacteriales* (8%). *Unclassified Archaea* and *Methanomicrobia* accounted for 6% each. At GCR11, the distribution was more balanced between the obligate acetoclasts (*Methanosaeta,* 26%), hydrogenotrophs (*Methanobacterium*-8.7%, *Methanospirillum*-4.9% and *Methanopyrus*-5.8%) and C1-methanogens (*Methanosarcinaceae*, 22%) with *unclassified Archaea* accounting for 5%. The co-existence of methanogenic *Archaea* with multiple different pathways could be attributed to the comparatively lower gas production rates observed at GCR11. The different precursors required for methane synthesis by each group may lead to more substrate competition with other diverse groups of bacteria effective lowering methanogenesis in the ND layer. Methanogenesis at GCR13 was primarily dominated by acetoclasts (*Methanosaeta*-40%) and hydrogenotrophs

(*Methanobacterium*-17.4%, *Methanomicrobiales* – 7% and *Methanospirillum* – 3.7%) with 6% *unclassified Archaea*. The higher abundance of *Methanosaeta* at GCR13 corresponded with higher G_{ebu} of 22 and 72 mmol/m^2/d in 2012 and 2013, respectively, compared to 7 and 48 mmol/m^2/d for GCR11.

The GAL at all sites had lower archaeal diversity and sequence counts compared to other layers with the composition of archaeal groups varying with site. The archaeal structure at GCR2-GAL was completely different from other sites, primarily composed of unclassified *Archaea* (81%) and a small fraction of *Methanosaeta* (4.7%) and *Methanomethylovorans* (2%). At GCR6, 11 and 13 *Methanosaeta* was the most abundant group, representing 45%, 39% and 64%, of the total respectively. C1-methylotrophic methanogens that include *Methanosarcinaceae*, *Methanomethylovorans* and *Methanosarcina* had higher abundance at GCR6 (29%) compared to GCR11 and 13. In contrast, hydrogenotrophs exhibited higher abundance at GCR11 (23%) and GCR6 (13%) but were essentially absent at GCR13 except for *Methanopyrus* representing 2.5% of sequences. The higher OM content in the GAL layer at GCR11 may have stimulated the increased abundance of hydrogenotrophs at this site.

The proportion of hydrogenotrophs, acetoclasts and C1-methylotrophic methanogens in the OrgC layer varied greatly by site. Hydrogenotrophs were the most abundant methanogenic *Archaea* at GCR13, with *Methanobacterium* and *Methanobrevibacter* accounting for 73% of sequences while Methanosaeta represented only 9.5%. In contrast, *Methanosaeta* (66.7%) was the most abundant group at GCR6, with hydrogenotrophs and C1-methylotrophic methanogens representing only 12.6% and 2.3%, respectively. Similarly, acetoclastic *Methanosaeta* was most abundant at GCR2 (39.5%) followed by hydrogenotrophs (29%), primarily *Methanocorpusculum*, and C1-methylotrophic methanogens (4.4%). GCR11 had a higher

abundance of C1-methylotrophic methanogens primarily *Methanosarcinaceae* (52.5%). The site also had significant numbers of acetoclastic *Methanosaeta* (26.4%) and lower abundance of hydrogenotrophs (8% of the sequences). In summary, C1-methylotrophic and hydrogenotrophic methanogenesis dominated at sites GCR11 and 13, respectively, whereas GCR6 was dominated by acetoclasts and GCR2 had a more diverse methanogenic metabolic capability.

Total sequence counts in CSed layers were similar to those observed in the ND layers. Acetoclastic methanogenesis was the predominant gas production pathway at all sites, (similar to pre-capping findings and in the ND layer). *Archaea* from the methylotrophic methanogen group were effectively absent at all sites with *Methanosarcina* representing <1% at all sites and *Methanomethylovorans* completely absent (Table 5.12). GCR6 had the highest abundance of *Methanosaeta* (68.2% of sequences) while hydrogenotrophs *Methanobacterium* and *Methanomicrobiales* accounted for 13.5% and 7.7% respectively. At GCR11, *Methanosaeta* accounted for 57.1% of the total sequences and hydrogenotrophs were primarily composed of *Methanobacterium* (7.4%) and *Methanomicrobiales* (21.7%). GCR2 and 13 had a similar distribution of *Archaea* with *Methanosaeta* representing for 40.7% and 47.2% respectively and hydrogenotrophs accounting for 31.4% and 17.1%, respectively. The hydrogenotrophs were primarily composed of *Methanobacterium*, *Methanobrevibacter* and *Methanomicrobiales* spp.

Similar to pre-capping conditions, acetoclastic methanogenesis was the dominant pathway at all sites and high gas producing sites having higher abundances of *Methanosaeta* compared to *Methanobacterium*. Site GCR 6 had elevated abundance of *Methanosaeta* and *Methanobacterium* throughout the core, which is consistent with the extremely high field gas production rates. GCR 11 and 13 had higher abundances of *Methanosaeta* and *Methanobacterium* in the ND layer, whereas *Methanosaeta* dominated the CSed layer in these

sites. GCR2 had the lowest gas production and lowest abundances of methanogenic *Archaea* compared to other sites, even though OC and OM content in GCR2 were similar to other sites. This diverse archaeal structure and low sequence counts in the ND and CSed layer suggests inhibition of acetoclastic methanogenesis and development of a more diverse population of *Archaea* and *Bacteria* at GCR2, possibly due to competition for acetate and other methanogenic precursors. For example, *Methanosaeta* abundance in the CSed layer (40% of the sequences) was only 13,000. This is compared to 43,000, 30,000 and 73,000 at sites GCR 6, 11 and 13, respectively.

Phylogenetic analysis of post-capping sediment core DNA extracts also revealed the greater prevalence of AOA compared to pre-capping levels. This suggests greater nitrification of ammonia in the anaerobic zone post-capping. Only sites with abundance greater than 1% are mentioned here although all sections in each site exhibited presence of AOA. In ND layer, *Candidatus Nitrososphaera* abundance was observed at 5.1% and 5.3% for sites GCR11 and 13. Elevated abundances of *Candidatus Nitrososphaera* (up to 15% of total *Archaea*) was observed in the OrgC layer for sites GCR2, 6, 11 and 13. These were the highest levels observed among all layers. Similarly, the GAL layer exhibited 7.7% and 2.5% abundance in *Candidatus Nitrososphaera* for sites GCR2 and 6 respectively and *Candidatus Nitrosocaldus* (another genera of AOA) were present in high amounts (9 – 13% of total *Archaea*) in the CSed layer at sites GCR 2 and 13. Previous research has shown that Ammonia Oxidizing Bacteria (AOB) dominate in systems with direct inorganic ammonia input (Jia and Conrad 2009, Pratscher, Dumont, and Conrad 2011), whereas AOA are more prevalent in environments where ammonification of organic matter is the primary source of ammonia (Di et al. 2010, Offre, Prosser, and Nicol 2009, Stahl and de la Torre 2012). The presence of AOA in increasing abundance with sediment depth

is consistent with previous findings of the affinity for organic sources of ammonia. Given the very high TOC and OM in GCR sediment, we would expect nitrate to be rapidly consumed near the SWI. Slow rates of ammonification of OM would lead to AOA outcompeting AOB in low ammonia environments (Stahl and de la Torre 2012). These findings further highlight the significance of this recently discovered AOA nitrification pathway in aquatic sediment, as nearly all previous studies have found them in relatively clean environments such as the ocean and Lake Superior (Bollmann, Bullerjahn, and McKay 2014).

5.5 Conclusion

The phylogenetic analysis of methanogenic *Archaea* provided insights into the distribution of methanogens at each site and serves as a tool to evaluate variations in field gas production rates. Acetoclastic *Methanosaeta* representing around 40% of the sequences and were numerically dominant in pre-capping sediment. GCR6 (one of the highest gas-producing sites), had significantly elevated levels of *Methanosaeta* compared to *Methanobacterium*. Field measured gas production rates were also significantly ($p<0.05$) correlated with *Methanosaeta* abundance, suggesting that acetoclastic methanogenesis controls gas production rates in the pre-capping river sediment. The archaeal community structure exhibited a balance in the distribution of sequences of class *Methanomicrobia* and *Methanobacteria* between the two reaches, with higher abundances of *Methanobacteria* in Reach 1 compared to Reach 2. *Methanobacteria* is primarily composed of hydrogenotrophic methanogens and consequently the proportion of gas produced by this pathway is expected to be higher in Reach 1 compared to Reach 2. Correlation analysis also revealed a greater abundance of *Methanobrevibacter* in sites with recalcitrant and low OM levels, whereas *Methanosaeta* and *Methanosarcina* exhibited higher abundance in sediment with more labile OM.

Following capping, the comparative distribution of archaeal genera varied from site to site among the four layers, suggesting that a variety of environmental and geochemical factors influenced their spatial distribution. In terms of field gas production rates, *Methanosaeta* abundance was correlated with the observed variability in gas production in monitoring years 2012 and 2013. Gas production rates were not significantly correlated with *Methanosaeta* for 2014 monitoring year in which gas production rates declined considerably. Gas production in the ND, GAL and the OrgC layer likely involved the three major pathways of hydrogenotrophic, methylotrophic and acetoclastic methanogenesis due to the presence of diverse methanogenic *Archaea* pertaining to each metabolic pathway. *Methanosaeta* abundance increased with sediment depth for all sites except for GCR6 where *Methanosaeta* was dominant throughout the core, explaining the consistently high gas production rates measured at this site. In contrast, hydrogenotrophic *Methanobacterium* were more abundant in the surficial sediment compared to deeper sections. This is suggestive of a preference for hydrogenotrophic methanogenic pathway with the increase in lability of the organic carbon in the ND layer. It was not clear why GCR6 had elevated *Methanosaeta* abundance in the GAL and OrgC layer although the OM and OC content were comparable to other sites. GCR6 also exhibited very high levels of *Methanosaeta* in pre-capping sediment, suggesting that some other parameter or biogeochemical features of site GC6 not captured in this study influences methanogenic *Archaea* distribution.

Microbial community structure analysis provided conclusive evidence that the contaminated sediment zone has methanogenic *Archaea* at levels higher or comparable to that observed in the New Deposit layer (ND). This demonstrates that the CSed layer is still biologically active with regards to methanogenesis. The increasing *Methanosaeta* abundance with sediment depth is suggestive of higher gas production in deeper sediment compared to the ND layer. The archaeal

distribution in the CSed layers were similar to those observed in pre-capping surficial sediment (primarily dominated by acetoclasts and hydrogenotrophs) with negligible presence of C1-methylotrophic methanogens. This analysis along with the findings from the incubation study discussed in Chapter 3 provide multiple lines of evidence suggesting that the CSed zone is capable of continued gas production.

Comparative analysis of pre and post-capping archaeal distribution in surficial sediment showed that the labile nature of fresh OM in the ND layer resulted in a more diverse archaeal microbiome, particularly at site GCR2 with 24% unclassified *Archaea*. The abundance of methylotrophic methanogens increased significantly in the surficial zone especially at sites GCR2 and 13. The increased lability of the OM resulted in a positive shift in relative abundance of hydrogenotrophic methanogens compared to acetoclastic *Methanosaeta*. Thus capping resulted in a more diversified methanogenic ecosystem in the GCR surficial sediment.

The analysis also revealed the presence of AOA that included the genera *Candidatus Nitrososphaera* and *Candidatus Nitrosocaldus*. Post-capping archaeal abundances showed increasing levels of AOA with depth. This is suggestive of ammonia synthesis in deeper sediment through either dissimilatory nitrate reduction (at sites near the HSD outfall) or ammonification of organic matter. The high prevalence of this recently discovered group in a highly polluted aquatic environment suggests that they play a more broadly important role in the nitrogen cycle, as nitrification of ammonia to nitrite is the rate-limiting step in the nitrification process.

Figure 0.24 Distribution of Archaeal community structure in post-cap GCR2 –ND layer.

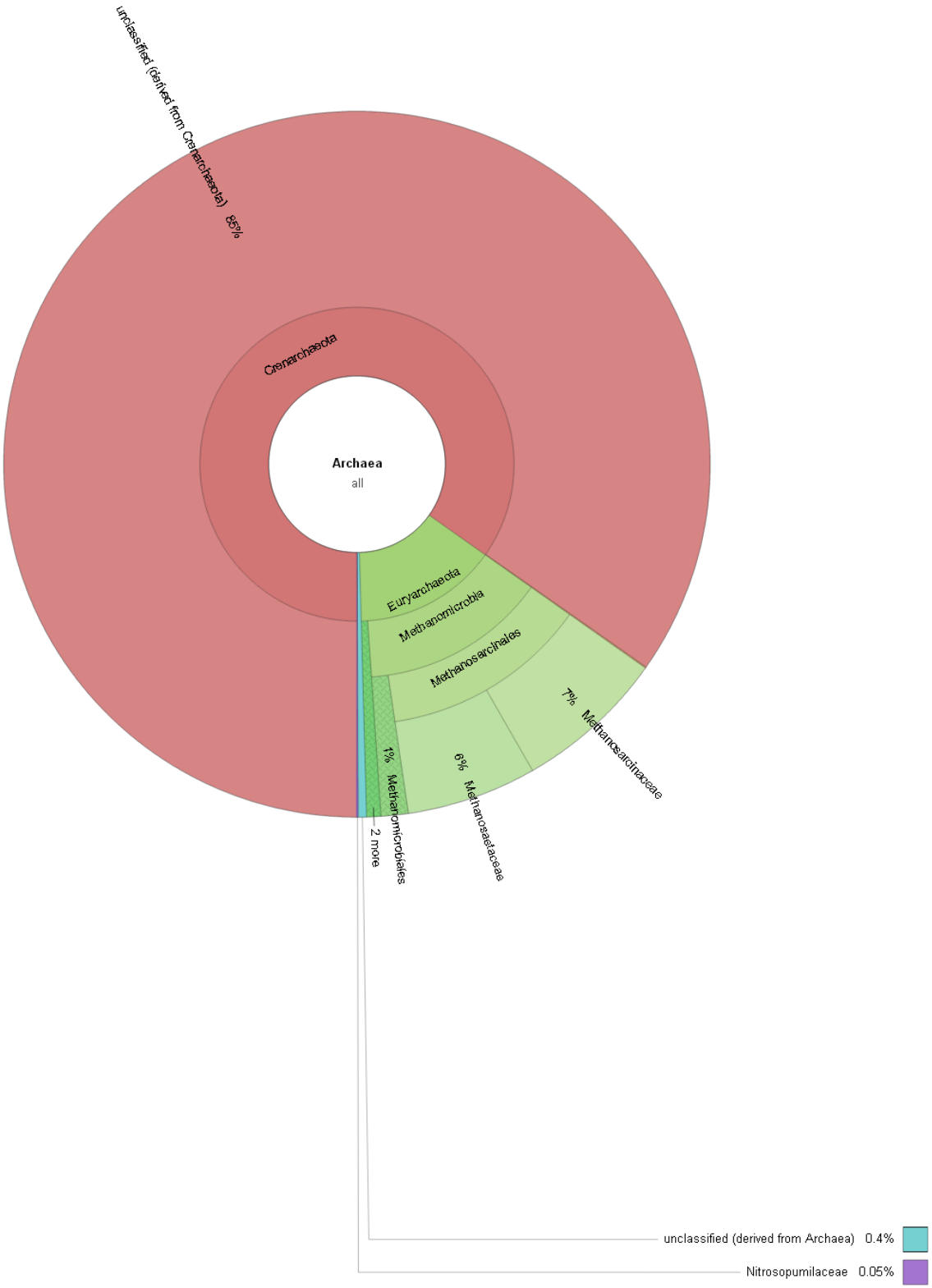

Figure 0.25 Distribution of Archaeal community structure in post-cap GCR2 -GAL layer.

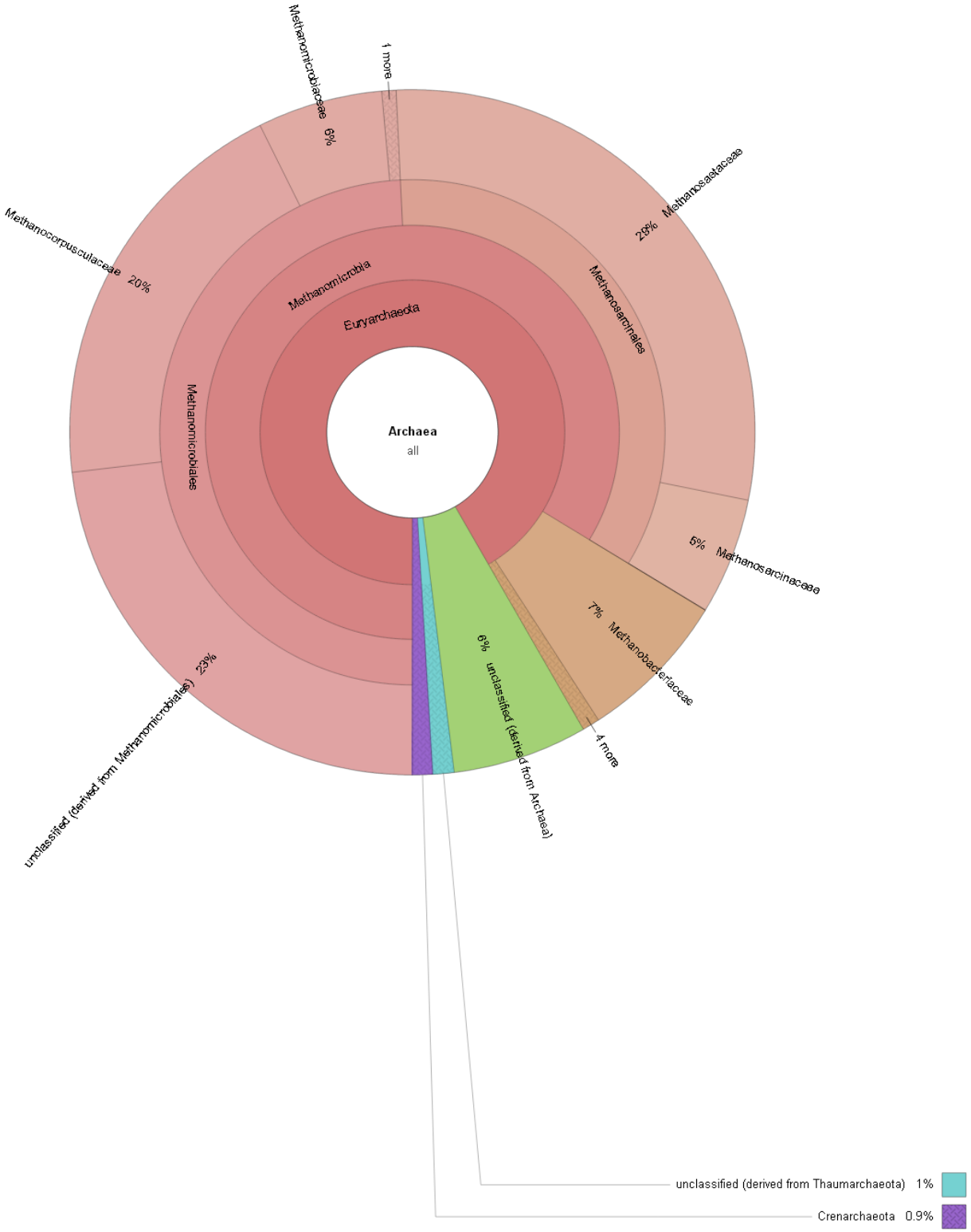

Figure 0.26 Distribution of Archaeal community structure in post-cap GCR2 -OrgC layer.

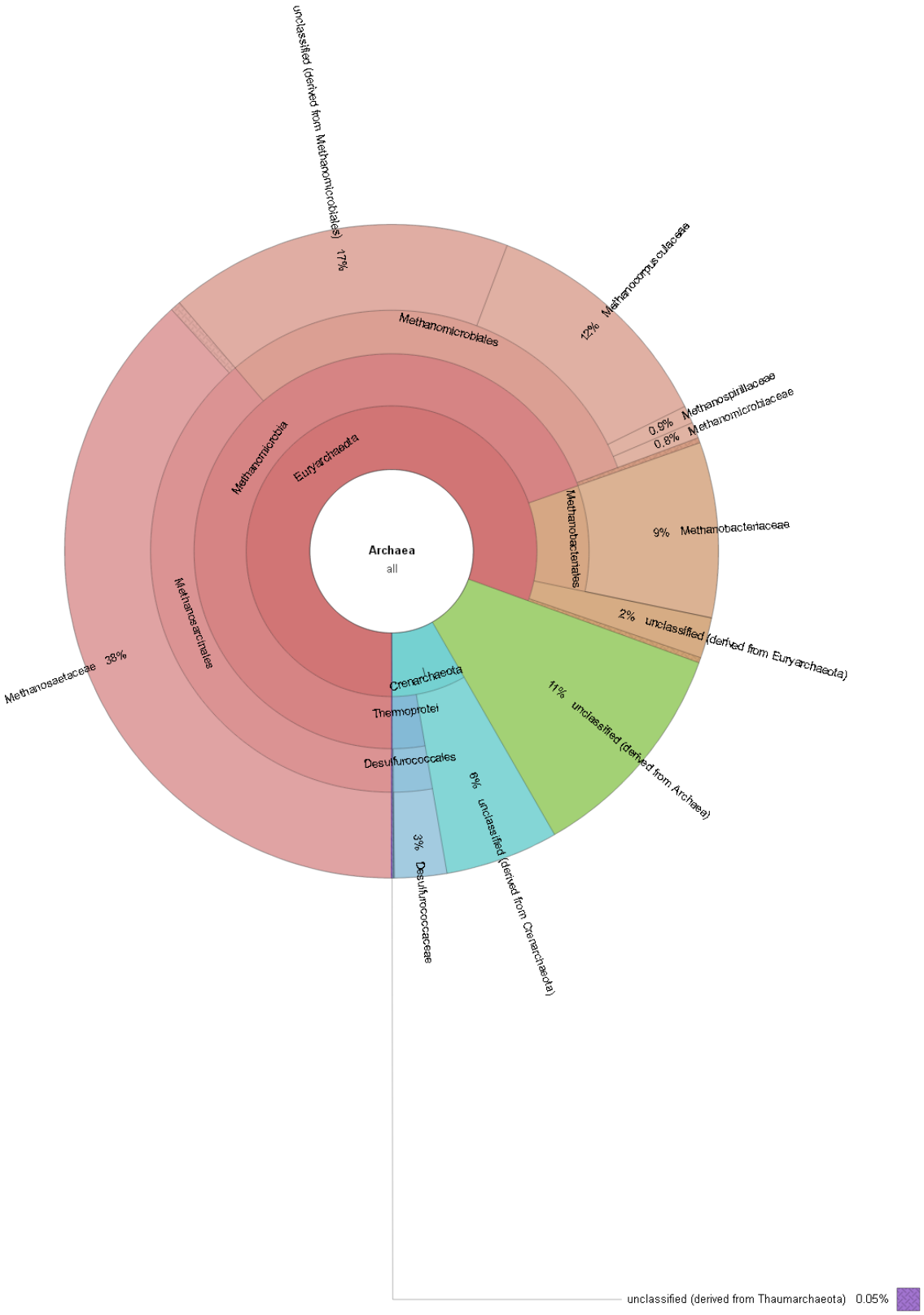

Figure 0.27 Distribution of Archaeal community structure in post-cap GCR2 -CSed layer.

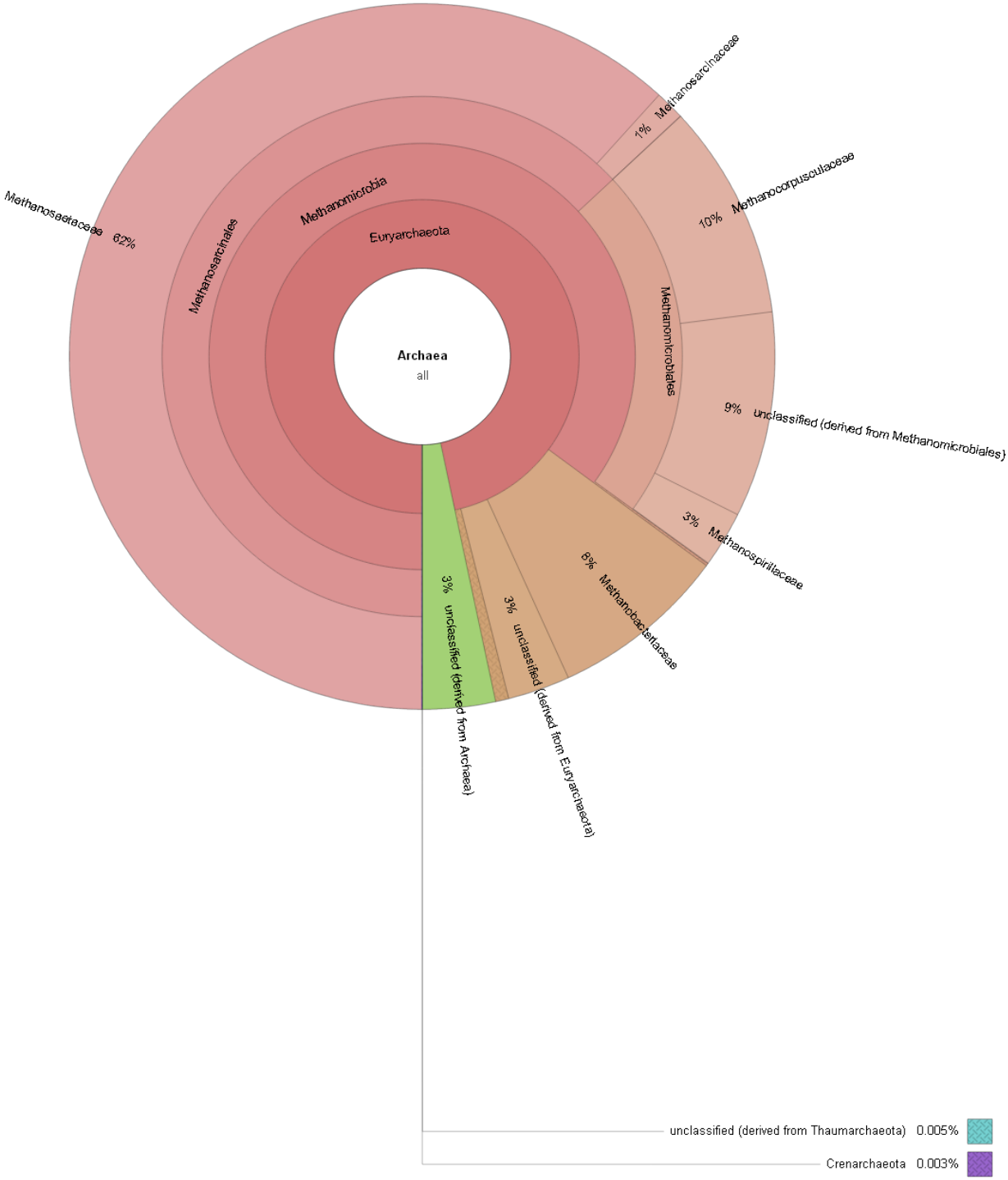

Figure 0.28 Distribution of Archaeal community structure in post-cap GCR6 -ND layer.

Figure 0.29 Distribution of Archaeal community structure in post-cap GCR6 -GAL layer.

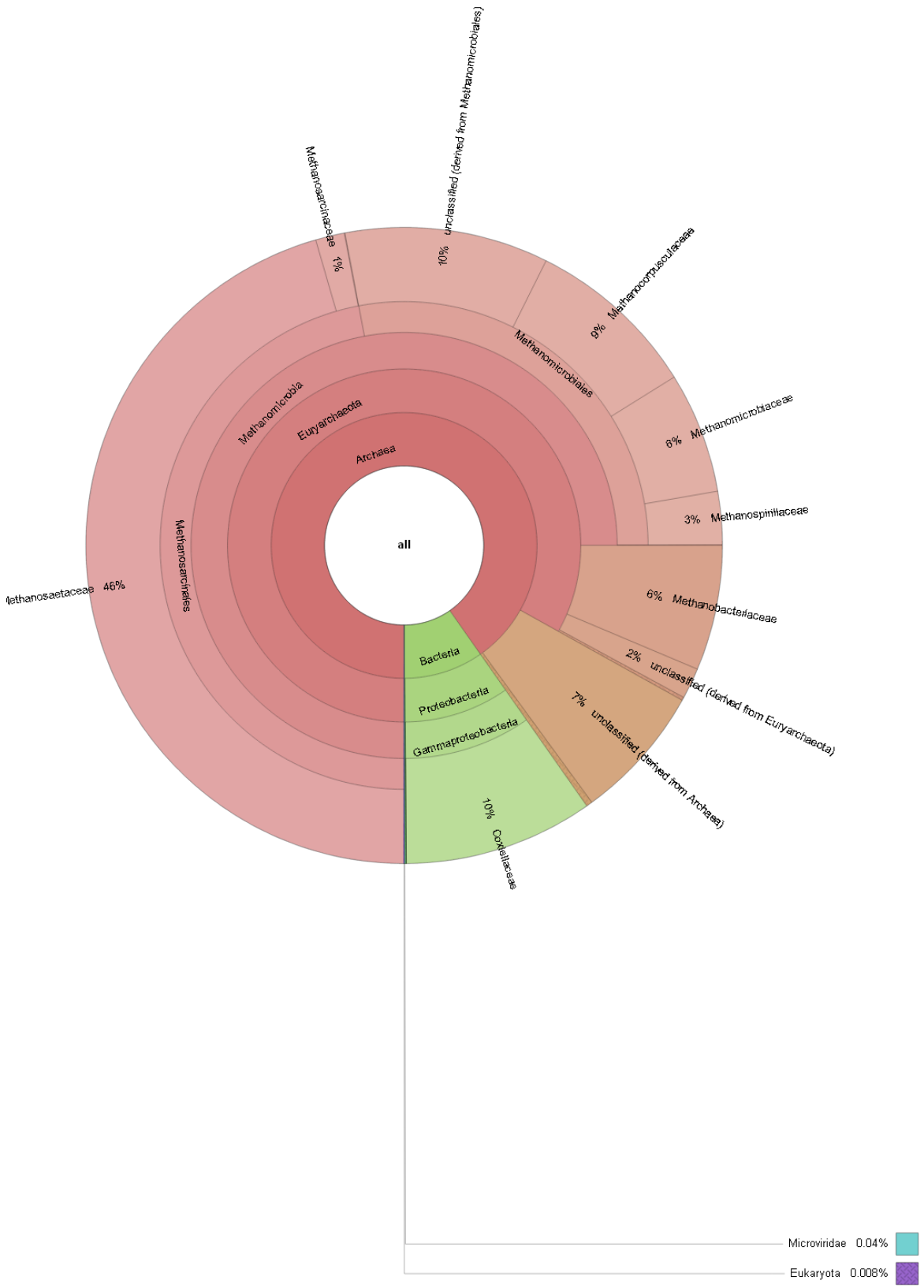

Figure 0.30 Distribution of Archaeal community structure in post-cap GCR6 -OrgC layer.

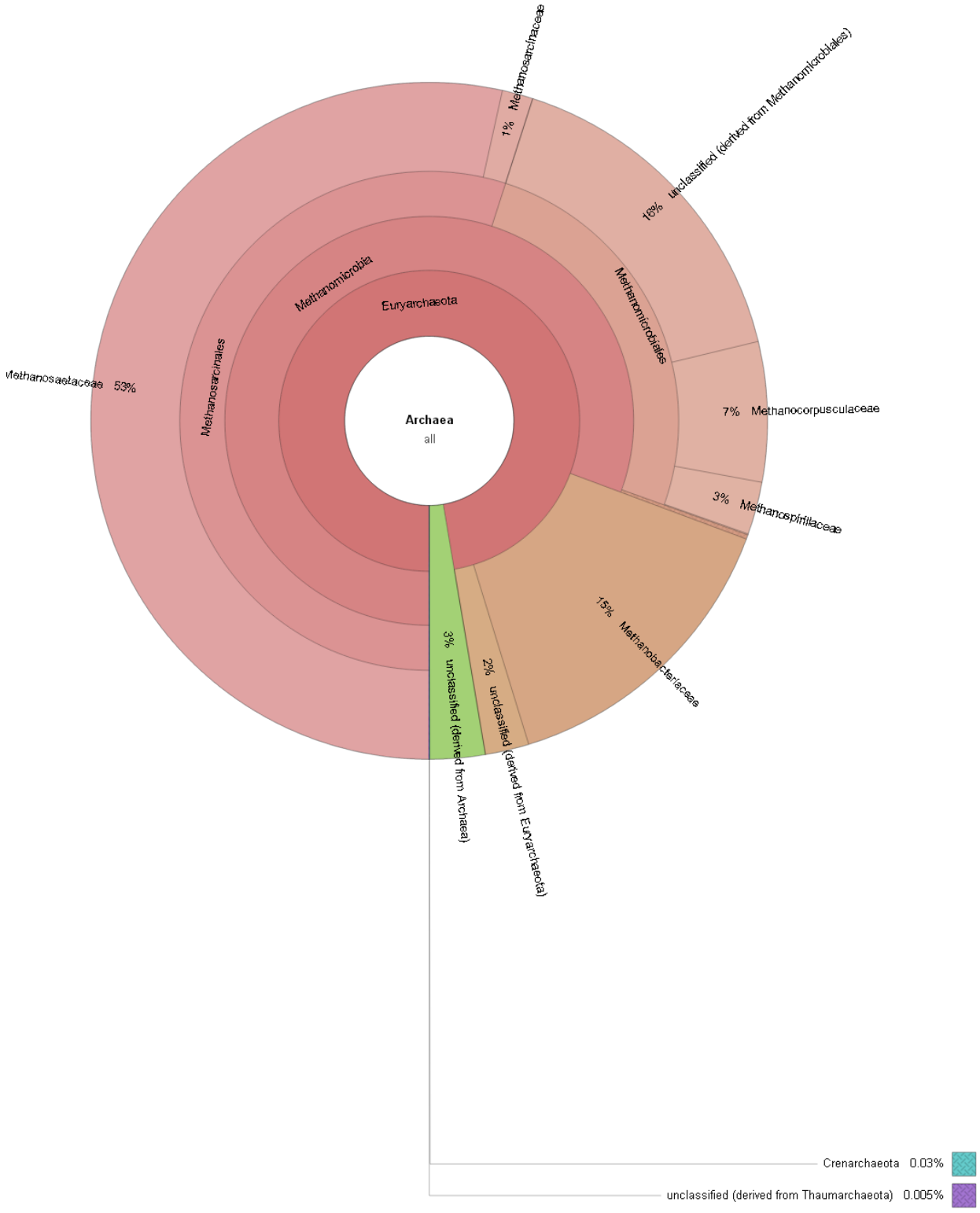

Figure 0.31 Distribution of Archaeal community structure in post-cap GCR6 -CSed layer.

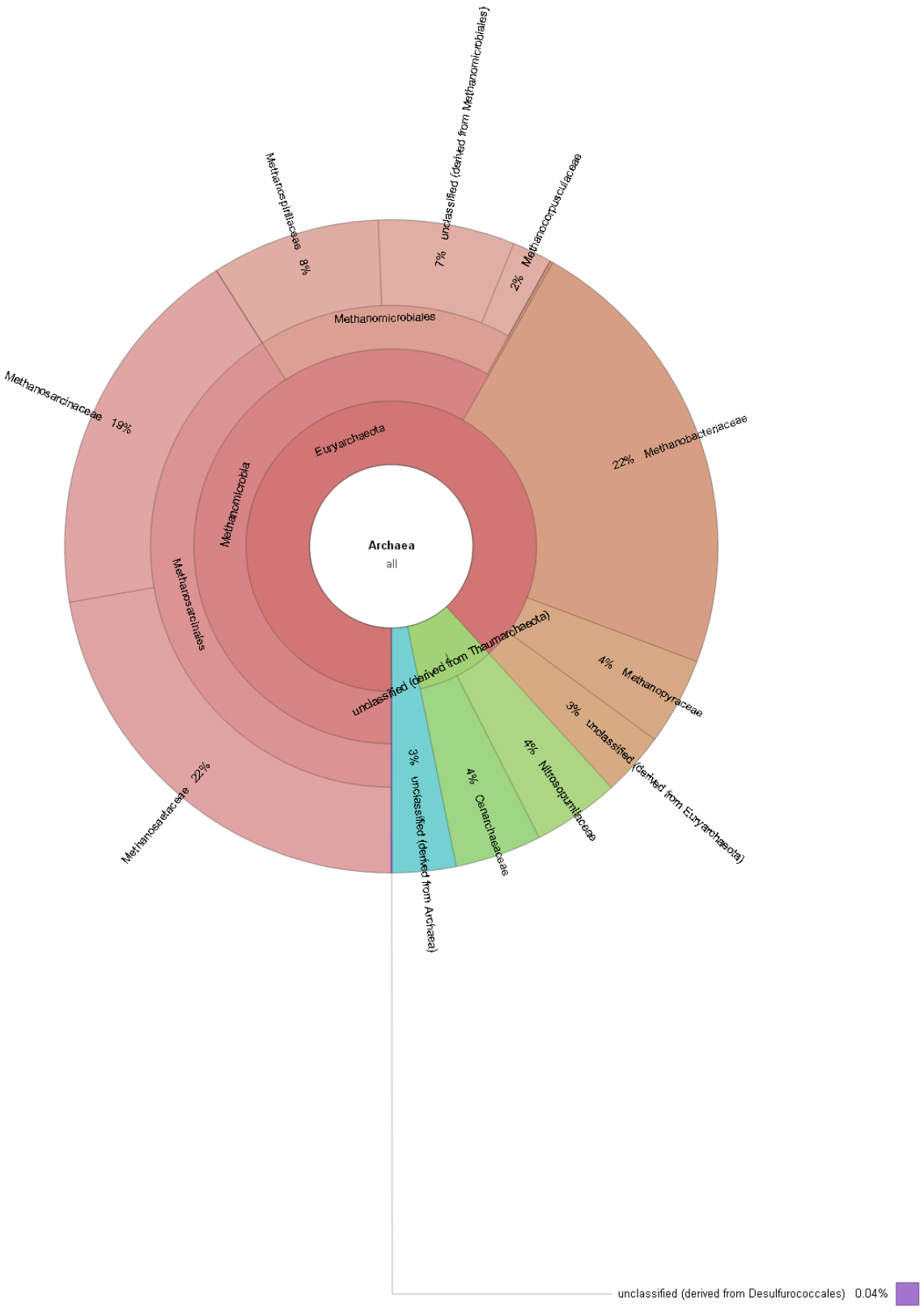

Figure 0.32 Distribution of Archaeal community structure in post-cap GCR11 -ND layer.

Figure 0.33 Distribution of Archaeal community structure in post-cap GCR11 -GAL layer.

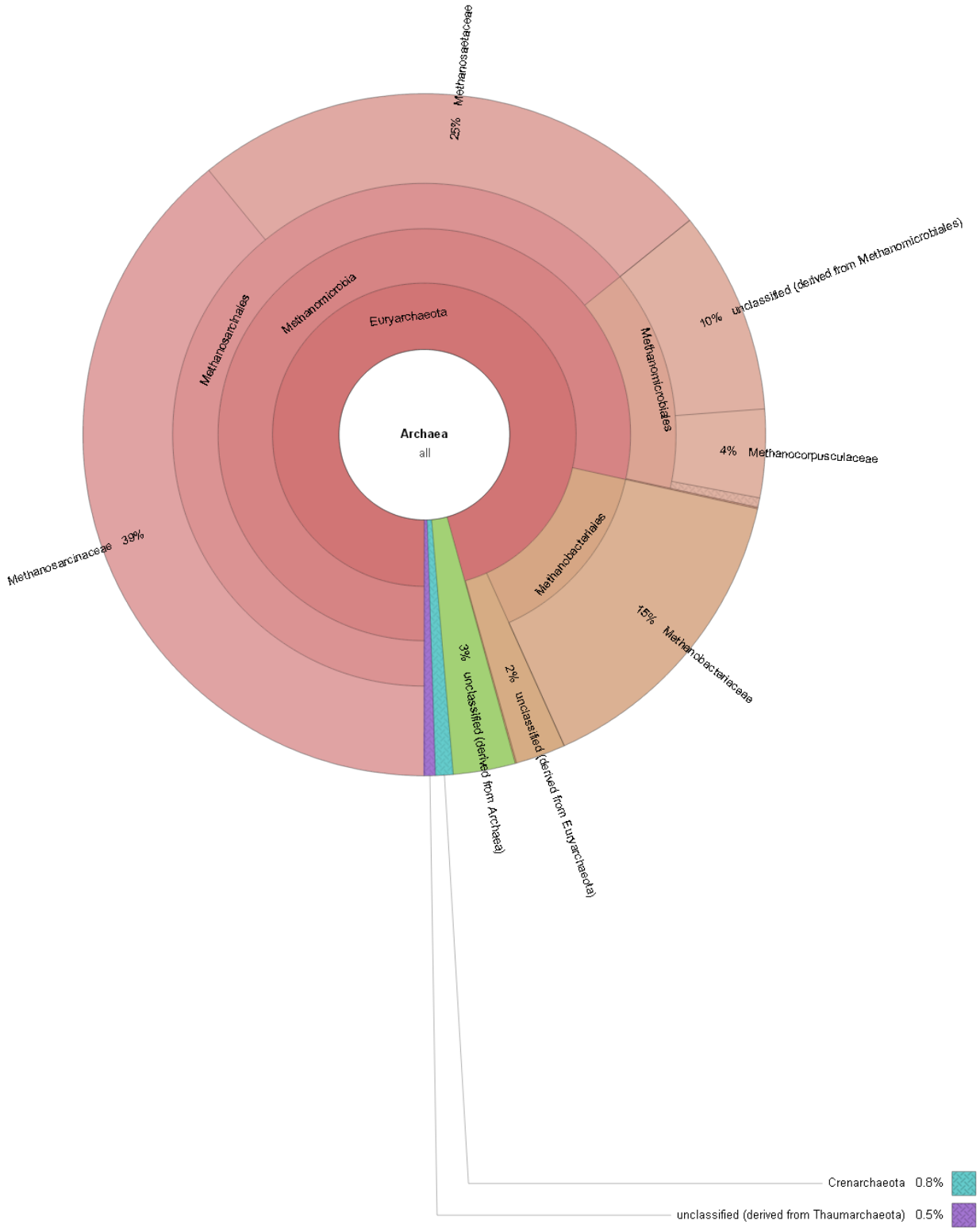

Figure 0.34 Distribution of Archaeal community structure in post-cap GCR11 -OrgC layer.

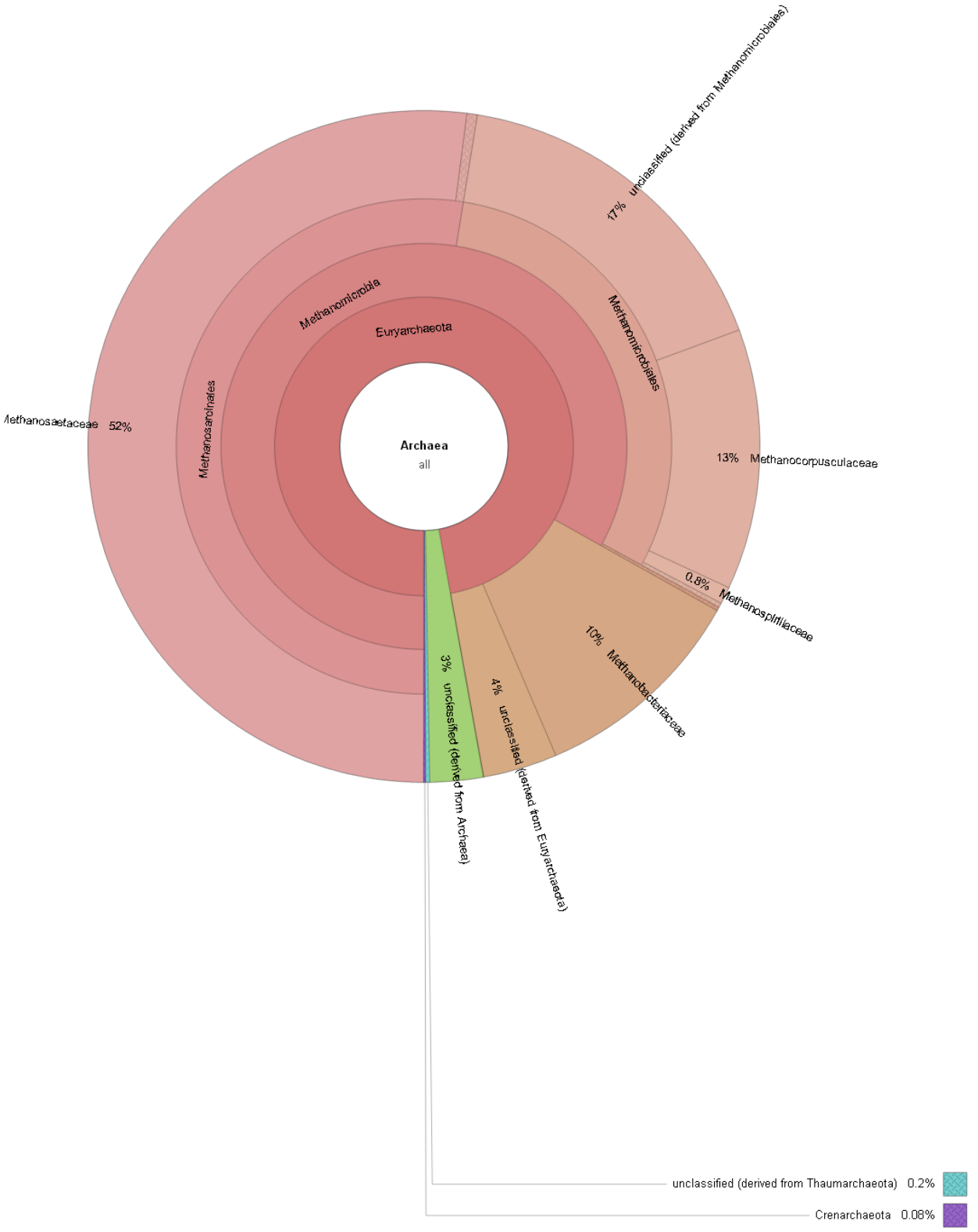

Figure 0.35 Distribution of Archaeal community structure in post-cap GCR11 -CSed layer.

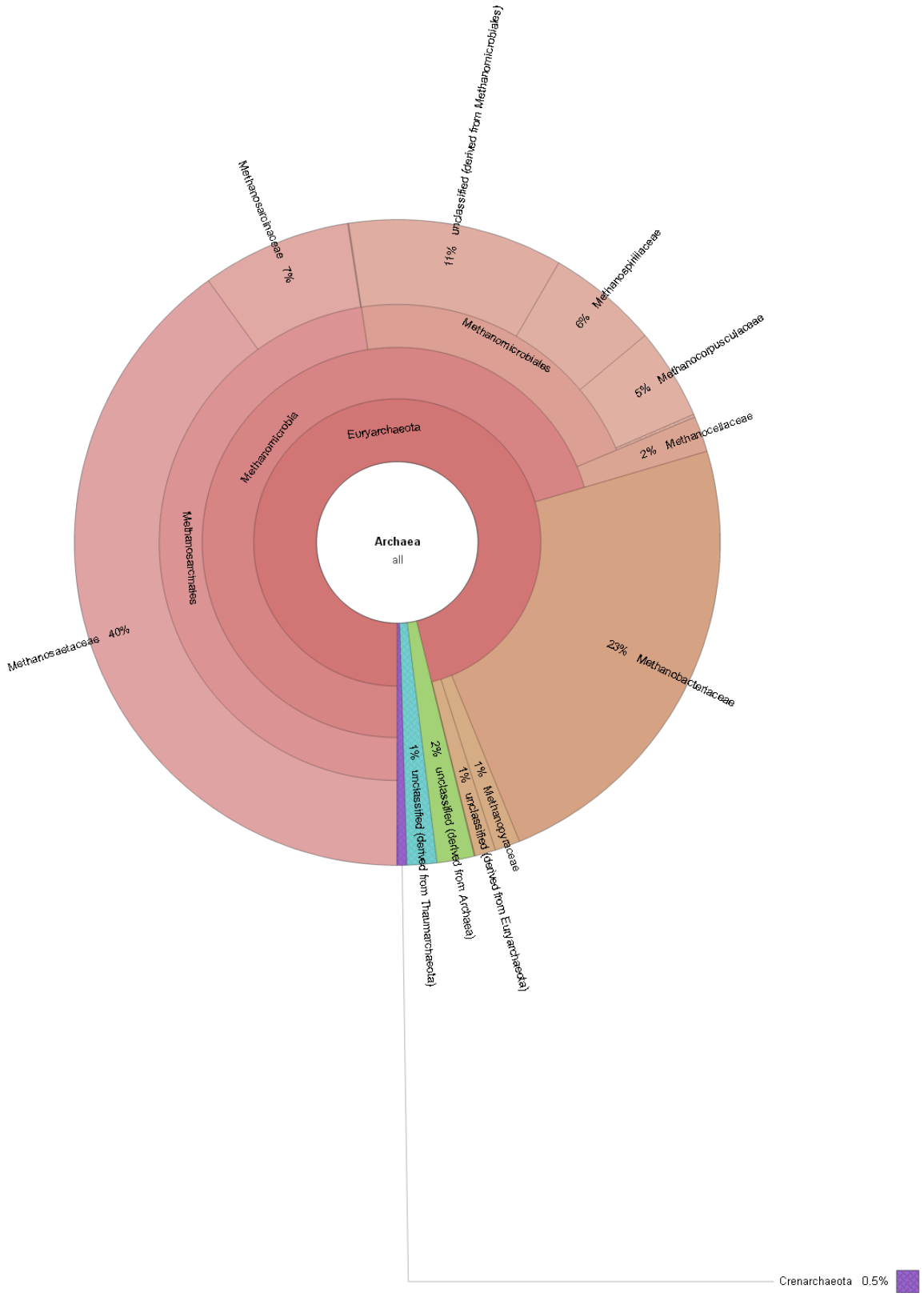

Figure 0.36 Distribution of Archaeal community structure in post-cap GCR13 -ND layer.

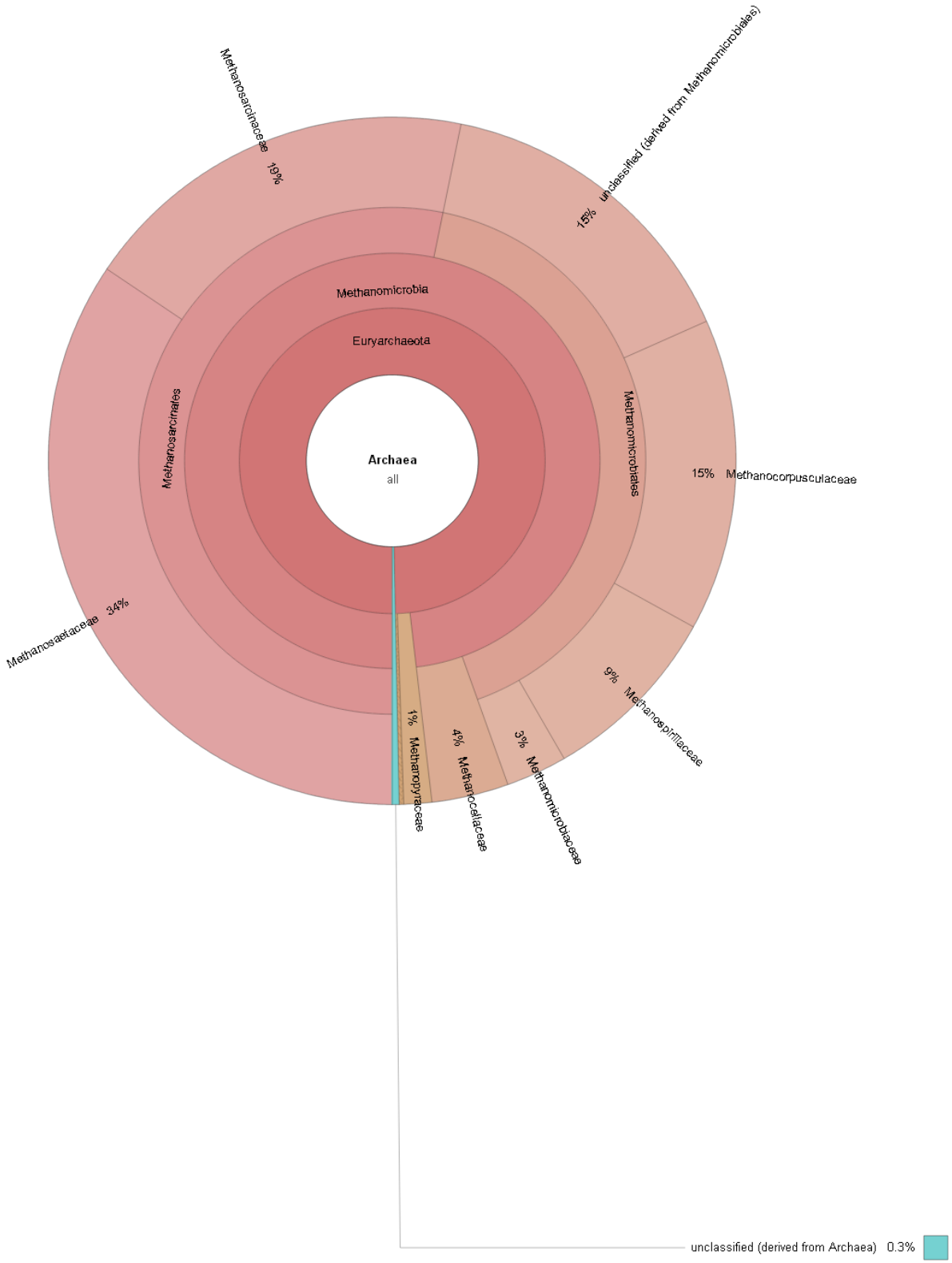

Figure 0.37 Distribution of Archaeal community structure in post-cap GCR13 -GAL layer.

Figure 0.38 Distribution of Archaeal community structure in post-cap GCR13 -OrgC layer.

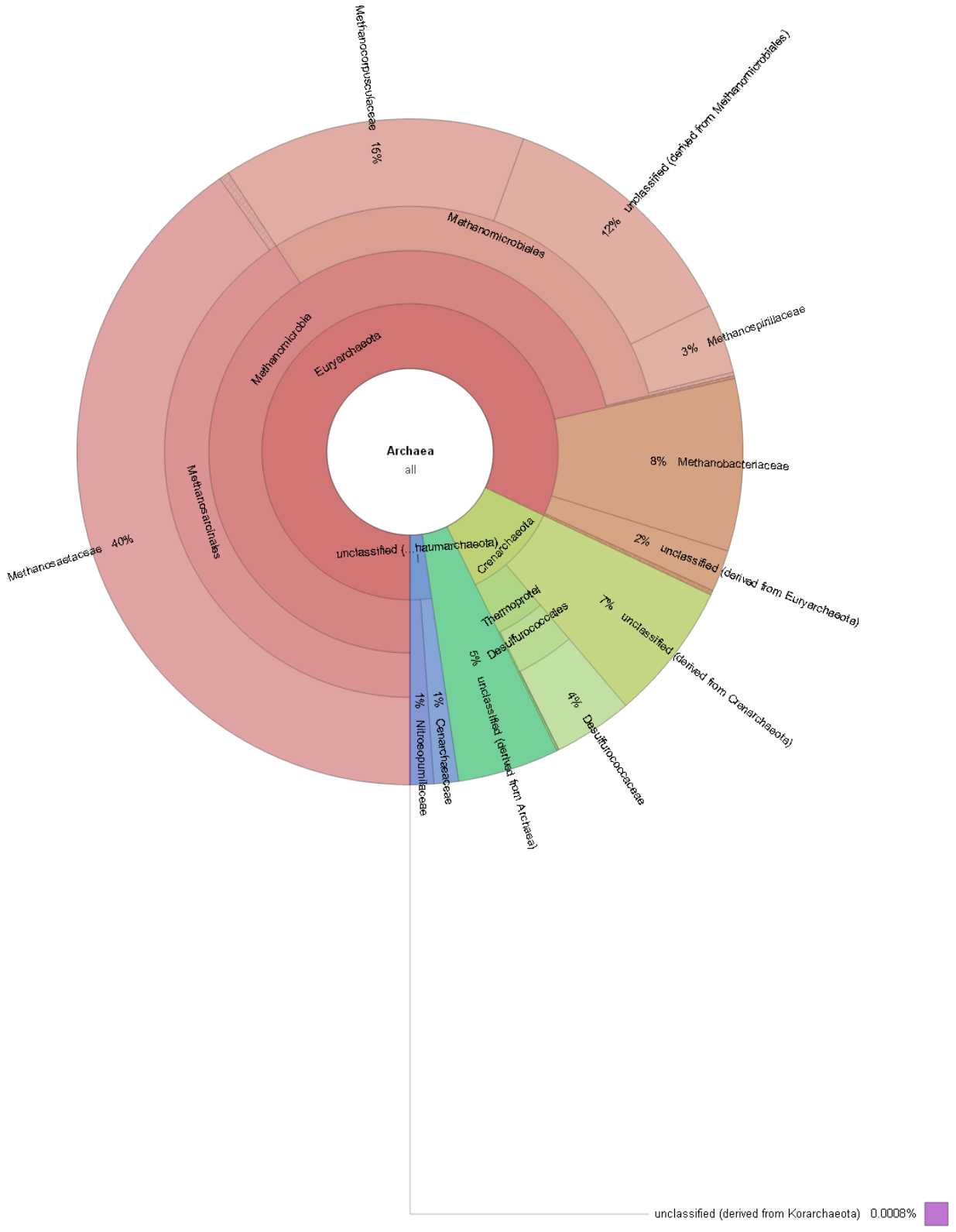

Figure 0.39 Distribution of Archaeal community structure in post-cap GCR13 –Csed layer.

CHAPTER VI GROUNDWATER SURFACE WATER EXCHANGE MODELING

6.1 Introduction

Research over the past fifty years has significantly improved our scientific understanding of the biogeochemical processes and complex fluid dynamics that exists in the hyporheic zone of interaction between surface water (SW) and ground water (GW) (Boano et al. 2014). A variety of biogeochemical processes (enhanced redox cycling of metals, nutrient transformations, and organic carbon respiration) occur in the hyporheic zone that affects the fate of dissolved constituents near the sediment-water interface (SWI) (Böhlke et al. 2009, Fuller and Harvey 2000, Haggerty et al. 2009). These processes represent an interplay between the microbial communities and the supply of important electron acceptors and donors (O_2, NO_3^-, N_2O, NH_4^+, SO_4^{2-}, CH_4) that are transported by subsurface flows (Hedin et al. 1998). For example, Fuller et al (Fuller and Harvey 2000) observed reactive trace metal uptake in the order of 52%, 27% and 36% of stream water concentration for Co, Ni and Zn, in the hyporheic zone. Nitrogen cycling in the form of denitrification and nitrification are also known to occur in the shallow subsurface, and are typically limited by the supply of dissolved organic carbon (DOC) (Hedin et al. 1998). The hyporheic zone can also act as a source and sink of DOC to the benthos, (Findlay et al. 1993, Fiebig and Lock 1991) by immobilizing DOC as it passes through the sediment or by generating DOC from the biodegradation of organic matter in the hyporheic zone (Hornberger, Bencala, and McKnight 1994, Schindler and Krabbenhoft 1998). Thus, hyporheic flows can play an important role in regulation of nitrogen cycle in the environment. In the case of larger scale hyporheic flows, groundwater discharge to streams can transport pollutants to surface water and conversely,

polluted surface water and its interaction with contaminated sediments can transport contaminants to underlying aquifers in losing streams.

The interconnected nature of SW-GW systems has led to regulations such as the European Union Water Framework Directive (WFD, 2000) that mandate a more integrated management of the hydrologic systems. Furthermore, human activity, global warming and related climatic changes can alter the nature of interaction between groundwater and SW systems. For example, land use changes in a watershed such as rapid urbanization, can lead to increase in temperature of surface water runoff in response to increase in the area of hot pavements and impact rate dependent biogeochemical processes, fish health and ecological processes (Nelson and Palmer 2007, Wang and Kanehl 2003). Thus, for sustainable management of water resources it is essential to effectively monitor the nature of interaction between SW-GW systems that may vary over time.

Factors that influence the magnitude and scale of hyporheic exchange include: magnitude and spatial variability of hydraulic conductivity, hydraulic gradient and presence of streambed features such as dunes, sandbars and riffles (Bhaskar, Harvey, and Henry 2012, Arrigoni et al. 2008). Streambed features can influence the hydrostatic and hydrodynamic forces acting at the (SWI) and can induce hyporheic flows at spatial scales in the range of the stream depth. Hydrostatic forces are induced by variations in streambed topography such as large boulders, riffles, steps and cascades leading to spatial variability in hyporheic exchange whereas hydrodynamic forces are driven by changes in momentum transfer to the streambed and increase with stream velocity (Elliot and Brooks 1997). Hydrodynamic forces driven hyporheic flows occur at spatial scales less than the stream depth and are associated with smaller bed form variations such as sand riffles and dunes, cobbles and grain clusters (Boano et al. 2014). Hyporheic exchanges are typically interlinked with larger scale groundwater fluxes due to the

shared response of near and far field hydraulic gradients and this may suppress the spatial extent of the hyporheic zone (Bhaskar, Harvey, and Henry 2012). For example, groundwater discharge/recharge in a direction opposite to direction of hyporheic flow can reduce the depth of hyporheic zone and total hyporheic flow (Harvey, Wagner, and Bencala 1996, Cardenas and Wilson 2007a, Bhaskar, Harvey, and Henry 2012). Consequently, the hyporheic flux is influenced by groundwater flux and Reynolds number (as a function of stream velocity and bed form geometry) (Cardenas and Wilson 2007b). Temporal variability in hyporheic fluxes has been reported by several researchers and are primarily due to changes in hydraulic gradients induced by rain events and fluctuations in the groundwater table (Briggs et al. 2012, Hatch et al. 2006, Keery et al. 2007). Temporal variability can also be induced by changes in hydraulic properties of the sediment such as scouring and the plugging effect of fine sediments (Keery et al. 2007).

The dynamic nature of hyporheic exchanges, its significant role in biogeochemical processes and impacts due to activity makes it essential to monitor GW-SW interaction. Conventional methods for measurement of hyporheic fluxes include tracer based measurements and hydraulic based measurements using mini-piezometers, seepage meters, slug tests, incremental stream flow measurements and hydrograph separation methods (Kalbus, Reinstorf, and Schirmer 2006). Each method has its own limitations, uncertainties, assumptions and characteristic temporal and spatial scales (Hatch et al. 2006). Using heat as a natural tracer to measure hyporheic exchanges is a relatively less used technique but provides several advantages. Particularly the ability to measure the temporal variability of hyporheic fluxes (Stonestrom and Constantz 2003) and the relative simplicity in collecting streambed temperature data, makes this approach more attractive. Moreover, recent advances in sensor technology has enabled the collection of highly accurate long term streambed temperature profiles. Also, the availability of low cost sensors have

provided the ability to deploy multiple sensor arrays to effectively characterize spatial variability in hyporheic fluxes (Becker et al. 2004, Conant 2004). The fact that the thermal properties of sediment is largely independent of texture and varies over a narrow range of values (in contrast to hydraulic conductivity), lowers the uncertainty associated with flux estimates compared to the traditional methods (Stonestrom and Constantz 2003).

In the case of a capped river-bed, hyporheic flows can facilitate the transport of nutrients, metals and DOCs to the contaminated sediment zone and stimulate production of biogenic gases from partly decomposed detritus. Increase in gas ebullition rates can cause cap damage (Viana, Yin, Xhao, et al. 2007, Yuan et al. 2007, Himmelheber, Taillefert, et al. 2008, Reible et al. 2006) and reduce the design life of an active cap. Hyporheic flows are also known to regulate the streambed and water temperature which can affect the rate of biogeochemical processes and abundance of aquatic biota (Arrigoni et al. 2008, Caissie 2006). The former can increase gas production and the latter can increase benthic fluxes to the water column. River restoration efforts such dredging and installation of a multi-layer cap material can dramatically alter hydraulic properties, hydraulic gradients and bed form geometry of the restored system. A multi-layer is generally comprised of coarse to fine sand and gravel with vastly different hydraulic properties compared to naturally occurring sediment. Also, cap placement is known to cause sediment consolidation resulting in altered hydraulic conductivity and permeability in the sediment zone below the cap. Consequently, post-capping evaluation of GW-SW exchange is essential to ensure cap performance and design breakthrough times. This study aims to utilize streambed temperature profiles together with heat flux modelling to assess the direction and magnitude of hyporheic exchange in a contaminated urban river that has undergone shallow dredging and capping.

6.2 Materials and Methods

Sediment temperature was recorded at twelve sites (designated GCR 1-6 and GCR 8-13) along a 2 Km stretch of the west branch of the Grand Calumet River (WBGCR) from Columbia Ave to Indianapolis Blvd. A plan view of the study site and temperature logger locations is shown in Figure 6.1**.** Permitted discharge from the Hammond Sanitary District (HSD) wastewater treatment plant located near site GCR10 accounts for 90% of flow in the WBGCR with water levels significantly impacted by rain events. Sites GCR11-13 located upstream of the outfall are characterized by low stream velocities or stagnant water resulting in poor water quality and algal growth suppressing sun light penetration to the streambed. Stream restoration involved dredging contaminated sediment up to a depth of 60 cm followed by construction of an active cap layer with a total thickness of 45 cm. The cap design included a bottom 15 cm adsorptive layer composed of a 5:1 sand and organoclay mixture. A 30 cm thick sand/gravel-armoring layer was constructed over the adsorptive layer for protection against erosion. The armoring layer contained up to 10% or more of gravel. Stream depth varied between 0.6 – 1 m, with stream width ranging from 50 – 70 m. Sediment temperature was recorded from June to November for three consecutive post-capping years from 2012 to 2014. Temperature data were collected at 45 minute intervals with Hobo temperature data loggers (UA-002-08) installed at depths of +25 cm, 0 cm, -25 cm, -50 cm, -75 cm, -100 cm and -200 cm at six monitoring locations (GCR 2, 6, 8, 9, 11 and 13) from June to November. Temperature profiles for sites GCR1, 3, 4, 5, 10 and 12 were recorded for depths of 0 and -25 cm from late August to November. Site GCR8 was left uncapped due to the presence of an underwater oil pipeline in close proximity and thus served as a non-capped control. The temperature loggers were attached externally to a 0.64 cm hollow PVC pipe at appropriate depths using zip ties and secured using duct tape. The PVC pipes were

filled with sand and capped at both ends to provide sufficient rigidity to allow penetration through the cap and into the sediment at depths down to 2m below the SWI. The temperature logger has an operational range of -20 °C to 70 °C with a measurement accuracy of ±0.53 °C and a resolution of 0.14 °C. The logger array was installed in the streambed by manually pushing it into the sediment to the appropriate depth. The -200 cm temperature logger (intended to be representative of the groundwater temperature), was installed inside a 3.2 cm hollow PVC pipe filled with sand and sealed with end caps. Multiple holes were drilled on the PVC pipe at the logger location up to a depth of 3 cm above and below logger placement to allow for rapid equilibration of pore water temperature around the logger.

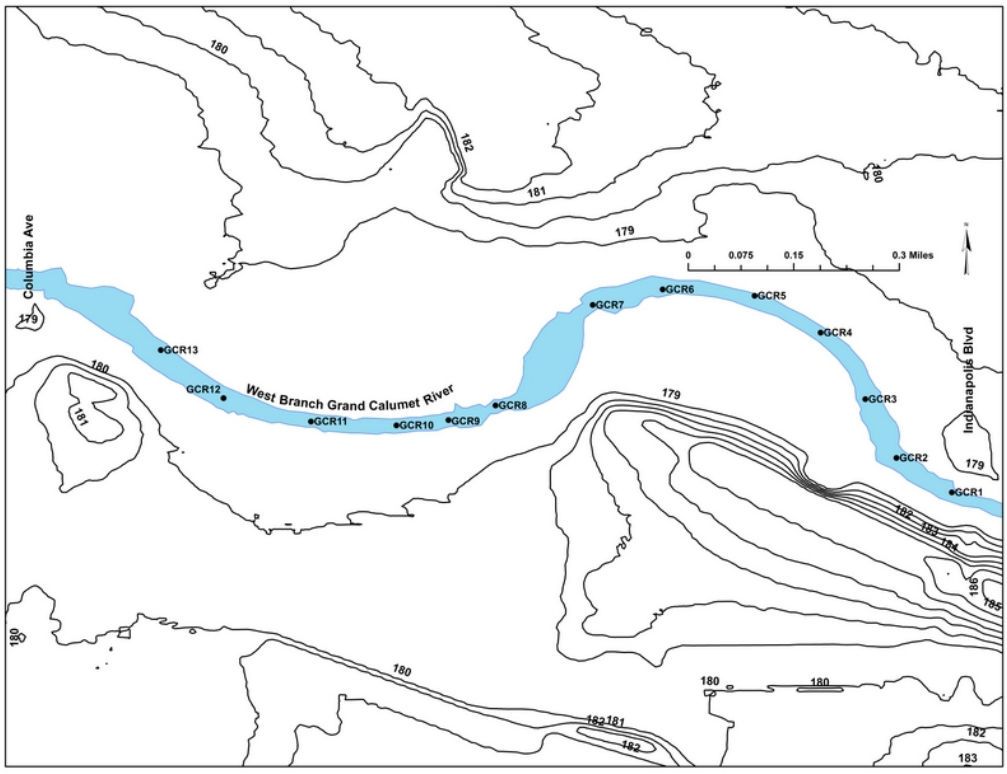

Figure 0.1 Shows the location of temperature arrays during three years of post-cap monitoring in a 2 Km stretch of West Branch Grand Calumet River (WBGCR) from Columbia Ave to Indianapolis Blvd.

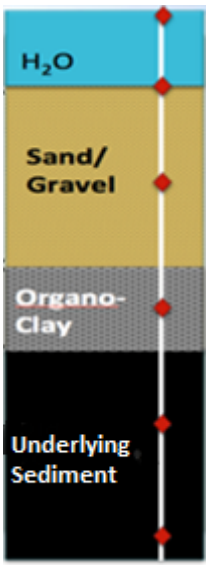

Figure 0.2 Approximate location of temperature sensors in relation to the sand-gravel armor and organoclay layers of the active cap and contaminated sediment zone shown in black.

6.3 Analytical Methods for Flux Measurement from Temperature Time Series

Heat transport in streambed occurs by three mechanisms: conduction of heat through the sediment-water matrix, advection, and hydrodynamic dispersion of water moving through the streambed. The one-dimensional conduction-advection-dispersion model for heat and fluid transport (1D-HFT) in porous media is given as follows (Stallman 1965, Bredehoeft and Papaopulos 1965, Hatch et al. 2006, Keery et al. 2007, Anderson 2005):

$$\frac{\partial T}{\partial t} = \frac{\lambda_e}{c\rho}\frac{\partial^2 T}{\partial z^2} - \left[\frac{c_w \rho_w q}{c\rho}\right]\left(\frac{\partial T}{\partial z}\right) \tag{0.1}$$

Where T is the temperature, z is distance below the SWI, t is time, λ_e is the effective thermal conductivity of the fluid-sediment matrix, ρ is sediment density, ρ_w is density of water, c is the bulk heat capacity of the sediment, c_w is the specific heat capacity of water and q is the vertical Darcy velocity expressed as flow per unit area. The pore water seepage velocity (v_z) is related to

the Darcy velocity as $q = nv_z$, where n is the sediment bed porosity. The ratio $\frac{\lambda_e}{c\rho}$ is the thermal diffusivity of the medium and is represented by κ_e. Thermal diffusivity incorporates heat transport by conduction and dispersion and is expressed as (McCallum et al. 2012):

$$\kappa_e = \frac{\lambda_e}{c\rho} + \beta \left(\frac{c_w \rho_w}{c\rho} q \right)^2$$

Where β is the thermal dispersivity coefficient which is dependent on grain size and fluid velocity (Molina-Giraldo, Bayer, and Blum 2011). There are conflicting views on the assignment of appropriate thermal dispersivity values (Anderson 2005). Some researchers assign values in the range of solute dispersivity (De Marsily 1986, Smith and Chapman 1983) while others have chosen to ignore β (Bear 1972, Woodbury and Smith 1985) arguing that the effect of dispersion is either negligible or represented in the effective thermal conductivity term; especially at larger length scales. Molina-Giraldo et al and Hatch et al (Hatch et al. 2006, Molina-Giraldo, Bayer, and Blum 2011) demonstrated the significance of choosing appropriate dispersivity values for accurate estimation of seepage rates especially at higher flow rates when relative error becomes large.

There are several analytical solutions to 1D-heat transport equation depending on the assumptions and boundary conditions. Bredehoef and Papadapolous (Bredehoeft and Papaopulos 1965) provided a solution to 1-D HFT for a single temperature profile data, assuming steady state flow of heat and water. Schmidt et al (Schmidt, Bayer-Raich, and Schirmer 2006) modified the Bredehoef and Papadapolous (1965) solution and presented an objective function to calculate the value of the Darcy velocity that best fits a vertical temperature profile for homogeneous streambed of depth L, assuming changes in temperature are due solely to water fluxes. Silliman (Silliman, Ramirez, and McCabe 1995) presented an analytical solution, assuming homogeneous

thermal and hydraulic properties and that temperature changes result solely from advective and conductive transport of temperature perturbations at the SWI. Their solution is similar to the 1D advection-diffusion solute transport equation and is given as follows.

$$\Delta T(z,t) = \frac{\Delta T_w}{2}\left[erfc\left(\frac{z - Zt}{2\sqrt{\kappa_e t}}\right) + exp\left(\frac{Zz}{\kappa_e}\right) erfc\left(\frac{z + Zt}{2\sqrt{\kappa_e t}}\right)\right] \quad (0.2)$$

Where $\kappa_e = \frac{\lambda_e}{c\rho}$, is the effective thermal diffusivity (cm^2/s), $Z = \frac{nv_z}{\gamma}$, $\gamma = \frac{c\rho}{c_w\rho_w}$ and ΔT_w is the change in surface water temperature. $\Delta T(z,t)$ is the incremental change in temperature in response to a temperature change of ΔT_w. The actual temperature is obtained by assuming an initial temperate of T_0 and summing the incremental temperature changes over the modeling period. Becker et al (Becker et al. 2004) applied the Silliman analytical solution to establish the groundwater discharge rate at Ischua Creek, NY. Conant et al (Conant 2004) developed an empirical model relating measured streambed temperature to discharge or recharge rates.

Stallman (1965) (Stallman 1965) presented a mathematical solution to the 1D HFT assuming sinusoidal temperature variations at the surface, vertical flow with no thermal gradient. He demonstrated the applicability of the method to detect fluxes up to 2 cm/d from diurnal temperature fluctuations and up to 0.1cm/d from annual temperature fluctuations (Lapham 1989). Goto et al (Goto, Yamano, and Kinoshita 2005) introduced the concept of the specific penetration depth with non-dimensional parameters to identify three types of flow regimes (pure conduction, advection dominated, and transition between the two regimes) and accurately modeled streambed response under recharge and discharge conditions for marine sediments. The specific penetration depth is the depth at which the amplitude of fluctuation is e^{-1} of that at the surface and can be used to determine appropriate logger burial depths in planning a streambed

temperature survey. The solution to Eq 6.1 for periodic variations in temperature is given as (Hatch et al. 2006)

$$T(z,t) = A\,exp\left(\frac{v_{TF}z}{2\kappa_e} - \frac{z}{2\kappa_e}\sqrt{\frac{\alpha + {v_{TF}}^2}{2}}\right) cos\left(\frac{2\pi t}{P} - \frac{z}{2\kappa_e}\sqrt{\frac{\alpha - {v_{TF}}^2}{2}}\right) \tag{0.3}$$

Where A is the amplitude, P is the period of temperature variation, v_{TF} is the velocity of the thermal front ($v_{TF} = v_z/\gamma;$) and $\alpha = \sqrt{{v_{TF}}^4 + (8\pi\,.\frac{\kappa_e}{P})^2}$. The streambed temperature response is a nonlinear function of κ_e, v_{TF}, P and z ; parameters that control the conductive and advective components of heat flow. The first term in equation (6.3) defines the decrease in amplitude and the second term defines the shift in phase of the temperature response with increasing depth. Hatch et al (Hatch et al. 2006) split the amplitude and phase shift terms in equation (6.3) and introduced amplitude and phase shift ratios for pairs of temperature measurements with uniform thermal and hydraulic properties between measurement depths, described in the following equations:

Amplitude Ratio:
$$A_r = exp\left\{\frac{\Delta z}{2\kappa_e}\left(v_{TF} - \sqrt{\frac{\alpha + {v_{TF}}^2}{2}}\right)\right\} \tag{0.4}$$

Phase Shift Ratio:
$$\Delta\emptyset = \frac{P\Delta z}{4\pi\kappa_e}\sqrt{\frac{\alpha - {v_{TF}}^2}{2}} \tag{0.5}$$

Equations 6.4 and 6.5 can be rearranged to represent the velocity of the thermal front as a function of amplitude and phase shift ratios as follows:

$$v_{TF,Ar} = \frac{2\kappa_e}{\Delta z}\ln A_r + \sqrt{\frac{\alpha + {v_{TF}}^2}{2}} \tag{0.6}$$

$$v_{TF,\Delta\emptyset} = \sqrt{\alpha - 2\left(\frac{\Delta\emptyset 4\pi\kappa_e}{P\Delta z}\right)^2} \quad (0.7)$$

The pore water velocity (v_z) can be calculated from thermal front velocity from (v_{TF}=v_z/γ). Equations 6.6 and 6.7 provide two independent methods to estimate fluid velocity each with its own set of limitations and uncertainty (Hatch et al. 2006). The phase shift relationship provides magnitude of thermal velocity but with no direction, due to thermal velocity appearing inside the square root function (Eq 6.4). The method involves filtering the raw temperature data to remove noise from high frequency temperature variations and identify the diurnal temperature variation corresponding to a frequency of 1 d^{-1}. This is followed by processing the temperature data computationally with a peak picking program that identifies the peak amplitude and phase shift for each day. The output is used to calculate A_r and $\Delta\emptyset$ from which the thermal front velocity v_{TF} can be fit iteratively. The amplitude ratio provides greater sensitivity at lower seepage rates, whereas the phase shift provides greater sensitivity at higher seepage rates (Hatch et al. 2006). However, amplitude ratio method provides more accurate measurement of velocity compared to phase shift estimates under non-ideal environmental conditions such as lack of clear sinusoidal fluctuations. This was shown by Rau et al (Rau et al. 2010) who compared seepage velocities derived from A_r and $\Delta\emptyset$ and identified discrepancies in computed values attributable to the uncertainty in thermal properties that resulted in violation of the model assumptions. However, time series estimates rely upon thermal properties, which have smaller uncertainties compared to hydraulic properties. As a result these methods are expected to provide a more accurate and consistent estimate of v_z (Lautz 2010).

Keery et al (Keery et al. 2007) used an extension of the Stallman et al analytical method along with dynamic harmonic regression (DHR) filtering of raw temperature data. DHR filtering

identifies the component frequencies of the temperature time series and provides an absolute value of amplitude variation as a function of time. This method provides sub-daily of time varying flow rates whereas the Hatch method provides only daily seepage velocities. The relation between the amplitude of a temperature time series at two monitoring depths is given as:

$$A_{z,t+\Delta t} = A_{0,t} e^{-az} \tag{0.8}$$

Where,

$$a = \left[\left(\kappa^2 + \frac{\xi^4}{4} \right)^{\frac{1}{2}} + \frac{\xi^2}{2} \right] - \xi \tag{0.9}$$

$$\kappa = \frac{\pi c \rho}{\lambda_e \tau} \tag{0.10}$$

$$\xi = \frac{v_z c_w \rho_w}{2\lambda_e} \tag{0.11}$$

Equation 6.8, based on change in amplitude of the temperature signal, is rearranged in terms of fluid velocity (v_z), amplitude attenuation and thermal properties as follows (Keery et al. 2007):

$$\left(\frac{H^3 D}{4z} \right) {v_z}^3 - \left(\frac{5H^2 D^2}{4z^2} \right) {v_z}^2 + \left(\frac{2HD^3}{z^3} \right) v_z + \left(\frac{\pi c \rho}{\lambda_e \tau} \right) - \frac{D^4}{z^4} = 0 \tag{0.12}$$

Where,

$$D = ln\left(\frac{A_{z,t+\Delta t}}{A_{0,t}} \right) \; and \; H = \frac{c_w \rho_w}{\lambda_e}$$

Similarly the vertical fluid velocity derived from phase shift in sinusoidal temperature signal is expressed as:

$$v_z = \left(\frac{c^2 \rho^2 z^2}{\Delta t^2 c_w^2 \rho_w^2} - \frac{16\pi^2 \Delta t^2 \lambda_e^2}{\tau^2 z^2 c_w^2 \rho_w^2} \right)^{\frac{1}{2}} \tag{0.13}$$

6.3.1 Combining Amplitude Ratio (A_r) and Phase($\Delta\emptyset$) shift to calculate thermal diffusivity and thermal front velocity

McCallum et al (McCallum et al. 2012) combined equations 6.6 and 6.7, (assuming that the thermal front velocity calculated from amplitude ratio ($v_{TF,Ar}$) and phase shift ($v_{TF,\Delta\emptyset}$) are consistent to) derive a single equation for the thermal front velocity front (v_{TF}) and effective thermal diffusivity (κ_e) that incorporates A_r and $\Delta\emptyset$

$$v_{TF} = \frac{\Delta z(P^2 ln^2 A_r - 4\pi^2 \Delta\emptyset^2)}{\Delta\emptyset\sqrt{16\pi^4\Delta\emptyset^4 + 8P^2\pi^2\Delta\emptyset^2 ln^2 A_r + P^4 ln^4 A_r}} \quad (0.14)$$

$$\kappa_e = \frac{\Delta z^2 P^2 ln A_r(4\pi^2\Delta\emptyset^2 - P^2 ln^2 A_r)}{\Delta\emptyset(P^2 ln^2 A_r + 4\pi^2\Delta\emptyset^2)(P^2 ln^2 A_r - 4\pi^2\Delta\emptyset^2)} \quad (0.15)$$

The advantage of this approach is that both v_{TF} and κ_e are independent of each other and can be calculated without using an iterative approach for streambeds with unknown κ_e values.

In a similar fashion, Luce et al (Luce et al. 2013) combined amplitude and phase shift into a dimensionless velocity term (η) expressed as,

$$\eta = -\frac{\ln(A_r)}{\Delta\emptyset} \quad (0.16)$$

Luce et al also introduced the concept of a dampening depth (z_d). The dampening depth has been used successfully to measure sediment scouring and to estimate the ideal burial depth for the temperature measurement (Luce et al. 2013, Tonina, Luce, and Gariglio 2014). However, Rau et al (Rau et al. 2015) argued that the inability of current signal processing methods to deal with non-stationarity can introduce errors under transient conditions during which scouring is measured and should be treated with caution. The dampening depth, thermal diffusivity and

advective thermal velocity (v_{TF}) are expressed as follows (Goto, Yamano, and Kinoshita 2005, Luce et al. 2013)

$$z_d = \sqrt{\frac{\kappa_e P}{\pi}} \tag{0.17}$$

$$\kappa_e = \frac{2\pi\eta\Delta z^2}{P(ln^2(A_r) + \Delta z^2)} \tag{0.18}$$

$$v_{TF} = \frac{2\pi\Delta z(1-\eta^2)}{P\sqrt{(1+\eta^2)(ln^2(A_r) + \Delta z^2)}} \tag{0.19}$$

The Darcy velocity can be then be computed from v_{TF} using the following relationship:

$$q = \left(n + (1-n)\frac{c_s}{c_w}\right) v_{TF} \tag{0.20}$$

Where n is the porosity and c_s and c_w are the volumetric heat capacity of the solids and water, respectively. The major advantage of the McCallum and Luce methods is that they do not require inputs for physical and thermal properties of the streambed to calculate the thermal velocity and effective thermal diffusivity. This effectively removes any associated error caused by approximation of these parameters. Both McCallum and Luce report that thermal diffusivity estimates exceeded typical values under transient flux conditions induced by rapid changes in stream stage.

6.4 Processing Temperature Data

Raw temperature data contain temperature fluctuations of varying frequency and noise depending on the sensor accuracy and sampling rate. Temperature data processing is essential to accurately identify the phase and amplitude of the temperature signal. Hatch et al used a simple band pass filter (0.9 $d^{-1} \leq (f) \leq 1.1\ d^{-1}$) to smooth the discretized dataset and increase resampling times. Simple band pass filtering of data sets with noise or low diel signal variations can

introduce errors resulting in spurious amplitude ratios and phase shift values (Shanafield, Hatch, and Pohll 2011). Keery et al was the first to utilize DHR in temperature data analysis. DHR utilizes Fourier analysis of non-stationary signals and was developed by Young et al (Young, Pedregal, and Tych 1999). The method uses time variable spectral coefficients (in contrast to standard Fourier analysis) for analysis of non-stationary signals (Rau et al. 2015, Vogt et al. 2010, Young, Pedregal, and Tych 1999). Rau et al (Rau et al. 2015) investigated the accuracy of four signal processing techniques and concluded DHR is the best overall method with the least root mean square error (RMSE). All signal processing methods introduce edge effects at the beginning and end of the analysis, resulting in inaccurate amplitude and phase shift values (Hatch et al. 2006, Keery et al. 2007, Vogt et al. 2010, Rau et al. 2015). Consequently two cycles of the temperature oscillation are typically discarded at both ends (Keery et al. 2007). The MATLAB® code for DHR processing in available in CAPTAIN toolbox (Young et al. 2010) and can be readily implemented.

In this paper we attempt to utilize the MaCallum method to estimate seepage flux in the top 25 cm of the streambed at all the 12 sites using the VFLUX MATLAB code for temperature data analysis. The sinusoidal temperature signal was not of sufficient amplitude and strength to apply the methodology for sensor pairs deeper than 25cm due to poor amplitude and phase shift extraction. VFLUX integrates DHR signal processing using the CAPTAIN toolbox to extract the fundamental diurnal signal to compute the Darcy velocity using MaCallum, Luce, Hatch and Keery methods outlined above (Gordon et al. 2012). The program has provisions to resample the raw data to reduce the sampling rate to improve DHR filtering. A resampling rate of 12 samples per day is suggested for data with higher frequency sampling rates (Rau et al. 2015). Oversampling can cause incorrect signal identification while implementing the standard

frequency domain optimization routine in DHR filtering (Vogt et al. 2010). The program provides tools for performing sensitivity analysis by specifying a maximum, minimum and base value for each sediment and thermal input parameter. The program also provides Monto Carlo error analysis to provide a confidence interval for the flux estimate. We also attempt to model the steady state Darcy flux for sensor pairs below 25cm using the forward modeling approach outlined by Silliman et al (Silliman, Ramirez, and McCabe 1995), assuming negligible dispersion and appropriate thermal properties. Considering that there is limited hyporheic flow at depths below 25 cm (as evidenced in the temperature profile data) our assumption of negligible dispersion is justified.

Model inputs include sediment physical parameters and thermal properties for each sensor pair as shown in Table 6.1. Physical parameters were characterized from sediment cores obtained from site GCR2, 6, 11 and 13. For sites without a sediment core, average values calculated from the four sites were used as model input. Thermal conductivity and volumetric heat capacity values were obtained from Lapham et al (Lapham 1989) using the coarse grained curve for 0-50 cm sediment depths (considering the cap is 45 cm thick) and the fine grained curve for depths greater than 50 cm. The new sedimentation on top of the cap was between 1 to 3 cm and consisted of fine grained, organic-rich material. This was negligible compared to the sensor spacing of 25 cm and was not included in the modeling. Sediment core depths ranged between 40-60 cm, with cap thickness ranging between 30-42 cm. The average properties of contaminated sediment material obtained from the cores were used for flux calculations at depths greater than 50 cm. The higher parameter variability observed for sediments 25-50 cm (i.e. larger σ) are attributed to the fact that multiple sediment types (contaminated sediment and cap material) were present in these depth ranges.

Table 0.1 Porosity and dry bulk density measurements obtained from sediment cores at sites GCR2, GCR6, GCR11 and GCR13. Shown are mean ± SEM (σ)

Site	Depth	Porosity		Wet Bulk Density (g/cm^3)		Dry Bulk Density (g/cm^3)		Thermal Conductivity (cal/sec-cm°C)	Heat Capacity ($cal/cm^3°C$)
		Mean	σ	Mean	σ	Mean	σ		
	0-25	0.41	0.06	1.87	0.07	1.55	0.17	0.005	0.63
GCR2	25-50	0.44	0.14	1.89	0.13	1.61	0.12	0.005	0.63
	>50	0.67	0.00	1.46	0.02	0.79	0.01	0.002	0.85
	0-25	0.41	0.09	1.87	0.15	1.57	0.21	0.005	0.63
GCR6	25-50	0.58	0.22	1.63	0.33	1.17	0.56	0.003	0.73
	>50	0.83	0.02	1.17	0.03	0.39	0.03	0.002	0.85
	0-25	0.49	0.17	1.81	0.28	1.33	0.47	0.004	0.67
GCR11	25-50	0.67	0.26	1.40	0.38	0.72	0.62	0.002	0.85
	>50	0.86	0.02	1.15	0.03	0.31	0.04	0.002	0.85
	0-25	0.41	0.12	1.89	0.17	1.58	0.31	0.005	0.63
GCR13	25-50	0.56	0.21	1.50	0.31	0.91	0.47	0.002	0.85
	>50	0.74	0.06	1.37	0.01	0.73	0.01	0.002	0.85
	0-25	0.43	0.04	1.86	0.17	1.51	0.12	0.004	0.65
Mean	25-50	0.56	0.09	1.61	0.29	1.11	0.39	0.003	0.77
	>50	0.78	0.09	1.29	0.02	0.56	0.24	0.002	0.85

6.5 Results and Discussion

6.5.1 Streambed temperature fluctuations

A strong diurnal temperature fluctuation was observed in the water column (+25 cm depth) with a sinusoidal pattern observed at most sites reflecting the daily solar heating and cooling cycles. (Figure 6.3-6). Sinusoidal temperature fluctuations were observed up to a depth of -25 cm with the amplitude decreasing with depth. At site GCR 13 the 0 cm logger did not exhibit the same degree of sinusoidal fluctuation as observed at other sites. This was attributed to the highly turbid and stagnant water column at the west end the reach that prevented solar penetration and resultant heating of the streambed. The surface water (+25 cm) and the streambed (0 cm) showed a general pattern of warming from June to mid-September at all sites. During this period, the temperature at shallow sediment depths were always higher than at deeper sediment depths. Although the surface water temperature decreased on two occasions in July and August the sediment temperature profiles had consistently negative temperature gradients with depth. A transition period begins after mid-September, where the streambed retains heat while the surficial sediment temperature is colder. This resulted in cooler temperatures at shallow depths of 0 and -25 cm, and warmer temperatures at -50 and -75 cm. The decreasing temperature gradient was maintained at depths below -50 cm. This suggests the transport of heat to deeper sediment depths dominated by heat conduction. By mid-October the temperature profile was inversed with temperatures at 100 cm depth warmer than those at 0, -25, -50 and -75 cm. This increasing sediment temperature with depth gradient continued over the winter period until warmer temperatures heated the surface in mid-March (data not shown). A similar winter temperature profile inversion was observed in streambed records from Maules Creek in Australia (Rau et al. 2010). Data from sites GCR-2, 6, 11 &13 were used to evaluate streambed response to increase

in temperature at SWI and evaluate evidence of groundwater upwelling. Data from the period 6/6/2013 to 6/25/2013 was used, during which there was a consistent increase in mean daily temperature at the SWI. The streambed temperature at these sites increased between 3.52 to 0.61 °C at depths from -25 to -200cm, in response to a 3.74 °C increase in mean temperature at SWI. The average temperature increase during this period was similar at the 0 cm and -25cm depths, suggesting relatively rapid transport of heat in the armor layer, and slower heat transport in the deeper organoclay and contaminated sediment layers. The sinusoidal temperature fluctuations observed at the SWI (0 cm) was partially attenuated at the -25 cm depth, and no clear sinusoidal variations were observed in deeper sediment layers. Temperature profiles characteristic of rapid groundwater upwelling are evidenced by lack of temperature gradients or possible inversion of gradients with surficial streambed temperatures similar to those observed in deeper sediment layers. For example Schmidt et al (Schmidt, Bayer-Raich, and Schirmer 2006) observed streambed temperature in the range of observed groundwater temperature (monitored at 1 m to 5 m depth) at a depth of -50cm and -10cm in sediments with high groundwater upwelling. In GCR, the average daily temperature at 50 cm was significantly different than that observed at -100 cm and -200 cm, indicating the absence of groundwater upwelling at all sites (Table 6.2). Instead the temperature data observed at all four sites is characteristic of a losing stream or one with no advection where the movement of pore water into the hyporheic zone results in temperature changes mimicking the temperature trends at the surface.

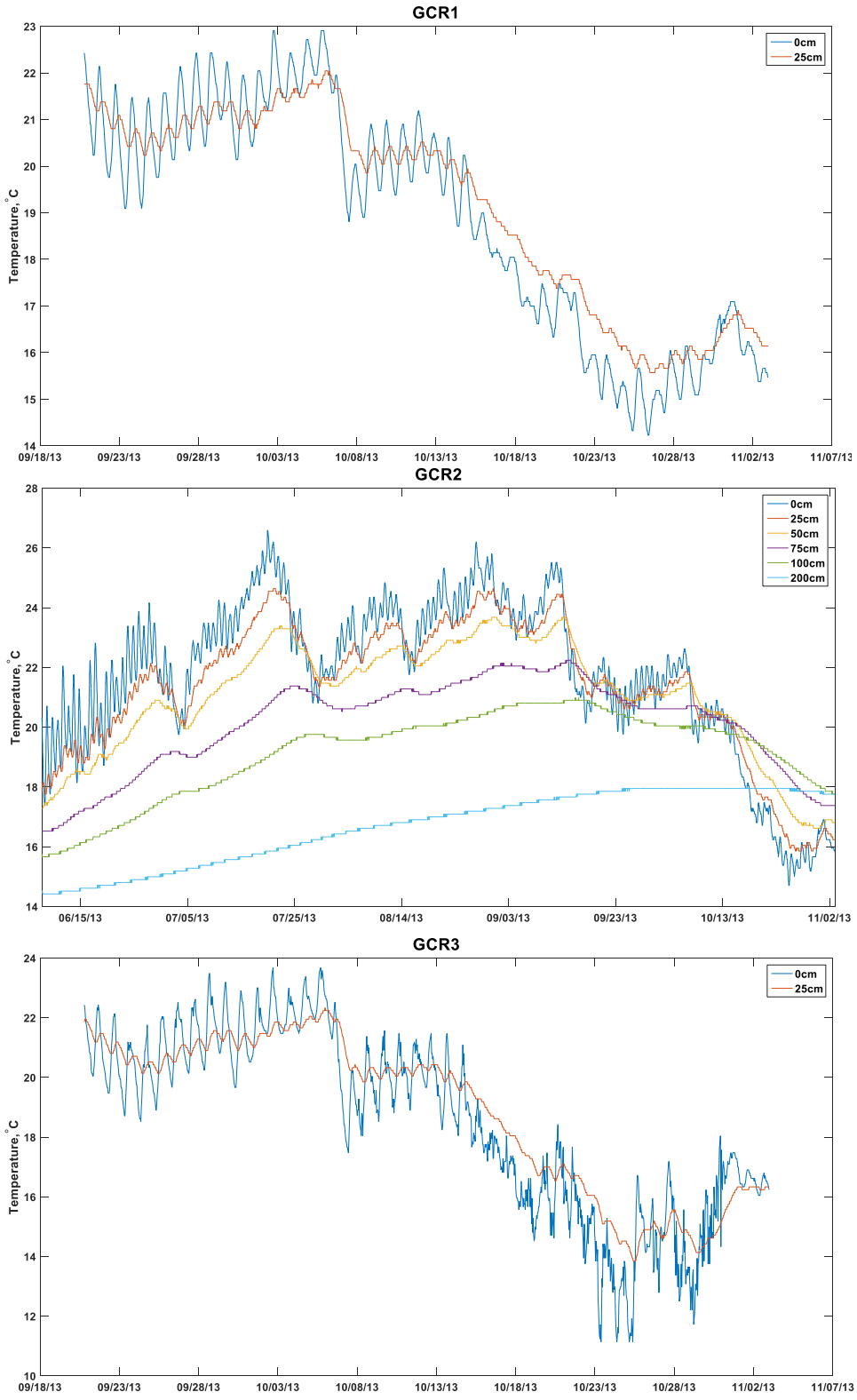

Figure 0.3 Sediment temperature from June 1 to Nov 7 at sites GCR 1-3.

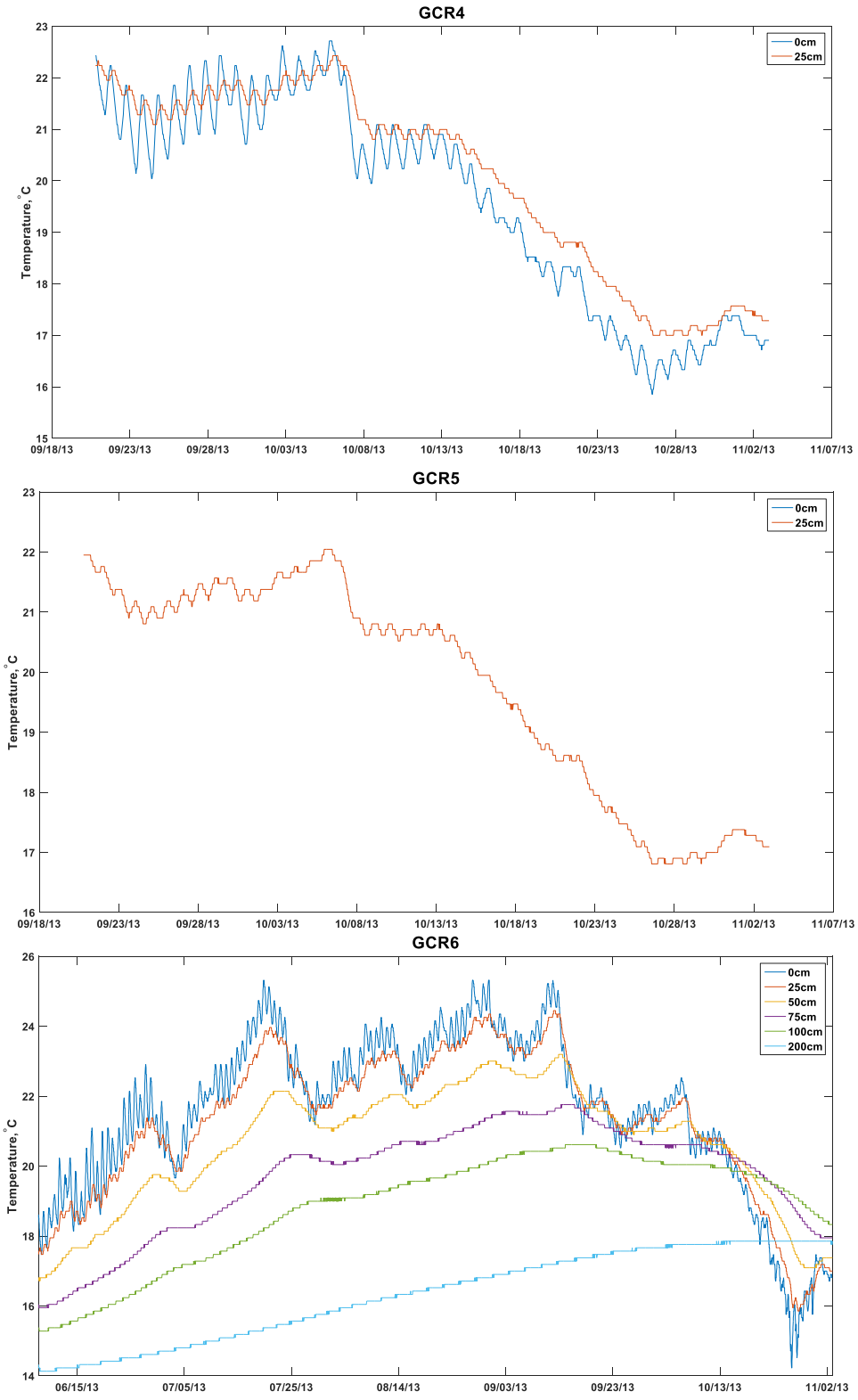

Figure 0.4 Sediment temperature from June 1 to Nov 7 at GCR4-6. Note: 0 cm probe malfunctioned at GCR5 resulting in no recorded temperature.

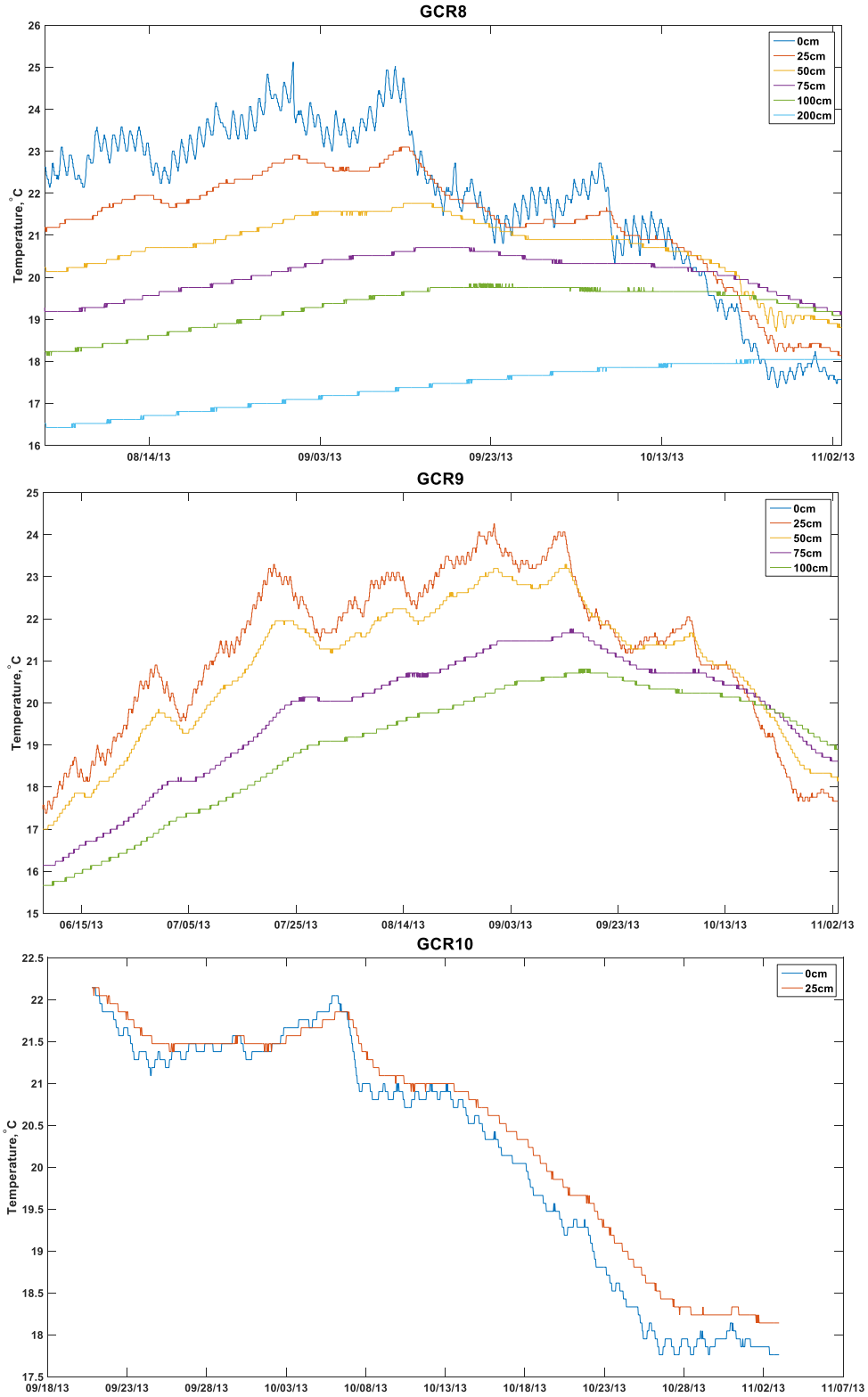

Figure 0.5 Sediment from June 1 to Nov 7 at GCR8-10. September to November for sites GCR8 and 10 and June to November for GCR9. Note: 0cm probe at GCR9 malfunctioned, resulting in no recorded temperature.

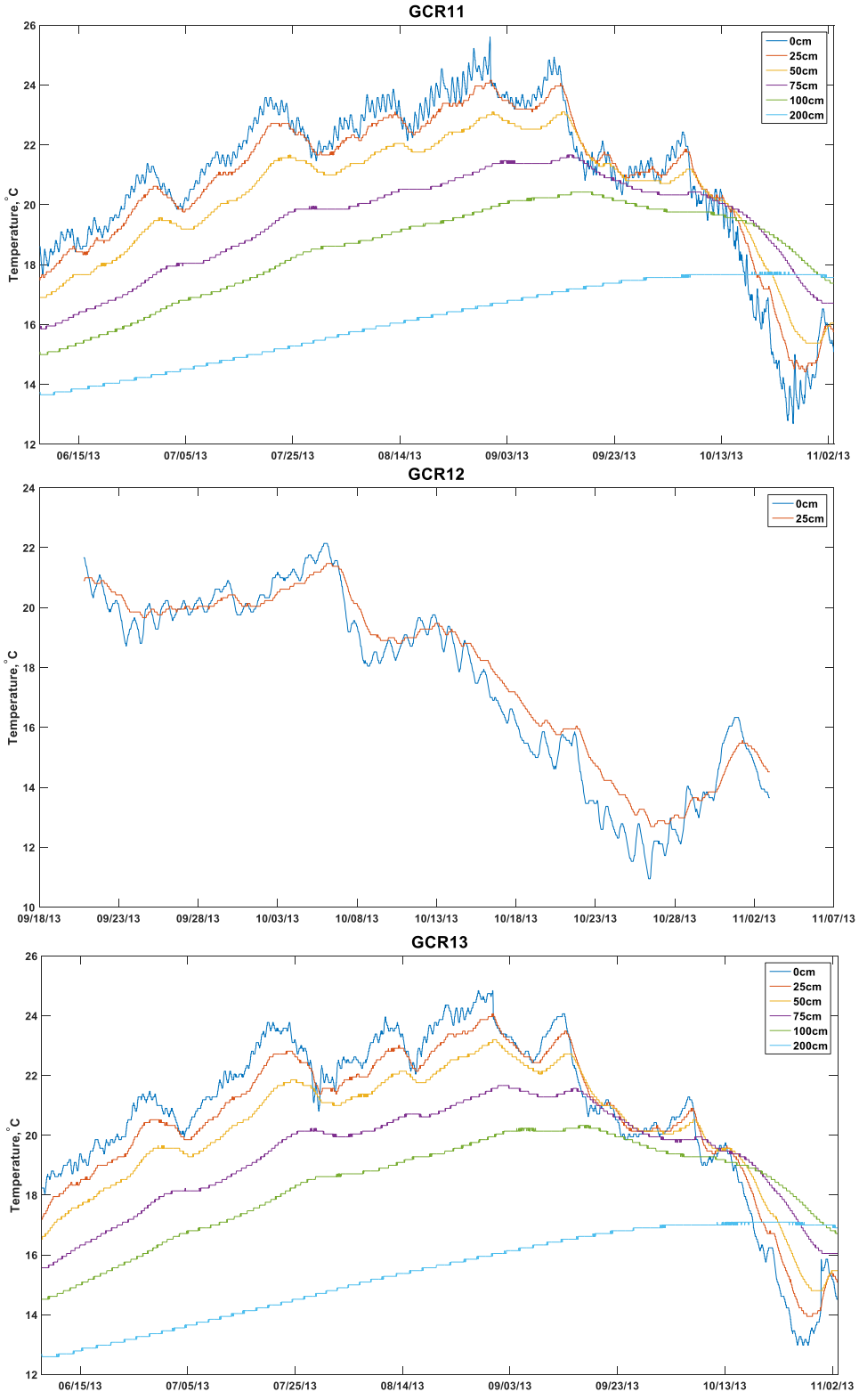

Figure 0.6 Sediment temperature from June 1 to Nov 7 at sites GCR11-13

Table 0.2 Average daily temperature recorded for different depths at the start and end of a distinct surface warming period and observed streambed response represented as temperature increase.

Site	Depth	Average Daily Temp (06/6/13) (°C)	Average Daily Temp (06/25/13) (°C)	Temperature Increase, (°C)
GCR13	0cm	18.24	21.30	3.06
	-25cm	17.20	20.52	3.32
	-50cm	16.55	19.51	2.96
	-75cm	15.57	17.76	2.19
	-100cm	14.52	16.19	1.67
	-200cm	12.59	13.37	0.77
GCR11	0cm	18.11	21.19	3.08
	-25cm	17.56	20.51	2.96
	-50cm	16.90	19.33	2.43
	-75cm	15.86	17.58	1.72
	-100cm	15.00	16.30	1.30
	-200cm	13.65	14.27	0.61
GCR6	0cm	18.05	21.90	3.85
	-25cm	17.54	21.23	3.69
	-50cm	16.79	19.61	2.82
	-75cm	15.95	17.83	1.88
	-100cm	15.28	16.63	1.34
	-200cm	14.13	14.61	0.48
GCR2	0cm	18.87	22.95	4.08
	-25cm	18.02	21.97	3.96
	-50cm	17.28	20.79	3.51
	-75cm	16.52	18.82	2.30
	-100cm	15.66	17.32	1.66
	-200cm	14.42	15.00	0.57

Streambed temperature profiles exhibit differences in response to varied thermal and hydraulic properties. Larger diurnal temperature fluctuations were observed at sites GCR1-6 compared to sites 9-13. This may be influenced in part by a lack of streambank tree canopy together with the strong influence of the HSD outfall discharging warmer water to the stream. The uncapped site GCR8 had only minor diurnal temperature variation at -25 cm depth. This was likely due to the fine sediment with high organic matter content and corresponding low thermal conductivity <0.002 cal/cm^3 ºC throughout the sediment column. This resulted in a lack of a clear sinusoidal trend and resulting poor amplitude and phase shift identification. Site GCR10 was immediately downstream of the HSD outfall, resulting in limited diurnal temperature fluctuations and the absence of clear sinusoidal trend (Figure 6.5). In contrast sites GCR11-13 had strong sinusoidal variations at the 0 cm but lower amplitude temperature fluctuations than those observed at sites GCR1-6. The air temperature decreased significantly after October 13, 2013 and this change was accompanied by significantly lower temperature amplitudes at all sites. Consequently, flux estimates using the McCallum method were determined from the start of the monitoring period to Oct 13th 2013 for all monitoring locations except sites GCR 5, 8, 9 and 10.

6.5.2 Dynamic Harmonic Regression Analysis

The raw temperature data contains multiple harmonics that requires filtering to isolate the frequency (d-^{1}) of interest. The presence of multiple peaks within a diurnal temperature record makes the manual identification of peaks at two depths complicated. Also the non-stationarity of the temperature signal makes identification of amplitude and time lag inaccurate if computed from just the maximum and minimum values (Gordon et al. 2012,

Lautz 2010). For example, the amplitude calculated from the maximum temperature and the preceding or proceeding minimum will result in two different amplitude values for the same day. DHR is a robust filtering technique that makes identification of diurnal signal even under quickly changing temperature trends and allows for fully automated selection of extrema without manual intervention. The VFLUX MATLAB code (Gordon et al. 2012) implements the CAPTAIN toolbox DHR filtering routine requiring inputs of r-factor, windows, Pf, n, beta, K_{cal}, C_{scal} and C_{wcal}. The r-factor is a positive integer representing a reduction factor to reduce the sampling rate to 12 d^{-1}, as oversampling may lead to errors in output (Gordon 2015). In our current study temperature data were recorded at 45 min intervals resulting in 32 samples per day and an r-factor = (32/12)≈3. The rest of the inputs are windows=1 for 0 to -25cm depth, fundamental period Pf = 1 d, n is the measured sediment porosity, beta = thermal dispersivity (in meters) (for Hatch and Keery et al methods), K_{cal}= thermal conductivity (cal/sec-cmºC), C_{scal} = heat capacity of sediment (cal/cm^3ºC), C_{wcal} = heat capacity of water (cal/cm^3ºC). The sediment and thermal properties corresponding to the 0-25 cm depth range are presented in Table 6.1. The DHR signal processing routine in VFLUX produces two diagnostic plots for each time series that includes the autoregression spectrum ARSPEC and a plot of the actual data and the model fit. The DHR model is an unobserved component model where an observed variable (such as temperature) is related to one or more components that are dependent on perceived features of the data represented by their characteristic spectral properties (Young 2011). The temperature time-series can be represented by the following basic DHR model equation:

$$y(k) = T(k) + C(k) + S(k) + e(k)$$

Where $y(k)$ is the observed temperature, $T(k)$ is the long term trend, $C(k)$ is the cyclical component representing the diurnal temperature variation, $S(k)$ is the seasonal component and $e(k)$ is the irregular component representing any unpredictable variations in the time series. The ARSPEC plot of each time-series was evaluated for the strength of the diurnal signal (represented by y-axis in the plot) at the fundamental signal period of 10.7 d^{-1} representing the $C(k)$ component. The half peak to the left of the fundamental peak represents the long term trend$T(k)$. The presence of peaks at the second and third harmonics indicates intra-day variations in the temperature signal represented by the seasonal and irregular components in the model equation. ARSPEC output for depths 0 and -25 cm are presented in Figures 6.7-11. The fundamental signal period is shown together with the first (5.35 d^{-1}), second (3.6 d^{-1}), third (2.7 d^{-1}) and fourth (2.1 d^{-1}) harmonics represented by vertical red lines. The McCallum method was utilized for all sites with at least one peak at the fundamental period of 10.7 samples/cycle representing the diurnal variation of sufficient strength. Strong peaks were observed at the fundamental period and first harmonic for all sites at 0 cm depth, indicating a strong diurnal signal in response to solar heating of the streambed. Fundamental period peaks were observed at -25 cm depth at all sites except GCR10 and GCR8. A malfunctioning 0 cm sensor at sites GCR9 and GCR5 precluded determination of flux at these sites, thus fluxes were calculated at eight of the twelve study sites. First harmonic peaks were not discernable at most sites at the -25 cm depth. DHR signal processing was able to isolate the sinusoidal trend in the temperature data, and these data were used to calculate the amplitude and phase shift of the temperature signal at the fundamental period for both depths. An example of the sinusoidal signal extracted from the raw temperature data is

provided in Figure 6.12 for site GCR1. The 0 cm sensor provided a strong sinusoidal signal at the fundamental period with an amplitude of 1 – 2 ºC. The amplitude of the signal decreased over time in response to the onset of colder water temperatures during the latter part of the monitoring period. Amplitude at the -25 cm sensor at GCR1 was comparatively weaker in the range of 0.4 ºC. Amplitude was extracted from the sinusoidal temperature signal for all the eight modeled sites. A noticeable decrease in amplitude was observed after mid October 2013 at all modeled sites. Consequently the flux calculations were limited to the section of data prior to the date. The amplitude ratio and phase shift was thus extracted from the filtered DHR output and used for flux calculations.

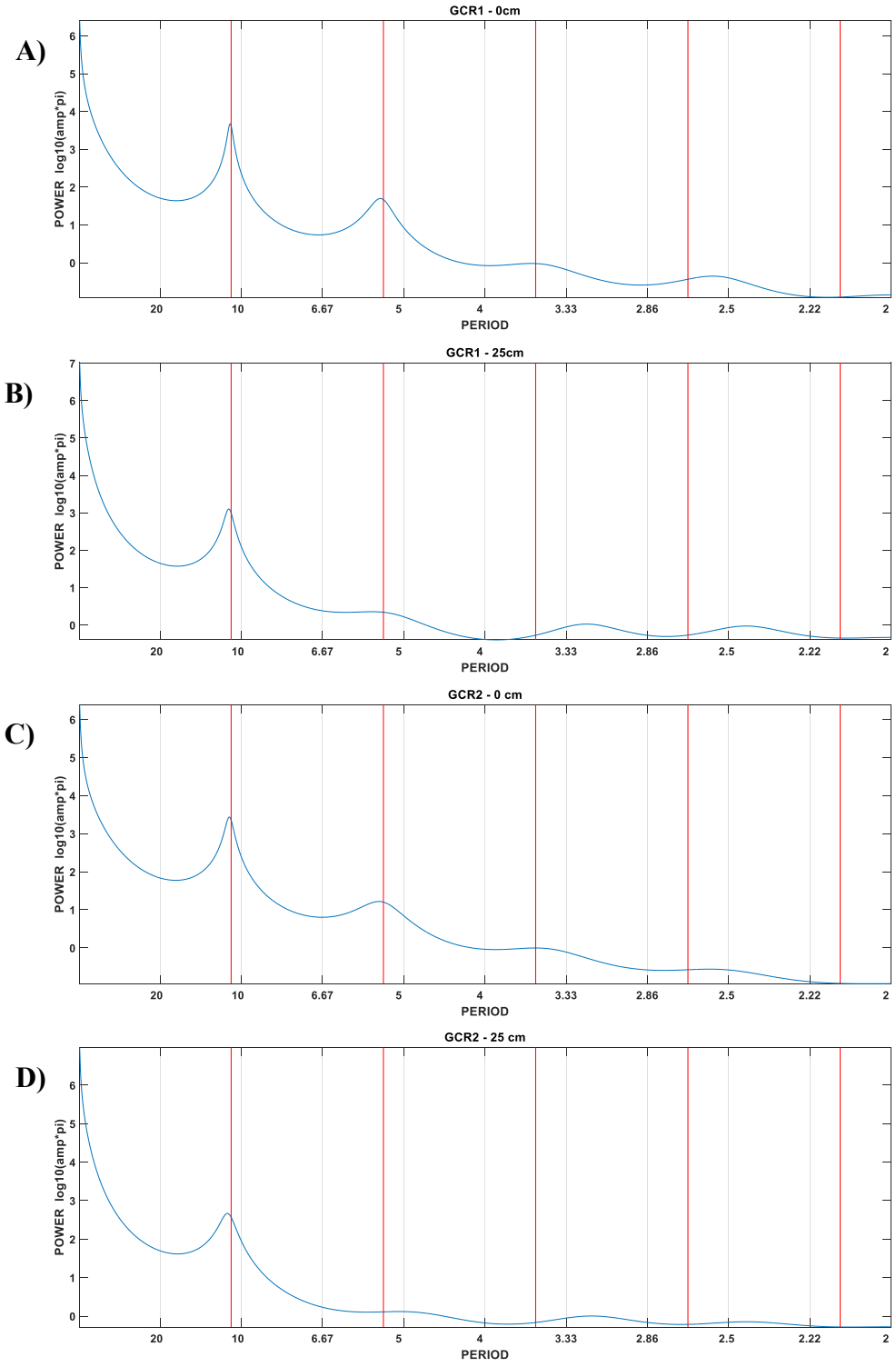

Figure 0.7 ARSPEC output for sites GCR1 and GCR2 at model depths 0 and -25 cm. Strong peaks are observed at the fundamental period for both sites.

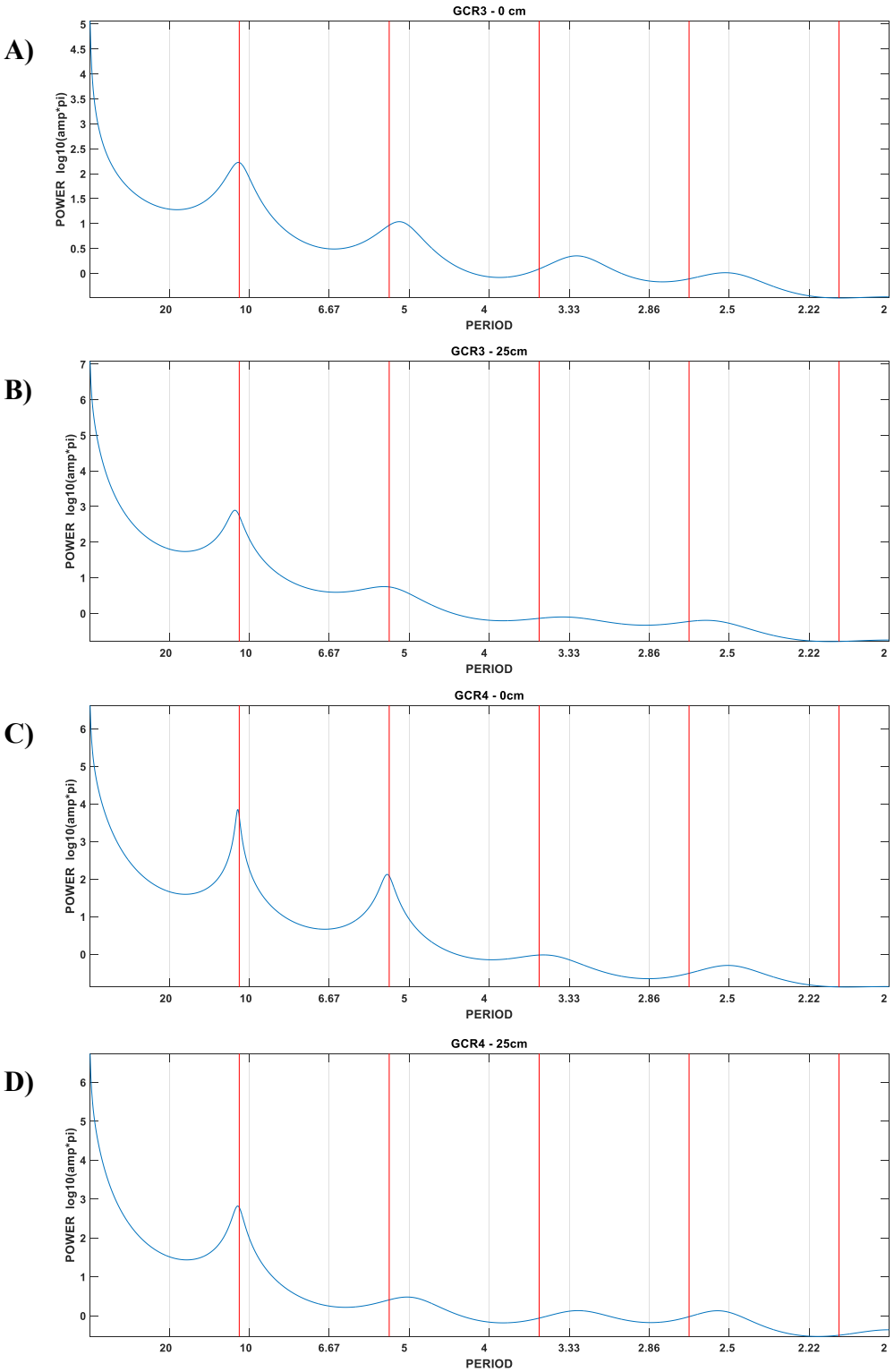

Figure 0.8 ARSPEC output for sites GCR3 and GCR4 at model depths 0 and -25cm. Strong peaks are observed at the fundamental period for both sites.

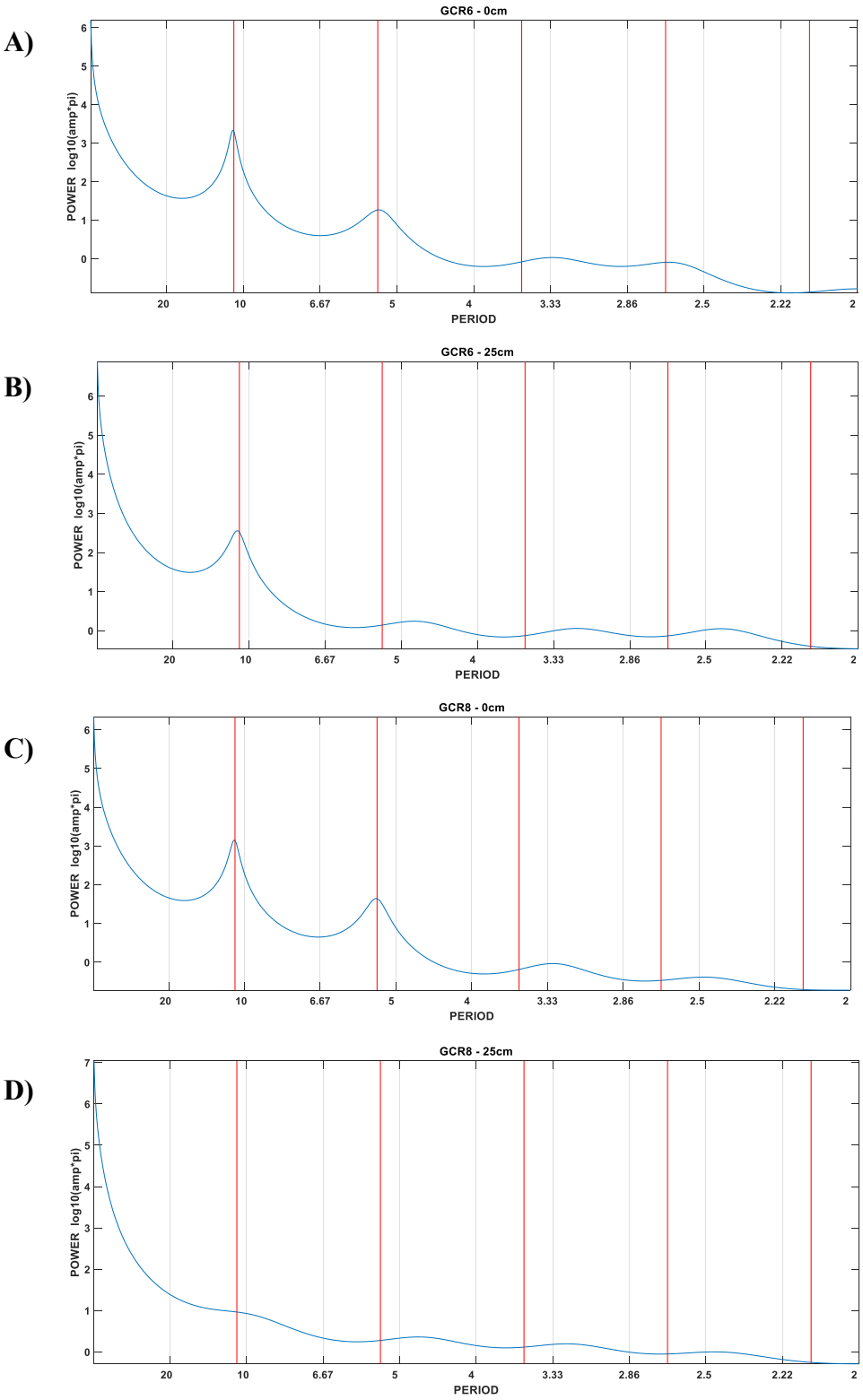

Figure 0.9 ARSPEC output for sites GCR6 and GCR8 at model depths 0 and -25cm. Strong peaks are observed at the fundamental period for GCR6. A strong peak is not observed at the -25cm depth for GCR8 indicating weak diurnal temperature fluctuation.

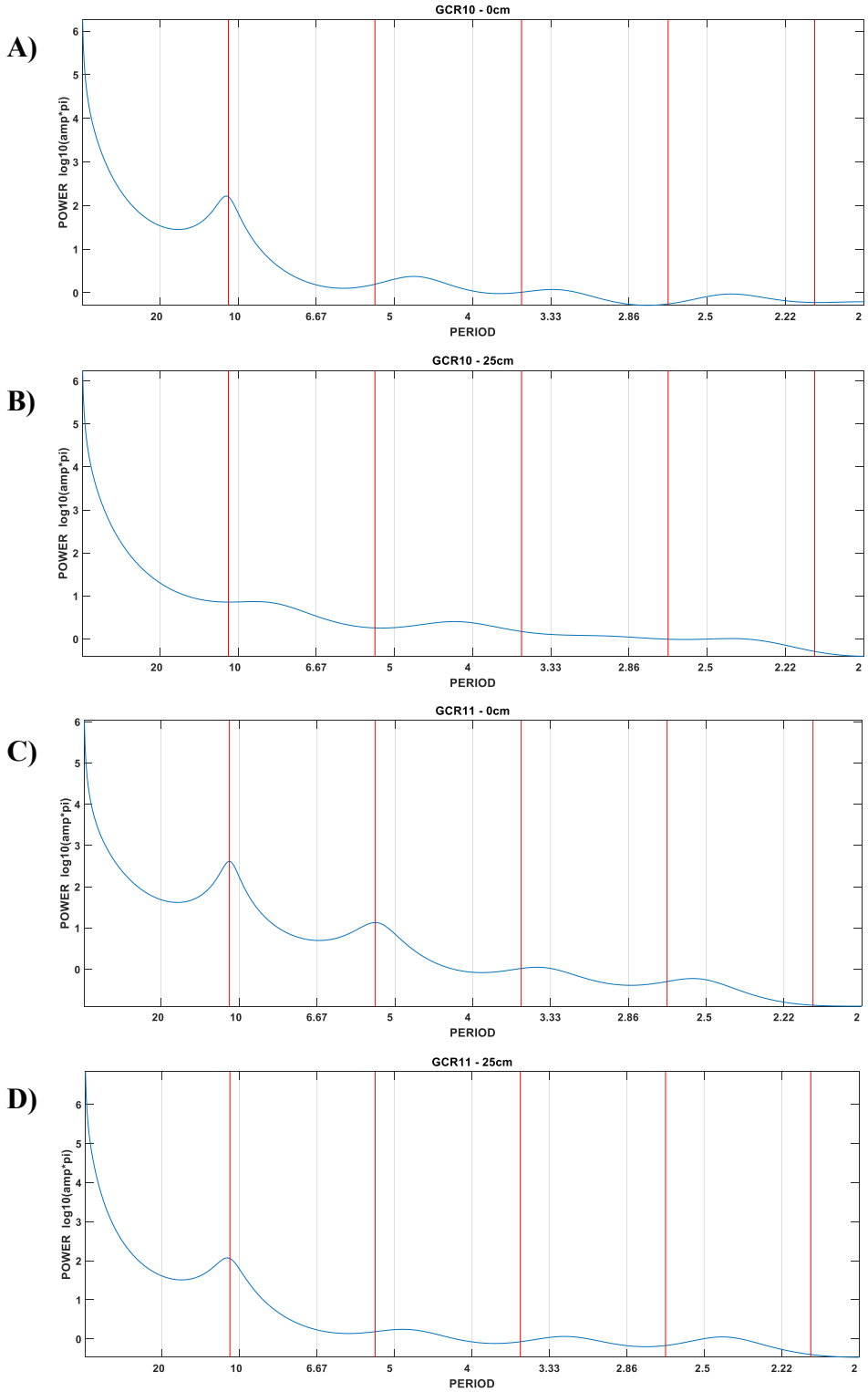

Figure 0.10 ARSPEC output for sites GCR10 and GCR11 at model depths 0 and -25cm. Strong peaks are observed at the fundamental period at both depths for GCR11 and 0cm depth at GCR10. No identifiable peak is seen for -25cm depth for GCR10.

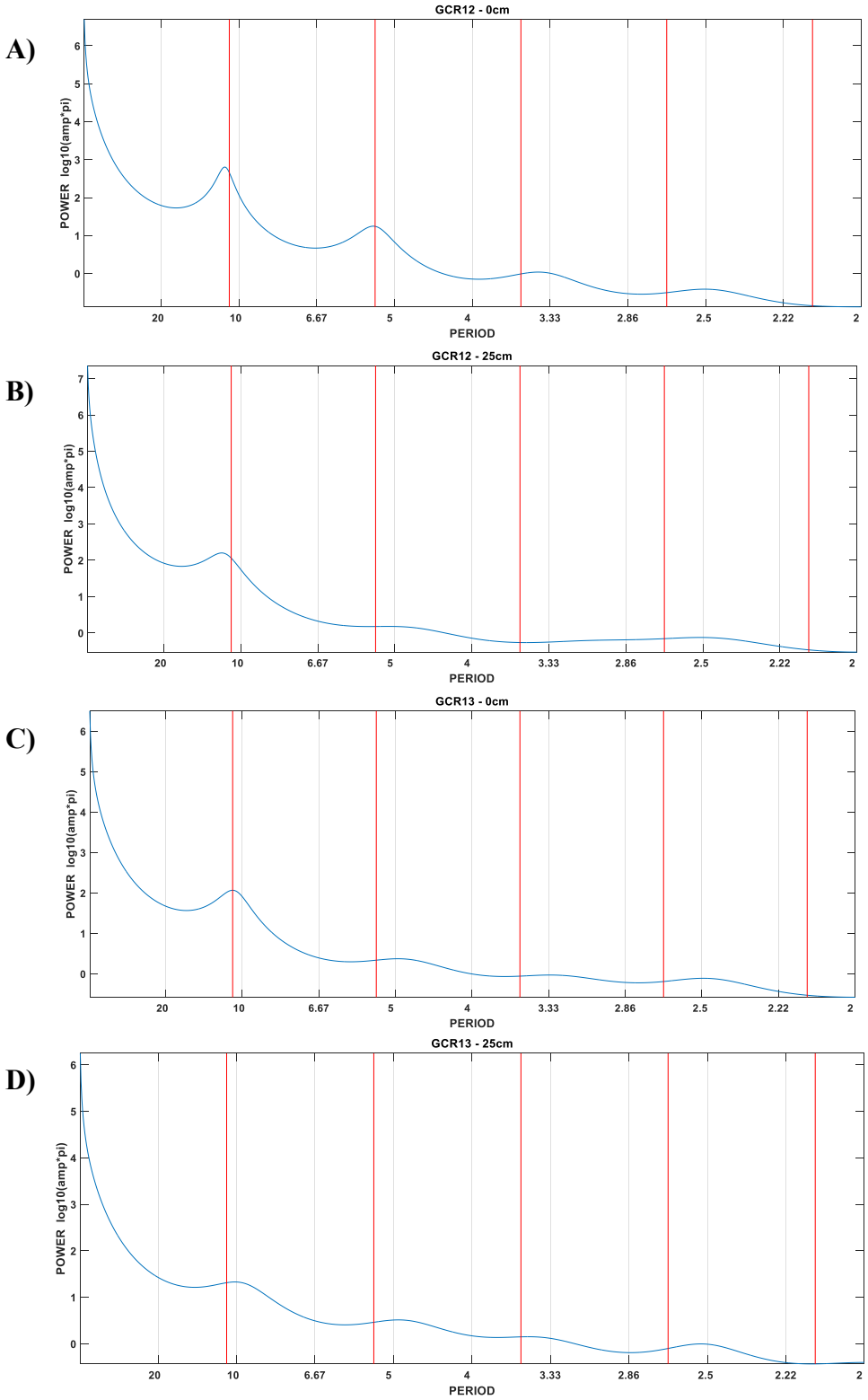

Figure 0.11 ARSPEC output for sites GCR12 and GCR13 at model depths 0 and -25cm. Strong peaks are observed at 0cm depth for both sites with and no identifiable peak at -25cm depth for GCR13.

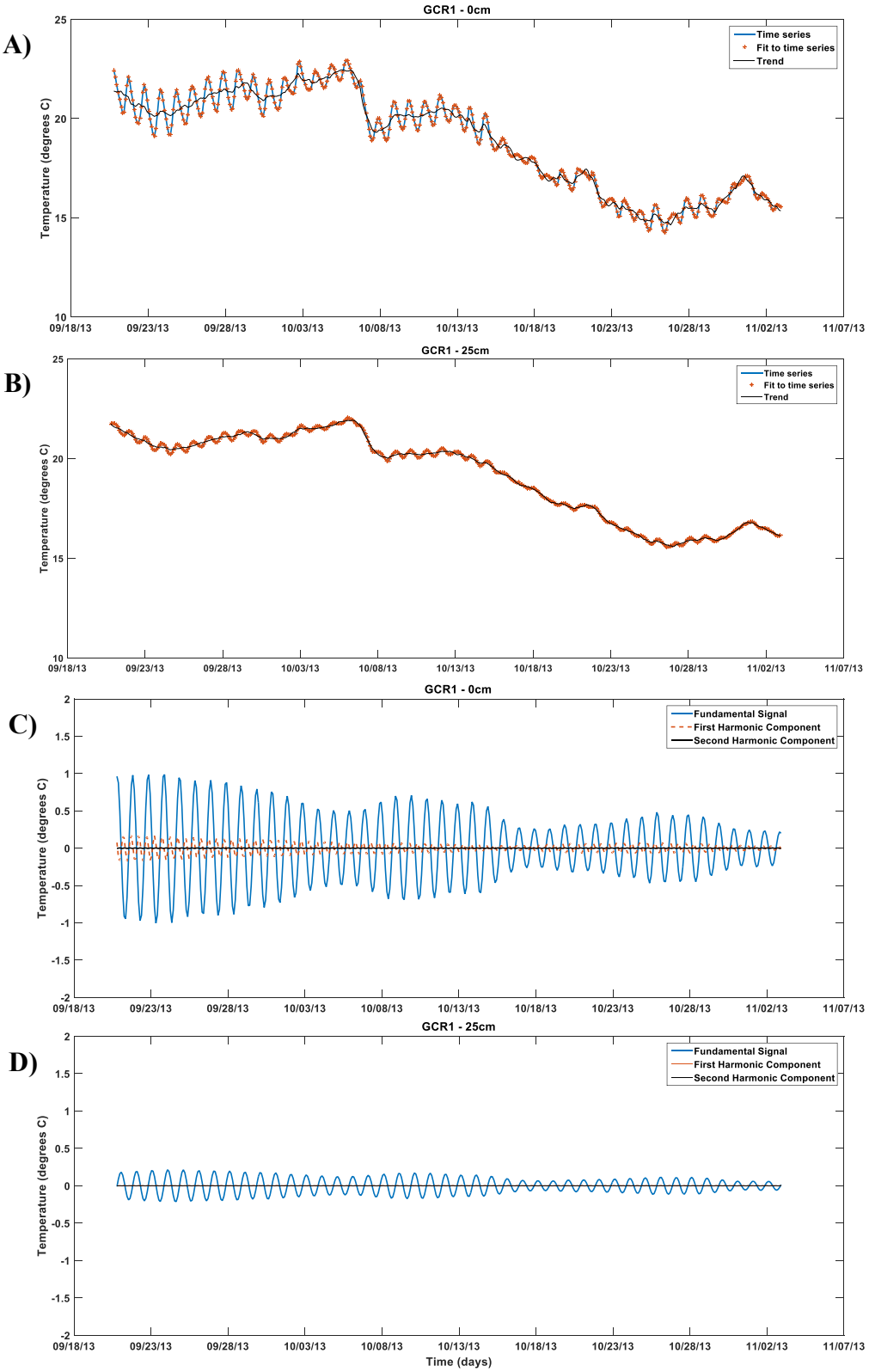

Figure 0.12 DHR fit to temperature data and trend are shown in A) and B). Extracted signal at the fundamental period, first and second harmonics are shown in C) and D).

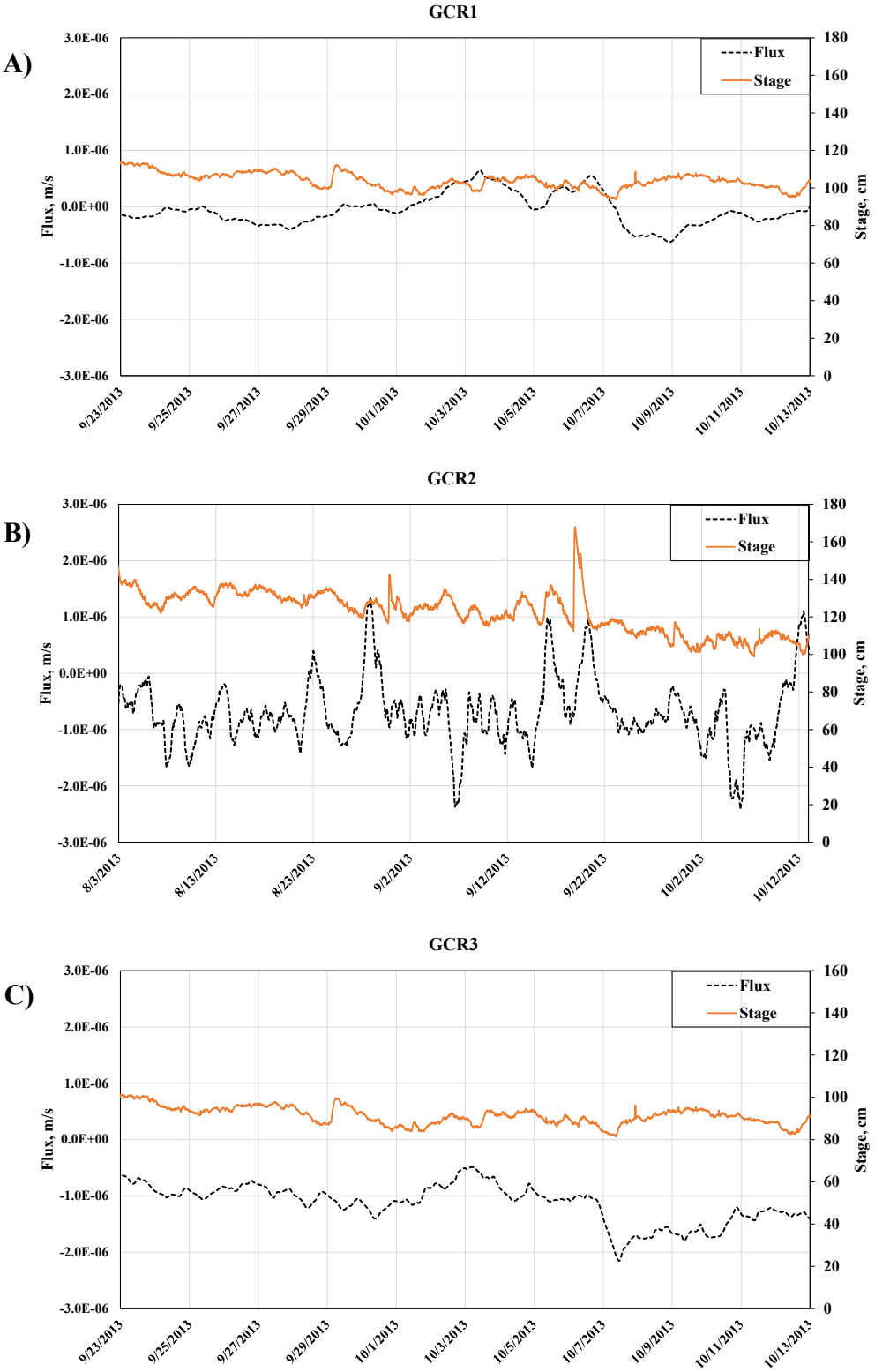

Figure 0.13 Calculated Darcy fluxes compared to river stage over the monitoring period for sites A) GCR1, B) GCR2 and C) GCR3.

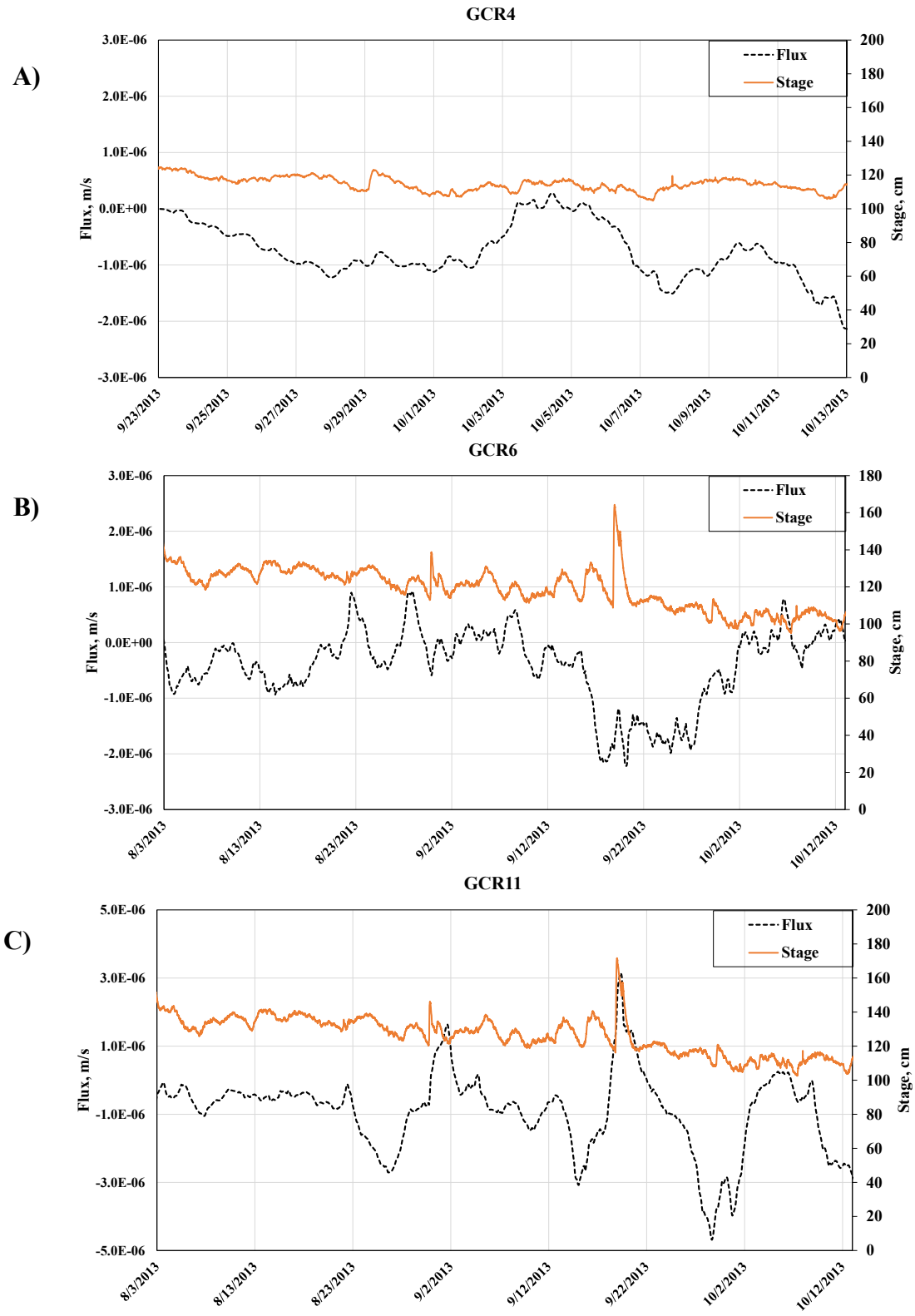

Figure 0.14 Calculated Darcy fluxes compared to river stage over the monitoring period for sites A) GCR4, B) GCR6 and C) GCR11.

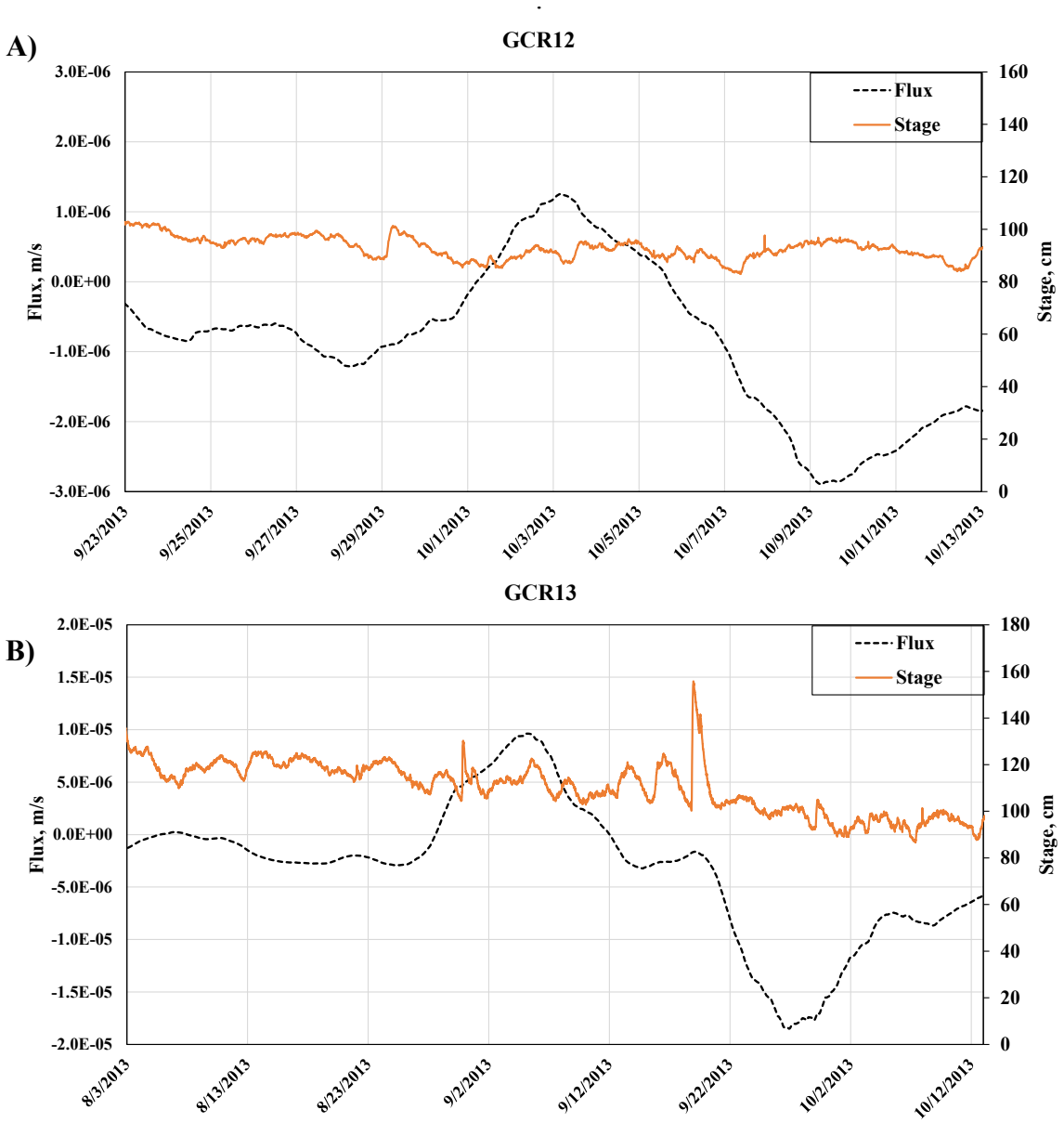

Figure 0.15 Calculated Darcy fluxes compared to river stage over the monitoring period for sites A) GCR12 and B) GCR13.

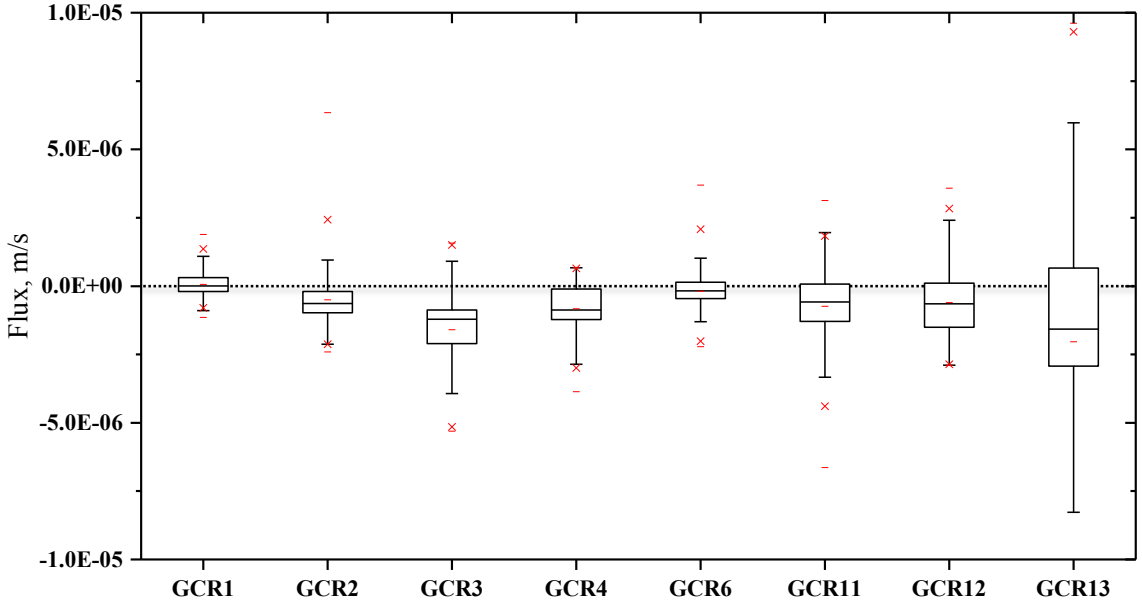

Figure 0.16 Box and whisker plot of fluxes for all modeled sites. (-) beyond the whiskers represent max and min, (-) inside the box represent the mean, box represents 75th percentile and 25th percentile and horizontal line across the box represents the median.

6.5.3 McCallum Method Darcy Flux Estimation

An advantage of using DHR is that it allows sub-daily flux calculations from the sub-daily amplitude ratio and phase-shift values extracted from the signal. The only input parameters required for flux calculation are all known: porosity (n), specific heat capacity of sediment (c_s) and water (c_w) using equation 12. VFLUX can then be used to calculate the Darcy flux using the McCallum method for every amplitude ratio and phase shift value extracted by DHR analysis. These data represent the average flux between the sensor pair at midpoint (12.5 cm) depth. The calculated fluxes were plotted as a function of time along with field measured water depth data from the relevant sampling period in 2013. In the McCallum model positive flux values indicate gaining conditions where groundwater discharges into the stream and negative values represent losing conditions

with stream water entering the hyporheic zone. Box and Whisker plot for the range of observed fluxes at each site is shown in Figure 6.16. Greater range of fluxes are observed at sites GCR11, 12 and 13 compared to sites in reach 2 (GCR1-6) with predominantly losing condition at all sites. GCR1 was the only site with gaining conditions with a very low flux value of $6.3x10^{-8}$ m/s. Sites GCR2 and 13 had higher fluxes compared to other sites, in the range of $-2x10^{-6}$ m/s. At GCR1 there was no strong evidence of the fluxes being influenced by changes in stage but primarily due to the low fluctuation in water depth observed during the monitoring period (Figure 6.13A). Site GCR2 had higher fluctuations in fluxes with clear indication of rapid changes in flux in response to changes in stage (Figure 6.13B). The monitoring period from 9/12 to 09/23 consisted of three significant flood events seen by the three peaks in the stage plot where the water depth increase by 20-40 cm. The flood events induced a rapid increase in discharge to the shallow subsurface. It is interesting to note that the magnitude and direction of flux changed rapidly during these flood events, before settling down to magnitudes similar to those observed prior to the storm event.

This rapid response was likely caused by discharge of bank storage back into the river, as was observed at Maules Creek (McCallum et al. 2012). All gaining fluxes observed at GCR2 were preceded by an increase in stage except for an inexplicable GW discharge event observed around 10/12/2013. Site GCR3 was consistently losing stream water throughout the monitoring period with limited fluctuations. GCR4 had surface water recharge for the majority of the monitoring period, except for a slight shift to discharge conditions around the first week of October. GCR6 had higher fluxes changes (mean flux

= -1.9x10^{-7} m/s) with increase in recharge fluxes after high flow events, as was observed at GCR2. Site GCR6 exhibited periodic discharge fluxes early in the monitoring period, followed by consistent periods of surfacewater recharge as the water stage decreased in October. This response likely can be attributed to the complex interaction between the GCR-6 and the entrance to Roxana Marsh. GCR6 is located at the mouth of the marsh and there is potential for subsurface flows from the marsh back into the river under low flow conditions.

In reach 2, GCR11 was characterized by recharge conditions with higher recharge fluxes after storm events during two time periods around September 1st and 18th. It is intresting to note that the streambed temperature dropped significantly during both time periods indicating transient conditions (The impact of transient conditions on model performance will be discussed later). GCR12 and 13 were under recharge conditions for the majority of the monitoring period with the minimal fluctutations. Both sites had a stready increase in flux to discharge conditions from the last week of August to first week of September, followed by a period of increasing recharge before stabilizing to recharge fluxes of 2x10^{-6} and 1x10^{-5} m/s for GCR12 and 13, respectively.

The flux estimates at all sites except GCR13 varied within a relatively narrow range of values (Figure 6.16). These fluxes were comparable to fluxes measured at three piezometer locations just east of GCR1 (Figure 6.17) by Tetra Tech Inc (personal communication). In general, the observed fluxes at the uncapped piezometer locations were (in the range of -1.5E-8 to 2.0E-8 m/s) comparable to (-2.0E-6 to 1.0E-6 m/s) those estimated from McCullam method.

The time variant seepage flux estimated from the McCallum method provides a better understanding of the streambed GW-SW interaction including direction and magnitude. In contrast, conventional methods do not allow this level of temporal resolution.

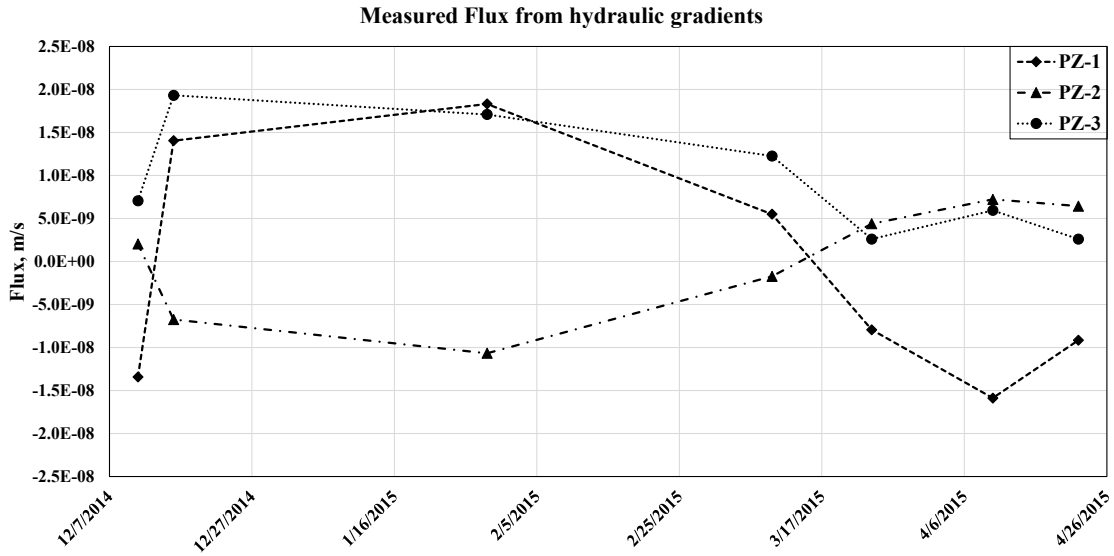

Figure 0.17 Fluxes measured by piezometer at three uncapped locations immediately east of GCR1 in 2014/2015. Data from James Wescott, TetraTech, Chicago.

6.5.4 Limitations and Uncertainty in flux estimates

The physical and thermal properties of the streambed required in flux calculations are porosity (n) and specific heat capacity of sediment (c_s) and water (c_w). The heat capacity of water is, essentially constant in the measured temperature range of 15 – 23 ºC while the other two are variable in-situ. Therefore, it is important to perform an accurate analysis of the flux calculation that takes into account this variability. For this we chose the Monte Carlo analytical technique of performing simulations with randomly varying the model parameters. Monte Carlo simulation was performed for 1000 realizations by selecting random values for porosity and heat capacity from a normal distribution of input mean and standard deviation (Table 6.1). Mean and standard deviation of porosity were calculated from average of sediment core sections in the 0 – 25 cm depth (0.4 ± 0.1)

and specific heat capacity values of 980 ± 145 J/kg ºC were used based on literature values (McCallum et al. 2012). The Monte Carlo flux simulations were performed with mean and upper and lower uncertainty limits of ±2σ (Figure 6.18-20). Monte Carlo simulation allows us also to evaluate whether flux estimates are real by comparing the fluxes calculated at each site along with the range of flux estimates due to uncertainty in c_s and n.

The results of these analyses demonstrate that the uncertainty associated with porosity and specific heat capacity is low at all sites. There is a slight increase in uncertainty with increase in the magnitude of the estimated flux velocity. This is primarily caused by greater dispersion at low porosity, which decreases the path length and increases dispersion as the velocity increases. Uncertainty in flux estimates are also caused by transient conditions where rapid changes in flux cause temperature changes in the streambed at time scales less than the resolution obtained from DHR filtering. This interpretation is supported by previous results in the literature. McCallum et al (McCallum et al. 2012) observed greater uncertainty at higher fluxes caused by violation of the steady state model assumption, and is generally evidenced by unreasonable estimates of thermal diffusivity. However Rau et al (Rau et al. 2015) argued against the violation of steady state and demonstrated that the uncertainty is caused by a signal processing artifact in which short term flux changes induce non-stationarity in the temperature signal. The non-stationarity is too fast to be precisely delineated by Fourier based filtering methods that use a harmonically forced solution of fixed time and frequency (Rau et al. 2015). However DHR was the best performing filtering techniques with the lowest root mean square error (RMSE) among all methods considered.

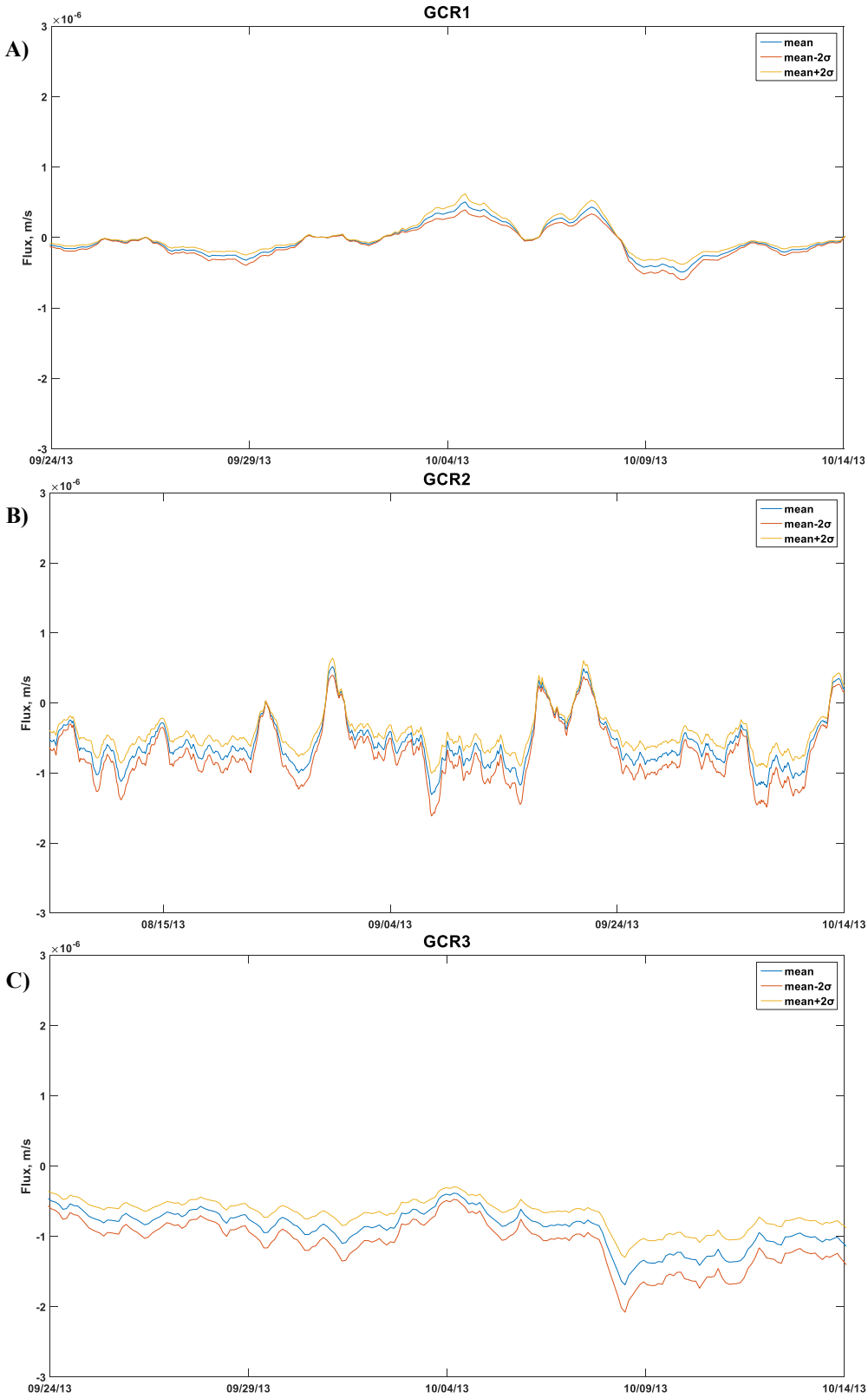

Figure 0.18 Monte Carlo Analysis of flux estimate incorporating uncertainty in porosity and specific heat capacity for sites A) GCR1, B) GCR2, C) GCR3 from Aug-Oct 2013.

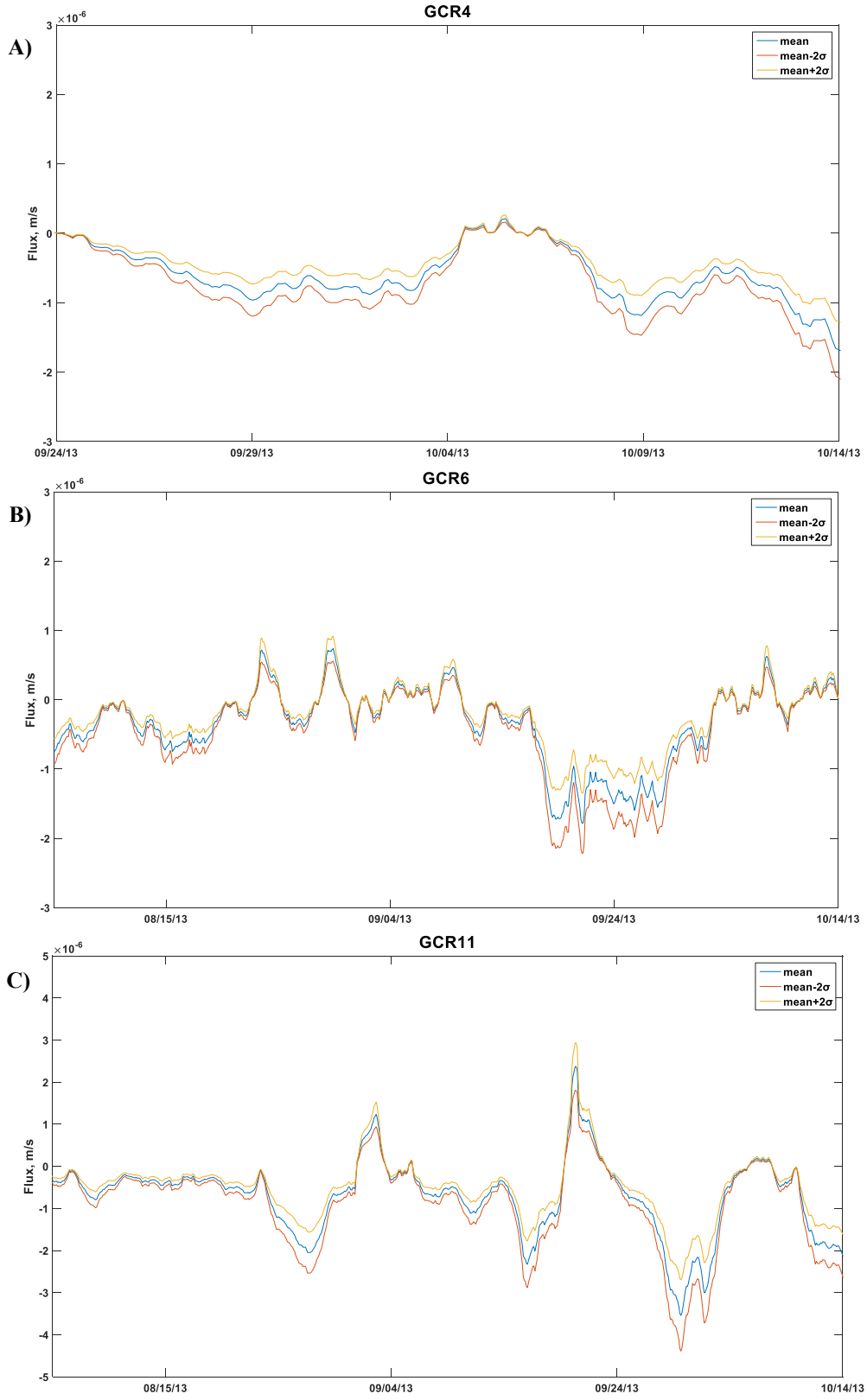

Figure 0.19 Monte Carlo Analysis of flow estimates incorporating uncertainty in porosity and specific heat capacity for sites A) GCR4, B) GCR6, C) GCR11 from Aug-Oct 2013.

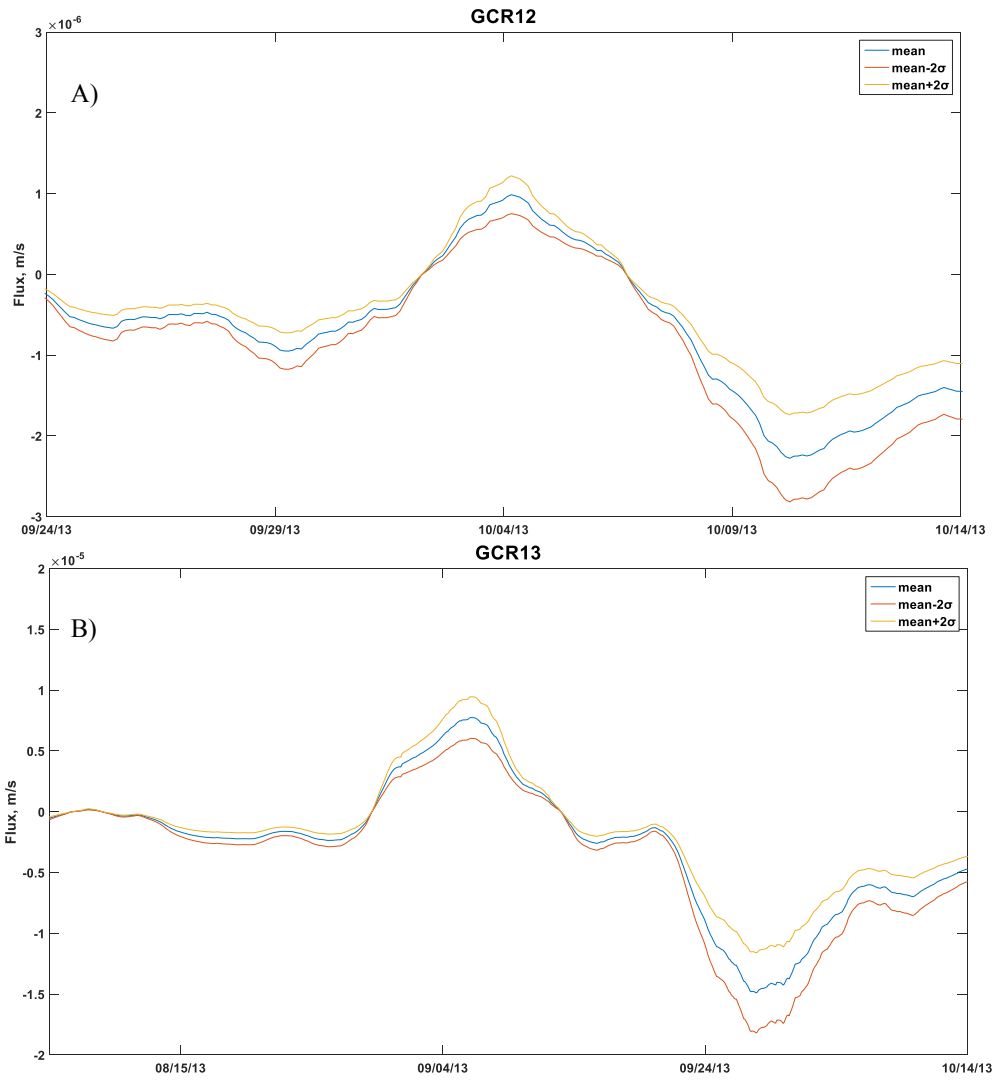

Figure 0.20 Monte Carlo Analysis of flow estimates incorporating uncertainty in porosity and specific heat capacity for sites A) GCR12, B) GCR13 from Aug-Oct 2013.

Uncertainty in flux estimates can also be caused by low response time of the temperature logger. A sensor with low response time cannot capture the transient temperature changes accurately even at high logging rates. Also the precision and resolution of the sensor should be greater than the amplitude of temperature variation observed at the model depths. Consiquently uncertainity in flux estimates is greater as evidenced by wide range of fluxes observed at sites GCR12 and 13 (Figure 6.16) . Similarly the sensor resolution

relative to the temperature variation at 0 cm and -25 cm at site GCR8 resulted in an inability to accurately quantify flux at this site. There exists a trade off between burial depth and signal strength as a shallow burial depth may result in a higher amplitude ratio and a non-discernable phase shift in the temperature signal. Hence, in planning streambed temperature surveys it is geneally recommened to deploy multiple sensors with high precision in the top sediment layer to better capture the sinusoidal variation.

6.5.5 Forward Modelling of Streambed Temperature Data for depths below -25cm

We utilized a forward modelling approach to simulate streambed temperature for sensor pairs between -25 to -100cm depth at the six long-term monitoring sites, GCR2, 6, 8, 9, 11 and 13. The model uses temperature perturbations between sampling intervals at the sensor above the model depth to calculate the response at a distance z from the sensor assuming temperature at large depths remains constant. The temperature response at any depth (z) in response to a temperature change is give in equation 2 and repeated below.

$$\Delta T(z,t) = \frac{\Delta T_w}{2}\left[erfc\left(\frac{z - Zt}{2\sqrt{\kappa_e t}}\right) + exp\left(\frac{Zz}{\kappa_e}\right) erfc\left(\frac{z + Zt}{2\sqrt{\kappa_e t}}\right)\right] \quad (0.21)$$

Here, $\Delta T(z,t)$ is the incremental change in temperature in response to a temperature change of ΔT_w at the sensor above the model depth. Silliman et al (1993) developed a superposition solution that models the actual sediment temperature from the summation of all the $\Delta T(z,t)$ prior to time (t) and assuming an initial temperature T_0:

$$T_i(t) = T_0 + \sum \Delta T_i(z,\tau) \quad (0.22)$$

$$\kappa_e = \frac{\lambda_e}{c\rho} \quad (0.23)$$

Where, $\tau = t - t_i$. Each temperature record in the time series is subtracted from the previous value to create a time series of temperature change ΔT_w for the sensor above. T_0 is the pseudo initial condition representing the real temperature at the model depth. The assumption of T_0 results in the predicted temperature differing from actual values for up to the first 200 hrs of the model run and consequently is ignored for flux calculations. The model assumes that the temperature response is due solely to vertical flow of water at a constant velocity throughout the modeling time step. The model was run using measured values for porosity and Lapham curves-derived thermal conductivity (λ_e) and volumetric heat capacity (c) (Table 1) (Lapham 1989). The vertical flow velocity was calculated by minimizing the RMSE between measured temperature record and model response. The onset of the temperature transition period in the temperature profile starting from mid-September resulted in a poor fit to the measured temperature. Consequently, forward modeling was performed for the period of 06/06/13 to 09/15/13 ignoring the first 200hrs of model run (Figure 6.21-22). The measured temperature plots for depths 50 to 100 cm exhibit progressively lower temperature fluctuations with increasing depths. Also, diurnal temperature variations were not observed at these depths.

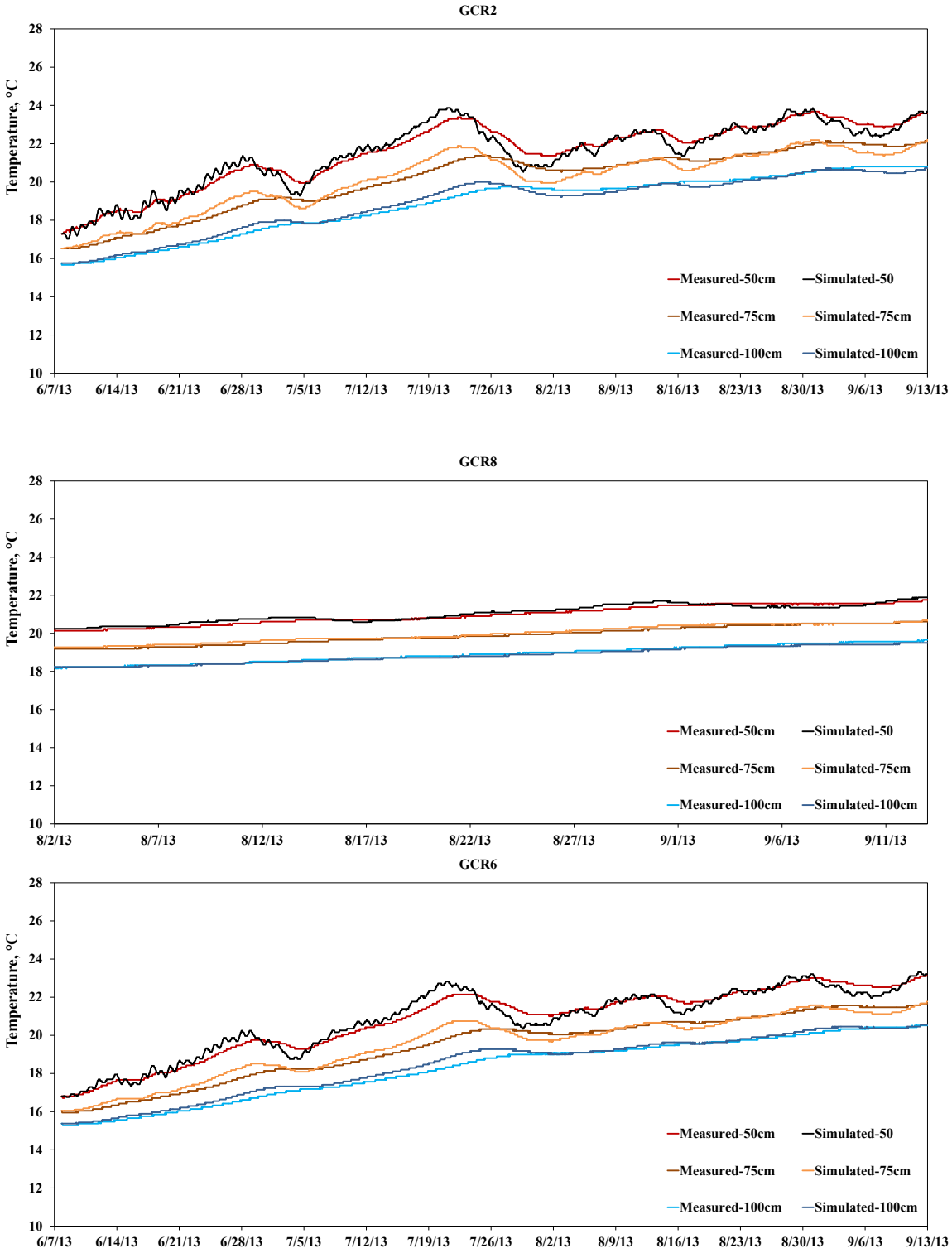

Figure 0.21 Measured and simulated temperature at depths -50cm, -75cm, -100cm for sites GCR2, 6 and 8.

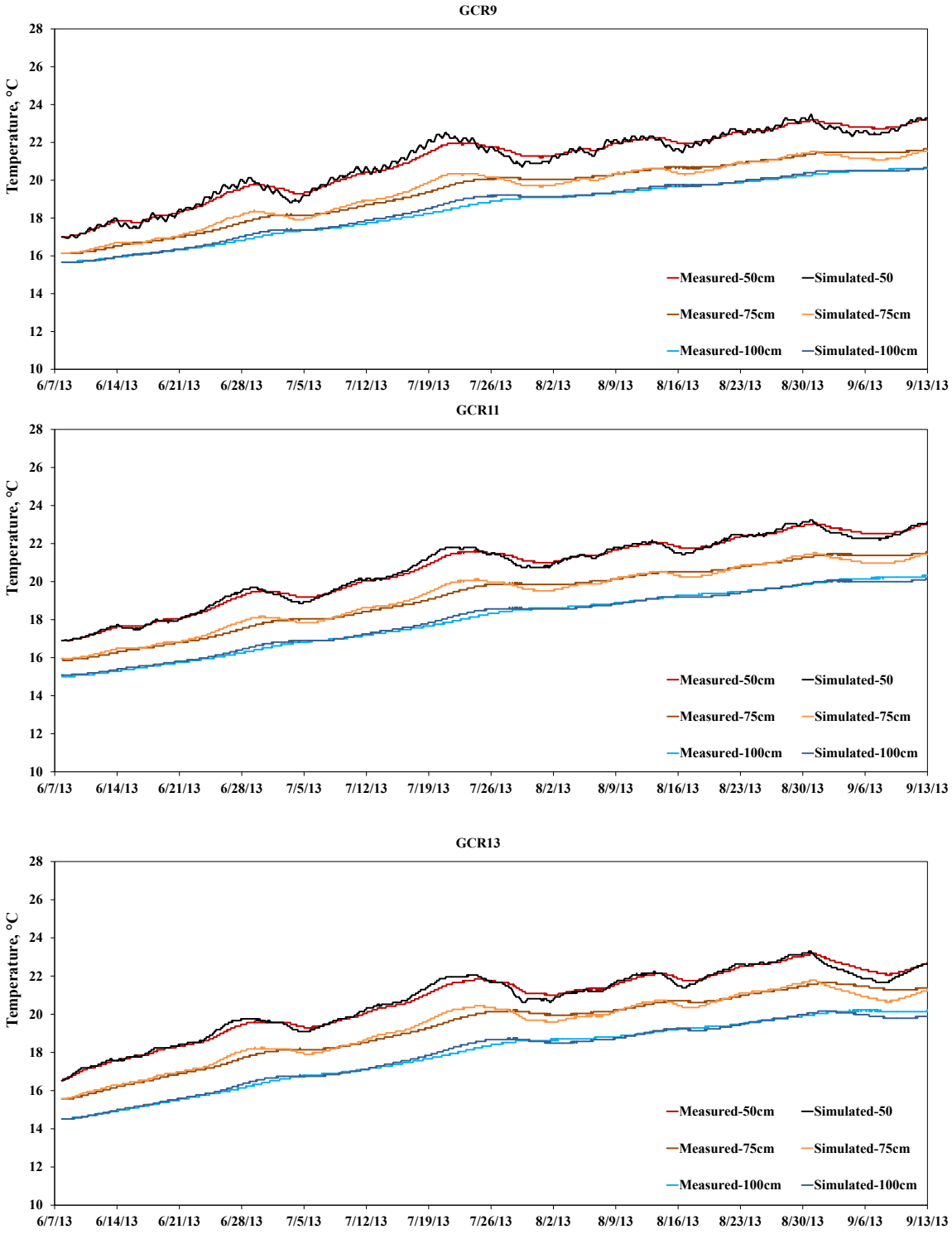

Figure 0.22 Measured and simulated temperature at depths -50cm, -75cm, -100cm for sites GCR9, 11and 13.Less temperature is variability observed at these sites compared to GCR2 and GCR6.

In general the forward model provided a good fit to the measured temperature data capturing the long-term trend in temperature changes at the surface, although intra-day variations were not effectively captured due to sensor precision and sediment heterogeneity.

Darcy velocity estimates from the model fit compare well with the range of velocities previously observed from the McCallum model with all locations having downward velocity indicative of losing condition. The velocities observed at depths greater than 50 cm (representing the contaminated sediment layer) were in the range of 8-28 $x10^{-8}$ m/s and were similar in magnitude to those that were measured at a nearby site by piezometers (personal communication, James Westcott, Tetra Tech). The sediment in 25 – 50 cm zone consisted of both organoclay and contaminated sediment with hydraulic conductivities expectedly larger than those in the contaminated sediment zone. The model correctly predicted higher flow velocities in this depth zone in the range of 1-$6x10^{-6}$ m/s. The subsurface flow at GCR thus exhibited a pattern typically observed at recharge locations where the flow velocity decreases with depth in response to development of horizontal flow paths with increasing depths (Gordon et al. 2012, Briggs et al. 2012).

Table 0.3 Estimated Darcy velocity at all model sites for depth -50, -75 and -100cm depths.

Depth (cm)	Darcy Velocity, m/s					
	GCR 13	**GCR 11C**	**GCR 9**	**GCR 8**	**GCR 6**	**GCR 2**
25-50	5.6E-06	1.1E-06	1.1E-06	8.3E-08	8.3E-07	5.6E-06
50-75	5.6E-07	8.3E-08	1.1E-07	8.3E-08	8.3E-08	2.2E-07
75-100	2.8E-07	8.3E-08	8.3E-08	8.3E-08	8.3E-08	8.3E-08

6.5.6 Implications for capped sites

The fluxes calculated in the top 25 cm of the streambed are representative of vertical surface water exchange to the hyporheic zone. The significantly higher velocities in the armoring layer illustrates the importance of temperature array placement for accurate estimation of Darcy velocity. Velocities determined solely from temperature profiles in the upper armoring layer would overestimate the flux through the active cap by one to two orders of magnitude. These large velocities would suggest a violation of flow continuity in the 1D case, as the areas cannot vary by as much as the velocities do between the armoring layer and the lower cap and sediment layers. Rather, the high velocities likely result from riffle flow or other 2D flow in the porous and highly conductive armoring layer, as has been observed in other studies of streambed exchange [14]. The much higher velocities thus act to diminish temperature gradients in the armoring layer, and may rapidly transport dissolved constituents to the surface.

Given the above observations, it would not be acceptable to view the armor layer as being additionally protective of releases of dissolved constituents into or out of the contaminated sediment pore water beyond that of the underlying active cap. Further the rapid transport of heat across the gravel armor layer in response to higher thermal conductivity and flow velocity contradicts the argument that the armor layer can act as an insulating material in lowering underlying sediment temperatures and thereby decreasing temperature dependent gas production rates as has been argued (Huls and Costello 2005). Capping presents additional uncertainty for estimating flux from heat modeling due to presence of cap layers with widely differing characteristics. However, this can be overcome by using temperature arrays with high vertical resolution and proper sediment

characterization to reduce the associated uncertainty. In spite of these factors heat flux modeling provides a robust method for flux estimation as long as proper analytical methods are used with adequate sensor precision and spacing. The availability of computer programs (such as VFLUX) to process the raw temperature data has streamlined the implementation of the method to allow quantification of time varying flux estimates.

6.6 Conclusion

Analytical solutions for the 1D heat transport equation were successfully implemented to estimate transient Darcy velocity in surface sediment and steady state velocity at deeper depths in a capped sediment using McCallum method and Silliman forward modeling method. Both methods provided robust estimates of Darcy velocity, with higher fluxes in the armor layer and much lower fluxes in the organoclay and underlying contaminated sediment layers. All sites in GCR were found to be losing surface water to the hyporheic zone with evidence of possible gaining conditions at GCR1 on the edge of the cap. The fluxes were strongly influenced by changes in water depth in the stream, reflected by steep increases in net discharge after storm events. Some sites exhibited brief periods of return of bank storage after flood events followed by a return to normal rates of groundwater recharge. The time varying flux estimates provided greater insight into GW-SW exchange pattern at multiple sites along the complex capped stream. The depth varying flux estimates indicated the presence of horizontal hyporheic flow regimes. Although flux estimates across the organoclay layer were complicated by the presence of multiple material types, the method was able to provide relatively consistent estimates of the Darcy velocity that can be used for evaluating chemical breakthrough times and cap

performance with greater certainty. Utilizing heat flux as a tracer to provide flux estimates has great potential for usage as a standard monitoring tool in cap performance and post-capping ground-water surface water exchange assessment.

CHAPTER VII CONCLUSIONS AND IMPLICATIONS

The research described in this dissertation added to the current body of literature on the effectiveness of active capping in mitigating ebullition facilitated contaminant fluxes and in lowering gas ebullition rates, during an active capping sediment remediation in the WBCR. The pre-capping study in the WBCR provided a range of gas flux rates that were similar to that observed in the spring season for urban waterways in Chicago. The measured fluxes were compared with decomposition models in the literature to evaluate the real world applicability of these models in estimating gas ebullition rates. All tested models over predicted the field measured gas ebullition rates in the GCR. This was likely due in part to the fact that flux measurements in the WBGCR were made in late fall of each year when ebullition rates are expected to be lower.

The post-capping field study provided estimates of gas ebullition rates in contaminated sediments capped with permeable sand and organoclay active layer. To the best of my knowledge, only one study (Zhu et al. 2015) has previously reported on post-cap gas ebullition measured in a sand capped test cell (located in Reach 7 of the GCR). This three-year study presented here with measurements at thirteen sites provides a more comprehensive dataset on post-cap ebullition rates and the influence of environmental parameters. Fluxes at sites upstream of the HSD outfall were higher than the range of values (5- 35 mmol/m^2/d) reported in Zhu et al (Zhu et al. 2015), as the Reach 2 sites were influenced by a greater deposition of fresh organic matter on top of the cap. Fluxes at all other sites were within the range reported by Zhu et al [1] and average reductions in gas ebullition were 84%, 63% and 61% for the three post-cap years 2012, 2013 and 2014,

respectively. Comparison with environmental parameters revealed that the post-capping gas fluxes were strongly influenced by sediment temperature and water depth. The gas flux increase in 2013 was accompanied by sediment temperature increases, suggesting that higher temperatures significantly increased microbial kinetics. The study also provided a better understanding of previous research that suggested that the cap and armor acts as an insulating layer. In contrast to previous arguments in the literature, pre and post-capping sediment temperature data showed that the cap is more conductive to heat transport compared to native sediment. This has significant implications on gas production from the contaminated sediment zone below the cap.

Incubation experiments to assess gas production potential showed that cumulative gas production was similar in the CSed and ND layers, whereas the GAL ad OrgC layers exhibited minimal gas production. These results provide further evidence that the CSed layer is ebullition active and thus continued ebullition is likely following capping. Given that the extent of sediment available for gas production is much greater than that of the ND layer, we postulate that the majority of post-cap gas production occurs in the CSed layer, during the study duration. As the thickness of ND layer increases over the years, its contribution to ebullition fluxes is expected to increase, as evidenced by differences in ND layer thickness and ebullition rates at sites upstream of HSD outfall. Further as the CSed layer gets buried deeper, gas production in CSed will depend on availability of nutrients and bacterial/archaeal consortiums that are involved in anaerobic OM degradation and methanogenesis. Consequently, assessing the long-term impact would require continued monitoring of gas production rates.

This study also evaluated active capping performance in mitigating ebullition-facilitated metal and PAH transport. Metal fluxes were lowered by 89-97% with re-suspension of surficial sediment being the primary mode of transport. Any metal transport from beneath the cap is expected to be in the dissolved phase. PAH fluxes also fell sharply in the first year but increased to 60% of pre-capping levels in 2013 and followed again by a decrease in 2014.

The observed trend in PAH fluxes pattern furthered our hypothesis that CSed is ebullition active. The rise and fall of PAH flux in 2013 and 2014 were accompanied by a rise and fall of sediment temperature although average gas fluxes were similar. This suggests that the higher temperatures stimulated increased gas production in the CSed layer thereby increasing PAH partition and transport, resulting in higher measured fluxes. The similar fractional composition of individual PAHs in CSed and in the ebullition trap suggested that PAHs in the trap originated from the CSed layer. The gas fluxes in 2014 could be attributed to elevated gas production in the ND layer. It is postulated that continued deposition increased the thickness of the ND layer compared to 2013, explaining the higher gas and lower PAH fluxes observed in 2014.

Thus post-capping ebullition-facilitated contaminant transport originating from the CSed zone is primarily influenced by sediment temperature and water depth. This field study provided substantial evidence that there is potential for continued gas production from below the cap and for ebullition-facilitated PAH migration into the water column and atmosphere. Increases in average sediment temperatures could reactivate gas generation in the CSed layer, with subsequent potential for cap fracture, enhanced advective transport and lower design breakthrough times. This hypothesis can be further evaluated

by performing a similar study in the summer when the average temperatures are expected to be much higher, resulting in elevated PAH fluxes.

The impact of capping on the sediment Archaeal community structure was evaluated by using phylogenetic analysis of 16 sRNA genes from pre- and post-capping sediment. Analysis revealed an archaeal community structure dominated by methanogens in both pre-and post-capping sediment. Capping resulted in a more diverse distribution of methanogens in the surficial zone, with evidence of methanogenesis occurring via the three major methanogenic pathways: hydrogenotrophic, acetoclastic and C1methylotrophic methanogenesis. In pre-cap sediment, acetoclastic and hydrogenotrophic methanogens were more numerically dominant, with only negligible abundance of methylotrophic methanogens. Field measured gas fluxes were significantly correlated with *Methanosaeta* abundance in pre- and post-capping sediment, suggesting that acetoclastic methanogenesis controls gas production in the GCR. The presence of high abundances of *Methanosaeta* at in all four layers of GCR6 also explained the significantly higher gas production observed at this site. The sequence count and abundance of methanogenic *Archaea* were similar or higher in the CSed layer compared to ND, suggesting that the CSed layer is biologically active. The increasing *Methanosaeta* abundance with sediment depth was consistent with the presence of gas production in deeper sediment layers. Phylogenic analysis, along with results from the field study and incubation experiments provided conclusive evidence that the CSed layer is capable of continued gas production.

This research also explored the potential for using heat tracer methods to evaluate GW-SW interactions and to measure the Darcy velocity in different layers of post-cap

sediment. Two approaches utilizing amplitude/phase shift of sinusoidal signal and forward modeling were used to analyze temperature data in the top 25cm and deeper sediment layers, respectively. The McCallum method (McCallum et al. 2012) provided a more comprehensive insight into the nature of GW-SW interaction in the top 25 cm, with GW fluxes strongly influenced by stream depth and storm events. The analysis revealed that discharge conditions prevail in the top 25 cm at most sites and times, with brief periods of groundwater recharge following storm events. The Darcy flux decreased with depth in the OrgC and CSed layers, suggesting the presence of horizontal flow paths below the gravel layer. The steady-state flux estimated in the OrgC and CSed layers can be used to re-evaluate breakthrough times using the two layer steady state model (Lampert and Reible 2009) or CAPSIM, which are typically used in cap design and assessment. The higher velocities observed in the gravel layer suggest that the armor should not be viewed as additional protection against contaminant migration. Finally, the higher seepage velocities can rapidly transport heat and nutrients to the subsurface thereby increasing the potential for gas production below the cap. Heat tracer methods if implemented properly can provide Darcy estimates with lower uncertainty compared to traditional methods such as seepage meters, mini-piezometers and hydraulic conductivity measurements.

REFERENCES

Achtnich, Christof, Friedhelm Bak, and Ralf Conrad. 1995. "Competition for electron donors among nitrate reducers, ferric iron reducers, sulfate reducers, and methanogens in anoxic paddy soil." *Biology and Fertility of Soils* 19 (1):65-72.

Albert, Daniel B, Christopher S Martens, and Marc J Alperin. 1998. "Biogeochemical processes controlling methane in gassy coastal sediments—Part 2: groundwater flow control of acoustic turbidity in Eckernförde Bay Sediments." *Continental Shelf Research* 18 (14):1771-1793.

Anderson, Iain J, Magdalena Sieprawska-Lupa, Eugene Goltsman, Alla Lapidus, Alex Copeland, Tijana Glavina Del Rio, Hope Tice, Eileen Dalin, Kerrie Barry, and Sam Pitluck. 2009. "Complete genome sequence of Methanocorpusculum labreanum type strain Z." *Standards in Genomic Sciences* 1 (2):197.

Anderson, Mary P. 2005. "Heat as a ground water tracer." *Ground water* 43 (6):951-968.

Arrigoni, Alicia S, Geoffrey C Poole, Leal AK Mertes, Scott J O'Daniel, William W Woessner, and Steven A Thomas. 2008. "Buffered, lagged, or cooled? Disentangling hyporheic influences on temperature cycles in stream channels." *Water Resources Research* 44 (9).

Bae, Hee-Sung, M Elizabeth Holmes, Jeffrey P Chanton, K Ramesh Reddy, and Andrew Ogram. 2015. "Distribution, Activities, and Interactions of Methanogens and Sulfate-Reducing Prokaryotes in the Florida Everglades." *Applied and environmental microbiology* 81 (21):7431-7442.

Bamford, Holly A, Dianne L Poster, and Joel E Baker. 1999. "Temperature dependence of Henry's law constants of thirteen polycyclic aromatic hydrocarbons between 4 C and 31 C." *Environmental Toxicology and Chemistry* 18 (9):1905-1912.

Barber, Robert D, Liyang Zhang, Michelle Harnack, Maynard V Olson, Rajinder Kaul, Cheryl Ingram-Smith, and Kerry S Smith. 2011. "Complete genome sequence of Methanosaeta concilii, a specialist in aceticlastic methanogenesis." *Journal of bacteriology* 193 (14):3668-3669.

Basiliko, Nathan, and Joseph B Yavitt. 2001. "Influence of Ni, Co, Fe, and Na additions on methane production in Sphagnum-dominated Northern American peatlands." *Biogeochemistry* 52 (2):133-153.

Battelle. 2012. Sediment and Water Sampling, West Branch of the Grand Calumer River, Reaches 1 & 2 (Roxana Marsh).

Bear, Jacob. 1972. "Dynamics of fluids in porous media." *Eisevier, New York, 764p*.

Bear, Jacob. 2013. *Dynamics of fluids in porous media*: DoverPublications. com.

Becker, MW, T Georgian, H Ambrose, J Siniscalchi, and K Fredrick. 2004. "Estimating flow and flux of ground water discharge using water temperature and velocity." *Journal of Hydrology* 296 (1):221-233.

Bedessem, Marjorie E, Norbert G Swoboda-Colberg, and Patricia JS Colberg. 1997. "Naphthalene mineralization coupled to sulfate reduction in aquifer-derived enrichments." *FEMS Microbiology Letters* 152 (2):213-218.

Bhaskar, Aditi S, Judson W Harvey, and Eric J Henry. 2012. "Resolving hyporheic and groundwater components of streambed water flux using heat as a tracer." *Water Resources Research* 48 (8).

Boano, Fulvio, Judson W Harvey, Andrea Marion, Aaron I Packman, Roberto Revelli, Luca Ridolfi, and Anders Wörman. 2014. "Hyporheic flow and transport processes: Mechanisms, models, and biogeochemical implications." *Reviews of Geophysics* 52 (4):603-679.

Böhlke, John Karl, Ronald C Antweiler, Judson W Harvey, Andrew E Laursen, Lesley K Smith, Richard L Smith, and Mary A Voytek. 2009. "Multi-scale measurements and modeling of denitrification in streams with varying flow and nitrate concentration in the upper Mississippi River basin, USA." *Biogeochemistry* 93 (1-2):117-141.

Bollmann, Annette, George S Bullerjahn, and Robert Michael McKay. 2014. "Abundance and diversity of ammonia-oxidizing archaea and bacteria in sediments of trophic end members of the Laurentian Great Lakes, Erie and Superior." *PloS one* 9 (5):e97068.

Boon, Paul I, and Alison Mitchell. 1995. "Methanogenesis in the sediments of an Australian freshwater wetland: Comparison with aerobic decay, and factors controlling methanogenesis." *FEMS Microbiology Ecology* 18 (3):175-190.

Boone, David R, William B Whitman, and Pierre Rouvière. 1993. "Diversity and taxonomy of methanogens." In *Methanogenesis*, 35-80. Springer.

Boopathy, R. 2000. "Factors limiting bioremediation technologies." *Bioresource technology* 74 (1):63-67.

Borrel, Guillaume, Anne-Catherine Lehours, Olivier Crouzet, Didier Jézéquel, Karl Rockne, Amélie Kulczak, Emilie Duffaud, Keith Joblin, and Gérard Fonty. 2012. "Stratification of Archaea in the deep sediments of a freshwater meromictic lake: vertical shift from methanogenic to uncultured archaeal lineages." *PloS one* 7 (8):e43346.

Bosse, U, P Frenzel, and R Conrad. 1993. "Inhibition of methane oxidation by ammonium in the surface layer of a littoral sediment." *FEMS Microbiology Ecology* 13 (2):123-134.

Brannon, James M, Douglas Gunnison, Daniel E Averett, James L Martin, and Rex L Chen. 1989. Analyses of impacts of bottom sediments from Grand Calumet River and Indiana Harbor Canal on water quality. DTIC Document.

Bredehoeft, JD, and IS Papaopulos. 1965. "Rates of vertical groundwater movement estimated from the Earth's thermal profile." *Water Resources Research* 1 (2):325-328.

Bremner, JM, and ANDA M BLACKMER. 1978. "Nitrous oxide: emission from soils during nitrification of fertilizer nitrogen." *Science* 199 (4326):295-296.

Bridgham, Scott D, and Curtis J Richardson. 1992. "Mechanisms controlling soil respiration (CO< sub> 2</sub> and CH< sub> 4</sub>) in southern peatlands." *Soil Biology and Biochemistry* 24 (11):1089-1099.

Briggs, Martin A, Laura K Lautz, Jeffrey M McKenzie, Ryan P Gordon, and Danielle K Hare. 2012. "Using high-resolution distributed temperature sensing to quantify spatial and temporal variability in vertical hyporheic flux." *Water Resources Research* 48 (2).

Brochier, Céline, Patrick Forterre, and Simonetta Gribaldo. 2004. "Archaeal phylogeny based on proteins of the transcription and translation machineries: tackling the Methanopyrus kandleri paradox." *Genome biology* 5 (3):R17-R17.

Brochier-Armanet, Céline, Bastien Boussau, Simonetta Gribaldo, and Patrick Forterre. 2008. "Mesophilic Crenarchaeota: proposal for a third archaeal phylum, the Thaumarchaeota." *Nature Reviews Microbiology* 6 (3):245-252.

Brown, John F, Helen Feng, Donna L Bedard, Michael J Brennan, James C Carnahan, and Ralph J May. 1987. "Environmental dechlorination of PCBs." *Environmental Toxicology and Chemistry* 6 (8):579-593.

Butler, Ian B, Martin AA Schoonen, and David T Rickard. 1994. "Removal of dissolved oxygen from water: a comparison of four common techniques." *Talanta* 41 (2):211-215.

Cadillo-Quiroz, Hinsby, Joseph B Yavitt, and Stephen H Zinder. 2009. "Methanosphaerula palustris gen. nov., sp. nov., a hydrogenotrophic methanogen isolated from a minerotrophic fen peatland." *International Journal of Systematic and Evolutionary Microbiology* 59 (5):928-935.

Caissie, Daniel. 2006. "The thermal regime of rivers: a review." *Freshwater Biology* 51 (8):1389-1406.

Cardenas, M Bayani, and John L Wilson. 2007a. "Dunes, turbulent eddies, and interfacial exchange with permeable sediments." *Water Resources Research* 43 (8).

Cardenas, M Bayani, and John L Wilson. 2007b. "Exchange across a sediment–water interface with ambient groundwater discharge." *Journal of Hydrology* 346 (3):69-80.

Casper, Peter, Stephen C Maberly, Grahame H Hall, and Bland J Finlay. 2000. "Fluxes of methane and carbon dioxide from a small productive lake to the atmosphere." *Biogeochemistry* 49 (1):1-19.

Chaban, Bonnie, Sandy YM Ng, and Ken F Jarrell. 2006. "Archaeal habitats-from the extreme to the ordinary." *Canadian journal of microbiology* 52 (2):73-116.

Chanton, Jqfrey P, Christopher S Martens, and Cheryl A Kelley. 1989. "Gas transport from methane-saturated, tidal freshwater and wetland sediments." *Limnol. Oceanogr* 34 (5):807-819.

Che Aziz, Azivy. 2014. "Accumulation and Transformation of Halogenated Biphenyl and Diphenyl Ethers in Urban Sediments."

Chen, Da, Robert C Hale, and Robert J Letcher. 2015. "Photochemical and microbial transformation of emerging flame retardants: Cause for concern?" *Environmental Toxicology and Chemistry* 34 (4):687-699.

Chin, K-J, T Lueders, MW Friedrich, M Klose, and R Conrad. 2004. "Archaeal community structure and pathway of methane formation on rice roots." *Microbial ecology* 47 (1):59-67.

Chin, Kuk-Jeong, Thomas Lukow, Stephan Stubner, and Ralf Conrad. 1999. "Structure and function of the methanogenic archaeal community in stable cellulose-degrading enrichment cultures at two different temperatures (15 and 30° C)." *FEMS microbiology ecology* 30 (4):313-326.

Christensen, Torben R, Anna Ekberg, Lena Ström, Mihail Mastepanov, Nicolai Panikov, Mats Öquist, Bo H Svensson, Hannu Nykänen, Pertti J Martikainen, and Hlynur Oskarsson. 2003. "Factors controlling large scale variations in methane emissions from wetlands." *Geophysical Research Letters* 30 (7):1414.

Cole, James R, Benli Chai, Terry L. Marsh, Ryan J Farris, Qiong Wang, SA Kulam, S Chandra, Donna M McGarrell, Thomas M. Schmidt, and George M. Garrity.

2003. "The Ribosomal Database Project (RDP-II): previewing a new autoaligner that allows regular updates and the new prokaryotic taxonomy." *Nucleic acids research* 31 (1):442-443.

Coles, Janice RP, and Joseph B Yavitt. 2002. "Control of methane metabolism in a forested northern wetland, New York State, by aeration, substrates, and peat size fractions." *Geomicrobiology Journal* 19 (3):293-315.

Conant, Brewster. 2004. "Delineating and quantifying ground water discharge zones using streambed temperatures." *Groundwater* 42 (2):243-257.

Conrad, R. 1999. "Contribution of hydrogen to methane production and control of hydrogen concentrations in methanogenic soils and sediments." *FEMS Microbiology Ecology* 28 (3):193-202.

Conrad, Ralf, Christoph Erkel, and Werner Liesack. 2006. "Rice Cluster I methanogens, an important group of< i> Archaea</i> producing greenhouse gas in soil." *Current opinion in biotechnology* 17 (3):262-267.

Constantz, Jim. 1998. "Interaction between stream temperature, streamflow, and groundwater exchanges in alpine streams." *Water resources research* 34 (7):1609-1615.

Constantz, Jim, Amy E Stewart, Richard Niswonger, and Lisa Sarma. 2002. "Analysis of temperature profiles for investigating stream losses beneath ephemeral channels." *Water Resources Research* 38 (12):52-1-52-13.

Cornelissen, Gerard, Örjan Gustafsson, Thomas D Bucheli, Michiel TO Jonker, Albert A Koelmans, and Paul CM van Noort. 2005. "Extensive sorption of organic compounds to black carbon, coal, and kerogen in sediments and soils: mechanisms and consequences for distribution, bioaccumulation, and biodegradation." *Environmental Science & Technology* 39 (18):6881-6895.

Crozier, CR, I Devai, and RD DeLaune. 1995. "Methane and reduced sulfur gas production by fresh and dried wetland soils." *Soil Science Society of America Journal* 59 (1):277-284.

Cuthbert, MO, R Mackay, V Durand, M-F Aller, RB Greswell, and MO Rivett. 2010. "Impacts of river bed gas on the hydraulic and thermal dynamics of the hyporheic zone." *Advances in Water Resources* 33 (11):1347-1358.

Dalal, RC, DE Allen, SJ Livesley, and G Richards. 2008. "Magnitude and biophysical regulators of methane emission and consumption in the Australian agricultural, forest, and submerged landscapes: a review." *Plant and Soil* 309 (1-2):43-76.

Daniels, LACY, G Fulton, RW Spencer, and WH Orme-Johnson. 1980. "Origin of hydrogen in methane produced by Methanobacterium thermoautotrophicum." *Journal of bacteriology* 141 (2):694-698.

Davies, TR. 1973. "Isolation of bacteria capable of utilizing methane as a hydrogen donor in the process of denitrification." *Water Research* 7 (4):575-579.

De Marsily, Ghislain. 1986. Quantitative hydrogeology. Paris School of Mines, Fontainebleau.

DelSontro, Tonya, Daniel F McGinnis, Sebastian Sobek, Ilia Ostrovsky, and Bernhard Wehrli. 2010. "Extreme methane emissions from a Swiss hydropower reservoir: Contribution from bubbling sediments." *Environmental science & technology* 44 (7):2419-2425.

Demirel, Burak, and Paul Scherer. 2008. "The roles of acetotrophic and hydrogenotrophic methanogens during anaerobic conversion of biomass to methane: a review." *Reviews in Environmental Science and Bio/Technology* 7 (2):173-190.

DeSantis, Todd Z, Philip Hugenholtz, Neils Larsen, Mark Rojas, Eoin L Brodie, Keith Keller, Thomas Huber, Daniel Dalevi, Ping Hu, and Gary L Andersen. 2006. "Greengenes, a chimera-checked 16S rRNA gene database and workbench compatible with ARB." *Applied and environmental microbiology* 72 (7):5069-5072.

Di, Hong J, Keith C Cameron, Ju-Pei Shen, Chris S Winefield, Maureen O'Callaghan, Saman Bowatte, and Ji-Zheng He. 2010. "Ammonia-oxidizing bacteria and archaea grow under contrasting soil nitrogen conditions." *FEMS Microbiology Ecology* 72 (3):386-394.

Dixon, B. 1996. *Bioremediation is here to stay*.

Domenico, Patrick A, and Franklin W Schwartz. 1998. *Physical and chemical hydrogeology*. Vol. 44: Wiley New York.

Dong, Liang F, Cindy J Smith, Sokratis Papaspyrou, Andrew Stott, A Mark Osborn, and David B Nedwell. 2009. "Changes in benthic denitrification, nitrate ammonification, and anammox process rates and nitrate and nitrite reductase gene abundances along an estuarine nutrient gradient (the Colne Estuary, United Kingdom)." *Applied and environmental microbiology* 75 (10):3171-3179.

Dubey, Suresh Kumar, Alpana Singh, Takeshi Watanabe, Susumu Asakawa, Ankit Singla, Hironori Arai, and Kazuyuki Inubushi. 2014. "Methane production potential and methanogenic archaeal community structure in tropical irrigated Indian paddy soils." *Biology and Fertility of Soils* 50 (2):369-379.

Earley, Zachary M, Suhail Akhtar, Stefan J Green, Ankur Naqib, Omair Khan, Abigail R Cannon, Adam M Hammer, Niya L Morris, Xiaoling Li, and Joshua M Eberhardt. 2015. "Burn injury alters the intestinal microbiome and increases gut permeability and bacterial translocation." *PloS one* 10 (7):e0129996.

Eisen, Michael B, Paul T Spellman, Patrick O Brown, and David Botstein. 1998. "Cluster analysis and display of genome-wide expression patterns." *Proceedings of the National Academy of Sciences* 95 (25):14863-14868.

Elliot, AH, and NH Brooks. 1997. "Transfer of nonsorbing solutes to a streambed with bed forms: Laboratory experiments." *Water Resour. Res* 33 (1):137-151.

Falz, K Zepp, C Holliger, R Grosskopf, W Liesack, AN Nozhevnikova, B Müller, B Wehrli, and D Hahn. 1999. "Vertical distribution of methanogens in the anoxic sediment of Rotsee (Switzerland)." *Applied and environmental microbiology* 65 (6):2402-2408.

Farouki, Omar T. 1986. "Thermal properties of soils."

Fechner-Levy, Elizabeth J, and Harold F Hemond. 1996. "Trapped methane volume and potential effects on methane ebullition in a northern peatland." *OCEANOGRAPHY* 41 (7).

Fendinger, Nicholas J, Donald D Adams, and Dwight E Glotfelty. 1992. "The role of gas ebullition in the transport of organic contaminants from sediments." *Science of the total environment* 112 (2):189-201.

Ferry, James G, Paul H Smith, and RS Wolfe. 1974. "Methanospirillum, a New Genus of Methanogenic Bacteria, and Characterization of Methanospirillum hungatii sp. nov." *International Journal of Systematic Bacteriology* 24 (4):465-469.

Fiebig, Douglas M, and Maurice A Lock. 1991. "Immobilization of dissolved organic matter from groundwater discharging through the stream bed." *Freshwater Biology* 26 (1):45-55.

Findlay, Stuart, David Strayer, Cheikh Goumbala, and Kim Gould. 1993. "Metabolism of streamwater dissolved organic carbon in the shallow hyporheic zone." *Limnology and Oceanography* 38 (7):1493-1499.

Foght, Julia M, David L Gutnick, and Donald WS Westlake. 1989. "Effect of emulsan on biodegradation of crude oil by pure and mixed bacterial cultures." *Applied and environmental microbiology* 55 (1):36-42.

Förstner, Ulrich. 1981. "Metal transfer between solid and aqueous phases." In *Metal pollution in the aquatic environment*, 197-270. Springer.

Fritioff, Åsa, L Kautsky, and M Greger. 2005. "Influence of temperature and salinity on heavy metal uptake by submersed plants." *Environmental Pollution* 133 (2):265-274.

Fuller, Christopher C, and Judson W Harvey. 2000. "Reactive uptake of trace metals in the hyporheic zone of a mining-contaminated stream, Pinal Creek, Arizona." *Environmental science & technology* 34 (7):1150-1155.

Garcia, Jean-Louis, Bharat KC Patel, and Bernard Ollivier. 2000. "Taxonomic, Phylogenetic, and Ecological Diversity of Methanogenic< i> Archaea</i>." *Anaerobe* 6 (4):205-226.

Garrity, George M, Julia A Bell, and Timothy G Lilburn. 2004. "Taxonomic outline of the prokaryotes. Bergey's manual of systematic bacteriology." *Springer, New York, Berlin, Heidelberg*.

Ghosh, Upal, Richard G Luthy, Gerard Cornelissen, David Werner, and Charles A Menzie. 2011. "In-situ sorbent amendments: a new direction in contaminated sediment management." *Environmental Science & Technology* 45 (4):1163-1168.

Gidley, Philip T, Seokjoon Kwon, Alexander Yakirevich, Victor S Magar, and Upal Ghosh. 2012. "Advection dominated transport of polycyclic aromatic hydrocarbons in amended sediment caps." *Environmental science & technology* 46 (9):5032-5039.

Glissman, K, K-J Chin, P Casper, and R Conrad. 2004. "Methanogenic pathway and archaeal community structure in the sediment of eutrophic Lake Dagow: effect of temperature." *Microbial ecology* 48 (3):389-399.

Gordon, Ryan P, Laura K Lautz, Martin A Briggs, and Jeffrey M McKenzie. 2012. "Automated calculation of vertical pore-water flux from field temperature time series using the VFLUX method and computer program." *Journal of Hydrology* 420:142-158.

Gordon, Ryan P, Lautz, Laura K. 2015. VFLUX2 Documentation.

Goreau, Thomas J, Warren A Kaplan, Steven C Wofsy, Michael B McElroy, Frederica W Valois, and Stanley W Watson. 1980. "Production of NO2-and N2O by nitrifying bacteria at reduced concentrations of oxygen." *Applied and Environmental Microbiology* 40 (3):526-532.

Goto, Shusaku, Makoto Yamano, and Masataka Kinoshita. 2005. "Thermal response of sediment with vertical fluid flow to periodic temperature variation at the surface." *Journal of Geophysical Research: Solid Earth (1978–2012)* 110 (B1).

Graças, Diego A, Paulo R Miranda, Rafael A Baraúna, John A McCulloch, Rubens Ghilardi Jr, Maria Paula C Schneider, and Artur Silva. 2011. "Microbial diversity of an anoxic zone of a hydroelectric power station reservoir in Brazilian Amazonia." *Microbial ecology* 62 (4):853-861.

Green, Stefan J, Raghavee Venkatramanan, and Ankur Naqib. 2015. "Deconstructing the Polymerase Chain Reaction: Understanding and Correcting Bias Associated with Primer Degeneracies and Primer-Template Mismatches." *PloS one* 10 (5):e0128122.

Haggerty, Roy, Eugènia Martí, Alba Argerich, Daniel Von Schiller, and Nancy B Grimm. 2009. "Resazurin as a "smart" tracer for quantifying metabolically active transient storage in stream ecosystems." *Journal of Geophysical Research: Biogeosciences (2005–2012)* 114 (G3).

Hanson, Richard S, and Thomas E Hanson. 1996. "Methanotrophic bacteria." *Microbiological reviews* 60 (2):439-471.

Hao, Oliver J, Jin M Chen, Li Huang, and Robert L Buglass. 1996. "Sulfate-reducing bacteria." *Critical reviews in environmental science and technology* 26 (2):155-187.

Harvey, Judson W, Brian J Wagner, and Kenneth E Bencala. 1996. "Evaluating the reliability of the stream tracer approach to characterize stream-subsurface water exchange." *Water Resources Research* 32 (8):2441-2451.

Hatch, Christine E, Andrew T Fisher, Justin S Revenaugh, Jim Constantz, and Chris Ruehl. 2006. "Quantifying surface water–groundwater interactions using time series analysis of streambed thermal records: Method development." *Water Resources Research* 42 (10).

Hedin, Lars O, Joseph C von Fischer, Nathaniel E Ostrom, Brian P Kennedy, Michael G Brown, and G Philip Robertson. 1998. "Thermodynamic Constraints On Nitrogentransformations And Other Biogeochemicalprocesses At Soil-Stream Interfaces." *Ecology* 79 (2):684-703.

Himmelheber, David W, Martial Taillefert, Kurt D Pennell, and Joseph B Hughes. 2008. "Spatial and temporal evolution of biogeochemical processes following in situ capping of contaminated sediments." *Environmental science & technology* 42 (11):4113-4120.

Himmelheber, David W, Sara H Thomas, Frank E Löffler, Martial Taillefert, and Joseph B Hughes. 2008. "Microbial colonization of an in situ sediment cap and correlation to stratified redox zones." *Environmental science & technology* 43 (1):66-74.

Himmelheber, David W., Kurt D. Pennell, and Joseph B. Hughes. 2007. "Natural attenuation processes during in situ capping." *Environmental science & technology* 41 (15):5306-5313.

Hopmans, Jan W, Jirka Šimunek, and Keith L Bristow. 2002. "Indirect estimation of soil thermal properties and water flux using heat pulse probe measurements: Geometry and dispersion effects." *Water Resources Research* 38 (1):1006.

Hornberger, GM, KE Bencala, and DM McKnight. 1994. "Hydrological controls on dissolved organic carbon during snowmelt in the Snake River near Montezuma, Colorado." *Biogeochemistry* 25 (3):147-165.

Hou, AX, GX Chen, ZP Wang, Oswald Van Cleemput, and WH Patrick. 2000. "Methane and nitrous oxide emissions from a rice field in relation to soil redox and microbiological processes." *Soil Science Society of America Journal* 64 (6):2180-2186.

Huls, Hubert, and Michael Costello. 2005. "Designing assessments for decision making for remediation of contaminated sediments." Third International Conference on Remediation of Contaminated Sediments, New Orleans, LA, January 24-27.

Huson, Daniel H, Alexander F Auch, Ji Qi, and Stephan C Schuster. 2007. "MEGAN analysis of metagenomic data." *Genome research* 17 (3):377-386.

Huttunen, Jari T, K Matti Lappalainen, Erkki Saarijärvi, Tero Väisänen, and Pertti J Martikainen. 2001. "A novel sediment gas sampler and a subsurface gas collector used for measurement of the ebullition of methane and carbon dioxide from a eutrophied lake." *Science of the total environment* 266 (1):153-158.

Inubushi, K, S Otake, Y Furukawa, N Shibasaki, M Ali, AM Itang, and H Tsuruta. 2005. "Factors influencing methane emission from peat soils: comparison of tropical and temperate wetlands." *Nutrient cycling in Agroecosystems* 71 (1):93-99.

Itoh, Takashi, and Takao Iino. 2013. "Phylogeny and biological features of thermophiles." In *Thermophilic Microbes in Environmental and Industrial Biotechnology*, 249-270. Springer.

J.Constantz, D.A. Stonestrom;. 2004. "Using Temperature to Study Stream-Ground Water Exchanges." *USGS Fact Sheet*.

Jacobs, Patrick H., and Ulrich Förstner. 1999. "Concept of subaqueous capping of contaminated sediments with active barrier systems (ABS) using natural and modified zeolites." *Water research* 33 (9):2083-2087.

Jaynes, DB. 1990. "Temperature variations effect on field-measured infiltration." *Soil Science Society of America Journal* 54 (2):305-312.

Jia, Zhongjun, and Ralf Conrad. 2009. "Bacteria rather than Archaea dominate microbial ammonia oxidation in an agricultural soil." *Environmental microbiology* 11 (7):1658-1671.

Jiang, B, SN Parshina, W Van Doesburg, BP Lomans, and AJM Stams. 2005. "Methanomethylovorans thermophila sp. nov., a thermophilic, methylotrophic methanogen from an anaerobic reactor fed with methanol." *International journal of systematic and evolutionary microbiology* 55 (6):2465-2470.

Jobbágy, Esteban G, and Robert B Jackson. 2000. "The vertical distribution of soil organic carbon and its relation to climate and vegetation." *Ecological applications* 10 (2):423-436.

Johnson, Nathan W, Danny D Reible, and Lynn E Katz. 2010. "Biogeochemical Changes and Mercury Methylation beneath an In-Situ Sediment Cap†." *Environmental science & technology* 44 (19):7280-7286.

Josefsson, Sarah, Morten Schaanning, Göran S Samuelsson, Jonas S Gunnarsson, Ida Olofsson, Espen Eek, and Karin Wiberg. 2012. "Capping efficiency of various carbonaceous and mineral materials for in situ remediation of polychlorinated dibenzo-p-dioxin and dibenzofuran contaminated marine sediments: Sediment-to-

water fluxes and bioaccumulation in boxcosm tests." *Environmental science & technology* 46 (6):3343-3351.

Joulian, C, B Ollivier, BKC Patel, and Pierre-Armand Roger. 1998. "Phenotypic and phylogenetic characterization of dominant culturable methanogens isolated from ricefield soils." *FEMS Microbiology Ecology* 25 (2):135-145.

Kaiser, Jocelyn. 2000. "Just how bad is dioxin?" *Science* 288 (5473):1941-1944.

Kalbus, E, F Reinstorf, and M Schirmer. 2006. "Measuring methods for groundwater–surface water interactions: a review." *Hydrology and Earth System Sciences* 10 (6):873-887.

Keery, John, Andrew Binley, Nigel Crook, and Jonathan WN Smith. 2007. "Temporal and spatial variability of groundwater–surface water fluxes: development and application of an analytical method using temperature time series." *Journal of Hydrology* 336 (1):1-16.

Keller, Michael, and Robert F Stallard. 1994. "Methane emission by bubbling from Gatun Lake, Panama." *Journal of Geophysical Research: Atmospheres (1984–2012)* 99 (D4):8307-8319.

Kittelmann, Sandra, Henning Seedorf, William A Walters, Jose C Clemente, Rob Knight, Jeffrey I Gordon, and Peter H Janssen. 2013. "Simultaneous amplicon sequencing to explore co-occurrence patterns of bacterial, archaeal and eukaryotic microorganisms in rumen microbial communities." *PLoS One* 8 (2):e47879.

Knowles, Roger. 1982. "Denitrification." *Microbiological reviews* 46 (1):43.

Knox, Anna S, Michael H Paller, and Jesse Roberts. 2012. "Active capping technology—New approaches for in situ remediation of contaminated sediments." *Remediation Journal* 22 (2):93-117.

Knox, Anna Sophia, Michael H Paller, Danny D Reible, Xingmao Ma, and Ioana G Petrisor. 2008. "Sequestering agents for active caps—remediation of metals and organics." *Soil & sediment contamination* 17 (5):516-532.

Koike, Isao, and Akihiko Hattori. 1978. "Denitrification and ammonia formation in anaerobic coastal sediments." *Applied and Environmental Microbiology* 35 (2):278-282.

Könneke, Martin, Anne E Bernhard, R José, Christopher B Walker, John B Waterbury, and David A Stahl. 2005. "Isolation of an autotrophic ammonia-oxidizing marine archaeon." *Nature* 437 (7058):543-546.

Kuiper, Irene, Ellen L. Lagendijk, Guido V. Bloemberg, and Ben J. J. Lugtenberg. 2004. "Rhizoremediation: a beneficial plant-microbe interaction." *Molecular Plant-Microbe Interactions* 17 (1):6-15.

Kurr, Margit, Robert Huber, Helmut König, Holger W Jannasch, Hans Fricke, Antonio Trincone, Jakob K Kristjansson, and Karl O Stetter. 1991. "Methanopyrus kandleri, gen. and sp. nov. represents a novel group of hyperthermophilic methanogens, growing at 110 C." *Archives of Microbiology* 156 (4):239-247.

Laanbroek, Hendrikus J, Harm J Geerligs, Lolke Sijtsma, and Hans Veldkamp. 1984. "Competition for sulfate and ethanol among Desulfobacter, Desulfobulbus, and Desulfovibrio species isolated from intertidal sediments." *Applied and environmental microbiology* 47 (2):329-334.

Lampert, David J, and Danny Reible. 2009. "An analytical modeling approach for evaluation of capping of contaminated sediments." *Soil and Sediment Contamination* 18 (4):470-488.

Lapham, Wayne W. 1989. Use of temperature profiles beneath streams to determine rates of vertical ground-water flow and vertical hydraulic conductivity. Dept. of the Interior, US Geological Survey; USGPO; Books and Open-File Reports Section, US Geological Survey [distributor].

Lautz, Laura K. 2010. "Impacts of nonideal field conditions on vertical water velocity estimates from streambed temperature time series." *Water Resources Research* 46 (1).

Li, An, Karl J Rockne, Neil Sturchio, Wenlu Song, Justin C Ford, and Hua Wei. 2009. "PCBs in sediments of the Great Lakes–Distribution and trends, homolog and chlorine patterns, and in situ degradation." *Environmental pollution* 157 (1):141-147.

Liu, Chunhua, Jennifer A Jay, Raveendra Ika, James P Shine, and Timothy E Ford. 2001. "Capping efficiency for metal-contaminated marine sediment under conditions of submarine groundwater discharge." *Environmental science & technology* 35 (11):2334-2340.

Lomans, Bart P, Ronald Maas, Rianne Luderer, Huub JM Op den Camp, Arjan Pol, Chris van der Drift, and Godfried D Vogels. 1999. "Isolation and characterization of Methanomethylovorans hollandica gen. nov., sp. nov., isolated from freshwater sediment, a methylotrophic methanogen able to grow on dimethyl sulfide and methanethiol." *Applied and environmental microbiology* 65 (8):3641-3650.

Lomans, Bart P, A Smolders, Lucienne M Intven, Arjan Pol, De Op, and C Van Der Drift. 1997. "Formation of dimethyl sulfide and methanethiol in anoxic freshwater sediments." *Applied and Environmental Microbiology* 63 (12):4741-4747.

Lovley, Derek R. 1991. "Dissimilatory Fe (III) and Mn (IV) reduction." *microbiological reviews* 55 (2):259.

Lovley, Derek R, John D Coates, Elizabeth L Blunt-Harris, Elizabeth JP Phillips, and Joan C Woodward. 1996. "Humic substances as electron acceptors for microbial respiration." *Nature* 382 (6590):445-448.

Lovley, Derek R, Stephen J Giovannoni, David C White, James E Champine, EJP Phillips, Yuri A Gorby, and Steve Goodwin. 1993. "Geobacter metallireducens gen. nov. sp. nov., a microorganism capable of coupling the complete oxidation of organic compounds to the reduction of iron and other metals." *Archives of microbiology* 159 (4):336-344.

Lovley, Derek R, and Michael J Klug. 1986. "Model for the distribution of sulfate reduction and methanogenesis in freshwater sediments." *Geochimica et Cosmochimica Acta* 50 (1):11-18.

Lovley, Derek R, and Elizabeth JP Phillips. 1986. "Organic matter mineralization with reduction of ferric iron in anaerobic sediments." *Applied and environmental microbiology* 51 (4):683-689.

Lovley, Derek R, and Elizabeth JP Phillips. 1987. "Competitive mechanisms for inhibition of sulfate reduction and methane production in the zone of ferric iron reduction in sediments." *Applied and Environmental Microbiology* 53 (11):2636-2641.

Lovley, Derek R, and Elizabeth JP Phillips. 1988. "Novel mode of microbial energy metabolism: organic carbon oxidation coupled to dissimilatory reduction of iron or manganese." *Applied and environmental microbiology* 54 (6):1472-1480.

Lovley, Derek R. 2000. "Anaerobic benzene degradation." *Biodegradation* 11 (2-3):107-116.

Luce, Charles H, Daniele Tonina, Frank Gariglio, and Ralph Applebee. 2013. "Solutions for the diurnally forced advection-diffusion equation to estimate bulk fluid velocity and diffusivity in streambeds from temperature time series." *Water Resources Research* 49 (1):488-506.

Mackay, Donald, Wan Ying Shiu, and Russell P Sutherland. 1979. "Determination of air-water Henry's law constants for hydrophobic pollutants." *Environmental Science & Technology* 13 (3):333-337.

Makkar, Randhir S, and Karl J Rockne. 2003. "Comparison of synthetic surfactants and biosurfactants in enhancing biodegradation of polycyclic aromatic hydrocarbons." *Environmental Toxicology and Chemistry* 22 (10):2280-2292.

MallaáShrestha, Pravin. 2014. "A new model for electron flow during anaerobic digestion: direct interspecies electron transfer to Methanosaeta for the reduction of carbon dioxide to methane." *Energy & Environmental Science* 7 (1):408-415.

Martens, Christopher S, Cheryl A Kelley, Jeffrey P Chanton, and William J Showers. 1992. "Carbon and hydrogen isotopic characterization of methane from wetlands and lakes of the Yukon-Kuskokwim delta, western Alaska." *Journal of Geophysical Research: Atmospheres (1984–2012)* 97 (D15):16689-16701.

Martens, Christopher S., and J. Val Klump. 1980. "Biogeochemical cycling in an organic-rich coastal marine basin—I. Methane sediment-water exchange processes." *Geochimica et Cosmochimica Acta* 44 (3):471-490. doi: http://dx.doi.org/10.1016/0016-7037(80)90045-9.

Martínez-Jerónimo, Fernando, Jade Lizette Cruz-Cisneros, and Leonardo García-Hernández. 2008. "A comparison of the response of< i> Simocephalus mixtus</i>(Cladocera) and< i> Daphnia magna</i> to contaminated freshwater sediments." *Ecotoxicology and environmental safety* 71 (1):26-31.

Matson, Pamela A, and Robert C Harriss. 2009. *Biogenic trace gases: measuring emissions from soil and water*: John Wiley & Sons.

McCallum, AM, MS Andersen, GC Rau, and RI Acworth. 2012. "A 1-D analytical method for estimating surface water–groundwater interactions and effective thermal diffusivity using temperature time series." *Water Resources Research* 48 (11).

McCartney, Daryl M, and Jan A Oleszkiewicz. 1993. "Competition between methanogens and sulfate reducers: effect of COD: sulfate ratio and acclimation." *Water Environment Research*:655-664.

McCartney, DM, and JA Oleszkiewicz. 1991. "Sulfide inhibition of anaerobic degradation of lactate and acetate." *Water Research* 25 (2):203-209.

McDonough, Kathleen M, and David A Dzombak. 2005. "Microcosm experiments to assess the effects of temperature and microbial activity on polychlorinated biphenyl transport in anaerobic sediment." *Environmental science & technology* 39 (24):9517-9522.

McKew, Boyd A, Alex J Dumbrell, Joe D Taylor, Terry J McGenity, and Graham JC Underwood. 2013. "Differences between aerobic and anaerobic degradation of microphytobenthic biofilm-derived organic matter within intertidal sediments." *FEMS microbiology ecology* 84 (3):495-509.

McLinn, Eugene L, and Thomas R Stolzenburg. 2009. "Ebullition-Facilitated Transport of Manufactured Gas Plant Tar from Contaminated Sediment." *Environmental toxicology and chemistry* 28 (11):2298-2306.

McNally, Dan L, James R Mihelcic, and Donald R Lueking. 1998. "Biodegradation of three-and four-ring polycyclic aromatic hydrocarbons under aerobic and denitrifying conditions." *Environmental science & technology* 32 (17):2633-2639.

Meyers, Philip A, and Brian J Eadie. 1993. "Sources, degradation and recycling of organic matter associated with sinking particles in Lake Michigan." *Organic Geochemistry* 20 (1):47-56.

Middelburg, Jack J. 1989. "A simple rate model for organic matter decomposition in marine sediments." *Geochimica et Cosmochimica Acta* 53 (7):1577-1581.

Mittal, Menka, and Karl J Rockne. 2008. "Indole production by Pseudomonas stutzeri strain NAP-3 during anaerobic naphthalene biodegradation in the presence of dimethyl formamide." *Journal of Environmental Science and Health Part A* 43 (9):1027-1034.

Mogollón, José M, Ivan L'Heureux, Andrew W Dale, and Pierre Regnier. 2009. "Methane gas-phase dynamics in marine sediments: A model study." *American journal of science* 309 (3):189-220.

Molina-Giraldo, Nelson, Peter Bayer, and Philipp Blum. 2011. "Evaluating the influence of thermal dispersion on temperature plumes from geothermal systems using analytical solutions." *International Journal of Thermal Sciences* 50 (7):1223-1231.

MOLONGOSKI, JOHN J, and MICHAEL J KLUG. 1980. "Anaerobic metabolism of particulate organic matter in the sediments of a hypereutrophic lake*." *Freshwater Biology* 10 (6):507-518.

Monograph, Iarc. 1983. "Evaluation of the carcinogenic risk of chemicals to humans." *Polynuclear Aromatic Compounds, Part* 1:245.

Morris, Stephan W, Mark N Kirstein, Marcus B Valentine, Kristopher G Dittmer, David N Shapiro, David L Saltman, and A Thomas Look. 1994. "Fusion of a kinase gene, ALK, to a nucleolar protein gene, NPM, in non-Hodgkin's lymphoma." *Science* 263 (5151):1281-1284.

Mosier, Arvin, Reiner Wassmann, Louis Verchot, Jennifer King, and Cheryl Palm. 2004. "Methane and nitrogen oxide fluxes in tropical agricultural soils: sources, sinks and mechanisms." In *Tropical Agriculture in Transition—Opportunities for Mitigating Greenhouse Gas Emissions?*, 11-49. Springer.

Murphy, Paul, Andre Marquette, Danny Reible, and Gregory V. Lowry. 2006. "Predicting the performance of activated carbon-, coke-, and soil-amended thin layer sediment caps." *Journal of Environmental Engineering* 132 (7):787-794.

Nakajima, F., Anders Baun, Anna Ledin, and P. Mikkelsen. 2005. "A novel method for evaluating bioavailability of polycyclic aromatic hydrocarbons in sediments of an urban stream." *Water Science & Technology* 51 (3-4):275-281.

Nelson, Kären C, and Margaret A Palmer. 2007. "Stream Temperature Surges Under Urbanization and Climate Change: Data, Models, and Responses1." *JAWRA Journal of the American Water Resources Association* 43 (2):440-452.

Nüsslein, Bernhard, Kuk-Jeong Chin, Werner Eckert, and Ralf Conrad. 2001. "Evidence for anaerobic syntrophic acetate oxidation during methane production in the profundal sediment of subtropical Lake Kinneret (Israel)." *Environmental microbiology* 3 (7):460-470.

Oberbremer, A, R Müller-Hurtig, and F Wagner. 1990. "Effect of the addition of microbial surfactants on hydrocarbon degradation in a soil population in a stirred reactor." *Applied Microbiology and biotechnology* 32 (4):485-489.

Oen, Amy MP, Elisabeth ML Janssen, Gerard Cornelissen, Gijs D Breedveld, Espen Eek, and Richard G Luthy. 2011. "In situ measurement of PCB pore water concentration profiles in activated carbon-amended sediment using passive samplers." *Environmental science & technology* 45 (9):4053-4059.

Office, Us-Epa Great Lakes National Program. 1998. "Realizing Remediation: A Summary of Contaminated Sediment Remediation Activities in the Great Lakes Basin."

Offre, Pierre, James I Prosser, and Graeme W Nicol. 2009. "Growth of ammonia-oxidizing archaea in soil microcosms is inhibited by acetylene." *FEMS microbiology ecology* 70 (1):99-108.

Olsta, James T, and C Hornaday. 2007. "Installation of an in-situ cap at a superfund site." Battelle Conference Savannah, Paper D-025.

Ondov, Brian D, Nicholas H Bergman, and Adam M Phillippy. 2011. "Interactive metagenomic visualization in a Web browser." *BMC bioinformatics* 12 (1):385.

Paiva, Sandra, Frederic Devaux, Sonia Barbosa, Claude Jacq, and Margarida Casal. 2004. "Ady2p is essential for the acetate permease activity in the yeast Saccharomyces cerevisiae." *Yeast* 21 (3):201-210.

Parsons, Myles L. 1970. "Groundwater thermal regime in a glacial complex." *Water Resources Research* 6 (6):1701-1720.

Perelo, Louisa Wessels. 2010. "Review: in situ and bioremediation of organic pollutants in aquatic sediments." *Journal of hazardous materials* 177 (1):81-89.

Pratscher, Jennifer, Marc G Dumont, and Ralf Conrad. 2011. "Ammonia oxidation coupled to CO2 fixation by archaea and bacteria in an agricultural soil." *Proceedings of the National Academy of Sciences* 108 (10):4170-4175.

Prieme, Anders. 1994. "Production and emission of methane in a brackish and a freshwater wetland." *Soil Biology and Biochemistry* 26 (1):7-18.

Pruesse, Elmar, Christian Quast, Katrin Knittel, Bernhard M Fuchs, Wolfgang Ludwig, Jörg Peplies, and Frank Oliver Glöckner. 2007. "SILVA: a comprehensive online resource for quality checked and aligned ribosomal RNA sequence data compatible with ARB." *Nucleic acids research* 35 (21):7188-7196.

Quadrini, James D, Heather M VanDewalker, Joseph E Mihm, and Lawrence J McShea. 2003. "Pilot-scale demonstration of in situ capping of PCB-containing sediments in the lower Grasse River." *Remediation Journal* 14 (1):33-53.

Raghoebarsing, Ashna A, Arjan Pol, Katinka T Van de Pas-Schoonen, Alfons JP Smolders, Katharina F Ettwig, W Irene C Rijpstra, Stefan Schouten, Jaap S Sinninghe Damsté, Huub JM Op den Camp, and Mike SM Jetten. 2006. "A

microbial consortium couples anaerobic methane oxidation to denitrification." *Nature* 440 (7086):918-921.

Rau, Gabriel C, Martin S Andersen, Andrew M McCallum, and Richard Ian Acworth. 2010. "Analytical methods that use natural heat as a tracer to quantify surface water–groundwater exchange, evaluated using field temperature records." *Hydrogeology Journal* 18 (5):1093-1110.

Rau, Gabriel C, Mark O Cuthbert, Andrew M McCallum, Landon JS Halloran, and Martin S Andersen. 2015. "Assessing the accuracy of 1-D analytical heat tracing for estimating near-surface sediment thermal diffusivity and water flux under transient conditions." *Journal of Geophysical Research: Earth Surface* 120 (8):1551-1573.

Reible, D, Xiaoxia Lu, Lisa Moretti, Jasmine Galjour, and Xingmao Ma. 2007. "Organoclays for the capping of contaminated sediments." Fifth International Conference on Remediation of Contaminated Sediments, Savannah, GA.

Reible, Danny, David Lampert, David Constant, Robert D. Mutch Jr, and Yuewei Zhu. 2006. "Active capping demonstration in the Anacostia River, Washington, DC." *Remediation Journal* 17 (1):39-53.

Rockne, K, and R Kaliappan. 2013. Post-capping sediment gas ebullition study Grand Calumet River, western brach reaches 1 and 2. United States Army Corps of Engineers-Chicago District.

Rockne, K, R Kaliappan, and G Bourgon. 2011. Sediment gas ebullition study Grand Calumet RIver, western branch reaches 1 and 2. Submitted to United States Army Corps-Chicago District.

Rockne, K, P Viana, and K Yin. 2010. Sediment Ebullition and Flux Studies at Bubbly Creek, Chicago, IL, Final Report. United State Army Corps of Engineers Chicago District.

Rockne, Karl J, and Patrick L Brezonik. 2006. "Nutrient removal in a cold-region wastewater stabilization pond: importance of ammonia volatilization." *Journal of environmental engineering* 132 (4):451-459.

Rockne, Karl J, Joanne C Chee-Sanford, Robert A Sanford, Brian P Hedlund, James T Staley, and Stuart E Strand. 2000. "Anaerobic naphthalene degradation by microbial pure cultures under nitrate-reducing conditions." *Applied and Environmental Microbiology* 66 (4):1595-1601.

Rockne, Karl J, and Krishna R Reddy. 2003. "Bioremediation of contaminated sites." *Invited Theme Paper, International e-Conference on Modern Trends in Foundation Engineering: Geotechnical Challenges and Solutions, Indian Institute of Technology, Madras, India*.

Rockne, Karl J, and Stuart E Strand. 1998. "Biodegradation of bicyclic and polycyclic aromatic hydrocarbons in anaerobic enrichments." *Environmental science & technology* 32 (24):3962-3967.

Rockne, Karl J, and Stuart E Strand. 2001. "Anaerobic biodegradation of naphthalene, phenanthrene, and biphenyl by a denitrifying enrichment culture." *Water research* 35 (1):291-299.

Roden, Eric E. 2003. "Diversion of electron flow from methanogenesis to crystalline Fe (III) oxide reduction in carbon-limited cultures of wetland sediment microorganisms." *Applied and environmental microbiology* 69 (9):5702-5706.

Rouse, Joseph D., David A. Sabatini, R. Eric Brown, and Jeffrey H. Harwell. 1996. "Evaluation of ethoxylated alkylsulfate surfactants for use in subsurface remediation." *Water Environment Research* 68 (2):162-168.

Roy, Réal, and Roger Knowles. 1994. "Effects of methane metabolism on nitrification and nitrous oxide production in polluted freshwater sediment." *Applied and environmental microbiology* 60 (9):3307-3314.

Sakai, Sanae, Hiroyuki Imachi, Satoshi Hanada, Akiyoshi Ohashi, Hideki Harada, and Yoichi Kamagata. 2008. "Methanocella paludicola gen. nov., sp. nov., a methane-producing archaeon, the first isolate of the lineage 'Rice Cluster I', and proposal of the new archaeal order Methanocellales ord. nov." *International Journal of Systematic and Evolutionary Microbiology* 58 (4):929-936.

Sarmiento, Felipe B, John A Leigh, and William B Whitman. 2011. "Genetic systems for hydrogenotrophic methanogens." *Methods in enzymology* 494:43-73.

Schindler, John E, and David P Krabbenhoft. 1998. "The hyporheic zone as a source of dissolved organic carbon and carbon gases to a temperate forested stream." *Biogeochemistry* 43 (2):157-174.

Schlegel, Katharina, Cornelia Welte, Uwe Deppenmeier, and Volker Müller. 2012. "Electron transport during aceticlastic methanogenesis by Methanosarcina acetivorans involves a sodium-translocating Rnf complex." *FEBS Journal* 279 (24):4444-4452.

Schmidt, C, M Bayer-Raich, and M Schirmer. 2006. "Characterization of spatial heterogeneity of groundwater-stream water interactions using multiple depth streambed temperature measurements at the reach scale." *Hydrology and Earth System Sciences Discussions* 3 (4):1419-1446.

Segers, Reinoud. 1998. "Methane production and methane consumption: a review of processes underlying wetland methane fluxes." *Biogeochemistry* 41 (1):23-51.

Shanafield, Margaret, Christine Hatch, and Greg Pohll. 2011. "Uncertainty in thermal time series analysis estimates of streambed water flux." *Water Resources Research* 47 (3).

Shima, Seigo, David A Hérault, Albrecht Berkessel, and Rudolf K Thauer. 1998. "Activation and thermostabilization effects of cyclic 2, 3-diphosphoglycerate on enzymes from the hyperthermophilic Methanopyrus kandleri." *Archives of microbiology* 170 (6):469-472.

Silliman, Stephen E, and David F Booth. 1993. "Analysis of time-series measurements of sediment temperature for identification of gaining vs. losing portions of Juday Creek, Indiana." *Journal of Hydrology* 146:131-148.

Silliman, Stephen E, Jose Ramirez, and Raye L McCabe. 1995. "Quantifying downflow through creek sediments using temperature time series: One-dimensional solution incorporating measured surface temperature." *Journal of Hydrology* 167 (1):99-119.

Simpson, Stuart L, Ian D Pryor, Ben R Mewburn, Graeme E Batley, and Dianne Jolley. 2002. "Considerations for capping metal-contaminated sediments in dynamic estuarine environments." *Environmental science & technology* 36 (17):3772-3778.

Slesarev, Alexei I, Katja V Mezhevaya, Kira S Makarova, Nikolai N Polushin, Olga V Shcherbinina, Vera V Shakhova, Galina I Belova, L Aravind, Darren A Natale,

and Igor B Rogozin. 2002. "The complete genome of hyperthermophile Methanopyrus kandleri AV19 and monophyly of archaeal methanogens." *Proceedings of the National Academy of Sciences* 99 (7):4644-4649.

Smith, Douglas R, Lynn A Doucette-Stamm, C Deloughery, H Lee, J Dubois, T Aldredge, R Bashirzadeh, D Blakely, R Cook, and K Gilbert. 1997. "Complete genome sequence of Methanobacterium thermoautotrophicum deltaH: functional analysis and comparative genomics." *Journal of Bacteriology* 179 (22):7135.

Smith, Kerry S, and Cheryl Ingram-Smith. 2007. "Methanosaeta, the forgotten methanogen?" *Trends in microbiology* 15 (4):150-155.

Smith, Leslie, and David S Chapman. 1983. "On the thermal effects of groundwater flow: 1. Regional scale systems." *Journal of Geophysical Research: Solid Earth (1978–2012)* 88 (B1):593-608.

Sokol, Roger C, O-Seob Kwon, Charlotte M Bethoney, and G-Yull Rhee. 1994. "Reductive dechlorination of polychlorinated biphenyls in St. Lawrence River sediments and variations in dechlorination characteristics." *Environmental science & technology* 28 (12):2054-2064.

Spang, Anja, Anja Poehlein, Pierre Offre, Sabine Zumbrägel, Susanne Haider, Nicolas Rychlik, Boris Nowka, Christel Schmeisser, Elena V Lebedeva, and Thomas Rattei. 2012. "The genome of the ammonia-oxidizing Candidatus Nitrososphaera gargensis: insights into metabolic versatility and environmental adaptations." *Environmental microbiology* 14 (12):3122-3145.

Stahl, David A, and José R de la Torre. 2012. "Physiology and diversity of ammonia-oxidizing archaea." *Annual review of microbiology* 66:83-101.

Stallman, RW. 1965. "Steady one-dimensional fluid flow in a semi-infinite porous medium with sinusoidal surface temperature." *Journal of Geophysical Research* 70 (12):2821-2827.

Stetter, Karl O, and Günther Gaag. 1983. "Reduction of molecular sulphur by methanogenic bacteria."

Stonestrom, David Arthur, and Jim Constantz. 2003. *Heat as a tool for studying the movement of ground water near streams*: US Dept. of the Interior, US Geological Survey.

Ström, L, T Olsson, and G Tyler. 1994. "Differences between calcifuge and acidifuge plants in root exudation of low-molecular organic acids." *Plant and Soil* 167 (2):239-245.

Sultrac. 2010. Basis of Design Repor: Remedial Design West Branch Grand Calumet River Roxana Marsh and Reaches 1 and 2 Hammond, Lake County, Indiana.

Suzuki, Seitaro. 1960. "Percolation measurements based on heat flow through soil with special reference to paddy fields." *Journal of Geophysical Research* 65 (9):2883-2885.

Tarnocai, Charles, JG Canadell, EAG Schuur, Peter Kuhry, G Mazhitova, and S Zimov. 2009. "Soil organic carbon pools in the northern circumpolar permafrost region." *Global biogeochemical cycles* 23 (2).

Thebrath, B, F Rothfuss, MJ Whiticar, and R Conrad. 1993. "Methane production in littoral sediment of Lake Constance." *FEMS Microbiology Letters* 102 (3-4):279-289.

Thomas, Courtney, David Lampert, and Danny Reible. 2014. "Remedy performance monitoring at contaminated sediment sites using profiling solid phase microextraction (SPME) polydimethylsiloxane (PDMS) fibers." *Environmental Science: Processes & Impacts* 16 (3):445-452.

Tonina, Daniele, Charles Luce, and Frank Gariglio. 2014. "Quantifying streambed deposition and scour from stream and hyporheic water temperature time series." *Water Resources Research* 50 (1):287-292.

Treusch, Alexander H, Sven Leininger, Arnulf Kletzin, Stephan C Schuster, Hans-Peter Klenk, and Christa Schleper. 2005. "Novel genes for nitrite reductase and Amo-related proteins indicate a role of uncultivated mesophilic crenarchaeota in nitrogen cycling." *Environmental Microbiology* 7 (12):1985-1995.

USEPA. "Polychlorinated Biphenyls Retrived from: http://www.epa.gov/wastes/hazard/tsd/pcbs/about.htm." http://www.epa.gov/wastes/hazard/tsd/pcbs/about.htm.

USEPA. 1987. "An Overview of Sediment Quality in the United States."

USEPA. 1992. "Sediment classification methods compendium. EPA-823-R-006."

USEPA. 1996. "Soil screening guidance technical background document." *Office of Solid Waste and Emergency Response, Washington, DC EPA/540* 95.

USEPA. 1998. Contaminated Sediment Management Strategy. edited by Office of Water.

USEPA. 2004. "The Incidence and Severity of Sediment Contamination in Surface Waters of the United States."

USEPA. 2005. "Contaminated sediment remediation guidance for hazardous waste sites." *Office of Solid Waste and Emergency Response*.

USEPA. 2008. Polycyclic Aromatic Hydrocarbons (PAHs). Retrived from http://www.epa.gov/osw/hazard/wastemin/minimize/factshts/pahs.pdf. edited by Office of Solid Waste Washington D. C.

USEPA. 2015. "Grand Calumet River Area of Concern." USEPA Accessed April 27th http://www.epa.gov/greatlakes/aoc/grandcal/index.html.

Valentine, David W, Elisabeth A Holland, and David S Schimel. 1994. "Ecosystem and physiological controls over methane production in northern wetlands." *Journal of Geophysical Research: Atmospheres (1984–2012)* 99 (D1):1563-1571.

Viana, Priscilla, K Yin, K Xhao, and K Rockne. 2007. "Modeling and control of gas ebullition in capped sediments." Proceedings, 4th International Conference on Remediation of Contaminated Sediments. Battelle, Savannah, GA, USA, January.

Viana, Priscilla, Ke Yin, Xiuhong Zhao, and Karl Rockne. 2007. "Active sediment capping for pollutant mixtures: control of biogenic gas production under highly intermittent flows." *Land Contamination and Reclamation* 15 (4):413.

Viana, Priscilla Z, Ke Yin, and Karl J Rockne. 2008. "Modeling active capping efficacy. 1. Metal and organometal contaminated sediment remediation." *Environmental science & technology* 42 (23):8922-8929.

Viana, Priscilla Z, Ke Yin, and Karl J Rockne. 2012. "Field measurements and modeling of ebullition-facilitated flux of heavy metals and polycyclic aromatic hydrocarbons from sediments to the water column." *Environmental science & technology* 46 (21):12046-12054.

Vogt, Tobias, Philipp Schneider, Lisa Hahn-Woernle, and Olaf A Cirpka. 2010. "Estimation of seepage rates in a losing stream by means of fiber-optic high-resolution vertical temperature profiling." *Journal of Hydrology* 380 (1):154-164.

Wang, Lizhu, and Paul Kanehl. 2003. Influences of watershed urbanization and instream habitat on macroinvertebrates in cold water streams. Wiley Online Library.

West, Candida C., and Jeffrey H. Harwell. 1992. "Surfactants and subsurface remediation." *Environmental science & technology* 26 (12):2324-2330.

Whalen, SC. 2005. "Biogeochemistry of methane exchange between natural wetlands and the atmosphere." *Environmental Engineering Science* 22 (1):73-94.

Wilke, Andreas, Elizabeth M Glass, Jared Bischof, Daniel Braithwaite, Mark D'Souza, Wolfgang Gerlach, Travis Harrison, Kevin Keegan, Hunter Matthews, and Tobias Paczian. 2014. "MG-RAST Manual for version 3.3. 6, revision 9."

Williams, Richard T, and Ronald L Crawford. 1984. "Methane production in Minnesota peatlands." *Applied and Environmental Microbiology* 47 (6):1266-1271.

Winfrey, MR, and JG Zeikus. 1977. "Effect of sulfate on carbon and electron flow during microbial methanogenesis in freshwater sediments." *Applied and Environmental Microbiology* 33 (2):275-281.

Winterwerp, Johan C, and Walther GM Van Kesteren. 2004. *Introduction to the physics of cohesive sediment dynamics in the marine environment*: Elsevier.

Woodbury, Allan D, and Leslie Smith. 1985. "On the thermal effects of three-dimensional groundwater flow." *Journal of Geophysical Research: Solid Earth (1978–2012)* 90 (B1):759-767.

Yavitt, Joseph B, Gerald E Lang, and R Kelman Wieder. 1987. "Control of carbon mineralization to CH4 and CO2 in anaerobic, Sphagnum-derived peat from Big Run Bog, West Virginia." *Biogeochemistry* 4 (2):141-157.

Yin, Ke, Priscilla Viana, Xiuhong Zhao, and Karl Rockne. 2010. "Characterization, performance modeling, and design of an active capping remediation project in a heavily polluted urban channel." *Science of the total environment* 408 (16):3454-3463.

Young, Peter C. 2011. *Recursive estimation and time-series analysis: An introduction for the student and practitioner*: Springer Science & Business Media.

Young, Peter C, Diego J Pedregal, and Wlodek Tych. 1999. "Dynamic harmonic regression." *Journal of forecasting* 18 (6):369-394.

Young, Peter C, C James Taylor, Wlodek Tych, DJ Pedregal, and Paul G McKenna. 2010. "The Captain toolbox."

Yuan, Qingzhong. 2007. "Experimental and modeling studies of contaminant transport in capped sediments during gas bubble ebullition." Louisiana State University.

Yuan, Qingzhong, Kalliat T Valsaraj, and Danny D Reible. 2009. "A model for contaminant and sediment transport via gas ebullition through a sediment cap." *Environmental Engineering Science* 26 (9):1381-1391.

Yuan, Qingzhong, Kalliat T Valsaraj, Danny D Reible, and Clinton S Willson. 2007. "A laboratory study of sediment and contaminant release during gas ebullition." *Journal of the Air & Waste Management Association* 57 (9):1103-1111.

Zehnder, Alexander JB. 1988. *Biology of anaerobic microorganisms*: John Wiley and Sons Inc.

Zeikus, JG, and MR Winfrey. 1976. "Temperature limitation of methanogenesis in aquatic sediments." *Applied and environmental microbiology* 31 (1):99-107.

Zhao, Xiuhong, Laura Drumm, Ke Yin, and Karl J Rockne. 2009. "Segregation of the PAH-contaminated fraction of hydraulically dredged sediment." *Journal of Environmental Engineering* 135 (5):291-298.

Zheng, D, and L Raskin. 2000. "Quantification of Methanosaeta species in anaerobic bioreactors using genus-and species-specific hybridization probes." *Microbial ecology* 39 (3):246-262.

Zhu, Jinxing, Huajun Zheng, Guomin Ai, Guishan Zhang, Di Liu, Xiaoli Liu, and Xiuzhu Dong. 2012. "The genome characteristics and predicted function of methyl-group oxidation pathway in the obligate aceticlastic methanogens, Methanosaeta spp." *PloS one* 7 (5):e36756-e36756.

Zhu, Tengyi, Dafang Fu, Chad T. Jafvert, and Rajendra Prasad Singh. 2015. "Modeling of gas generation from the river adjacent to the manufactured gas plant." *RSC Advances* 5 (13):9565-9573. doi: 10.1039/C4RA06627H.

Zimmerman, John R., Upal Ghosh, Rod N. Millward, Todd S. Bridges, and Richard G. Luthy. 2004. "Addition of carbon sorbents to reduce PCB and PAH bioavailability in marine sediments: Physicochemical tests." *Environmental science & technology* 38 (20):5458-5464.

Zinder, Stephen H. 1993. "Physiological ecology of methanogens." In *Methanogenesis*, 128-206. Springer.

APPENDIX

Table A0.1 Genus level classification and abundance of the15 most abundant *Archaea* in pre-capping surface sediment of site GCR 1.

Phylum	Class	Order	Family	Genus	Sequence Count	Abundance
Euryarchaeota	*Methanomicrobia*	*Methanosarcinales*	*Methanosaetaceae*	*Methanosaeta*	23236	40%
Euryarchaeota	*Methanobacteria*	*Methanobacteriales*	*Methanobacteriaceae*	*Methanobacterium*	21038	36%
Euryarchaeota	-	-	-	-	2264	4%
Euryarchaeota	*Methanomicrobia*	-	-	-	1775	3%
Euryarchaeota	*Methanobacteria*	*Methanobacteriales*	*Methanobacteriaceae*	-	1461	3%
Euryarchaeota	*Methanobacteria*	*Methanobacteriales*	*Methanobacteriaceae*	*Methanobrevibacter*	1416	2%
Euryarchaeota	*Methanomicrobia*	*Methanomicrobiales*	-	-	1264	2%
Unclassified (derived from Archaea)	*Unclassified (derived from Archaea)*	*Unclassified (derived from Archaea)*	*Unclassified (derived from Archaea)*	*Unclassified (derived from Archaea)*	1142	2%
Euryarchaeota	*Methanomicrobia*	*Methanomicrobiales*	*Unclassified (derived from Methanomicrobiales)*	*Methanolinea*	1140	2%
Euryarchaeota	*Methanomicrobia*	*Methanosarcinales*	*Methanosarcinaceae*	*Methanomethylovorans*	868	1%
Euryarchaeota	*Methanomicrobia*	*Methanosarcinales*	-	-	818	1%
Euryarchaeota	*Unclassified (derived from Euryarchaeota)*	*Unclassified (derived from Euryarchaeota)*	*Unclassified (derived from Euryarchaeota)*	*Unclassified (derived from Euryarchaeota)*	764	1%
Euryarchaeota	*Methanomicrobia*	*Methanocellales*	*Methanocellaceae*	*Methanocella*	352	1%
Euryarchaeota	*Methanomicrobia*	*Methanomicrobiales*	*Methanospirillaceae*	*Methanospirillum*	208	0%
Thaumarchaeota	*Unclassified (derived from Thaumarchaeota)*	*Unclassified (derived from Thaumarchaeota)*	*Unclassified (derived from Thaumarchaeota)*	*Candidatus Nitrososphaera*	115	0%

Table A0.2 Genus level classification and abundance of the15 most abundant *Archaea* in pre-capping surface sediment of site GCR 2.

Phylum	Class	Order	Family	Genus	Sequence Count	Abundance
Euryarchaeota	*Methanomicrobia*	*Methanosarcinales*	*Methanosaetaceae*	*Methanosaeta*	19555	48%
Euryarchaeota	*Methanobacteria*	*Methanobacteriales*	*Methanobacteriaceae*	*Methanobacterium*	11597	29%
Euryarchaeota	*Methanobacteria*	*Methanobacteriales*	*Methanobacteriaceae*	*Methanobrevibacter*	2290	6%
Euryarchaeota	*Methanomicrobia*	-	-	-	795	2%
Unclassified (derived from Archaea)	*Unclassified (derived from Archaea)*	*Unclassified (derived from Archaea)*	*Unclassified (derived from Archaea)*	*Unclassified (derived from Archaea)*	771	2%
Euryarchaeota	*Methanomicrobia*	*Methanosarcinales*	*Methanosarcinaceae*	*Methanomethylovorans*	743	2%
Euryarchaeota	-	-	-	-	677	2%
Euryarchaeota	*Unclassified (derived from Euryarchaeota)*	*Unclassified (derived from Euryarchaeota)*	*Unclassified (derived from Euryarchaeota)*	*Unclassified (derived from Euryarchaeota)*	515	1%
Euryarchaeota	*Methanomicrobia*	*Methanocellales*	*Methanocellaceae*	*Methanocella*	503	1%
Euryarchaeota	*Methanobacteria*	*Methanobacteriales*	*Methanobacteriaceae*	-	477	1%
Euryarchaeota	*Methanomicrobia*	*Methanomicrobiales*	-	-	469	1%
Crenarchaeota	*Thermoprotei*	*Desulfurococcales*	*Desulfurococcaceae*	-	354	1%
Crenarchaeota	-	-	-	-	347	1%
Unclassified (derived from Archaea)	*Unclassified (derived from Archaea)*	*Unclassified (derived from Archaea)*	*Unclassified (derived from Archaea)*	*Unclassified (derived from Archaea)*	321	1%
Euryarchaeota	*Methanomicrobia*	*Methanosarcinales*	-	-	177	0%

Table A0.3 Genus level classification and abundance of the15 most abundant *Archaea* in pre-capping surface sediment of site GCR 3.

Phylum	Class	Order	Family	Genus	Sequence Count	Abundance
Euryarchaeota	*Methanomicrobia*	*Methanosarcinales*	*Methanosaetaceae*	*Methanosaeta*	21752	55%
Euryarchaeota	*Methanobacteria*	*Methanobacteriales*	*Methanobacteriaceae*	*Methanobacterium*	6650	17%
Euryarchaeota	*Unclassified (derived from Euryarchaeota)*	*Unclassified (derived from Euryarchaeota)*	*Unclassified (derived from Euryarchaeota)*	*Unclassified (derived from Euryarchaeota)*	2078	5%
Unclassified (derived from Archaea)	*Unclassified (derived from Archaea)*	*Unclassified (derived from Archaea)*	*Unclassified (derived from Archaea)*	*Unclassified (derived from Archaea)*	1594	4%
Euryarchaeota	*Methanomicrobia*	*Methanomicrobiales*	-	-	1577	4%
Euryarchaeota	*Methanomicrobia*	-	-	-	1509	4%
Euryarchaeota	*Methanobacteria*	*Methanobacteriales*	*Methanobacteriaceae*	*Methanobrevibacter*	947	2%
Euryarchaeota	-	-	-	-	806	2%
Euryarchaeota	*Methanomicrobia*	*Methanomicrobiales*	*Unclassified (derived from Methanomicrobiales)*	*Methanolinea*	774	2%
Euryarchaeota	*Methanomicrobia*	*Methanosarcinales*	-	-	429	1%
Euryarchaeota	*Methanomicrobia*	*Methanomicrobiales*	*Methanocorpusculaceae*	*Methanocorpusculum*	389	1%
Euryarchaeota	*Methanobacteria*	*Methanobacteriales*	*Methanobacteriaceae*	-	285	1%
Euryarchaeota	*Methanomicrobia*	*Methanosarcinales*	*Methanosarcinaceae*	*Methanomethylovorans*	240	1%
Unclassified (derived from Archaea)	*Unclassified (derived from Archaea)*	*Unclassified (derived from Archaea)*	*Unclassified (derived from Archaea)*	*Unclassified (derived from Archaea)*	225	1%
Euryarchaeota	*Methanomicrobia*	*Methanomicrobiales*	*Methanospirillaceae*	*Methanospirillum*	189	0%
Euryarchaeota	*Methanomicrobia*	*Methanocellales*	*Methanocellaceae*	*Methanocella*	100	0%

Table A0.4 Genus level classification and abundance of the15 most abundant *Archaea* in pre-capping surface sediment of site GCR 4.

Phylum	Class	Order	Family	Genus	Sequence Count	Abundance
Euryarchaeota	*Methanomicrobia*	*Methanosarcinales*	*Methanosaetaceae*	*Methanosaeta*	21415	51%
Euryarchaeota	*Methanobacteria*	*Methanobacteriales*	*Methanobacteriaceae*	*Methanobacterium*	8594	21%
Euryarchaeota	-	-	-	-	5490	13%
Euryarchaeota	*Methanobacteria*	*Methanobacteriales*	*Methanobacteriaceae*	*Methanobrevibacter*	1932	5%
Unclassified (derived from Archaea)	*Unclassified (derived from Archaea)*	*Unclassified (derived from Archaea)*	*Unclassified (derived from Archaea)*	*Unclassified (derived from Archaea)*	731	2%
Euryarchaeota	*Methanomicrobia*	*Methanomicrobiales*	-	-	665	2%
Euryarchaeota	*Methanomicrobia*	-	-	-	613	1%
Euryarchaeota	*Methanomicrobia*	*Methanomicrobiales*	*Methanospirillaceae*	*Methanospirillum*	431	1%
Euryarchaeota	*Methanobacteria*	*Methanobacteriales*	*Methanobacteriaceae*	-	392	1%
Euryarchaeota	*Methanomicrobia*	*Methanomicrobiales*	*Unclassified (derived from Methanomicrobiales)*	*Methanolinea*	346	1%
Euryarchaeota	*Methanomicrobia*	*Methanosarcinales*	*Methanosarcinaceae*	-	200	0%
Euryarchaeota	*Methanomicrobia*	*Methanosarcinales*	*Methanosarcinaceae*	*Methanomethylovorans*	194	0%
Euryarchaeota	*Unclassified (derived from Euryarchaeota)*	*Unclassified (derived from Euryarchaeota)*	*Unclassified (derived from Euryarchaeota)*	*Unclassified (derived from Euryarchaeota)*	193	0%
Unclassified (derived from Archaea)	*Unclassified (derived from Archaea)*	*Unclassified (derived from Archaea)*	*Unclassified (derived from Archaea)*	*Unclassified (derived from Archaea)*	119	0%
Euryarchaeota	*Methanomicrobia*	*Methanomicrobiales*	*Methanocorpusculaceae*	*Methanocorpusculum*	99	0%

Table A0.5 Genus level classification and abundance of the15 most abundant *Archaea* in pre-capping surface sediment of site GCR 5.

Phylum	Class	Order	Family	Genus	Sequence Count	Abundance
Euryarchaeota	*Methanomicrobia*	*Methanosarcinales*	*Methanosaetaceae*	*Methanosaeta*	20734	55%
Euryarchaeota	*Methanobacteria*	*Methanobacteriales*	*Methanobacteriaceae*	*Methanobacterium*	7081	19%
Euryarchaeota	*Methanobacteria*	*Methanobacteriales*	*Methanobacteriaceae*	*Methanobrevibacter*	2782	7%
Crenarchaeota	*Unclassified (derived from Crenarchaeota)*	*Unclassified (derived from Crenarchaeota)*	*Unclassified (derived from Crenarchaeota)*	*Candidatus Nitrosocaldus*	1559	4%
Unclassified (derived from Archaea)	*Unclassified (derived from Archaea)*	*Unclassified (derived from Archaea)*	*Unclassified (derived from Archaea)*	*Unclassified (derived from Archaea)*	1441	4%
Euryarchaeota	-	-	-	-	979	3%
Euryarchaeota	*Methanomicrobia*	-	-	-	754	2%
Euryarchaeota	*Methanobacteria*	*Methanobacteriales*	*Methanobacteriaceae*	-	509	1%
Euryarchaeota	*Methanomicrobia*	*Methanomicrobiales*	-	-	475	1%
Euryarchaeota	*Methanomicrobia*	*Methanosarcinales*	*Methanosarcinaceae*	*Methanomethylovorans*	397	1%
Euryarchaeota	*Unclassified (derived from Euryarchaeota)*	*Unclassified (derived from Euryarchaeota)*	*Unclassified (derived from Euryarchaeota)*	*Unclassified (derived from Euryarchaeota)*	355	1%
Euryarchaeota	*Methanomicrobia*	*Methanomicrobiales*	*Methanospirillaceae*	*Methanospirillum*	197	1%
Euryarchaeota	*Methanomicrobia*	*Methanosarcinales*	*Methanosarcinaceae*	*Methanosarcina*	183	0%
Unclassified (derived from Archaea)	*Unclassified (derived from Archaea)*	*Unclassified (derived from Archaea)*	*Unclassified (derived from Archaea)*	*Unclassified (derived from Archaea)*	177	0%
Euryarchaeota	*Methanomicrobia*	*Methanomicrobiales*	*Unclassified (derived from Methanomicrobiales)*	*Methanolinea*	114	0%

Table A0.6 Genus level classification and abundance of the15 most abundant *Archaea* in pre-capping surface sediment of site GCR 6.

Phylum	Class	Order	Family	Genus	Sequence Count	Abundance
Euryarchaeota	*Methanomicrobia*	*Methanosarcinales*	*Methanosaetaceae*	*Methanosaeta*	27768	67%
Euryarchaeota	-	-	-	-	4354	11%
Euryarchaeota	*Methanomicrobia*	*Methanomicrobiales*	-	-	2541	6%
Euryarchaeota	*Methanobacteria*	*Methanobacteriales*	*Methanobacteriaceae*	*Methanobacterium*	1938	5%
Unclassified (derived from Archaea)	*Unclassified (derived from Archaea)*	*Unclassified (derived from Archaea)*	*Unclassified (derived from Archaea)*	*Unclassified (derived from Archaea)*	1507	4%
Euryarchaeota	*Methanomicrobia*	-	-	-	822	2%
Euryarchaeota	*Unclassified (derived from Euryarchaeota)*	*Unclassified (derived from Euryarchaeota)*	*Unclassified (derived from Euryarchaeota)*	*Unclassified (derived from Euryarchaeota)*	694	2%
Euryarchaeota	*Methanomicrobia*	*Methanocellales*	*Methanocellaceae*	*Methanocella*	456	1%
Euryarchaeota	*Methanobacteria*	*Methanobacteriales*	*Methanobacteriaceae*	*Methanobrevibacter*	257	1%
Euryarchaeota	*Methanomicrobia*	*Methanomicrobiales*	*Methanospirillaceae*	*Methanospirillum*	180	0%
Euryarchaeota	*Methanomicrobia*	*Methanosarcinales*	*Methanosarcinaceae*	*Methanosarcina*	168	0%
Unclassified (derived from Archaea)	*Unclassified (derived from Archaea)*	*Unclassified (derived from Archaea)*	*Unclassified (derived from Archaea)*	*Unclassified (derived from Archaea)*	157	0%
Euryarchaeota	*Methanobacteria*	*Methanobacteriales*	*Methanobacteriaceae*	-	110	0%
Euryarchaeota	*Methanomicrobia*	*Methanomicrobiales*	*Unclassified (derived from Methanomicrobiales)*	*Methanolinea*	105	0%
Euryarchaeota	*Methanomicrobia*	*Methanosarcinales*	*Methanosarcinaceae*	*Methanomethylovorans*	58	0%

Table A0.7 Genus level classification and abundance of the15 most abundant *Archaea* in pre-capping surface sediment of site GCR 7.

Phylum	Class	Order	Family	Genus	Sequence Count	Abundance
Euryarchaeota	*Methanomicrobia*	*Methanosarcinales*	*Methanosaetaceae*	*Methanosaeta*	17211	45%
Euryarchaeota	*Methanomicrobia*	*Methanosarcinales*	*Methanosarcinaceae*	-	5900	15%
Euryarchaeota	*Methanobacteria*	*Methanobacteriales*	*Methanobacteriaceae*	*Methanobacterium*	5558	15%
Euryarchaeota	-	-	-	-	1429	4%
Unclassified (derived from Archaea)	*Unclassified (derived from Archaea)*	*Unclassified (derived from Archaea)*	*Unclassified (derived from Archaea)*	*Unclassified (derived from Archaea)*	1198	3%
Euryarchaeota	*Methanobacteria*	*Methanobacteriales*	*Methanobacteriaceae*	*Methanobrevibacter*	1097	3%
Euryarchaeota	*Methanomicrobia*	-	-	-	1051	3%
Euryarchaeota	*Methanobacteria*	*Methanobacteriales*	*Methanobacteriaceae*	-	916	2%
Euryarchaeota	*Methanomicrobia*	*Methanomicrobiales*	-	-	648	2%
Euryarchaeota	*Unclassified (derived from Euryarchaeota)*	*Unclassified (derived from Euryarchaeota)*	*Unclassified (derived from Euryarchaeota)*	*Unclassified (derived from Euryarchaeota)*	547	1%
Crenarchaeota	*Thermoprotei*	*Desulfurococcales*	*Desulfurococcaceae*	-	417	1%
Euryarchaeota	*Methanomicrobia*	*Methanosarcinales*	*Methanosarcinaceae*	*Methanomethylovorans*	310	1%
Thaumarchaeota	*Unclassified (derived from Thaumarchaeota)*	*Unclassified (derived from Thaumarchaeota)*	*Unclassified (derived from Thaumarchaeota)*	*Candidatus Nitrososphaera*	280	1%
Euryarchaeota	*Methanomicrobia*	*Methanocellales*	*Methanocellaceae*	*Methanocella*	253	1%
Crenarchaeota	*Thermoprotei*	*Desulfurococcales*	*Desulfurococcaceae*	*Ignicoccus*	184	0%

Table A0.8 Genus level classification and abundance of the15 most abundant *Archaea* in pre-capping surface sediment of site GCR 8.

Phylum	Class	Order	Family	Genus	Sequence Count	Abundance
Euryarchaeota	*Methanomicrobia*	*Methanosarcinales*	*Methanosaetaceae*	*Methanosaeta*	33781	67%
Euryarchaeota	*Methanobacteria*	*Methanobacteriales*	*Methanobacteriaceae*	*Methanobacterium*	7457	15%
Euryarchaeota	*Methanomicrobia*	*Methanosarcinales*	*Methanosarcinaceae*	*Methanomethylovorans*	1568	3%
Euryarchaeota	*Methanomicrobia*	-	-	-	1320	3%
Euryarchaeota	*Methanobacteria*	*Methanobacteriales*	*Methanobacteriaceae*	*Methanobrevibacter*	1149	2%
Euryarchaeota	*Methanomicrobia*	*Methanomicrobiales*	-	-	880	2%
Euryarchaeota	*Methanomicrobia*	*Methanocellales*	*Methanocellaceae*	*Methanocella*	762	2%
Euryarchaeota	-	-	-	-	695	1%
Unclassified (derived from Archaea)	*Unclassified (derived from Archaea)*	*Unclassified (derived from Archaea)*	*Unclassified (derived from Archaea)*	*Unclassified (derived from Archaea)*	672	1%
Unclassified (derived from Archaea)	*Unclassified (derived from Archaea)*	*Unclassified (derived from Archaea)*	*Unclassified (derived from Archaea)*	*Unclassified (derived from Archaea)*	402	1%
Euryarchaeota	*Methanomicrobia*	*Methanomicrobiales*	*Unclassified (derived from Methanomicrobiales)*	*Methanolinea*	352	1%
Euryarchaeota	*Methanobacteria*	*Methanobacteriales*	*Methanobacteriaceae*	-	348	1%
Euryarchaeota	*Methanomicrobia*	*Methanomicrobiales*	*Methanospirillaceae*	*Methanospirillum*	267	1%
Euryarchaeota	*Unclassified (derived from Euryarchaeota)*	*Unclassified (derived from Euryarchaeota)*	*Unclassified (derived from Euryarchaeota)*	*Unclassified (derived from Euryarchaeota)*	186	0%
Euryarchaeota	*Methanomicrobia*	*Methanosarcinales*	-	-	122	0%

Table A0.9 Genus level classification and abundance of the15 most abundant *Archaea* in pre-capping surface sediment of site GCR 9.

Phylum	Class	Order	Family	Genus	Sequence Count	Abundance
Euryarchaeota	*Methanomicrobia*	*Methanosarcinales*	*Methanosaetaceae*	*Methanosaeta*	38880	56%
Euryarchaeota	*Methanobacteria*	*Methanobacteriales*	*Methanobacteriaceae*	*Methanobacterium*	11322	16%
Euryarchaeota	*Methanomicrobia*	*Methanomicrobiales*	-	-	9151	13%
Unclassified (derived from Archaea)	*Unclassified (derived from Archaea)*	*Unclassified (derived from Archaea)*	*Unclassified (derived from Archaea)*	*Unclassified (derived from Archaea)*	4043	6%
Euryarchaeota	*Methanomicrobia*	*Methanosarcinales*	*Methanosarcinaceae*	*Methanomethylovorans*	1183	2%
Euryarchaeota	*Methanomicrobia*	-	-	-	884	1%
Euryarchaeota	-	-	-	-	605	1%
Euryarchaeota	*Methanobacteria*	*Methanobacteriales*	*Methanobacteriaceae*	*Methanobrevibacter*	402	1%
Euryarchaeota	*Methanomicrobia*	*Methanomicrobiales*	*Methanospirillaceae*	*Methanospirillum*	382	1%
Euryarchaeota	*Methanomicrobia*	*Methanocellales*	*Methanocellaceae*	*Methanocella*	373	1%
Euryarchaeota	*Methanomicrobia*	*Methanosarcinales*	*Methanosarcinaceae*	*Methanosarcina*	357	1%
Euryarchaeota	*Methanomicrobia*	*Methanomicrobiales*	*Unclassified (derived from Methanomicrobiales)*	*Methanolinea*	316	0%
Euryarchaeota	*Methanopyri*	*Methanopyrales*	*Methanopyraceae*	*Methanopyrus*	217	0%
Euryarchaeota	*Methanomicrobia*	*Methanomicrobiales*	*Unclassified (derived from Methanomicrobiales)*	*Methanosphaerula*	171	0%
Euryarchaeota	*Methanobacteria*	*Methanobacteriales*	*Methanobacteriaceae*	-	136	0%

Table A0.10 Genus level classification and abundance of the15 most abundant *Archaea* in pre-capping surface sediment of site GCR 10.

Phylum	Class	Order	Family	Genus	Sequence Count	Abundance
Euryarchaeota	*Methanomicrobia*	*Methanosarcinales*	*Methanosaetaceae*	*Methanosaeta*	36834	59%
Euryarchaeota	*Methanobacteria*	*Methanobacteriales*	*Methanobacteriaceae*	*Methanobacterium*	8795	14%
Euryarchaeota	*Methanomicrobia*	*Methanomicrobiales*	-	-	4571	7%
Euryarchaeota	*Methanobacteria*	*Methanobacteriales*	*Methanobacteriaceae*	*Methanobrevibacter*	2720	4%
Unclassified (derived from Archaea)	*Unclassified (derived from Archaea)*	*Unclassified (derived from Archaea)*	*Unclassified (derived from Archaea)*	*Unclassified (derived from Archaea)*	2048	3%
Euryarchaeota	-	-	-	-	1836	3%
Euryarchaeota	*Methanomicrobia*	-	-	-	1789	3%
Euryarchaeota	*Methanomicrobia*	*Methanomicrobiales*	*Unclassified (derived from Methanomicrobiales)*	*Methanolinea*	810	1%
Euryarchaeota	*Methanomicrobia*	*Methanosarcinales*	*Methanosarcinaceae*	*Methanomethylovorans*	694	1%
Euryarchaeota	*Methanomicrobia*	*Methanomicrobiales*	*Methanospirillaceae*	*Methanospirillum*	677	1%
Euryarchaeota	*Methanobacteria*	*Methanobacteriales*	*Methanobacteriaceae*	-	350	1%
Euryarchaeota	*Methanomicrobia*	*Methanosarcinales*	*Methanosarcinaceae*	*Methanosarcina*	275	0%
Euryarchaeota	*Methanomicrobia*	*Methanomicrobiales*	*Unclassified (derived from Methanomicrobiales)*	*Methanosphaerula*	217	0%
Thaumarchaeota	*Unclassified (derived from Thaumarchaeota)*	*Unclassified (derived from Thaumarchaeota)*	*Unclassified (derived from Thaumarchaeota)*	*Candidatus Nitrososphaera*	178	0%
Unclassified (derived from Archaea)	*Unclassified (derived from Archaea)*	*Unclassified (derived from Archaea)*	*Unclassified (derived from Archaea)*	*Unclassified (derived from Archaea)*	142	0%

Table A0.11 Genus level classification and abundance of the15 most abundant *Archaea* in pre-capping surface sediment of site GCR 11.

Phylum	Class	Order	Family	Genus	Sequence Count	Abundance
Euryarchaeota	*Methanomicrobia*	*Methanosarcinales*	*Methanosaetaceae*	*Methanosaeta*	38151	58%
Euryarchaeota	*Methanobacteria*	*Methanobacteriales*	*Methanobacteriaceae*	*Methanobacterium*	14523	22%
Euryarchaeota	*Methanomicrobia*	-	-	-	2419	4%
Euryarchaeota	*Methanomicrobia*	*Methanomicrobiales*	*Methanocorpusculaceae*	*Methanocorpusculum*	1419	2%
Unclassified (derived from Archaea)	*Unclassified (derived from Archaea)*	*Unclassified (derived from Archaea)*	*Unclassified (derived from Archaea)*	*Unclassified (derived from Archaea)*	1363	2%
Euryarchaeota	-	-	-	-	1273	2%
Euryarchaeota	*Methanomicrobia*	*Methanomicrobiales*	*Methanospirillaceae*	*Methanospirillum*	1193	2%
Euryarchaeota	*Methanobacteria*	*Methanobacteriales*	*Methanobacteriaceae*	*Methanobrevibacter*	1142	2%
Euryarchaeota	*Methanobacteria*	*Methanobacteriales*	*Methanobacteriaceae*	-	1127	2%
Euryarchaeota	*Methanomicrobia*	*Methanomicrobiales*	-	-	937	1%
Euryarchaeota	*Methanomicrobia*	*Methanosarcinales*	*Methanosarcinaceae*	*Methanomethylovorans*	303	0%
Unclassified (derived from Archaea)	*Unclassified (derived from Archaea)*	*Unclassified (derived from Archaea)*	*Unclassified (derived from Archaea)*	*Unclassified (derived from Archaea)*	277	0%
Euryarchaeota	*Methanomicrobia*	*Methanomicrobiales*	*Unclassified (derived from Methanomicrobiales)*	*Methanolinea*	252	0%
Euryarchaeota	*Methanomicrobia*	*Methanosarcinales*	*Methanosarcinaceae*	*Methanosarcina*	244	0%
Euryarchaeota	*Methanomicrobia*	*Methanomicrobiales*	*Unclassified (derived from Methanomicrobiales)*	*Methanosphaerula*	216	0%

Table A0.12 Genus level classification and abundance of the15 most abundant *Archaea* in pre-capping surface sediment of site GCR 12.

Phylum	Class	Order	Family	Genus	Sequence Count	Abundance
Euryarchaeota	*Methanomicrobia*	*Methanosarcinales*	*Methanosaetaceae*	*Methanosaeta*	31786	62%
Euryarchaeota	*Methanobacteria*	*Methanobacteriales*	*Methanobacteriaceae*	*Methanobacterium*	8147	16%
Euryarchaeota	*Methanomicrobia*	-	-	-	3343	7%
Euryarchaeota	-	-	-	-	2333	5%
Euryarchaeota	*Methanomicrobia*	*Methanomicrobiales*	-	-	1212	2%
Unclassified (derived from Archaea)	*Unclassified (derived from Archaea)*	*Unclassified (derived from Archaea)*	*Unclassified (derived from Archaea)*	*Unclassified (derived from Archaea)*	1156	2%
Euryarchaeota	*Methanomicrobia*	*Methanomicrobiales*	*Unclassified (derived from Methanomicrobiales)*	*Methanolinea*	783	2%
Euryarchaeota	*Methanomicrobia*	*Methanomicrobiales*	*Methanospirillaceae*	*Methanospirillum*	464	1%
Unclassified (derived from Archaea)	*Unclassified (derived from Archaea)*	*Unclassified (derived from Archaea)*	*Unclassified (derived from Archaea)*	*Unclassified (derived from Archaea)*	347	1%
Euryarchaeota	*Methanomicrobia*	*Methanomicrobiales*	*Unclassified (derived from Methanomicrobiales)*	*Methanosphaerula*	341	1%
Euryarchaeota	*Methanobacteria*	*Methanobacteriales*	*Methanobacteriaceae*	*Methanobrevibacter*	259	1%
Euryarchaeota	*Methanomicrobia*	*Methanosarcinales*	*Methanosarcinaceae*	*Methanomethylovorans*	177	0%
Euryarchaeota	*Methanobacteria*	*Methanobacteriales*	*Methanobacteriaceae*	-	164	0%
Euryarchaeota	*Methanomicrobia*	*Methanosarcinales*	-	-	103	0%
Crenarchaeota	*Thermoprotei*	*Thermoproteales*	*Thermoproteaceae*	-	78	0%

Table A0.13 Genus level classification and abundance of the15 most abundant *Archaea* in pre-capping surface sediment of site GCR 13.

Phylum	Class	Order	Family	Genus	Sequence Count	Abundance
Euryarchaeota	*Methanomicrobia*	*Methanosarcinales*	*Methanosaetaceae*	*Methanosaeta*	49784	68%
Euryarchaeota	*Methanobacteria*	*Methanobacteriales*	*Methanobacteriaceae*	*Methanobacterium*	7704	11%
Unclassified (derived from Archaea)	*Unclassified (derived from Archaea)*	*Unclassified (derived from Archaea)*	*Unclassified (derived from Archaea)*	*Unclassified (derived from Archaea)*	4216	6%
Unclassified (derived from Archaea)	*Unclassified (derived from Archaea)*	*Unclassified (derived from Archaea)*	*Unclassified (derived from Archaea)*	*Unclassified (derived from Archaea)*	4069	6%
Euryarchaeota	-	-	-	-	2066	3%
Euryarchaeota	*Methanomicrobia*	-	-	-	1295	2%
Euryarchaeota	*Methanobacteria*	*Methanobacteriales*	*Methanobacteriaceae*	*Methanobrevibacter*	1092	1%
Euryarchaeota	*Methanomicrobia*	*Methanomicrobiales*	*Methanocorpusculaceae*	*Methanocorpusculum*	859	1%
Euryarchaeota	*Methanomicrobia*	*Methanosarcinales*	*Methanosarcinaceae*	*Methanosarcina*	491	1%
Euryarchaeota	*Methanomicrobia*	*Methanomicrobiales*	*Unclassified (derived from Methanomicrobiales)*	*Methanosphaerula*	381	1%
Euryarchaeota	*Methanomicrobia*	*Methanosarcinales*	*Methanosarcinaceae*	*Methanomethylovorans*	358	0%
Euryarchaeota	*Methanomicrobia*	*Methanomicrobiales*	*Methanospirillaceae*	*Methanospirillum*	307	0%
Euryarchaeota	*Methanomicrobia*	*Methanomicrobiales*	-	-	266	0%
Euryarchaeota	*Methanobacteria*	*Methanobacteriales*	*Methanobacteriaceae*	-	127	0%
Euryarchaeota	*Methanomicrobia*	*Methanosarcinales*	-	-	70	0%

Table A0.14 Genus level classification and abundance of the15 most abundant *Archaea* in post-capping sediment layer GCR 2 –ND.

Phylum	Class	Order	Family	Genus	Sequence Count	Abundance
Unclassified (derived from Archaea)	*Unclassified (derived from Archaea)*	*Unclassified (derived from Archaea)*	*Unclassified (derived from Archaea)*	*Unclassified (derived from Archaea)*	10252	24%
Euryarchaeota	*Methanobacteria*	*Methanobacteriales*	*Methanobacteriaceae*	*Methanobacterium*	8198	19%
Euryarchaeota	*Methanomicrobia*	*Methanosarcinales*	*Methanosarcinaceae*	-	6861	16%
Crenarchaeota	*Thermoprotei*	-	-	-	4428	10%
Euryarchaeota	*Methanomicrobia*	*Methanosarcinales*	*Methanosarcinaceae*	*Methanomethylovorans*	3774	9%
Euryarchaeota	*Methanomicrobia*	*Methanosarcinales*	*Methanosaetaceae*	*Methanosaeta*	3765	9%
Euryarchaeota	*Methanomicrobia*	*Methanocellales*	*Methanocellaceae*	*Methanocella*	2367	5%
Euryarchaeota	*Methanopyri*	*Methanopyrales*	*Methanopyraceae*	*Methanopyrus*	1397	3%
Euryarchaeota	-	-	-	-	337	1%
Euryarchaeota	*Unclassified (derived from Euryarchaeota)*	*Unclassified (derived from Euryarchaeota)*	*Unclassified (derived from Euryarchaeota)*	*Unclassified (derived from Euryarchaeota)*	317	1%
Thaumarchaeota	*Unclassified (derived from Thaumarchaeota)*	*Unclassified (derived from Thaumarchaeota)*	*Unclassified (derived from Thaumarchaeota)*	*Candidatus Nitrososphaera*	296	1%
Euryarchaeota	*Methanomicrobia*	-	-	-	259	1%
Euryarchaeota	*Methanobacteria*	*Methanobacteriales*	*Methanobacteriaceae*	*Methanobrevibacter*	197	0%
Euryarchaeota	*Methanomicrobia*	*Methanomicrobiales*	*Methanospirillaceae*	*Methanospirillum*	187	0%
Unclassified (derived from Archaea)	*Unclassified (derived from Archaea)*	*Unclassified (derived from Archaea)*	*Unclassified (derived from Archaea)*	*Unclassified (derived from Archaea)*	151	0%

Table A0.15 Genus level classification and abundance of the15 most abundant *Archaea* in post-capping sediment layer GCR 2 –GAL.

Phylum	Class	Order	Family	Genus	Sequence Count	Abundance
Unclassified (derived from Archaea)	*Unclassified (derived from Archaea)*	*Unclassified (derived from Archaea)*	*Unclassified (derived from Archaea)*	*Unclassified (derived from Archaea)*	1697	81%
Thaumarchaeota	*Unclassified (derived from Thaumarchaeota)*	*Unclassified (derived from Thaumarchaeota)*	*Unclassified (derived from Thaumarchaeota)*	*Candidatus Nitrososphaera*	161	8%
Euryarchaeota	*Methanomicrobia*	*Methanosarcinales*	*Methanosaetaceae*	*Methanosaeta*	99	5%
Euryarchaeota	*Methanomicrobia*	*Methanosarcinales*	*Methanosarcinaceae*	-	85	4%
Euryarchaeota	*Methanomicrobia*	*Methanosarcinales*	*Methanosarcinaceae*	*Methanomethylovorans*	41	2%
Euryarchaeota	*Methanopyri*	*Methanopyrales*	*Methanopyraceae*	*Methanopyrus*	5	0%
Euryarchaeota	*Methanobacteria*	*Methanobacteriales*	*Methanobacteriaceae*	*Methanobacterium*	3	0%
Euryarchaeota	*Methanomicrobia*	*Methanomicrobiales*	-	-	2	0%
Crenarchaeota	*Thermoprotei*	*Thermoproteales*	*Thermoproteaceae*	*Thermoproteus*	1	0%
Euryarchaeota	*Methanomicrobia*	*Methanomicrobiales*	*Unclassified (derived from Methanomicrobiales)*	*Methanolinea*	1	0%

Table A0.16 Genus level classification and abundance of the15 most abundant *Archaea* in post-capping sediment layer GCR 2 –OrgC.

Phylum	Class	Order	Family	Genus	Sequence Count	Abundance
Euryarchaeota	*Methanomicrobia*	*Methanosarcinales*	*Methanosaetaceae*	*Methanosaeta*	8408	39%
Euryarchaeota	*Methanomicrobia*	*Methanomicrobiales*	*Methanocorpusculaceae*	*Methanocorpusculum*	4400	21%
Thaumarchaeota	*Unclassified (derived from Thaumarchaeota)*	*Unclassified (derived from Thaumarchaeota)*	*Unclassified (derived from Thaumarchaeota)*	*Candidatus Nitrososphaera*	3203	15%
Euryarchaeota	*Methanomicrobia*	*Methanosarcinales*	*Methanosarcinaceae*	-	948	4%
Euryarchaeota	*Methanobacteria*	*Methanobacteriales*	*Methanobacteriaceae*	*Methanobrevibacter*	922	4%
Euryarchaeota	*Methanobacteria*	*Methanobacteriales*	*Methanobacteriaceae*	*Methanobacterium*	841	4%
Unclassified (derived from Archaea)	*Unclassified (derived from Archaea)*	*Unclassified (derived from Archaea)*	*Unclassified (derived from Archaea)*	*Unclassified (derived from Archaea)*	785	4%
Euryarchaeota	*Methanomicrobia*	-	-	-	584	3%
Euryarchaeota	*Methanomicrobia*	*Methanomicrobiales*	*Unclassified (derived from Methanomicrobiales)*	*Methanolinea*	254	1%
Euryarchaeota	*Methanomicrobia*	*Methanomicrobiales*	-	-	232	1%
Euryarchaeota	*Methanomicrobia*	*Methanosarcinales*	-	-	147	1%
Unclassified (derived from Archaea)	*Unclassified (derived from Archaea)*	*Unclassified (derived from Archaea)*	*Unclassified (derived from Archaea)*	*Unclassified (derived from Archaea)*	132	1%
Euryarchaeota	*Methanomicrobia*	*Methanomicrobiales*	*Methanomicrobiaceae*	*Methanoculleus*	110	1%
Euryarchaeota	*Methanomicrobia*	*Methanosarcinales*	*Methanosarcinaceae*	*Methanomethylovorans*	74	0%
Crenarchaeota	*Thermoprotei*	*Thermoproteales*	*Thermoproteaceae*	*Thermoproteus*	68	0%

Table A0.17 Genus level classification and abundance of the15 most abundant *Archaea* in post-capping sediment layer GCR 2 –CSed.

Phylum	Class	Order	Family	Genus	Sequence Count	Abundance
Euryarchaeota	*Methanomicrobia*	*Methanosarcinales*	*Methanosaetaceae*	*Methanosaeta*	13737	41%
Euryarchaeota	*Methanomicrobia*	*Methanomicrobiales*	-	-	4757	14%
Crenarchaeota	*Unclassified (derived from Crenarchaeota)*	*Unclassified (derived from Crenarchaeota)*	*Unclassified (derived from Crenarchaeota)*	*Candidatus Nitrosocaldus*	2947	9%
Euryarchaeota	*Methanobacteria*	*Methanobacteriales*	*Methanobacteriaceae*	*Methanobacterium*	2712	8%
Unclassified (derived from Archaea)	*Unclassified (derived from Archaea)*	*Unclassified (derived from Archaea)*	*Unclassified (derived from Archaea)*	*Unclassified (derived from Archaea)*	2400	7%
Euryarchaeota	*Methanobacteria*	*Methanobacteriales*	*Methanobacteriaceae*	*Methanobrevibacter*	1901	6%
Crenarchaeota	*Thermoprotei*	*Desulfurococcales*	*Desulfurococcaceae*	-	1324	4%
Euryarchaeota	*Methanomicrobia*	-	-	-	867	3%
Euryarchaeota	*Methanomicrobia*	*Methanomicrobiales*	*Unclassified (derived from Methanomicrobiales)*	*Methanolinea*	857	3%
Euryarchaeota	-	-	-	-	596	2%
Euryarchaeota	*Methanomicrobia*	*Methanomicrobiales*	*Methanomicrobiaceae*	*Methanoculleus*	452	1%
Unclassified (derived from Archaea)	*Unclassified (derived from Archaea)*	*Unclassified (derived from Archaea)*	*Unclassified (derived from Archaea)*	*Unclassified (derived from Archaea)*	217	1%
Euryarchaeota	*Methanomicrobia*	*Methanomicrobiales*	*Methanocorpusculaceae*	*Methanocorpusculum*	182	1%
Euryarchaeota	*Methanomicrobia*	*Methanocellales*	*Methanocellaceae*	*Methanocella*	103	0%

Table A0.18 Genus level classification and abundance of the15 most abundant *Archaea* in post-capping sediment layer GCR 6 –ND.

Phylum	Class	Order	Family	Genus	Sequence Count	Abundance
Euryarchaeota	*Methanomicrobia*	*Methanosarcinales*	*Methanosaetaceae*	*Methanosaeta*	43949	65%
Unclassified (derived from Archaea)	*Unclassified (derived from Archaea)*	*Unclassified (derived from Archaea)*	*Unclassified (derived from Archaea)*	*Unclassified (derived from Archaea)*	4224	6%
Euryarchaeota	*Methanomicrobia*	-	-	-	3929	6%
Euryarchaeota	*Methanobacteria*	*Methanobacteriales*	*Methanobacteriaceae*	*Methanobacterium*	3665	5%
Euryarchaeota	*Methanomicrobia*	*Methanomicrobiales*	-	-	2963	4%
Euryarchaeota	*Methanobacteria*	*Methanobacteriales*	*Methanobacteriaceae*	*Methanobrevibacter*	1707	3%
Euryarchaeota	-	-	-	-	1606	2%
Euryarchaeota	*Methanomicrobia*	*Methanomicrobiales*	*Methanospirillaceae*	*Methanospirillum*	1120	2%
Euryarchaeota	*Methanomicrobia*	*Methanomicrobiales*	*Unclassified (derived from Methanomicrobiales)*	*Methanolinea*	874	1%
Euryarchaeota	*Methanopyri*	*Methanopyrales*	*Methanopyraceae*	*Methanopyrus*	700	1%
Euryarchaeota	*Methanomicrobia*	*Methanosarcinales*	*Methanosarcinaceae*	*Methanomethylovorans*	503	1%
Euryarchaeota	*Methanomicrobia*	*Methanomicrobiales*	*Unclassified (derived from Methanomicrobiales)*	*Methanosphaerula*	343	1%
Euryarchaeota	*Methanomicrobia*	*Methanosarcinales*	-	-	296	0%
Thaumarchaeota	*Unclassified (derived from Thaumarchaeota)*	*Unclassified (derived from Thaumarchaeota)*	*Unclassified (derived from Thaumarchaeota)*	*Candidatus Nitrososphaera*	247	0%
Euryarchaeota	*Unclassified (derived from Euryarchaeota)*	*Unclassified (derived from Euryarchaeota)*	*Unclassified (derived from Euryarchaeota)*	*Unclassified (derived from Euryarchaeota)*	244	0%

Table A0.19 Genus level classification and abundance of the15 most abundant *Archaea* in post-capping sediment layer GCR 6 –GAL.

Phylum	Class	Order	Family	Genus	Sequence Count	Abundance
Euryarchaeota	*Methanomicrobia*	*Methanosarcinales*	*Methanosaetaceae*	*Methanosaeta*	20056	45%
Euryarchaeota	*Methanomicrobia*	*Methanosarcinales*	*Methanosarcinaceae*	-	10738	24%
Euryarchaeota	*Methanobacteria*	*Methanobacteriales*	*Methanobacteriaceae*	*Methanobacterium*	4783	11%
Euryarchaeota	*Methanomicrobia*	*Methanosarcinales*	*Methanosarcinaceae*	*Methanomethylovorans*	2021	5%
Euryarchaeota	*Methanomicrobia*	*Methanomicrobiales*	*Methanospirillaceae*	*Methanospirillum*	1169	3%
Thaumarchaeota	*Unclassified (derived from Thaumarchaeota)*	*Unclassified (derived from Thaumarchaeota)*	*Unclassified (derived from Thaumarchaeota)*	*Candidatus Nitrososphaera*	1103	2%
Euryarchaeota	*Methanomicrobia*	-	-	-	933	2%
Euryarchaeota	*Unclassified (derived from Euryarchaeota)*	*Unclassified (derived from Euryarchaeota)*	*Unclassified (derived from Euryarchaeota)*	*Unclassified (derived from Euryarchaeota)*	612	1%
Euryarchaeota	*Methanomicrobia*	*Methanomicrobiales*	-	-	574	1%
Unclassified (derived from Archaea)	*Unclassified (derived from Archaea)*	*Unclassified (derived from Archaea)*	*Unclassified (derived from Archaea)*	*Unclassified (derived from Archaea)*	475	1%
Euryarchaeota	*Methanobacteria*	*Methanobacteriales*	*Methanobacteriaceae*	*Methanobrevibacter*	397	1%
Euryarchaeota	*Methanomicrobia*	*Methanomicrobiales*	*Unclassified (derived from Methanomicrobiales)*	*Methanosphaerula*	369	1%
Euryarchaeota	*Methanopyri*	*Methanopyrales*	*Methanopyraceae*	*Methanopyrus*	338	1%
Crenarchaeota	*Thermoprotei*	-	-	-	290	1%
Unclassified (derived from Archaea)	*Unclassified (derived from Archaea)*	*Unclassified (derived from Archaea)*	*Unclassified (derived from Archaea)*	*Unclassified (derived from Archaea)*	220	0%

Table A0.20 Genus level classification and abundance of the15 most abundant *Archaea* in post-capping sediment layer GCR 6 –OrgC.

Phylum	Class	Order	Family	Genus	Sequence Count	Abundance
Euryarchaeota	*Methanomicrobia*	*Methanosarcinales*	*Methanosaetaceae*	*Methanosaeta*	36189	67%
Euryarchaeota	*Methanobacteria*	*Methanobacteriales*	*Methanobacteriaceae*	*Methanobacterium*	3783	7%
Euryarchaeota	*Methanomicrobia*	*Methanomicrobiales*	-	-	2990	6%
Euryarchaeota	*Methanomicrobia*	-	-	-	2262	4%
Euryarchaeota	*Methanobacteria*	*Methanobacteriales*	*Methanobacteriaceae*	*Methanobrevibacter*	1515	3%
Euryarchaeota	*Methanomicrobia*	*Methanomicrobiales*	*Methanospirillaceae*	*Methanospirillum*	1270	2%
Thaumarchaeota	*Unclassified (derived from Thaumarchaeota)*	*Unclassified (derived from Thaumarchaeota)*	*Unclassified (derived from Thaumarchaeota)*	*Candidatus Nitrososphaera*	1246	2%
Unclassified (derived from Archaea)	*Unclassified (derived from Archaea)*	*Unclassified (derived from Archaea)*	*Unclassified (derived from Archaea)*	*Unclassified (derived from Archaea)*	821	2%
Unclassified (derived from Archaea)	*Unclassified (derived from Archaea)*	*Unclassified (derived from Archaea)*	*Unclassified (derived from Archaea)*	*Unclassified (derived from Archaea)*	747	1%
Euryarchaeota	-	-	-	-	675	1%
Euryarchaeota	*Methanomicrobia*	*Methanosarcinales*	*Methanosarcinaceae*	-	603	1%
Euryarchaeota	*Methanomicrobia*	*Methanosarcinales*	*Methanosarcinaceae*	*Methanomethylovorans*	372	1%
Euryarchaeota	*Methanomicrobia*	*Methanomicrobiales*	*Unclassified (derived from Methanomicrobiales)*	*Methanosphaerula*	332	1%
Euryarchaeota	*Methanomicrobia*	*Methanomicrobiales*	*Unclassified (derived from Methanomicrobiales)*	*Methanolinea*	308	1%
Euryarchaeota	*Methanomicrobia*	*Methanosarcinales*	*Methanosarcinaceae*	*Methanosarcina*	280	1%

Table A0.21 Genus level classification and abundance of the15 most abundant *Archaea* in post-capping sediment layer GCR 6 –CSed.

Phylum	Class	Order	Family	Genus	Sequence Count	Abundance
Euryarchaeota	*Methanomicrobia*	*Methanosarcinales*	*Methanosaetaceae*	*Methanosaeta*	43373	68%
Euryarchaeota	*Methanobacteria*	*Methanobacteriales*	*Methanobacteriaceae*	*Methanobacterium*	8596	14%
Euryarchaeota	*Methanomicrobia*	*Methanomicrobiales*	-	-	4878	8%
Unclassified (derived from Archaea)	*Unclassified (derived from Archaea)*	*Unclassified (derived from Archaea)*	*Unclassified (derived from Archaea)*	*Unclassified (derived from Archaea)*	1559	2%
Euryarchaeota	-	-	-	-	1099	2%
Euryarchaeota	*Unclassified (derived from Euryarchaeota)*	*Unclassified (derived from Euryarchaeota)*	*Unclassified (derived from Euryarchaeota)*	*Unclassified (derived from Euryarchaeota)*	674	1%
Euryarchaeota	*Methanomicrobia*	-	-	-	646	1%
Euryarchaeota	*Methanomicrobia*	*Methanomicrobiales*	*Methanospirillaceae*	*Methanospirillum*	621	1%
Euryarchaeota	*Methanomicrobia*	*Methanomicrobiales*	*Unclassified (derived from Methanomicrobiales)*	*Methanosphaerula*	619	1%
Euryarchaeota	*Methanobacteria*	*Methanobacteriales*	*Methanobacteriaceae*	-	303	0%
Euryarchaeota	*Methanomicrobia*	*Methanomicrobiales*	*Unclassified (derived from Methanomicrobiales)*	*Methanolinea*	201	0%
Unclassified (derived from Archaea)	*Unclassified (derived from Archaea)*	*Unclassified (derived from Archaea)*	*Unclassified (derived from Archaea)*	*Unclassified (derived from Archaea)*	174	0%
Euryarchaeota	*Methanobacteria*	*Methanobacteriales*	*Methanobacteriaceae*	*Methanobrevibacter*	167	0%
Euryarchaeota	*Methanomicrobia*	*Methanosarcinales*	*Methanosarcinaceae*	*Methanomethylovorans*	160	0%
Euryarchaeota	*Methanomicrobia*	*Methanomicrobiales*	*Unclassified (Methanomicrobiales)*	*Methanoregula*	140	0%

Table A0.22 Genus level classification and abundance of the15 most abundant *Archaea* in post-capping sediment layer GCR 11 –ND.

Phylum	Class	Order	Family	Genus	Sequence Count	Abundance
Euryarchaeota	*Methanomicrobia*	*Methanosarcinales*	*Methanosaetaceae*	*Methanosaeta*	10564	26%
Euryarchaeota	*Methanobacteria*	*Methanobacteriales*	*Methanobacteriaceae*	*Methanobacterium*	7691	19%
Euryarchaeota	*Methanomicrobia*	*Methanosarcinales*	*Methanosarcinaceae*	*Methanomethylovorans*	4062	10%
Euryarchaeota	*Methanomicrobia*	*Methanosarcinales*	*Methanosarcinaceae*	-	2805	7%
Euryarchaeota	*Methanopyri*	*Methanopyrales*	*Methanopyraceae*	*Methanopyrus*	2385	6%
Unclassified (derived from Archaea)	*Unclassified (derived from Archaea)*	*Unclassified (derived from Archaea)*	*Unclassified (derived from Archaea)*	*Unclassified (derived from Archaea)*	2232	5%
Thaumarchaeota	*Unclassified (derived from Thaumarchaeota)*	*Unclassified (derived from Thaumarchaeota)*	*Unclassified (derived from Thaumarchaeota)*	*Candidatus Nitrososphaera*	2108	5%
Thaumarchaeota	*Unclassified (derived from Thaumarchaeota)*	*Nitrosopumilales*	*Nitrosopumilaceae*	*Nitrosopumilus*	2105	5%
Euryarchaeota	*Methanomicrobia*	*Methanomicrobiales*	*Methanospirillaceae*	*Methanospirillum*	2010	5%
Euryarchaeota	*Methanomicrobia*	*Methanosarcinales*	*Methanosarcinaceae*	*Methanosarcina*	1757	4%
Euryarchaeota	*Methanomicrobia*	*Methanomicrobiales*	*Unclassified (derived from Methanomicrobiales)*	*Methanosphaerula*	1363	3%
Euryarchaeota	*Methanobacteria*	*Methanobacteriales*	*Methanobacteriaceae*	-	552	1%
Euryarchaeota	*Unclassified (derived from Euryarchaeota)*	*Unclassified (derived from Euryarchaeota)*	*Unclassified (derived from Euryarchaeota)*	*Unclassified (derived from Euryarchaeota)*	398	1%
Euryarchaeota	*Methanomicrobia*	*Methanomicrobiales*	*Methanocorpusculaceae*	*Methanocorpusculum*	322	1%
Euryarchaeota	*Methanobacteria*	*Methanobacteriales*	*Methanobacteriaceae*	*Methanobrevibacter*	185	0%

Table A0.23 Genus level classification and abundance of the15 most abundant *Archaea* in post-capping sediment layer GCR 11 –GAL.

Phylum	Class	Order	Family	Genus	Sequence Count	Abundance
Euryarchaeota	*Methanomicrobia*	*Methanosarcinales*	*Methanosaetaceae*	*Methanosaeta*	10322	39%
Unclassified (derived from Archaea)	*Unclassified (derived from Archaea)*	*Unclassified (derived from Archaea)*	*Unclassified (derived from Archaea)*	*Unclassified (derived from Archaea)*	4552	17%
Euryarchaeota	*Methanobacteria*	*Methanobacteriales*	*Methanobacteriaceae*	*Methanobacterium*	2438	9%
Euryarchaeota	*Methanomicrobia*	*Methanomicrobiales*	*Unclassified (derived from Methanomicrobiales)*	*Methanosphaerula*	2383	9%
Euryarchaeota	*Methanomicrobia*	*Methanosarcinales*	*Methanosarcinaceae*	*Methanomethylovorans*	2078	8%
Euryarchaeota	*Methanomicrobia*	*Methanomicrobiales*	*Methanospirillaceae*	*Methanospirillum*	993	4%
Euryarchaeota	*Methanomicrobia*	*Methanosarcinales*	*Methanosarcinaceae*	*Methanosarcina*	976	4%
Euryarchaeota	*Unclassified (derived from Euryarchaeota)*	*Unclassified (derived from Euryarchaeota)*	*Unclassified (derived from Euryarchaeota)*	*Unclassified (derived from Euryarchaeota)*	639	2%
Euryarchaeota	*Methanomicrobia*	*Methanosarcinales*	*Methanosarcinaceae*	-	260	1%
Euryarchaeota	*Methanobacteria*	*Methanobacteriales*	*Methanobacteriaceae*	*Methanobrevibacter*	230	1%
Euryarchaeota	*Methanomicrobia*	*Methanomicrobiales*	-	-	230	1%
Euryarchaeota	*Methanopyri*	*Methanopyrales*	*Methanopyraceae*	*Methanopyrus*	226	1%
Euryarchaeota	*Methanomicrobia*	*Methanomicrobiales*	*Methanocorpusculaceae*	*Methanocorpusculum*	221	1%
Thaumarchaeota	*Unclassified (derived from Thaumarchaeota)*	*Unclassified (derived from Thaumarchaeota)*	*Unclassified (derived from Thaumarchaeota)*	*Candidatus Nitrososphaera*	215	1%
Euryarchaeota	*Methanomicrobia*	*Methanosarcinales*	*Methanosarcinaceae*	*Methanolobus*	131	0%

Table A0.24 Genus level classification and abundance of the15 most abundant *Archaea* in post-capping sediment layer GCR 11 –OrgC.

Phylum	Class	Order	Family	Genus	Sequence Count	Abundance
Euryarchaeota	*Methanomicrobia*	*Methanosarcinales*	*Methanosarcinaceae*	-	47853	51%
Euryarchaeota	*Methanomicrobia*	*Methanosarcinales*	*Methanosaetaceae*	*Methanosaeta*	24493	26%
Euryarchaeota	*Methanobacteria*	*Methanobacteriales*	*Methanobacteriaceae*	*Methanobacterium*	5317	6%
Unclassified (derived from Archaea)	*Unclassified (derived from Archaea)*	*Unclassified (derived from Archaea)*	*Unclassified (derived from Archaea)*	*Unclassified (derived from Archaea)*	3958	4%
Euryarchaeota	*Methanomicrobia*	*Methanomicrobiales*	-	-	2609	3%
Euryarchaeota	*Methanomicrobia*	-	-	-	1915	2%
Euryarchaeota	*Methanobacteria*	*Methanobacteriales*	*Methanobacteriaceae*	*Methanobrevibacter*	1815	2%
Thaumarchaeota	*Unclassified (derived from Thaumarchaeota)*	*Unclassified (derived from Thaumarchaeota)*	*Unclassified (derived from Thaumarchaeota)*	*Candidatus Nitrososphaera*	1160	1%
Crenarchaeota	*Thermoprotei*	*Thermoproteales*	*Thermoproteaceae*	-	847	1%
Euryarchaeota	*Methanomicrobia*	*Methanosarcinales*	*Methanosarcinaceae*	*Methanomethylovorans*	619	1%
Euryarchaeota	*Unclassified (derived from Euryarchaeota)*	*Unclassified (derived from Euryarchaeota)*	*Unclassified (derived from Euryarchaeota)*	*Unclassified (derived from Euryarchaeota)*	453	0%
Unclassified (derived from Archaea)	*Unclassified (derived from Archaea)*	*Unclassified (derived from Archaea)*	*Unclassified (derived from Archaea)*	*Unclassified (derived from Archaea)*	401	0%
Euryarchaeota	*Methanomicrobia*	*Methanosarcinales*	*Methanosarcinaceae*	*Methanosarcina*	271	0%
Euryarchaeota	*Methanomicrobia*	*Methanomicrobiales*	*Unclassified (derived from Methanomicrobiales)*	*Methanolinea*	264	0%
Euryarchaeota	*Methanomicrobia*	*Methanomicrobiales*	*Methanospirillaceae*	*Methanospirillum*	211	0%

Table A0.25 Genus level classification and abundance of the15 most abundant *Archaea* in post-capping sediment layer GCR 11 –CSed.

Phylum	Class	Order	Family	Genus	Sequence Count	Abundance
Euryarchaeota	*Methanomicrobia*	*Methanosarcinales*	*Methanosaetaceae*	*Methanosaeta*	77876	57%
Euryarchaeota	*Methanomicrobia*	*Methanomicrobiales*	-	-	29405	22%
Euryarchaeota	*Methanobacteria*	*Methanobacteriales*	*Methanobacteriaceae*	*Methanobacterium*	10070	7%
Unclassified (derived from Archaea)	*Unclassified (derived from Archaea)*	*Unclassified (derived from Archaea)*	*Unclassified (derived from Archaea)*	*Unclassified (derived from Archaea)*	3940	3%
Euryarchaeota	*Methanomicrobia*	*Methanomicrobiales*	*Unclassified (derived from Methanomicrobiales)*	*Methanolinea*	2208	2%
Euryarchaeota	*Methanobacteria*	*Methanobacteriales*	*Methanobacteriaceae*	-	2158	2%
Euryarchaeota	*Methanobacteria*	*Methanobacteriales*	*Methanobacteriaceae*	*Methanobrevibacter*	2109	2%
Euryarchaeota	-	-	-	-	1953	1%
Euryarchaeota	*Methanomicrobia*	-	-	-	1284	1%
Euryarchaeota	*Unclassified (derived from Euryarchaeota)*	*Unclassified (derived from Euryarchaeota)*	*Unclassified (derived from Euryarchaeota)*	*Unclassified (derived from Euryarchaeota)*	1209	1%
Euryarchaeota	*Methanomicrobia*	*Methanomicrobiales*	*Methanocorpusculaceae*	*Methanocorpusculum*	765	1%
Euryarchaeota	*Methanomicrobia*	*Methanomicrobiales*	*Methanospirillaceae*	*Methanospirillum*	736	1%
Euryarchaeota	*Methanomicrobia*	*Methanomicrobiales*	*Unclassified (derived from Methanomicrobiales)*	-	531	0%
Unclassified (derived from Archaea)	*Unclassified (derived from Archaea)*	*Unclassified (derived from Archaea)*	*Unclassified (derived from Archaea)*	*Unclassified (derived from Archaea)*	430	0%
Euryarchaeota	*Methanomicrobia*	*Methanosarcinales*	*Methanosarcinaceae*	*Methanomethylovorans*	301	0%

Table A0.26 Genus level classification and abundance of the15 most abundant *Archaea* in post-capping sediment layer GCR 13 –ND.

Phylum	Class	Order	Family	Genus	Sequence Count	Abundance
Euryarchaeota	*Methanomicrobia*	*Methanosarcinales*	*Methanosaetaceae*	*Methanosaeta*	23888	40%
Euryarchaeota	*Methanobacteria*	*Methanobacteriales*	*Methanobacteriaceae*	*Methanobacterium*	10407	17%
Euryarchaeota	*Methanomicrobia*	*Methanomicrobiales*	-	-	4331	7%
Unclassified (derived from Archaea)	*Unclassified (derived from Archaea)*	*Unclassified (derived from Archaea)*	*Unclassified (derived from Archaea)*	*Unclassified (derived from Archaea)*	3776	6%
Thaumarchaeota	*Unclassified (derived from Thaumarchaeota)*	*Unclassified (derived from Thaumarchaeota)*	*Unclassified (derived from Thaumarchaeota)*	*Candidatus Nitrososphaera*	3171	5%
Euryarchaeota	*Methanomicrobia*	*Methanomicrobiales*	*Methanospirillaceae*	*Methanospirillum*	2231	4%
Euryarchaeota	*Methanomicrobia*	-	-	-	1692	3%
Euryarchaeota	*Methanomicrobia*	*Methanosarcinales*	*Methanosarcinaceae*	-	1570	3%
Euryarchaeota	*Methanomicrobia*	*Methanocellales*	*Methanocellaceae*	*Methanocella*	1484	2%
Euryarchaeota	*Methanobacteria*	*Methanobacteriales*	*Methanobacteriaceae*	-	1173	2%
Euryarchaeota	*Methanopyri*	*Methanopyrales*	*Methanopyraceae*	*Methanopyrus*	1079	2%
Euryarchaeota	*Methanomicrobia*	*Methanosarcinales*	*Methanosarcinaceae*	*Methanolobus*	837	1%
Euryarchaeota	*Methanobacteria*	*Methanobacteriales*	*Methanobacteriaceae*	*Methanobrevibacter*	759	1%
Euryarchaeota	*Methanomicrobia*	*Methanomicrobiales*	*Unclassified (derived from Methanomicrobiales)*	*Methanolinea*	706	1%
Euryarchaeota	-	-	-	-	614	1%

Table A0.27 Genus level classification and abundance of the15 most abundant *Archaea* in post-capping sediment layer GCR 13 –GAL.

Phylum	Class	Order	Family	Genus	Sequence Count	Abundance
Euryarchaeota	*Methanomicrobia*	*Methanosarcinales*	*Methanosaetaceae*	*Methanosaeta*	958	64%
Euryarchaeota	*Methanomicrobia*	*Methanosarcinales*	*Methanosarcinaceae*	*Methanomethylovorans*	233	16%
Unclassified (derived from Archaea)	*Unclassified (derived from Archaea)*	*Unclassified (derived from Archaea)*	*Unclassified (derived from Archaea)*	*Unclassified (derived from Archaea)*	152	10%
Euryarchaeota	*Methanomicrobia*	*Methanocellales*	*Methanocellaceae*	*Methanocella*	102	7%
Euryarchaeota	*Methanopyri*	*Methanopyrales*	*Methanopyraceae*	*Methanopyrus*	37	2%
Euryarchaeota	*Methanomicrobia*	*Methanosarcinales*	*Methanosarcinaceae*	-	5	0%
Euryarchaeota	*Methanomicrobia*	*Methanosarcinales*	*Methanosarcinaceae*	*Methanolobus*	2	0%
Euryarchaeota	-	-	-	-	1	0%
Euryarchaeota	*Archaeoglobi*	*Archaeoglobales*	*Archaeoglobaceae*	-	1	0%
Euryarchaeota	*Methanomicrobia*	-	-	-	1	0%
Euryarchaeota	*Methanomicrobia*	*Methanomicrobiales*	-	-	1	0%
Euryarchaeota	*Methanomicrobia*	*Methanomicrobiales*	*Unclassified (derived from Methanomicrobiales)*	*Methanosphaerula*	1	0%

Table A0.28 Genus level classification and abundance of the15 most abundant *Archaea* in post-capping sediment layer GCR 13 –OrgC.

Phylum	Class	Order	Family	Genus	Sequence Count	Abundance
Euryarchaeota	*Methanobacteria*	*Methanobacteriales*	*Methanobacteriaceae*	*Methanobacterium*	5056	67%
Euryarchaeota	*Methanomicrobia*	*Methanosarcinales*	*Methanosaetaceae*	*Methanosaeta*	716	10%
Thaumarchaeota	*Unclassified (derived from Thaumarchaeota)*	*Unclassified (derived from Thaumarchaeota)*	*Unclassified (derived from Thaumarchaeota)*	*Candidatus Nitrososphaera*	580	8%
Euryarchaeota	*Methanobacteria*	*Methanobacteriales*	*Methanobacteriaceae*	*Methanobrevibacter*	409	5%
Euryarchaeota	*Methanomicrobia*	*Methanomicrobiales*	-	-	365	5%
Euryarchaeota	*Methanomicrobia*	*Methanosarcinales*	*Methanosarcinaceae*	-	142	2%
Unclassified (derived from Archaea)	*Unclassified (derived from Archaea)*	*Unclassified (derived from Archaea)*	*Unclassified (derived from Archaea)*	*Unclassified (derived from Archaea)*	79	1%
Crenarchaeota	-	-	-	-	62	1%
Euryarchaeota	*Methanomicrobia*	*Methanomicrobiales*	*Unclassified (derived from Methanomicrobiales)*	*Methanolinea*	37	0%
Euryarchaeota	*Methanomicrobia*	-	-	-	27	0%
Euryarchaeota	-	-	-	-	11	0%
Euryarchaeota	*Methanomicrobia*	*Methanomicrobiales*	*Methanomicrobiaceae*	*Unclassified (derived from Methanomicrobiaceae)*	3	0%
Euryarchaeota	*Methanomicrobia*	*Methanosarcinales*	*Methanosarcinaceae*	*Methanohalophilus*	3	0%
Crenarchaeota	*Unclassified (derived from Crenarchaeota)*	*Unclassified (derived from Crenarchaeota)*	*Unclassified (derived from Crenarchaeota)*	*Candidatus Nitrosocaldus*	2	0%
Euryarchaeota	*Methanomicrobia*	*Methanosarcinales*	*Methanosarcinaceae*	*Methanomethylovorans*	2	0%

Table A0.29 Genus level classification and abundance of the15 most abundant *Archaea* in post-capping sediment layer GCR 13 –CSed.

Phylum	Class	Order	Family	Genus	Sequence Count	Abundance
Euryarchaeota	*Methanomicrobia*	*Methanosarcinales*	*Methanosaetaceae*	*Methanosaeta*	30601	47%
Crenarchaeota	*Unclassified (derived from Crenarchaeota)*	*Unclassified (derived from Crenarchaeota)*	*Unclassified (derived from Crenarchaeota)*	*Candidatus Nitrosocaldus*	8420	13%
Euryarchaeota	*Methanomicrobia*	*Methanomicrobiales*	-	-	3627	6%
Euryarchaeota	*Methanomicrobia*	-	-	-	3578	6%
Crenarchaeota	*Thermoprotei*	*Desulfurococcales*	*Desulfurococcaceae*	-	2877	4%
Unclassified (derived from Archaea)	*Unclassified (derived from Archaea)*	*Unclassified (derived from Archaea)*	*Unclassified (derived from Archaea)*	*Unclassified (derived from Archaea)*	2767	4%
Euryarchaeota	*Methanobacteria*	*Methanobacteriales*	*Methanobacteriaceae*	*Methanobacterium*	2646	4%
Euryarchaeota	*Methanobacteria*	*Methanobacteriales*	*Methanobacteriaceae*	*Methanobrevibacter*	2595	4%
Euryarchaeota	*Methanomicrobia*	*Methanomicrobiales*	*Methanospirillaceae*	*Methanospirillum*	1300	2%
Thaumarchaeota	*Unclassified (derived from Thaumarchaeota)*	-	-	-	901	1%
Euryarchaeota	*Methanomicrobia*	*Methanomicrobiales*	*Methanocorpusculaceae*	*Methanocorpusculum*	880	1%
Euryarchaeota	-	-	-	-	758	1%
Euryarchaeota	*Methanomicrobia*	*Methanomicrobiales*	*Methanomicrobiaceae*	*Methanoculleus*	568	1%
Crenarchaeota	*Thermoprotei*	*Desulfurococcales*	*Desulfurococcaceae*	*Ignicoccus*	530	1%
Thaumarchaeota	*Unclassified (derived from Thaumarchaeota)*	*Nitrosopumilales*	*Nitrosopumilaceae*	*Nitrosopumilus*	483	1%

Table A0.30 Pearson's correlation between dominant pre-cap methanogenic archaeal genera, sediment chemical parameters and field gas ebullition rates

	Pearson's Co-efficient							
	OM	**OC**	**BC**	**BOD/COD ratio**	**COD/TOC ratio**	**Gas Ebullition rate**	**TMetals**	**TPAH**
Methanosaeta	0.512	0.326	-0.037	0.734	-0.245	0.623	0.276	0.247
Methanobacterium	-0.36	-0.348	-0.248	-0.072	0.203	-0.121	0.013	0.064
Methanobrevibacter	-0.668	-0.652	-0.141	-0.501	0.509	-0.061	-0.467	-0.205
Methanolinea	-0.069	-0.016	-0.196	-0.282	0.399	-0.236	-0.022	-0.12
Methanomethylovorans	-0.181	-0.27	-0.546	0.081	0.234	-0.125	0.444	0.436
Methanocella	-0.059	-0.029	-0.243	-0.106	0.02	-0.34	0.374	0.103
Candidatus Nitrososphaera	-0.524	-0.596	-0.645	-0.184	0.639	-0.192	-0.401	-0.143
Methanospirillum	0.351	0.212	-0.273	0.396	-0.061	-0.092	0.241	0.141
Methanocorpusculum	0.183	0.122	0.112	0.358	-0.324	0.333	-0.035	-0.076
Methanosarcina	0.184	-0.017	-0.066	0.71	0.016	0.667	0.041	0.317
Methanopyrus	0.248	0.161	-0.411	0.577	-0.011	-0.268	0.72	0.873
Methanosphaerula	0.318	0.183	0.01	0.494	-0.251	0.641	-0.128	-0.049

Table A0.31 Pearson's coefficient between dominant post-cap methanogenic archaeal genera, sediment chemical parameters and field gas ebullition rates.

	Pearson's Coefficient					
	OM	**OC**	**BC**	**2012_Gas**	**2013_Gas**	**2014_Gas**
Unclassified Archaea	-0.244	-0.248	-0.227	-0.432	-0.33	-0.354
Unclassified Euryarchaeota	0.441	0.419	0.471	0.287	**0.576**	0.282
Thermoprotei	**0.801**	0.163	**0.518**	-0.45	-0.29	-0.36
Methanomicrobia	0.091	-0.007	0.035	0.352	0.411	0.364
Methanomicrobiales	**0.785**	**0.789**	0.854	-0.153	-0.087	-0.192
Methanosarcinaceae	0.014	0.197	0.114	-0.18	0.072	-0.261
Methanobacteriaceae	-0.277	-0.125	-0.424	0.005	-0.158	-0.115
Methanosaeta	0.411	0.423	0.364	**0.534**	**0.634**	**0.479**
Methanobacterium	-0.157	-0.126	-0.16	0.297	-0.086	0.304
Methanobrevibacter	-0.024	-0.116	0.114	0.003	-0.255	0.108
Methanospirillum	-0.327	-0.326	-0.418	0.335	0.12	0.239
Methanolinea	0.368	0.339	**0.544**	-0.106	-0.136	-0.058
Methanopyrus	**0.59**	**0.539**	**0.783**	-0.233	-0.353	-0.296
Methanomethylovorans	-0.181	-0.283	-0.196	-0.084	-0.248	-0.113
Methanosphaerula	-0.194	-0.18	-0.192	-0.224	-0.1	-0.326
Candidatus Nitrososphaera	-0.44	-0.406	-0.436	-0.21	-0.319	-0.127
Methanosarcina	-0.253	-0.247	-0.256	-0.282	-0.173	**-0.397**
Methanocella	**-0.523**	-0.493	**-0.526**	-0.306	-0.388	-0.191
Methanocorpusculum	-0.155	-0.156	-0.144	-0.361	-0.266	-0.274
Methanoculleus	0.072	-0.044	0.261	-0.153	-0.471	-0.04
Methanoregula	-0.082	-0.012	-0.013	**0.586**	**0.802**	**0.644**
Methanosarcinales	**-0.995**	**-0.862**	**-0.556**	-0.71	-0.481	**-0.551**
Thermoproteaceae	0.274	0.037	**-0.556**	**0.574**	-0.204	**0.612**
Desulfurococacaea	**-0.822**	**-0.666**	0.074	-0.71	-0.481	**-0.551**
Candidatus Nitrosocaldus	-0.171	-0.466	**-0.891**	**0.574**	-0.204	**0.612**
Ignicoccus	-0.283	**-0.542**	**-0.975**	**0.923**	**0.636**	**0.989**

VITA

Raja Shankar Kaliappan

EDUCATION:

PhD Student, Environmental Engineering *GPA:* 4.0 / 4.0

University of Illinois at Chicago (*Expected: Spring '15)*

Master of Environmental Engineering *GPA:* 4.0 / 4.0

Illinois Institute of Technology, Chicago, Illinois *(Dec '08)*

Bachelor of Engineering in Civil Engineering *GPA:* 8.28 / 10.00

College of Engineering Guindy, Anna University, Chennai, India (*May '05*)

RESEARCH EXPERIENCE:

Graduate Researcher, UIC, Applied Environmental Biotechnology Lab (Aug '09-Present)

- Evaluating the efficacy of active capping technology in mitigating gas ebullition rates and ebullition facilitated contaminant fluxes at the Grand Calumet River Indiana
- Exposure Assessment of Atrazine in Drinking water in five Midwestern states in the corn-belt region.

Graduate Researcher, IIT, Chicago (May-Dec '07)

- Site-specific Class A Biosolids Treatment Technologies for sludge treatment at MWRDGC

TEACHING EXPERIENCE:

Graduate Teaching Assistant: University of Illinois at Chicago (Aug '09-Present)

Served as teaching assistant with responsibilities of conducting weekly labs, evaluating assignments/exams and substitute lecturer in Fluid Mechanics, Water Resources Engineering, Strength of Materials and Engineering Hydrology

PROFESSIONAL EXPERIENCE:

Engineering Intern O'Hare Modernization Program (June'08-Aug '09)

Assisted the City of Chicago Construction and Design team with reviewing change orders, line item changes, design drawings and specifications for O'Hare Airport Runway projects.

JOURNAL PUBLICATIONS, CONFERENCE PROCEEDINGS, POSTERS AND TECHNICAL REPORTS:

R. Kaliappan and K. Rockne (2015), Paper and Platform Presentation: Estimating Post-cap Groundwater/Surface Water Exchange at the Grand Calumet River, Indiana Using Streambed Temperature Profiles. In: Eighth International Conference on Remediation of Contaminated Sediments, New Orleans, Louisiana, USA, Jan 12th -13th 2015.

R. Kaliappan and K. Rockne (2015), Platform Presentation: Three-Year Post-Cap Gas Ebullition Monitoring Study on the Grand Calumet River Indiana, Reaches I and II. In: Eighth International Conference on Remediation of Contaminated Sediments, New Orleans,Louisiana, USA, Jan 12th 2015.

Kavitha, S.; Brindha, G. J.; Gloriana, A. S.; **Rajashankar, K**.; Yeom, I. T.; Banu, J. R., Enhancement of aerobic biodegradability potential of municipal waste activated sludge by ultrasonic aided bacterial disintegration. *Bioresource technology* 2016, *200*, 161-169

Sharmila, V. G.; Kavitha, S.; **Rajashankar, K**.; Yeom, I. T.; Banu, J. R., Effects of titanium dioxide mediated dairy waste activated sludge deflocculation on the efficiency of bacterial disintegration and cost of sludge management. *Bioresource technology* **2015,** *197*, 64-71

K. Rockne and **R. Kaliappan** (2013) Gas Ebullition Monitoring Pre and Post Dredging/Active Capping in the Grand Calumet River, Indiana. In: Seventh International Conference on Remediation of Contaminated Sediments, Dallas, Texas, USA, February 6th 2013.

Rockne, K. J., **R. Kaliappan**, et al. (2013). Report: Post Capping Sediment Gas Ebullition Study, Grand Calumet River, Western Branch, Reaches 1 and 2. USACE-Chicago District, University of Illinois at Chicago.

R. Jones, L. Stayner, M. Turyk, **R. Kaliappan**, K. Rockne, K. Almberg, E. Banda, J. Graber, R. Anderson, and L. Conroy (Sept 2013). Report: A Linkage Study of Health Outcome Data in Children and Agrichemical Water Contamination Data in the Midwest. Environmental Public Health Tracking Program.

Kaliappan, R., R. Jones, K. Rockne, L. Stayner, M. Turyk, J. Graber, R. Anderson, K. Almberg, and L. Conroy. Atrazine levels in IL Community Water System Drinking Water as Revealed by the Atrazine Monitoring Program Dataset. Presented at the 2012 Water Research Forum, University of Illinois at Chicago, April 10, 2012, Chicago, IL.

K. Rockne, **Kaliappan, R**., R. Jones, L. Stayner, M. Turyk, J. Graber, R. Anderson, K. Almberg, and L. Conroy. Atrazine levels in Illinois Community Water System Drinking Water as Revealed by the Atrazine Monitoring Program Dataset. Presented at the 2012 WATERCON 2012, a joint conference of the IL-AWWA and IWEA, March 19-22, 2012, Springfield, IL.

Almberg, Kirsten, Mary Turyk, Roger Gibson, Judith Graber, Rachael Jones, **Raja Kaliappan**, Elizabeth Banda et al. "P-107: A Linkage Study of Adverse Birth Outcomes with Agricultural Land Use Practices in Missouri, 2004-2008."*Epidemiology* 23, no. 5S (2012).

Rockne, K. J., **R. Kaliappan**, et al. (2011). Report: Sediment Gas Ebullition Study, Grand Calumet River, Western Branch, Reaches 1 and 2. USACE Chicago District, University of Illinois at Chicago.

Kaliappan. R, Rockne. K.J, "Biological Gas Production in Sediments Pollutes the Water Column in the Grand Calumet River, Indiana". Poster: UIC Student Research Forum 2011.

Rockne, Karl, **Raja Kaliappan**, and Priscilla Viana. "Importance of sediment gas ebullition in sediment-to-water contaminant flux." In: Abstracts of Papers of the American Chemical Society, vol. 242. American Chemical Society, 2011.

AWARDS AND ACTIVITIES:

- UIC Board of Trustees Scholarship, Fall 2015
- Graduate Student Council Representative, Civil and Materials Engineering, UIC, 2013-Present
- Mentor, High School students from Illinois Science and Math Academy, 2011
- Award for Outstanding Academic Excellence, Illinois Institute of Technology, 2008
- Illinois Institute of Technology Graduate College Dean's Fellowship, 2006
- Professional Memberships: ASCE (member#10415167), WEFTEC, Illinois